3 April 2009 | $10

Science

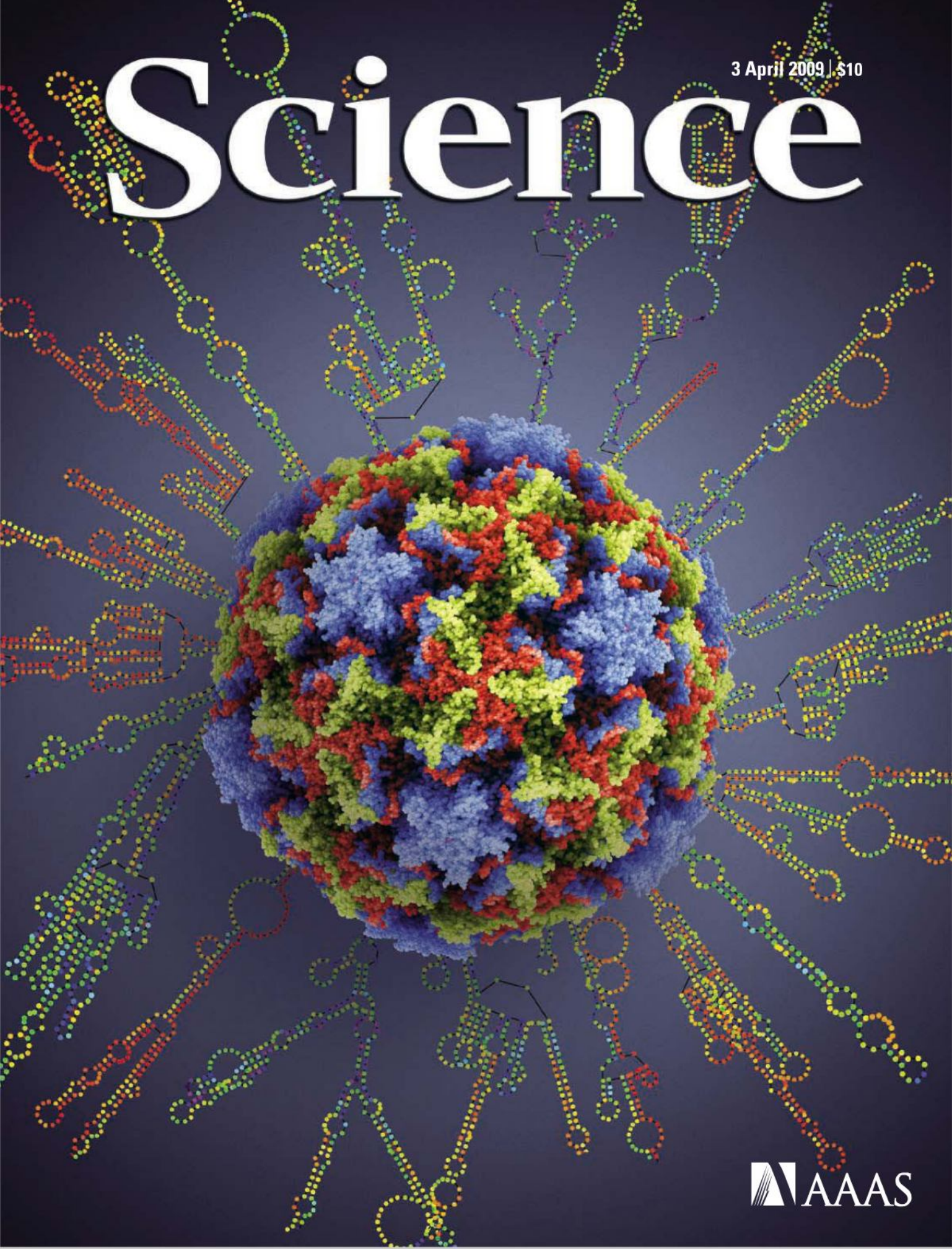

AAAS


Just imagine...

Go ahead, ask the big questions.

Our miRNA and noncoding RNA profiling portfolio makes it possible.

The NCode™ miRNA and ncRNA systems deliver faster, more complete answers. In one powerful portfolio, you can find answers to address your entire workflow, from sample preparation to data validation—or optimize any step along the way. From the first high-density array with both noncoding and mRNA content to data-rich miRNA microarrays to the highly sensitive miRNA labeling system that enables hybridization in as little as 8 hours, you'll have everything you need to advance your research. So ask your big questions and get answers at **www.invitrogen.com/ncode**.

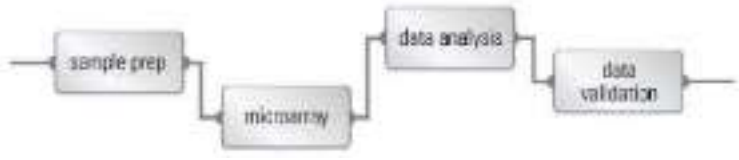

invitrogen™

GE Healthcare

Coordinate your application focus. Achieve greater operational efficiency.

GE Healthcare is focused on helping you develop efficient biopharmaceutical process flows and eliminating wasteful practices, taking your value stream to new frontiers. Through our wide range of technology platforms and services, upstream and downstream from process development to final manufacturing scale, GE Healthcare can connect you to the power of operational excellence.

Learn more about operational excellence at: www.gelifesciences.com/opex

imagination at work

GE Healthcare Bio-Sciences AB, a General Electric Company
Björkgatan 30, 751 84 Uppsala, Sweden

GE04-09. First printetd 09/2008.

EDITORIAL

NEWS OF THE WEEK

NEWS FOCUS

LETTERS

BOOKS *ET AL.*

POLICY FORUM

PERSPECTIVES

REVIEW

BREVIA

CONTENTS continued >>

page 28

page 38

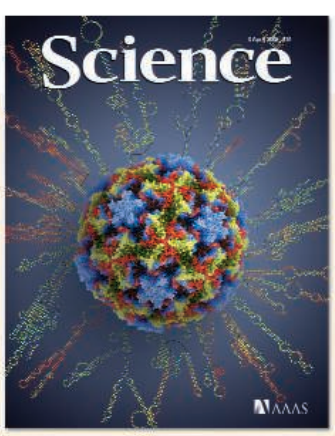

COVER

QuteMol-rendered image of human rhinovirus 3 (Protein Data Bank ID: 1rhi) illustrating virion topography. Red, blue, and yellow denote the three major surface capsid proteins; examples of RNA regional motifs are colored according to predicted base-pairing fidelity. Sequence diversity within the major surface proteins contributes to the wide range of immunogenic serotypes characteristic of the "common cold." See page 55.

Image: H. Adam Steinberg and Jean-Yves Sgro/ University of Wisconsin–Madison

DEPARTMENTS

Published by AAAS

page 42

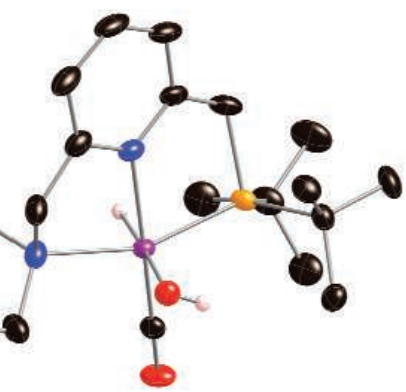

pages 44 & 74

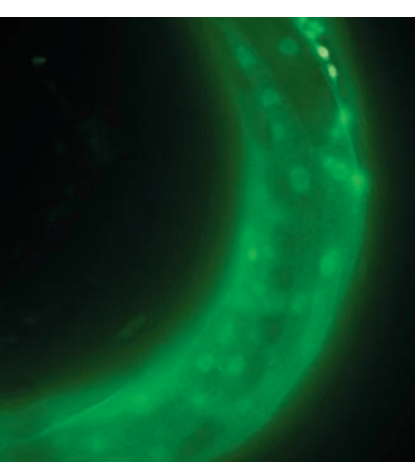

page 95

RESEARCH ARTICLE

REPORTS

Published by AAAS

SCIENCEONLINE

SCIENCEXPRESS
www.sciencexpress.org

Extinction-Reconsolidation Boundaries: Key to Persistent Attenuation of Fear Memories
M.-H. Monfils et al.

Behavioral manipulations can reverse a learned fearful association in rats.
10.1126/science.1167975

Understanding the Spreading Patterns of Mobile Phone Viruses
P. Wang et al.

Current mobile phone usage prevents major mobile virus outbreaks, but conditions could arise leading to a phone epidemic.
10.1126/science.1167053

Apicomplexan Parasites Co-Opt Host Calpains to Facilitate Their Escape from Infected Cells
R. Chandramohanadas et al.

A host protease helps newly replicated microbial parasites escape from incubator cells.
10.1126/science.1171085

Size and Shape of Saturn's Moon Titan
H. A. Zebker et al.

Titan's poles lie at lower elevations than the equator, perhaps explaining its high-latitude hydrocarbon lakes.
10.1126/science.1168905

Fabricating Genetically Engineered High-Power Lithium Ion Batteries Using Multiple Virus Genes
Y. J. Lee et al.

A genetically modified virus is used to form an efficient cathodic battery material.
10.1126/science.1171541

SCIENCENOW
www.sciencenow.org
Highlights From Our Daily News Coverage

The Keen Eyes of a Gamer
Playing shoot-and-kill video games improves visual acuity.

For Migrating Birds, Eating = Exercise
Sandpipers boost their fitness by gorging on omega-3–rich shrimp.

How Choosing Changes You
Could deciding on a beach vacation make you less fond of mountains?

SCIENCESIGNALING
www.sciencesignaling.org
The Signal Transduction Knowledge Environment

EDITORIAL GUIDE: Why We Need Quantitative Dynamic Models
R. Iyengar

Quantitative models provide insight into the mechanisms of cellular behavior and should enable personalized disease intervention.

RESEARCH ARTICLE: Phosphorylation of Nogo Receptors Suppresses Nogo Signaling, Allowing Neurite Regeneration
Y. Takei

Extracellular phosphorylation of Nogo receptors by casein kinase II blocks agonist binding.

PERSPECTIVE: Reversing DNA Methylation: New Insights from Neuronal Activity–Induced Gadd45b in Adult Neurogenesis
H. Wu and Y. E. Sun

Gadd45b causes epigenetic modification of promoters for *Bdnf* and *Fgf* genes in postmitotic neurons in response to neuronal activity.

PERSPECTIVE: Syndecans Shed Their Reputation as Inert Molecules
M. D. Bass et al.

The shedding of the extracellular domain of a transmembrane proteoglycan can be controlled by its cytoplasmic domain.

SCIENCECAREERS
www.sciencecareers.org/career_magazine
Free Career Resources for Scientists

Taken for Granted: The Jackpot's Consequences
B. L. Benderly

Opinions are mixed about the ultimate impact of the huge federal stimulus on early-career scientists.

A Quiet Scientist Returns to His Roots
E. Pain

After working in several countries and research fields, Tiago Fleming Outeiro returned home to Portugal and fundamental biology.

April 2009 Funding News
J. Fernández

Learn about the latest in research funding, scholarships, fellowships, and internships.

SCIENCEPODCAST
www.sciencemag.org/multimedia/podcast
Free Weekly Show

Download the 3 April *Science* Podcast to hear about renewal of cardiac muscle cells in the human heart, automating science, the origins of flowering plants, and more.

ORIGINSBLOG
blogs.sciencemag.org/origins
A History of Beginnings

SCIENCEINSIDER
blogs.sciencemag.org/scienceinsider
Science Policy News and Analysis

SCIENCENOW
Shoot more, see more.

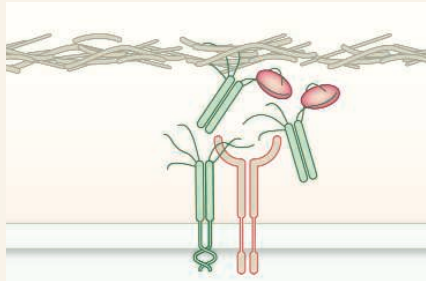

SCIENCESIGNALING
Shedding syndecan ectodomains.

SCIENCECAREERS
Did science really hit the jackpot?

SCIENCE (ISSN 0036-8075) is published weekly on Friday, except the last week in December, by the American Association for the Advancement of Science, 1200 New York Avenue, NW, Washington, DC 20005. Periodicals Mail postage (publication No. 484460) paid at Washington, DC, and additional mailing offices. The title SCIENCE is a registered trademark of the AAAS. Domestic individual membership and subscription (51 issues): $146 ($74 allocated to subscription). Domestic institutional subscription (51 issues): $835; Foreign postage extra: Mexico, Caribbean (surface mail) $55; other countries (air assist delivery) $85. First class, airmail, student, and emeritus rates on request. Canadian rates with GST available upon request, GST #1254 88122. Publications Mail Agreement Number 1069624. **Printed in the U.S.A.**

Change of address: Allow 4 weeks, giving old and new addresses and 8-digit account number. **Postmaster:** Send change of address to AAAS, P.O. Box 96178, Washington, DC 20090–6178. **Single-copy sales:** $10.00 current issue, $15.00 back issue prepaid includes surface postage; bulk rates on request. **Authorization to photocopy** material for internal or personal use under circumstances not falling within the fair use provisions of the Copyright Act is granted by AAAS to libraries and other users registered with the Copyright Clearance Center (CCC) Transactional Reporting Service, provided that $20.00 per article is paid directly to CCC, 222 Rosewood Drive, Danvers, MA 01923. The identification code for *Science* is 0036-8075. *Science* is indexed in the *Reader's Guide to Periodical Literature* and in several specialized indexes.

AAAS
ADVANCING SCIENCE, SERVING SOCIETY

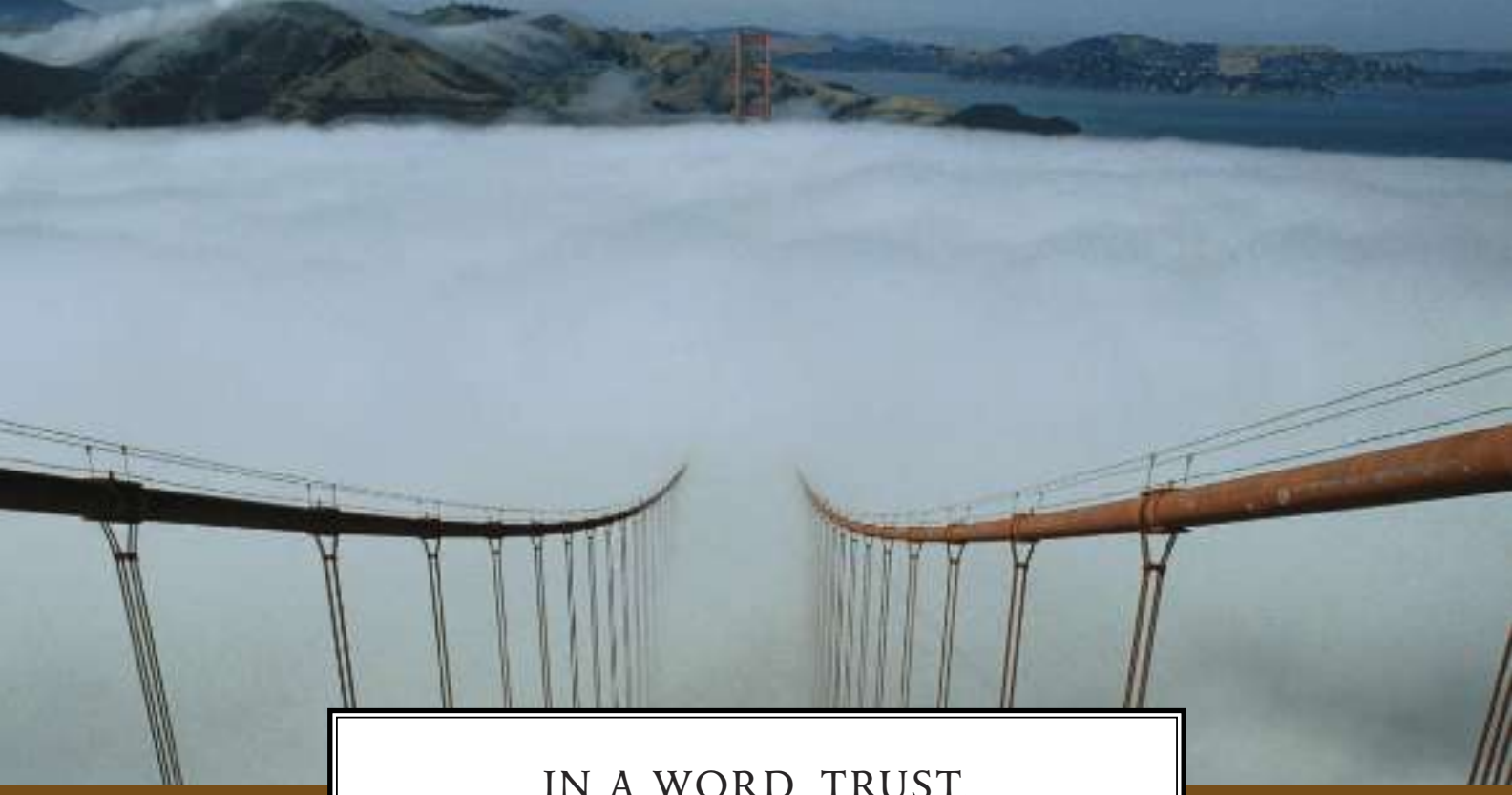

IN A WORD, TRUST.

T4 DNA Ligase

New England Biolabs is dedicated to providing our customers with guaranteed enzyme performance. Our recombinant T4 DNA Ligase is the most extensively used ligase for cloning experiments and other applications, including sample preparation and next generation sequencing. It is available at exceptional value, and an even greater value when purchased in large quantities for high throughput technologies. For cohesive, blunt, simple or complex reactions, make T4 DNA Ligase from NEB your first choice.

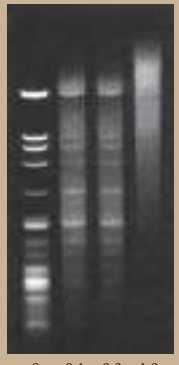

Ligation of blunt-ended HaeIII fragments of Lambda DNA using various amounts of T4 DNA Ligase (400,000 cohesive end units/ml) in a 20 µl reaction volume. Reactions were incubated for 30 minutes at 16°C.

Ligation of HindIII fragments (4-base overhang) of Lambda DNA using 1 cohesive end unit (1µl of 1:400 dilution) of T4 DNA Ligase. Reactions were incubated at 25°C.

Advantages:

Quality - Highly pure enzyme with no lot-to-lot variation

Convenience - Choose original T4 DNA Ligase or the Quick Ligation Kit to meet the demands of a variety of reaction conditions

Flexibility - Active at room temperature or 16°C; reaction times run from 5 minutes to overnight

Robustness - Active in a variety of reaction buffers

T4 DNA Ligase* RI
Regular Concentration **M0202S/L**
For standard cloning reactions

High Concentration **M0202T/M**
For large or difficult constructs

Quick Ligation™ Kit* RI **M2200S/L**
For ligation of cohesive or blunt-end DNA fragments in 5 minutes at room temperature

RI = Recombinant
*NEB ligase products are BSA-free

For more information regarding customization and OEM opportunities, please contact **oem@neb.com**

New England Biolabs, Inc. is an ISO 9001 certified company

NEW ENGLAND BioLabs® Inc.
enabling technologies in the life sciences

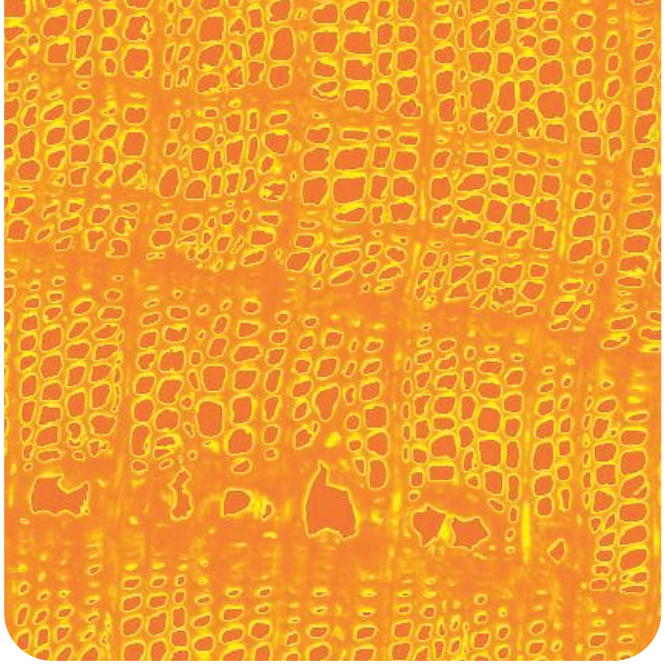

<< Warm in the Past

During the Medieval Climate Anomaly (approximately 800 to 1300 A.D.) temperatures in Europe were generally warmer than immediately before or after. The source of that warmth is hotly debated. **Trouet *et al.*** (p. 78) present a reconstruction of the North Atlantic Oscillation—the dominant mode of atmospheric circulation variability in the North Atlantic region—that extends back to the middle of the Medieval Climate Anomaly, based on data from Moroccan tree rings and a Scottish stalagmite. The North Atlantic Oscillation, it seems, was in a persistently positive state during the Medieval Climate Anomaly. The authors suggest that prevailing La Niña–like conditions during medieval times was initiated by high levels of irradiance and amplified by enhanced Atlantic Meridional Overturning Circulation.

Healing Heart

Damage to the heart through age or disease can lead to loss of heart muscle cells. Although cell transplantation therapies are being investigated to replace these cells, there would be certain advantages if the heart tissue could regenerate its own cells. To find out how many, if any, cells the human heart normally replaces over time, **Bergmann *et al.*** (p. 98; see the Perspective by **Murry and Lee**) made use of ^{14}C measurements in heart cells from adults of various ages. Atmospheric ^{14}C levels were elevated during times of aboveground testing of nuclear bombs around the 1950s and have declined since such tests were banned. Cells formed in different years reflect these differing levels of ^{14}C. Considerable amounts of DNA synthesis was observed in heart cells well after birth, such that a sturdy fraction of an adult's cardiac DNA seems not to be as old as the body it resides in. The extent to which this finding reflects new growth of cells during life, or represents tissue repair remains to be seen.

Malleable Hydrogels

Hydrogels consist of highly swollen polymer networks. Because their properties can be controlled through the specific constituent polymer chemistry, and because they can be made to degrade with time, hydrogels have been used, for example, as scaffolds in tissue engineering. Hydrogels, however, are difficult to pattern into complex shapes because of the high cross-link density, and it is difficult to modify or tune their properties after hydrogel formation. **Kloxin *et al.*** (p. 59) have developed a family of photodegradable hydrogels that can be patterned and shaped after gelation and show how dynamic tuning of the gel properties can be used to manipulate cell function and differentiation.

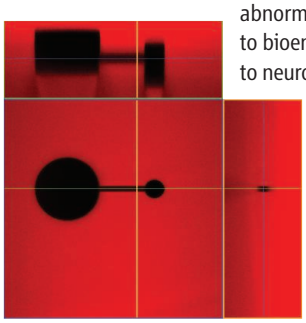

CREDITS (TOP TO BOTTOM): WERNER SCHOCH; JEM ROWLAND; KLOXIN *ET AL.*

Let Your Motor Do the Walking

A challenge in designing a molecular motor is to ensure that its motion is biased in a particular direction to allow it to do work, potentially through harnessing otherwise random fluctuations. **Omabegho *et al.*** (p. 67; see the Perspective by **Sherman**) report the construction of a DNA-based bipedal motor system that can walk along a DNA track. The system operates using two fuel strands, where the by-products of the reaction from the first fuel strand are required for the second, driving a ratcheting motion along the track.

Redox Redux in Alzheimer's Disease

Neurodegenerative disorders involve a series of pathophysiological changes. Oxidative or nitrosative stress can induce a profound and abnormal degree of mitochondrial fission, leading to bioenergetic compromise, which may contribute to neurodegenerative disorders. **Cho *et al.*** (p. 102) describe a critical nitrosylation event induced by nitrosative stress in the pathogenesis of sporadic cases of Alzheimer's disease. Dynamin-related protein 1 (Drp1), which is known to be important for mitochondrial fission, is activated by S-nitrosylation, a redox reaction of NO with a critical cysteine thiol. The nitrosylation event is triggered by oligomerized amyloid-β peptide and appears to mediate the synaptic damage known to occur early in Alzheimer's disease. Thus, the pathogenesis of Alzheimer's disease involves a redox component, which may help to explain why redox metals can contribute to neuronal damage in Alzheimer's disease.

Intelligent Machines?

How can we make sense out of the enormous volume of scientific data that is now being generated, and would a robot be able to replace a research assistant, postdoc, or even the principal investigator in a biological laboratory? (See the Perspective by **Waltz and Buchanan**.) **Schmidt and Lipson** (p. 81) developed an algorithm that substitutes a combination of brute force and mathematical strategies to solve a problem that challenges human reasoning.

Given raw data on the behavior of a physical system like a pendulum, the algorithm searched the gamut of possible equations of mathematical physics consistent with the data and converged on fundamental equations of motion originally derived by Hamilton and Lagrange. **King *et al.*** (p. 85) describe a robot programmed not only to conduct experiments on yeast metabolism with little to no human intervention, but also to reason about its results and plan appropriate next experiments. The robot, Adam, filled in the blanks of unknown enzymes required to account for a biochemical and bioinformatic description of metabolism and genomics, and identified orphan enzymes that were confirmed (by humans) to function in yeast metabolism.

Published by AAAS

Eppendorf & Science Prize for

Neurobiology

$25,000 Prize

Get recognized!

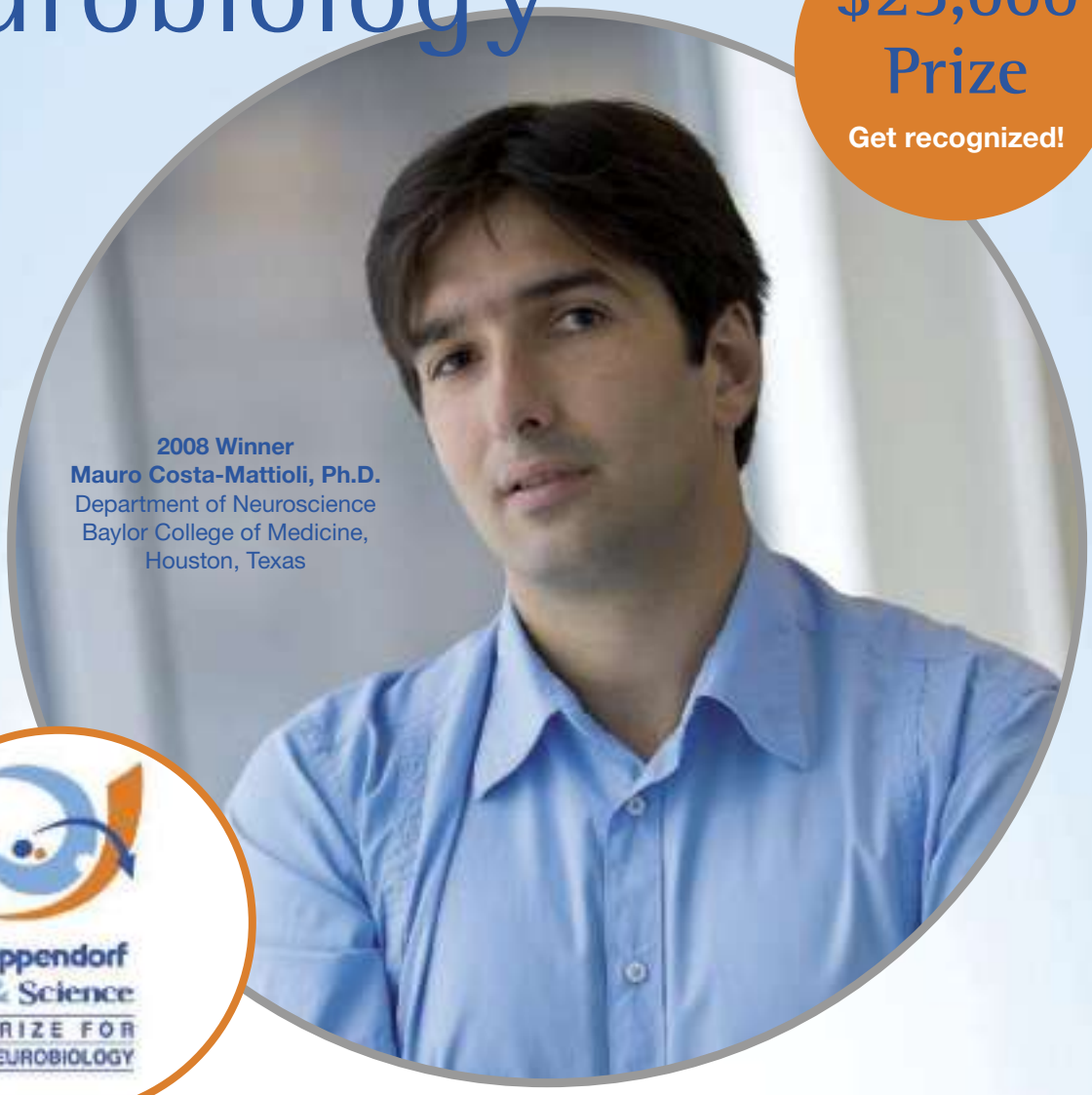

2008 Winner
Mauro Costa-Mattioli, Ph.D.
Department of Neuroscience
Baylor College of Medicine,
Houston, Texas

eppendorf & Science PRIZE FOR NEUROBIOLOGY

Deadline for entries
June 15, 2009

For more information
www.eppendorf.com/prize

This annual international research prize recognizes accomplishments in neurobiology research based on methods of molecular and cell biology. The winner and finalists are selected by a committee of independent scientists, chaired by the Editor-in-Chief of *Science*. Past winners include postdoctoral scholars and assistant professors.

To be eligible, you must be 35 years of age or younger. If you´re selected as this year´s winner, you will receive $25,000, have your work published in the prestigious journal *Science* and be invited to visit Eppendorf in Hamburg, Germany.

eppendorf
In touch with life

Science
AAAS

Kurstin Roe Photography

Bruce Alberts is Editor-in-Chief of *Science*.

Science for Science

ATTITUDES ABOUT CAREER PATHS HAVE CHANGED FOR THE CURRENT GENERATION OF SCIENCE graduate students and postdoctoral fellows. A recent survey of more than 1000 of these young scientists at the University of California, San Francisco (UCSF), reveals an unusually broad range of career aspirations. Less than half select becoming academic researchers like their mentors as their first choice. One senses that we are reaching a tipping point, where students who prefer to work in the world of public policy, government, precollege education, industry, or law will no longer be viewed as deserting science. Faculty and students can then begin to talk honestly about a whole range of respected, science-related career possibilities. This is crucial, because we must promote the movement of scientists into many occupations and environments if our end goal is to effectively apply science and its values to solving global problems.*

The problem is not confined to the interactions between professors and young scientists. Many potential employers who would benefit from having a talented scientist work for them have an overly narrow view of what scientists do, and some may even feel intimidated by the idea of working with a scientist. The best way to change such attitudes is by increasing the contacts between scientists and the rest of society. The American Association for the Advancement of Science has a long-standing tradition of internships and fellowships that intersect the worlds of science and policy, technology, law, and the media. And UCSF will experiment with a new program that would provide all graduate students with the opportunity to spend 3 months of a 5-year Ph.D. degree experience working as an apprentice in a setting outside the usual academic laboratory.

There are new efforts at bringing scientists together with policymakers at all levels of government. For example, the California Council on Science and Technology (CCST) has just announced a program, funded by the Gordon and Betty Moore Foundation in collaboration with others, to provide 1-year Policy Fellowships to the California State Legislature.† Many other governments around the world would certainly benefit from a similar infusion of scientific expertise. All of these programs will require that we provide our students with the additional skills they will need to be successful as they interface with other professions. And the international scientific community must serve as an important resource that remains connected with, and supports, scientists in other careers.

As Editor-in-Chief, I want to encourage and support not only research scientists, but everyone who would use their science in productive ways for society. In 1995, *Science* launched its *Science* Careers Web site (then called *Science*'s Next Wave), which promotes a wide range of successful careers for scientists while also advertising worldwide job opportunities. We now want to build on this tradition by providing new avenues for connecting scientists with each other, whatever their career paths. To this end, in the News and Commentary sections we will continue coverage of the evolving ways in which science is being applied to societal issues—ranging from education to law to public policy. In this way, we can connect our readership to the many opportunities for scientists to contribute to our world, while helping potential employers appreciate the advantages of having someone on their team who can connect them to the valuable resources and strengths of the scientific community.

In addition, *Science* is currently working on new ways to connect subcommunities of scientists with similar aims in order to increase their success. An initial version of a new connection Web site, the Clinical and Translational Science Network, will be launched soon. We also want to reach out to the young scientists entering the many career paths now opening. What are your needs for networking and community support? Readers with examples of highly effective communities that have been established electronically are likewise urged to post those ideas at *Science*, using the links below.

– Bruce Alberts

10.1126/science.1174131

Post a comment: www.sciencemag.org/sciext/post/040309.dtl **Read comments:** www.sciencemag.org/sciext/read/040309.dtl

Science* **320, 155 (2008). †www.fellows.ccst.us

Cell-free protein expression delivers data faster

Now, Get the Most Reliable System for Your Specific Needs

Express proteins in hours instead of days. Referenced in thousands of citations, Promega is the choice for cell-free expression. Select your system from the most comprehensive product portfolio commercially available. Whether you require eukaryotic- or prokaryotic-based expression from either DNA or RNA templates, Promega has the right system for you.

E. coli expression

Transform and overnight growth

DAY 1

Induction and protein expression

DAY 2-3

Purification/dialysis

DAY 4

Use in application

DAY 5

Total: 4-5 DAYS

TnT® Quick System

Add DNA directly to TnT® Master Mix, express protein

1 Hour

Use directly in application

Total: 1 Hour

6992MD

To select the best system for your needs visit: www.promega.com/selectors/tnt/

TODAY COULD BE THE DAY.

Promega

CREDITS (TOP TO BOTTOM): NASA/ESA AND M. J. JEE (JOHNS HOPKINS UNIVERSITY); ADAPTED FROM JEANNE LAWRENCE AND JOHN MCNEIL

ASTROPHYSICS

Stripped in the Dark

Galaxies appear to reside inside dark-matter halos, which over time gather in large clusters held together by the force of gravity. These can be violent places. Dark-matter halos collide and interact with one another, and as they get closer to the cluster's core, they can have matter stripped off them and be ripped apart by strong tidal forces. Although it is not possible to detect dark matter directly, its presence can be inferred from the gravitational effects it has on luminous matter. One such effect is gravitational lensing, whereby light is deflected by the presence of massive objects, producing elongated images of the objects behind them. By analyzing the distorted shapes it is possible to derive the mass distribution of the objects acting as a lens, a technique Natarajan *et al.* used to study the dark-matter halos in the massive lensing cluster Cl 0024+16. They found that the halo masses decreased with decreasing distance to the center of the cluster, as predicted by theories of cosmic structure formation; this result is mimicked in numerically simulated clusters, strengthening the evidence for tidal stripping in clusters of galaxies. — MJC

Astrophys. J. **693**, 970 (2009).

CHEMISTRY

Arene Choreography

Selective substitution of benzene derivatives is a key component of pharmaceutical and fine chemicals synthesis. In general, the easiest positions to modify are the ring carbons directly adjacent to or across from electron-rich substituents already present. Electron-withdrawing groups, in contrast, tend to reduce inherent reactivity toward further substitution, thus hampering direct synthetic strategies for a wide range of desirable products. Zhang *et al.* have addressed this challenge through careful ligand design in palladium-catalyzed addition (via C-H activation) of unsaturated esters to electron-poor arenes to yield olefin-substituted products. The optimal, pyridine-based ligand was sufficiently electron-rich to facilitate reoxidation of the metal after an addition cycle, but also strategically bulky so as to hinder coordination of a second such ligand after the first had bound, thereby leaving a site open for the weakly coordinating arene substrate. The catalyst selectively appended acrylate and cinnamate derivatives at the meta position (two carbons away) of nitro-, trifluoromethyl-, and ester-substituted arenes. More conventional, directed palladium-catalyzed addition facilitated further substitution at the ring carbons in between. The method complements a recently reported meta-selective arylation employing a copper catalyst (see Phipps and Gaunt, Reports, 20 March 2009, p. 1593). — JSY

J. Am. Chem. Soc. **131**, 10.1021/ja900327e (2009).

NEUROSCIENCE

Cleanup After a Breakup

When nerves are damaged, the parts of the axon fibers that are distal to the point of damage become disconnected from the neuronal cell body whence regulatory and metabolic support comes. The distal axonal segment usually degenerates in a characteristic manner termed Wallerian degeneration. The signals that bring about the orderly disintegration and cleanup of axonal debris are the subject of a study by Miller *et al.* When the axons of *Drosophila* olfactory neurons were broken by removal of the antennae, the remaining axon segments disintegrated in wild-type flies; however, in flies in which the protein kinase DLK had been deleted, disintegration proceeded much more slowly. Similarly, in mice, the disintegration of damaged axons in dorsal root ganglia cultures and in sciatic nerves in vivo was slowed in the absence of DLK. The downstream kinase JNK, through which DLK acts, functions in the disconnected axon segment early after the damage occurs. — PJH

Nat. Neurosci. **12**, 10.1038/nn.2290 (2009).

CELL BIOLOGY

Embodied RNA

More than half of the RNA transcribed from the genome is not translated into protein. A few of the larger noncoding RNAs (ncRNAs) have been found to regulate specific processes such as the silencing of the inactive X chromosome, whereas other ncRNAs may be involved in compartmentalized functions. Paraspeckles are intranuclear bodies that were identified 7 years ago and were predicted to function in mRNA processing as they contain proteins that bind DNA and RNA. Clemson *et al.* find that *NEAT1*, a 4-kb ncRNA, participates in nuclear compartmentalization by forming and maintaining paraspeckles. *NEAT1* RNA localized to paraspeckles in both human and mouse cells and bound to other paraspeckle proteins such as PSP1. Paraspeckles formed at the sites of *NEAT1* transcription, and cells depleted of *NEAT1* contained no paraspeckles. — HP*

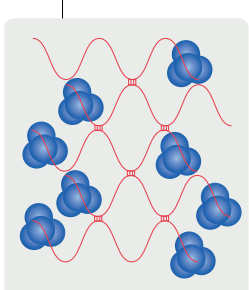

Paraspeckle architecture; RNA, red; protein, blue.

Mol. Cell **33**, 10.1016/j.molcel.2009.01.026 (2009).

*Helen Pickersgill is a locum editor in *Science*'s editorial department.

Published by AAAS

www.sciencemag.org

Science

1200 New York Avenue, NW
Washington, DC 20005
Editorial: 202-326-6550, FAX 202-289-7562
News: 202-326-6581, FAX 202-371-9227
Bateman House, 82-88 Hills Road
Cambridge, UK CB2 1LQ
+44 (0) 1223 326500, FAX +44 (0) 1223 326501

Subscription Services For change of address, missing issues, new orders and renewals, and payment questions: 866-434-AAAS (2227) or 202-326-6417, FAX 202-842-1065. Mailing addresses: AAAS, P.O. Box 96178, Washington, DC 20090-6178 or AAAS Member Services, 1200 New York Avenue, NW, Washington, DC 20005

Institutional Site Licenses please call 202-326-6755 for any questions or information

Reprints: Author Inquiries 800-635-7181
Commercial Inquiries 803-359-4578

Permissions 202-326-7074, FAX 202-682-0816

Member Benefits AAAS/Barnes&Noble.com bookstore www.aaas.org/bn; AAAS Online Store www.apisource.com/aaas/ code MKB6; AAAS Travels: Betchart Expeditions 800-252-4910; Apple Store www.apple/eppstore/aaas; Bank of America MasterCard 1-800-833-6262 priority code FAA3YU; Cold Spring Harbor Laboratory Press Publications www.cshlpress.com/affiliates/aaas.htm; GEICO Auto Insurance www.geico.com/landingpage/go51.htm?logo=17624; Hertz 800-654-2200 CDP#343457; Office Depot https://bsd.officedepot.com/portalLogin.do; Seabury & Smith Life Insurance 800-424-9883; Subaru VIP Program 202-326-6417; VIP Moving Services www.vipmayflower.com/domestic/index.html; Other Benefits: AAAS Member Services 202-326-6417 or www.aaasmember.org.

science_editors@aaas.org	(for general editorial queries)
science_letters@aaas.org	(for queries about letters)
science_reviews@aaas.org	(for returning manuscript reviews)
science_bookrevs@aaas.org	(for book review queries)

Published by the American Association for the Advancement of Science (AAAS), *Science* serves its readers as a forum for the presentation and discussion of important issues related to the advancement of science, including the presentation of minority or conflicting points of view, rather than by publishing only material on which a consensus has been reached. Accordingly, all articles published in *Science*—including editorials, news and comment, and book reviews—are signed and reflect the individual views of the authors and not official points of view adopted by AAAS or the institutions with which the authors are affiliated.

AAAS was founded in 1848 and incorporated in 1874. Its mission is to advance science, engineering, and innovation throughout the world for the benefit of all people. The goals of the association are to: enhance communication among scientists, engineers, and the public; promote and defend the integrity of science and its use; strengthen support for the science and technology enterprise; provide a voice for science on societal issues; promote the responsible use of science in public policy; strengthen and diversify the science and technology workforce; foster education in science and technology for everyone; increase public engagement with science and technology; and advance international cooperation in science.

Information for Authors
See pages 807 and 808 of the 6 February 2009 issue or access www.sciencemag.org/about/authors

EDITOR-IN-CHIEF **Bruce Alberts**
EXECUTIVE EDITOR **Monica M. Bradford**
NEWS EDITOR **Colin Norman**
MANAGING EDITOR, RESEARCH JOURNALS **Katrina L. Kelner**
DEPUTY EDITORS **R. Brooks Hanson, Barbara R. Jasny, Andrew M. Sugden**

Editorial SENIOR EDITOR/PERSPECTIVES Lisa D. Chong; SENIOR EDITORS Gilbert J. Chin, Pamela J. Hines, Paula A. Kiberstis (Boston), Marc S. Lavine (Toronto), Beverly A. Purnell, L. Bryan Ray, Guy Riddihough, H. Jesse Smith, Phillip D. Szuromi (Tennessee), Valda Vinson; ASSOCIATE EDITORS Kristen L. Mueller, Jake S. Yeston, Laura M. Zahn; ONLINE EDITOR Stewart Wills; ASSOCIATE ONLINE EDITORS Robert Frederick, Tara S. Marathe; WEB CONTENT DEVELOPER Martyn Green; BOOK REVIEW EDITOR Sherman J. Suter; ASSOCIATE LETTERS EDITOR Jennifer Sills; EDITORIAL MANAGER Cara Tate; SENIOR COPY EDITORS Jeffrey E. Cook, Cynthia Howe, Harry Jach, Barbara P. Ordway, Trista Wagoner; COPY EDITORS Chris Filiatreau, Lauren Kmec; EDITORIAL COORDINATORS Carolyn Kyle, Beverly Shields; PUBLICATIONS ASSISTANTS Ramatoulaye Diop, Joi S. Granger, Jeffrey Hearn, Lisa Johnson, Scott Miller, Jerry Richardson, Jennifer A. Seibert, Brian White, Anita Wynn; EDITORIAL ASSISTANTS Carlos L. Durham, Emily Guise, Michael Hicks, Patricia M. Moore; EXECUTIVE ASSISTANT Sylvia S. Kihara; ADMINISTRATIVE SUPPORT Maryrose Madrid

News DEPUTY NEWS EDITORS Robert Coontz, Eliot Marshall, Jeffrey Mervis, Leslie Roberts; CONTRIBUTING EDITORS Elizabeth Culotta, Polly Shulman; NEWS WRITERS Yudhijit Bhattacharjee, Adrian Cho, Jennifer Couzin, David Grimm, Constance Holden, Jocelyn Kaiser, Richard A. Kerr, Eli Kintisch, Andrew Lawler (New England), Greg Miller, Elizabeth Pennisi, Robert F. Service (Pacific NW), Erik Stokstad; INTERN Jackie D. Grom; CONTRIBUTING CORRESPONDENTS Dan Charles, Jon Cohen (San Diego, CA), Daniel Ferber, Ann Gibbons, Robert Koenig, Mitch Leslie, Charles C. Mann, Virginia Morell, Evelyn Strauss, Gary Taubes; COPY EDITORS Linda B. Felaco, Melvin Gatling, Melissa Raimondi; ADMINISTRATIVE SUPPORT Scherraine Mack, Fannie Groom; BUREAUS New England: 207-549-7755, San Diego, CA: 760-942-3252, FAX 760-942-4979, Pacific Northwest: 503-963-1940

Production DIRECTOR James Landry; SENIOR MANAGER Wendy K. Shank; ASSISTANT MANAGER Rebecca Doshi; SENIOR SPECIALISTS Steve Forrester, Chris Redwood; SPECIALIST Anthony Rosen; PREFLIGHT DIRECTOR David M. Tompkins; MANAGER Marcus Spiegler

Art DIRECTOR Yael Kats; ASSOCIATE ART DIRECTOR Laura Creveling; ILLUSTRATORS Chris Bickel, Katharine Sutliff; SENIOR ART ASSOCIATES Holly Bishop, Preston Huey, Nayomi Kevitiyagala; ART ASSOCIATE Jessica Newfield; PHOTO EDITOR Leslie Blizard

***Science* International**

Europe (science@science-int.co.uk) EDITORIAL: INTERNATIONAL MANAGING EDITOR Andrew M. Sugden; SENIOR EDITOR/PERSPECTIVES Julia Fahrenkamp-Uppenbrink; SENIOR EDITORS Caroline Ash, Stella M. Hurtley, Ian S. Osborne, Peter Stern; ASSOCIATE EDITOR Maria Cruz; LOCUM EDITOR Helen Pickersgill; EDITORIAL SUPPORT Deborah Dennison, Rachel Roberts, Alice Whaley; ADMINISTRATIVE SUPPORT John Cannell, Janet Clements; NEWS: EUROPE NEWS EDITOR John Travis; DEPUTY NEWS EDITOR Daniel Clery; CONTRIBUTING CORRESPONDENTS Michael Balter (Paris), John Bohannon (Vienna), Martin Enserink (Amsterdam and Paris), Gretchen Vogel (Berlin); INTERN Sara Coelho

Asia Japan Office: Asca Corporation, Eiko Ishioka, Fusako Tamura, 1-8-13, Hirano-cho, Chuo-ku, Osaka-shi, Osaka, 541-0046 Japan; +81 (0) 6 6202 6272, FAX +81 (0) 6 6202 6271; asca@os.gulf.or.jp; ASIA NEWS EDITOR Richard Stone (Beijing: rstone@aaas.org); CONTRIBUTING CORRESPONDENTS Dennis Normile (Japan: +81 (0) 3 3391 0630, FAX +81 (0) 3 5936 3531; dnormile@gol.com); Hao Xin (China: +86 (0) 10 6307 4439 or 6307 3676, FAX +86 (0) 10 6307 4358; cindyhao@gmail.com); Pallava Bagla (South Asia: +91 (0) 11 2271 2896; pbagla@vsnl.com)

EXECUTIVE PUBLISHER **Alan I. Leshner**
PUBLISHER **Beth Rosner**

Fulfillment Systems and Operations (membership@aaas.org); DIRECTOR Waylon Butler; SENIOR SYSTEMS ANALYST Jonny Blaker; CUSTOMER SERVICE SUPERVISOR Pat Butler; SPECIALISTS Latoya Casteel, LaVonda Crawford, Vicki Linton, April Marshall; DATA ENTRY SUPERVISOR Cynthia Johnson; SPECIALISTS Eintou Bowden, Tarrika Hill, William Jones

Business Operations and Administration DIRECTOR Deborah Rivera-Wienhold; ASSISTANT DIRECTOR, BUSINESS OPERATIONS Randy Yi; MANAGER, BUSINESS ANALYSIS Michael LoBue; MANAGER, BUSINESS OPERATIONS Jessica Tierney; FINANCIAL ANALYSTS Priti Pamnani, Celeste Troxler; RIGHTS AND PERMISSIONS: ADMINISTRATOR Emilie David; ASSOCIATE Elizabeth Sandler; MARKETING DIRECTOR Ian King; MARKETING MANAGER Allison Pritchard; MARKETING ASSOCIATES Aimee Aponte, Alison Chandler, Mary Ellen Crowley, Julianne Wielga, Wendy Wise; MARKETING EXECUTIVE Jennifer Reeves; MARKETING/MEMBER SERVICES EXECUTIVE Linda Rusk; DIRECTOR, SITE LICENSING Tom Ryan; DIRECTOR, CORPORATE RELATIONS Eileen Bernadette Moran; PUBLISHER RELATIONS, eRESOURCES SPECIALIST Kiki Forsythe; SENIOR PUBLISHER RELATIONS SPECIALIST Catherine Holland; PUBLISHER RELATIONS, EAST COAST Phillip Smith; PUBLISHER RELATIONS, WEST COAST Philip Tsolakidis; FULFILLMENT SUPERVISOR Iquo Edim; FULFILLMENT COORDINATOR Laura Clemens; ELECTRONIC MEDIA: MANAGER Lizabeth Harman; PROJECT MANAGER Trista Snyder; ASSISTANT MANAGER Lisa Stanford; SENIOR PRODUCTION SPECIALISTS Christopher Coleman, Walter Jones; PRODUCTION SPECIALISTS Nichele Johnston, Kimberly Oster

Advertising DIRECTOR, WORLDWIDE AD SALES Bill Moran

Product (science_advertising@aaas.org); MIDWEST/WEST COAST/W. CANADA Rick Bongiovanni: 330-405-7080, FAX 330-405-7081; EAST COAST/E. CANADA Laurie Faraday: 508-747-9395, FAX 617-507-8189; UK/EUROPE/ASIA Roger Goncalves: TEL/FAX +41 43 243 1358; JAPAN Mashy Yoshikawa: +81 (0) 3 3235 5961, FAX +81 (0) 3 3235 5852; SENIOR TRAFFIC ASSOCIATE Deiandra Simms

Commercial Editor Sean Sanders: 202-326-6430

Project Director, Outreach Brianna Blaser

Classified (advertise@sciencecareers.org); INSIDE SALES MANAGER: MIDWEST/CANADA Daryl Anderson: 202-326-6543; INSIDE SALES REPRESENTATIVE Karen Foote: 202-326-6740; KEY ACCOUNT MANAGER Joribah Able; NORTHEAST Alexis Fleming: 202-326-6578; SOUTHEAST Tina Burks: 202-326-6577; WEST Nicholas Hintibidze: 202-326-6533; SALES COORDINATORS Rohan Edmonson, Shirley Young; INTERNATIONAL: SALES MANAGER Tracy Holmes: +44 (0) 1223 326525, FAX +44 (0) 1223 326532; SALES Susanne Kharraz, Dan Pennington, Alex Palmer; SALES ASSISTANT Louise Moore; JAPAN Mashy Yoshikawa: +81 (0) 3 3235 5961, FAX +81 (0) 3 3235 5852; ADVERTISING PRODUCTION OPERATIONS MANAGER Deborah Tompkins; SENIOR PRODUCTION SPECIALIST/GRAPHIC DESIGNER Amy Hardcastle; SENIOR PRODUCTION SPECIALIST Robert Buck; SENIOR TRAFFIC ASSOCIATE Christine Hall; PUBLICATIONS ASSISTANT Mary Lagnaoui

AAAS Board of Directors RETIRING PRESIDENT, CHAIR James J. McCarthy; PRESIDENT Peter C. Agre; PRESIDENT-ELECT Alice Huang; TREASURER David E. Shaw; CHIEF EXECUTIVE OFFICER Alan I. Leshner; BOARD Alice Gast, Linda P. B. Katehi, Nancy Knowlton, Cherry A. Murray, Julia M. Phillips, Thomas D. Pollard, David S. Sabatini, Thomas A. Woolsey

AAAS
ADVANCING SCIENCE, SERVING SOCIETY

The TaqMan® OpenArray™ Genotyping System Enables…

Genotyping throughput that's out of this world.

One Person. One Day. Over 90,000 Genotypes.

The throughput capabilities of the TaqMan® OpenArray™ Genotyping System will astound you. This stellar new genotyping solution combines two world-class technologies. Our TaqMan® Genotyping Assays provide high quality results using proven TaqMan® Assay chemistry, and OpenArray™ technology utilizes nanoliter fluidics enabling one person to generate over 90,000 genotypes a day. With superior flexibility and less than 30 minutes of hands-on time, you'll get genotyping that is faster, easier, and more cost-effective than ever before.

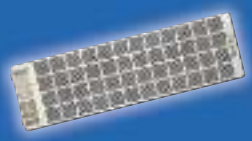

▶ Each TaqMan® OpenArray™ Genotyping Plate is equivalent to eight standard 384-well plates.

To explore new horizons in genotyping, visit info.appliedbiosystems.com/taqmanopenarray

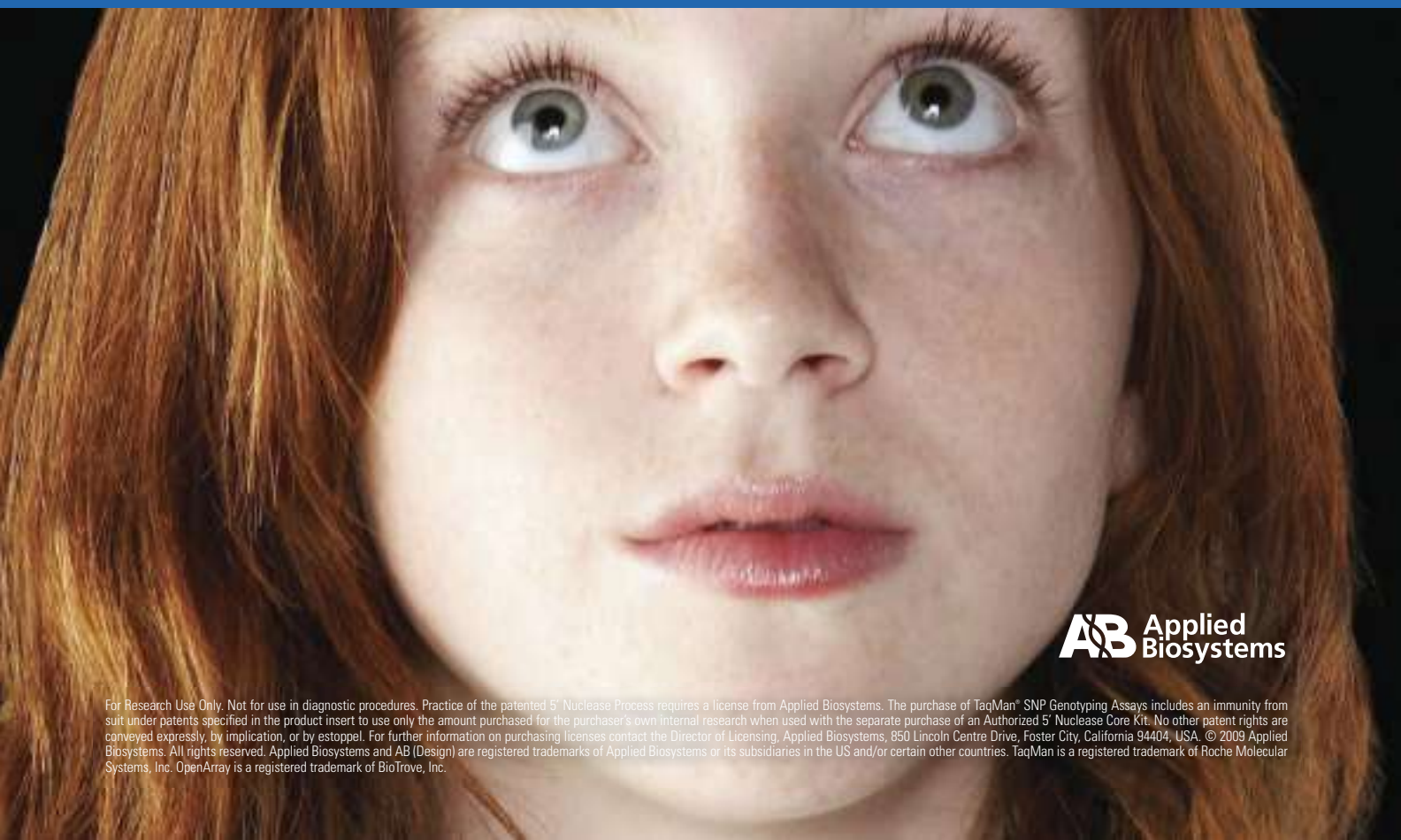

Applied Biosystems

2009 Gordon Research SEMINARS

a new offering for graduate students and post docs

Apply Today!

- **Give a talk** – speakers are selected from submitted abstracts
- **Present a poster** and get valuable feedback and suggestions
- **Network with your peers** in an informal atmosphere
- **Engage in scientific discussions** at the forefront of your field
- **Interact with leaders** who may serve as mentors during your career
- **Gain the confidence to participate in a GRC** – apply to both the GRS & GRC

The following 2009 Gordon Research Seminars (GRS) will be held immediately prior to a related GRC:

Bones & Teeth (GRS)*
July 11-12, 2009
University of New England, Maine

CAG Triplet Repeat Disorders (GRS)*
May 30-31, 2009
Waterville Valley Resort, New Hampshire

Catecholamines (GRS)
August 8-9, 2009
University of New England, Maine

Combinatorial Chemistry (GRS)*
June 6-7, 2009
Colby-Sawyer College, New Hampshire

Dendrites: Molecules, Structure & Function (GRS)
May 16-17, 2009
Il Ciocco Hotel and Resort, Italy

Inorganic Chemistry (GRS)*
June 20-21, 2009
University of New England, Maine

Magnetic Resonance (GRS)*
June 13-14, 2009
University of New England, Maine

Nuclear Physics (GRS)*
July 11-12, 2009
Bryant University, Rhode Island

Organometallic Chemistry (GRS)
July 11-12, 2009
Salve Regina University, Rhode Island

Phagocytes (GRS)*
June 6-7, 2009
Waterville Valley Resort, New Hampshire

Plant Cell Walls (GRS)*
August 1-2, 2009
Bryant University, Rhode Island

Plant Metabolic Engineering (GRS)
July 11-12, 2009
Waterville Valley Resort, New Hampshire

Polyamines (GRS)
June 20-21, 2009
Waterville Valley Resort, New Hampshire

Polymers (GRS)*
June 20-21, 2009
Mount Holyoke College, Massachusetts

** The Kenan Institute for Engineering, Technology & Science at North Carolina State University generously provided seed money to all new Gordon Research Seminars in 2009.*

*visit **www.grc.org** for more information*

Girl frog comes on to guy with red sac.

Dark Attraction

Nocturnal tree frogs use their unique call to lure females through the night, but could the color of their sacs also help to drive the ladies mad?

The sight of a pulsating vocal sac can excite a frog. To see if color could also be a turn-on, scientists at the Muséum National d'Histoire Naturelle in Paris exposed 70 female frogs to two computer screens displaying images of a male, adjusted to appear as he would at night. Speakers alternately played identical male calls; the only difference was that on one screen the male had a dark red vocal sac and on the other, a pale brown one. If a female lingered for 30 seconds in a "choice area" near either image, she was assumed to be signifying a desired mate.

Females were overwhelmingly drawn to the image of a frog with a darker, more colorful sac. Some climbed onto the screen to solicit the virtual frog. So even when lights are low, sac coloration may signal a quality mate, says evolutionary biologist Marc Théry, co-author of a paper online 25 March in *Biological Sciences.*

"This is a fascinating paper," says ecology graduate student Victoria Arch of the University of California, Los Angeles. It shows "the importance of considering multimodal cues" in mating, even in nocturnal species.

An Abel Geometer

Mikhail Gromov of the Institut des Hautes Études Scientifiques (IHES) in Bures-sur-Yvette, France, has won this year's $950,000 Abel Prize in mathematics from the Norwegian Academy of Science and Letters.

The Russian-born Gromov, 65, also a scholar at the Courant Institute of Mathematical Sciences in New York City, has made advances in the fields of symplectic and Riemannian geometry, which are closely tied to areas such as general relativity and string theory. He also founded the modern study of "geometric group theory," which injects notions of distance and curvature into the study of finite algebraic structures.

"Misha is often radical in his judgments," says IHES Director Jean-Pierre Bourguignon. But that pays off in unconventional insights, including new connections between mathematics and biology. For example, Gromov, with a co-author, proved a "theorem" on the virtual certainty of unicellular life in pond water: Within a mathematical framework that stipulates what it takes for a random arrangement of chemicals to be considered living, they find, the "live" states vastly outnumber the "dead" ones.

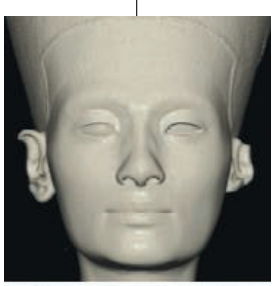

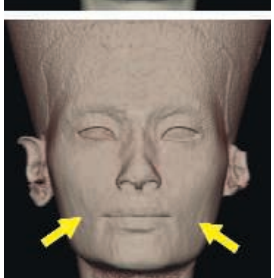

Pharaonic PhotoShop

The famous 3300-year-old bust of Egypt's Queen Nefertiti is more than just a pretty face. Researchers at the Imaging Science Institute in Berlin, Germany, have used computed tomography scans to reveal that the limestone core under the millimeters-thick stucco skin is a slightly different sculpture. This inner face is probably closer to her true likeness, researchers report in the 31 March issue of *Radiology*.

The alterations yield intriguing clues to the nobility's aesthetic ideals, the study's authors say. "Nefertiti's bust … is an intersection between realism and stylization," says institute director Alexander Huppertz, the lead author. The inner sculpture has wrinkles at the corners of its mouth and a small bump on its nose; the sculptor eliminated those flaws by pasting them over with stucco for the final sculpture. Although most of the makeover was designed to flatter the queen, one element was not: The sculptor made the corners of Nefertiti's eyelids more pronounced in the final version. Huppertz says that could have been done to denote the queen's maturity and wisdom. "None of us really knows what the Egyptians' ideals were in those days," says Nicholas Reeves, curator of Egyptian art at Eton College in Windsor, United Kingdom. "But I would say the sculptor only made improvements."

Woe in Congo

An orphaned chimpanzee awaits a buyer in Buta, in the northern Democratic Republic of the Congo. Cleveland Hicks, a graduate student at the Institute for Biodiversity and Ecosystem Dynamics at the University of Amsterdam, recently spent 13 months surveying the area. He reports that diamond and gold mining in the hitherto pristine Gangu forest is leading to destruction of habitat and an upsurge in the bushmeat trade (see www.wasmoethwildlife.org).

CREDITS (LEFT TO RIGHT): MARY THERY AND DORIS GOMEZ; HUPPERTZ *ET AL.*, *RADIOLOGY*, APRIL 2009. VOL 251; THURSTON CLEVELAND HICKS

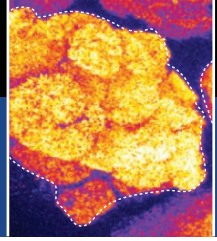

Multitasking while sleeping
22

Science's champion
24

INFECTIOUS DISEASE

Hitting Early, Epidemic Meningitis Ravages Nigeria and Niger

Nigeria and Niger are reeling from one of the worst meningococcal meningitis epidemics in years. Already, the epidemic has sickened at least 25,000 people, more than 17,000 in Nigeria alone, and killed 1500. World Health Organization (WHO) experts caution that those numbers may be underestimates and warn that the worst is yet to come. F. Marc LaForce of the Meningitis Vaccine Project (MVP), a nonprofit effort to develop an affordable vaccine to prevent such epidemics, worries that "this may be a repeat of 1996–97," when the largest epidemic ever to hit Nigeria caused more than 100,000 cases and 11,000 deaths.

WHO, Médecins Sans Frontières (MSF), and others have rushed in teams to help state and local health officials deal with the outbreak. Several million doses of the scarce and outmoded emergency vaccine, which has limited effectiveness, have been released from the global stockpile and have begun arriving in both countries. Antibiotics have been sent as well to supplement country supplies. But meningitis experts fear these efforts may be too little, too late to curb the epidemic, which started unusually early this season, now in its 14th week.

The grim task now is triage. There is simply not enough of the existing, 1960s–era vaccine to protect everybody at risk—50 million in Nigeria alone. That leaves the International Coordinating Group (ICG) on Vaccine Provision for Epidemic Meningitis Control, a collaborative effort of WHO, MSF, UNICEF, and the International Federation of Red Cross and Red Crescent Societies, with the unenviable task of deciding which countries and states get how much.

Caused by the bacterium *Neisseria meningitidis*, meningitis is an infection of the thin membranes that line the brain and spinal cord. It is a frequent scourge of the countries of the African meningitis belt, which stretches from Ethiopia to Senegal. Almost every year, waves of meningococcal meningitis arrive with the harmattan, the hot, dry wind that signals the start of the dry season in December or January, and then dissipate with the first rains, usually in May. Left untreated, meningitis kills roughly half of its victims; even with prompt treatment, up to 10% die and up to 25% are left with deafness or other disabilities.

Although epidemic meningitis comes like clockwork to Africa—for reasons that remain largely a mystery—no one can predict exactly where it will hit or how severe the outbreak will be. Nigeria and Niger have been largely spared in recent years—the disease tends to "jump around," says LaForce. Every 10 years or so, a perfect storm of environmental and population conditions combine to spawn massive outbreaks across the entire belt, like the one in 1996–97 that killed more than 25,000 in 10 countries and sickened 250,000.

Because of this unpredictable epidemiology and the shortage and limited efficacy of the existing polysaccharide vaccine—immunity lasts just 3 years—WHO recommends that it be used in mass campaigns to control epidemics, not to prevent them. ICG releases the vaccine, effective against the main epidemic strain, serogroup A, only when a country can demonstrate that an epidemic has begun and the strain has been confirmed by lab analysis—a tall order in some remote areas. (This year, as usual, the predominant strain is serogroup A, but some W135 is circulating.)

WHO estimates that if a country can launch a mass vaccination campaign within 3 to 4 weeks of the epidemic's onset, roughly 70% of cases can be prevented. But the application request can be onerous, concedes epidemiologist William Perea, who coordinates WHO's epidemic readiness and interventions in Geneva, and often the vaccine arrives too late to do much good. In Nigeria, the first batch of 1.5 million doses of vaccine arrived in early March, in week 8 of the season; several million more doses are on the way. By week 5, six local government areas had already passed the epidemic threshold, and that number skyrocketed to 28 in week 8 and has kept climbing. Says Perea, "It is too soon to say whether it is having an effect on the epidemic curve," which usually peaks 14 or 15 weeks into the season. Niger was better prepared this year, as it had 2 million doses of vaccine prepositioned and also applied earlier to the ICG.

Similarly, antibiotics can save lives, and overall supplies seem sufficient in both countries. But "they are not close enough to the patient," says Stéphane Hugonnet, a WHO epidemiologist working with the hardest hit states in northern Nigeria. "The end result is either the drug is given quite late or another drug is given. Overall, case management is quite poor."

Right now the biggest struggle is to get the vaccine where it can do the most good, say

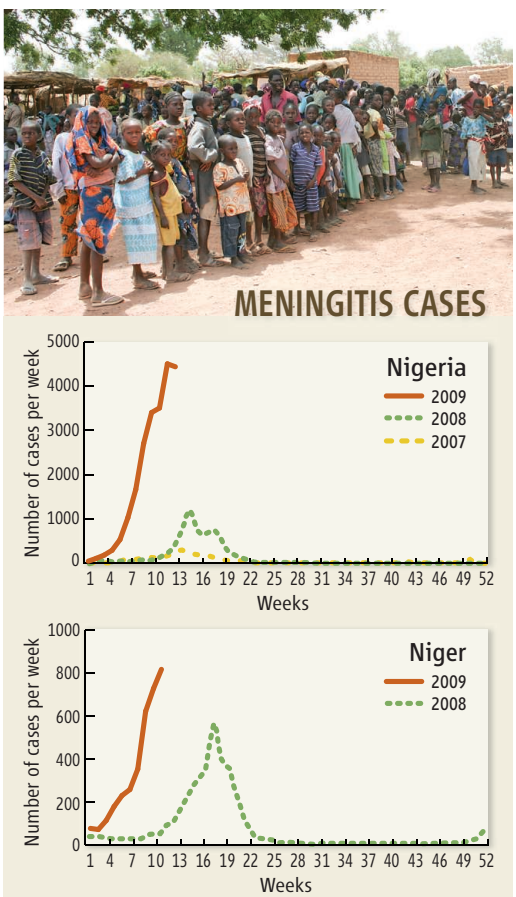

Straight line. Bacterial meningitis hit early and hard in Nigeria and Niger in 2009. Mass vaccination campaigns, like the one above in Burkina Faso in 2008, are launched after an epidemic has begun.

CREDITS: (SOURCE) WHO/MDSC; (IMAGE) MONIQUE BERLIER/MENINGITIS VACCINE PROJECT

Published by AAAS


Creationists gain some ground in Texas
25
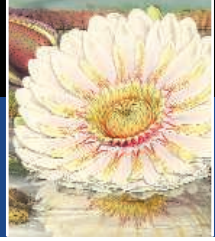
Darwin's "abominable mystery"
28
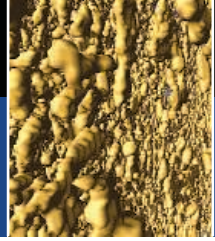
The mathematics of sea ice
32

Perea and Hugonnet: to densely populated areas where the epidemic is still on the rise or is expected to hit hard. If the epidemic is already waning, "it's a waste of resources," says Perea. "Unfortunately, countries don't always follow our epidemiologic recommendations." Nigeria, for instance, has been distributing the vaccine evenly among all states, "even if it is not needed." It's a tough call, he says. "Can you imagine being a minister of health of one of the states trying to explain that the curve is going down and they don't need vaccination?"

The rising toll is especially frustrating to LaForce of MVP, a partnership of the nonprofit PATH and WHO, because their inexpensive long-lasting conjugate vaccine designed to prevent such epidemics is almost ready (*Science*, 27 June 2008, p. 1710). Plans are being readied to vaccinate 5 million people, roughly half the vulnerable population, in Burkina Faso later this year; by then sufficient vaccine should be ready for a phased 6-year roll out across the rest of the meningitis belt. Citing the financial crisis, last year the GAVI Alliance, which was expected to fund the entire $370 million introduction package, provided just $29 million for 2009–10, as well as $55 million for the emergency stockpile. GAVI's decision was "very surprising" and "very, very frustrating," says Perea. "It is not clear what will happen in 2 years."

Meanwhile, Kader Konde, who directs WHO's Multi-Disease Surveillance Center in Burkina Faso, worries that there will not be enough of the emergency vaccine to get through this season. By week 11, ICG's emergency stockpile was down to 10 million doses. (Manufacturers held another 6 million.) Perea thinks they will squeak by. But if the stockpile drops too low and the epidemic doesn't wane, he says, "we are ready to consider the use of fractional doses. We are developing contingency plans."

–LESLIE ROBERTS

EPIDEMIOLOGY

Children's Study Exhibits Healthy Appetite

Perhaps the most ambitious long-term health study ever planned by the National Institutes of Health (NIH) has been hit by a NASA-style price shock: Once estimated at $3 billion over 25 years, the actual cost could be twice that much. The problem became public last week at a Capitol Hill hearing on the NIH budget. Acting NIH Director Raynard Kington said he has launched a high-level review of the plan to track the health of 100,000 children from before birth to age 21 and that the study will likely be scaled back.

The National Children's Study (NCS) grew out of a 2000 congressional directive to NIH to determine how environmental influences, from chemical contaminants to video games, shape the development of children and affect diseases such as autism and obesity. Researchers plan to recruit a diverse group of pregnant mothers at 105 sites around the United States by knocking on randomly selected doors (*Science*, 10 December 2004, p. 1883). Congress provided $192 million in funding this year to set up the sites and launch a pilot study.

Kington says he became concerned in early January, after Duane Alexander, director of the National Institute of Child Health and Human Development, which runs the NCS, told Kington's office of his staff's latest cost projections. They ranged from a low of $3.4 billion—well over a previous $2.7 billion price tag—to a high of $6 billion, depending on how many of the 28 hypotheses explored in the pilot phase are retained in the full study. Kington says he realized that "there was a fundamental problem in estimating the true costs."

Kington says he has now added "greatly heightened oversight." That includes asking Claude Lenfant, who retired as director of the National Heart, Lung, and Blood Institute 6 years ago, to return to NIH as his adviser on the study. "Obviously, [Lenfant] has incredible experience" overseeing large studies such as the Framingham Heart Study and the Women's Health Initiative, Kington notes. NIH will also take a longer pause than originally planned after the 1-year pilot, which began in January at two of seven sites, to revise the protocol and reassess the costs. The final protocol will be sent for review to a National Research Council panel that reviewed the study plan last year and, as it happens, urged a longer delay (*Science*, 30 May 2008, p. 1147).

Growing pains. NIH is struggling to control the cost of its plan to follow the health of 100,000 babies to age 21.

When trimming begins, Kington says he hopes the 100,000 sample size will be "the last thing" considered for cuts. But the size, number of hypotheses, and the protocols are all on the table. Pediatrician Philip Landrigan of Mount Sinai Medical Center in New York City, who helped conceive the NCS, hopes not to lose components such as in-home detailed assessments of each child's development, which are expensive. "We're just waiting to see how this works out," says Landrigan, whose team has knocked on more than 1000 doors in Queens and found that many women seem interested.

The budget problems come as no surprise to former NIH Director Elias Zerhouni, who wanted to zero out funding for the NCS. Zerhouni says he had "severe reservations" about the potential cost and felt NIH should complete the pilot before any decisions were made about proceeding with the full study. Instead, "Congress interfered" by providing the money to move ahead anyway. "It was political management," Zerhouni says, and "I don't think people should be shocked" at the result.

–JOCELYN KAISER

CREDIT: GEORGE DOYLE/STOCKBYTE/GETTY IMAGES

NEUROSCIENCE

Sleeping to Reset Overstimulated Synapses

The purpose of sleep is one of the toughest puzzles in biology. Some scientists think animals slumber primarily to save energy. Others have proposed that sleep has special relevance for learning and memory. A newer hypothesis borrows from both ideas, suggesting that sleep dials down synapses that have been cranked up by a day's worth of neural activity. Because stronger synapses use more energy and take up more space, the thinking goes, this synaptic cooldown helps conserve both energy and precious real estate in the brain. It also ensures that synapses don't max out and lose the ability to grow stronger if they're called upon to encode some new experience into memory the next day.

In this week's issue, two studies with fruit flies provide what some researchers say is the most compelling evidence to date for this provocative hypothesis. One finds that levels of several synaptic proteins increase during wakefulness and decline during sleep; the other finds a similar rise and fall in synapse number. "Together, these findings very clearly demonstrate that one major function of sleep is to reduce, on a structural level, synaptic connectivity in the brain," says Jan Born, a neuroscientist who studies sleep at the University of Lübeck in Germany and was not involved with either study.

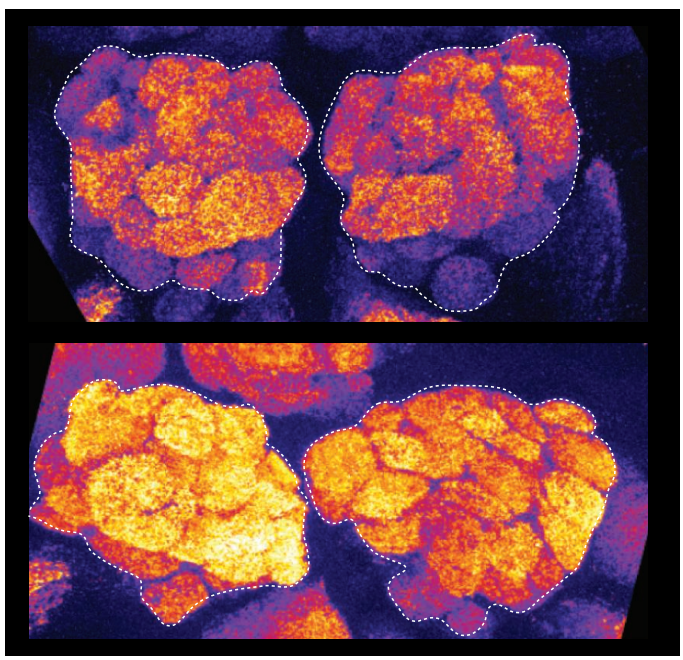

Sleepless synapses. After 16 hours without sleep (bottom panel), synaptic protein levels increase (indicated by warm colors) in the fruit fly brain.

CREDIT: G. GILESTRO *ET AL.*, *SCIENCE*

The so-called synaptic homeostasis hypothesis was first proposed about 5 years ago by neuroscientists Giulio Tononi and Chiara Cirelli at the University of Wisconsin, Madison. The idea had intuitive appeal and elegant simplicity but sparse experimental evidence. Since then, support has come from studies with rodents and people—and now, flies.

On page 109, Cirelli, Tononi, and postdoc Giorgio Gilestro report that depriving flies of sleep, either by periodically shaking the vials they call home or by forcing individual male flies to cohabitate with an unwelcome stranger (a male from another fly strain), resulted in higher levels of several synaptic proteins throughout the brain. Levels of these proteins, which included components of the transmitting and receiving sides of the synapse as well as proteins involved in neurotransmitter release, declined after flies had a chance to sleep. This pattern held up even when flies slept at odd hours, confirming that the proteins fluctuate with the sleep-wake cycle, not the time of day.

The second paper, on page 105, describes changes in synapse number during sleep. But the experiments weren't conceived as a direct test of the synaptic homeostasis hypothesis, says senior author Paul Shaw of Washington University in St. Louis, Missouri. Instead, the goal was to investigate how daytime activities influence subsequent sleep. Shaw's lab had previously found that flies sleep longer after social stimulation—either a fruit fly party in a vial or "courtship conditioning," in which a male fly learns the futility of trying to mate with another male doused with female pheromones (*Science*, 22 September 2006, p. 1775).

The main goal of the new study, led by Shaw's graduate student Jeffrey Donlea, was to investigate how these daytime experiences affect the sleep of mutant flies. The researchers found that disrupting any one of three genes, including *period*, an integral component of the circadian clock, prevented flies from sleeping longer after a socially stimulating day. Restoring the genes in just 16 so-called ventral lateral neurons—out of some 200,000 neurons in the fly brain—was enough to restore increased sleep after social enrichment.

These findings provide an intriguing link between two major regulators of sleep, Cirelli says. The circadian clock tells animals when to sleep, she explains, but the duration of sleep depends on how long they've been awake and what they've done during that time. The new findings suggest that some of the same cells and genes involved in regulating the circadian clock may also be involved in sensing sleep need.

In the same paper, Donlea and colleagues also report findings that seem to support the synaptic homeostasis hypothesis: They found that the same social experiences that increase the need for sleep also increase the number of synapses between lateral ventral neurons and their partners in the brainstem. After sleep, synapse numbers had declined.

Together, the two papers provide compelling evidence for synaptic downscaling during sleep, says Robert Stickgold, a neuroscientist at Harvard University who was initially skeptical of Tononi and Cirelli's hypothesis. Even so, Stickgold thinks it's unlikely that downscaling happens only during sleep or that synaptic strengthening is limited to waking hours. Human and rodent studies have suggested, for example, that sleep may be important for consolidating newly formed memories (*Science*, 9 March 2007, p. 1360), a process that's widely assumed to depend on strengthening synapses.

And in a 12 February *Neuron* paper, neuroscientist Marcos Frank and colleagues at the University of Pennsylvania reported that synaptic communication between neurons in the visual cortex of cats can grow stronger during sleep. Such findings "raise the question of whether downscaling is *all* that sleep can do to synapses," Frank says.

The apparently contradictory findings may just mean that the sleeping brain is multitasking, says Born. He suggests that an overall decrease in synaptic strength could help conserve space and energy in the brain, while at the same time synapses in specific neural circuits could be strengthened to reinforce newly encoded memories. **–GREG MILLER**

Published by AAAS

CREDIT: D. NORMILE/SCIENCE

Leftovers. Astronomer Yoshinori Yonekura plans to view the stars with retrofitted satellite dishes.

ASTRONOMY

Recycling, the Radio-Astronomical Way

TAKAHAGI, JAPAN—Two giant radio antennas on a hill above this small town may be an unlikely symbol of civic pride. But they are a reminder that the hardscrabble rural area 140 kilometers north of Tokyo was once at the telecommunications vanguard. The dishes are all that remains of Japan's first satellite receiving station. It went online 23 November 1963, just in time to carry live news reports of John F. Kennedy's assassination the previous day. When the telecom company shifted to optical fiber cables in 2007 and shuttered the station, local people sought a way to preserve their modest connection with history. As a result, the dishes are being reborn as radio telescopes for nearby Ibaraki University, to link into the formidable very long baseline interferometry (VLBI) array run by the National Astronomical Observatory of Japan (NAOJ) and as tools for stand-alone observations.

The antennas here are not the first telecom dishes to get a second, scientific lease on life, nor will they be the last. The next hand-me-down antenna due to come online is in Peru, where the Instituto Geofisico del Peru (IGP) in Lima is converting a 32-meter telecom antenna at Huancayo, in the country's central highlands. It's the latest example of the enthusiasm for radio-astronomical recycling. As optical fiber cables supplant more dishes around the world, more universities and observatories might take advantage of a low-cost opportunity to commence or expand observations.

The refurbished instruments are limited in the frequencies they can observe, and that causes some controversy. Makoto Miyoshi, a radio astronomer at NAOJ, thinks Japan's labor power and financial resources should be dedicated to cutting-edge science. "I feel that there are too many radio telescopes in Japan," he says. Hideyuki Kobayashi, another NAOJ radio astronomer, admits that 30-meter-class antennas are "banal." But he notes that competition for limited observing time on more powerful instruments is intense. For a small university, an antenna can attract students, involve the community, and yield important results if research is carefully targeted. And for a developing country with few observational instruments, like Peru, an old radio antenna provides entry into astrophysical research and future regional VLBI projects, says Jose Ishitsuka, an astronomer heading the IGP project.

Radio astronomers are scavengers par excellence. Almost from the inception of NASA's Deep Space Network in the late 1950s, many of its antennas used for satellite tracking and communications have been available on occasion for radio astronomy. Over the years, NASA donated a number of older antennas to observatories. In Japan, three universities took over government antennas that previously used VLBI techniques to track crustal deformations in the earthquake-prone country.

Outmoded telecom antennas are the latest boon. In 1995, the University of Tasmania, Hobart, in Australia, acquired a 30-meter telecom dish in Ceduna, a town on Australia's southern coast about 850 kilometers west of Adelaide, and converted it into a radio telescope. In Japan in 2001, KDDI, an international phone service provider, donated a 32-meter antenna at its earth station in western Yamaguchi Prefecture to NAOJ, with management granted to Yamaguchi University. Then several years ago, KDDI started shutting down Ibaraki Earth Station and offered the two dishes to NAOJ and Ibaraki University. "We recognized [the antennas] would have a big impact on radio astronomy in Japan," says Ibaraki radio astronomer Munetake Momose.

The gifts require some renovation. For starters, the frequencies often need to be retuned. Ibaraki University must address another challenge: Although the dishes move, they were designed to point at geostationary satellites. The Ibaraki team must install a star-tracking system, data recorders, and other electronics. If all goes smoothly, they will begin observations in the spring of 2010—at a bargain price. Refitting the Ibaraki antennas will cost about $1.2 million. Building two new 32-meter antennas would have run roughly $44 million, says NAOJ's Kobayashi. Conversion "is a nice business, isn't it?" he asks.

The deal gets sweeter after factoring in the scientific rewards. The Ceduna radio telescope extended the east-west spread, or baseline, of the five-station Australian Long Baseline Array, resulting in higher quality images of active galactic nuclei, pulsars and masers, says Simon Ellingsen, a radio astronomer at University of Tasmania. As a standalone telescope, it has carved a niche by making extended observations of radio sources that vary greatly over hours or months. "The monitoring is yielding many new insights and puzzles in relation to radio variability," says Ellingsen. Among other things, the observations are helping sort out whether the sources are truly variable or if radio emissions are modulated by the interstellar medium near Earth.

In Japan, the Takahagi antennas will join seven others used to occasionally bolster the dedicated four-antenna VLBI Exploration of Radio Astrometry network. Training a denser array on a celestial object produces "a very clear image," says Kobayashi. The Yamaguchi telescope is also concentrating on long-term observations; it has detected curious variability in radio emissions from Cepheus A, a well-known star-forming region, says Kenta Fujisawa, who heads Yamaguchi's radio-astronomy efforts.

Yamaguchi University has also used its antenna to build community relations. Each year, Fujisawa gives 10 or so public lectures at which attendees can remotely operate the dish for real-time observations. Yamaguchi Prefecture "has astronomy as a part of its culture now," he says—not to mention a stellar commitment to recycling.

–DENNIS NORMILE

Published by AAAS

A big hit. Nancy Pelosi lights up a crowd that includes, from right, representatives Bart Gordon and Rush Holt, NSF Director Arden Bement, and science lobbyist Sam Rankin.

CREDIT: DAVE SCAVONE PHOTOGRAPHY

NEWSMAKER INTERVIEW

Nancy Pelosi: Foursquare for Science

As speaker of the House, Representative Nancy Pelosi (D–CA) provokes strong reactions. Republicans like to energize the party faithful by pinning her name to Democratic policies they oppose. But as far as most U.S. scientists are concerned, Pelosi can do no wrong as the leader of congressional Democrats.

Last week, at three events held within an 8-hour span on a single day in Washington, D.C., the community paid tribute to Pelosi's successful advocacy of bigger research budgets and, more broadly, the importance of supporting innovation in a time of economic turmoil. In turn, Pelosi told scientists they need to work even harder to sustain the gains made in the recent stimulus package, the 2009 spending bill, and the president's budget request for 2010 (*Science*, 6 March, p. 1274).

The host groups—the Task Force on the Future of American Innovation, the Coalition for National Science Funding (CNSF), and Research!America—delivered the same message at all three gatherings: Thank you for all that you've done for science, and keep up the good work. "We talked about the importance of steady and uninterrupted increases that at least keep up with inflation," said Robert Berdahl, president of the Association of American Universities in Washington, D.C., who attended the task force event. "We wanted to thank the speaker … and to say that we wanted to be able to keep thanking her."

Pelosi—who became the first woman speaker after Democrats captured the House of Representatives in November 2006—returned the favor, praising the scientific societies, university presidents, and industry leaders for their lobbying and reminding them that their work is far from over. "None of what we were able to do would have been possible without the mobilization of the outside scientific community," she told the CNSF gathering. A few hours later, as she accepted the founder's award from Research!America, she told the assembled biomedical bigwigs that "we need your help again to make President Obama's executive order on stem cell research the law of the land." The public is behind you, she assured both groups. "Every place I go, no matter what the audience, every time I say science, science, science, science—and I say it everywhere—the room bursts out in applause."

Donning her mantle as party leader, she used the events to take a swipe at the Bush Administration. "For a long time, science had not been in the forefront. It was faith or science, take your pick. Now we're saying that science is the answer to our prayers."

In the course of her "science day," Pelosi agreed to field a few questions from *Science*. Here are her answers. **–JEFFREY MERVIS**

Q: Are you worried that pressure to reduce the budget deficit will ultimately force Congress to trim the president's 2010 request for science?

N.P.: If we make these investments in science, we will be able to remain leaders of innovation and stay number one in global competitiveness. For example, we will be able to improve health care. And that's the biggest way to reduce the cost of many entitlement programs. It will also help us become energy independent. So these investments will actually help us lower the deficit.

Q: Do you favor making foreign students with newly minted Ph.D.s from U.S. universities eligible for green cards?

N.P.: Yes, I'm for that—we want to staple a green card to those diplomas. And I think we have a chance to do it as part of a comprehensive immigration reform bill. But not on its own.

Q: You've talked about the importance of international benchmarking. Do we need a system of national standards in math and science, rather than the current patchwork system across all 50 states?

N.P.: We need to take a look at that. I have a great deal of confidence in two people—Congressman George Miller [D–CA], who's chairman of the education committee, and Bart Gordon [D–TN], who's chairman of the science committee. One of the reasons we were able to move some of our initiatives on science education so quickly was because George, who also has jurisdiction over higher education, said to Bart, "You just take the ball and run with it." So between the two of them, I have confidence that they will be able to come up with something useful.

Q: Why has it been so hard to attract and retain minorities in math and science?

N.P.: One of the things we did in the [stimulus] package was to recognize that many of our historically black colleges and Hispanic-serving institutions have not been receiving the grants and whatever else they need because they don't have the facilities. So we tried to make them eligible for more funds, to build the facilities that will attract the scientists who will apply for the grants. And their success will attract students, which will lead to excellence. We've also talked to NIH and other agencies about the importance of getting scientists to address the health disparities in our country. But it's a real challenge.

Q: Will this Congress approve a permanent R&D tax credit for industry?

N.P.: Yes, I hope so. But we want it permanent, and we want it modernized.

Published by AAAS

SCIENCE EDUCATION

New Texas Standards Question Evolution, Fossil Record

New science standards for Texas schools strike a major blow to the teaching of evolution, say scientists and educators who last week tried unsuccessfully to block the adoption of last-minute amendments aimed at providing an opening for the teaching of creationism. The standards incorporate talking points from the intelligent design literature, including doubt that the fossil record provides convincing evidence of evolution. Supporters of the new standards, who prevailed on 27 March by a vote of 13 to 2, say the next step will be to press publishers to modify biology textbooks.

"I think the new standards are wonderful," says Don McLeroy, chair of the Texas Board of Education and a dentist who claims that "dogmatism about evolution" has sapped "America's scientific soul." McLeroy believes that biology texts, to meet the new standards, should include "an evaluation of the sudden appearance of fossils" and "an explanation of stasis or how certain organisms stay the same over time." He also wants the textbooks to declare there is no "scientific explanation for the origin of life" and that "unguided natural processes cannot account for the complexity of the cell."

CREDIT: HARRY CABLUCK/AP PHOTO

Dogged. Texas school board chair Don McLeroy and member Gail Lowe supported textbook language questioning evolution.

McLeroy is anticipating the state's adoption in 2 years of new biology textbooks. Because Texas is the second-largest textbook market in the United States, publishers have a strong incentive to be certified by the board as "conforming 100% to the state's standards," says Dan Quinn of the Texas Freedom Network in Austin, which has campaigned to keep creationism out of the science classroom. Quinn cited the example of a high school textbook on health education that was stripped of anatomical line drawings and references to sexuality and contraceptives before it was submitted for board approval in 2004.

Quinn and his colleagues thought they had won a major victory earlier in the 3-day meeting when the board voted to strike from the existing standards the requirement that teachers present the "strengths and weaknesses" of evolutionary theory. But the next day, conservatives won support for a similar phrase that calls on teachers to "analyze, evaluate, and critique scientific explanations in all fields of science by using empirical evidence, logical reasoning, and experimental and observational testing, including examining all sides of scientific evidence of those scientific explanations so as to encourage critical thinking by the student."

The new language covers two hot-button topics. Teachers will now be required to have their students "analyze and evaluate scientific explanations concerning the complexity of the cell" and "analyze and evaluate the evidence regarding formation of simple organic molecules and their organization into long complex molecules having information such as the DNA molecule for self-replicating life." Students will also be expected to "analyze and evaluate a variety of fossil types such as transitional fossils, proposed transitional fossils, significant fossil deposits with regard to their appearance, completeness, and alignments with scientific explanations in light of this fossil data."

The creationists were "dogged," says Eugenie Scott of the National Center for Science Education in Oakland, California. "It was like you put the stake in the heart of the vampire and it comes back." Moderates on the board may have failed to recognize the final amendments as intelligent design talking points, she added, because they were focused on the "strengths and weaknesses" clause.

–YUDHIJIT BHATTACHARJEE

*Science*Insider

From the *Science* Policy Blog

In Bonn, Germany, international negotiators to the U.N. **climate change** treaty began work this week on a successor to the Kyoto Accords, an effort they hope to finish by December in Copenhagen. "My team and I came here determined to make up for lost time," top U.S. negotiator Todd Stern told delegates. The United States also hopes to hold bilateral talks with the 15 or so biggest emitters around the world. Meanwhile, stateside, a key draft of climate legislation was released this week in the House of Representatives by Edward Markey (D–MA) and Henry Waxman (D–CA).

British scientists and biomedical institutions have rallied to oppose portions of a new European Union **animal-experimentation law**. Animal-rights advocates have pushed the E.U. law, which would create new ethical reviews and tougher minimum housing and care requirements. British scientists told *Science*Insider that they fear the new regime will create a mountain of paperwork.

The U.S. National Institutes of Health (NIH) announced that $60 million of the $10 billion it has received as part of the stimulus package for spending to boost the economy will be set aside for a competition on **autism research**. In 2008, NIH spent $118 million on the disease, so that's a big increase. Most of the rest of the stimulus funds will be spent on proposals already in the hopper, but National Institute of Mental Health Director Thomas Insel says he hopes that the autism funding can be distributed in the next 18 months if proposals are good.

Elsewhere … The blog offered regular updates on the Texas vote on science standards related to the **teaching of evolution** (left). It chronicled difficulties among the **Irish science** community to justify current funding in hard economic times and a new database of **Japanese research**. And it noted the frustration of some environmentalists that the Obama Administration, despite its green reputation, didn't endorse **Earth Hour**, an international effort to turn off the lights from 8:30 p.m. to 9:30 p.m. on 28 March.

For the full postings and more, go to **blogs.sciencemag.org/scienceinsider**.

Published by AAAS

CELL BIOLOGY

Overcoming Opposition, Brazil Banks on Stem Cells

SÃO PAULO, BRAZIL—Despite vocal opposition from religious groups, the Brazilian government has launched a major initiative in pluripotent stem cell research. In the past 3 weeks, eight university labs in four states started receiving the first payments of a 3-year, $9.3 million grant intended to reshape them into Cell Technology Centers.

The largest chunk, $2 million, will establish a National Laboratory for Human Embryonic Cells (LaNCE), split between the Federal University of Rio de Janeiro (UFRJ) and the University of São Paulo (USP). Run by Brazilian stem cell powerhouses Stevens Rehen in Rio and Lygia Pereira in São Paulo, the lab will create a national stem cell bank to supply lines of existing and newly derived human embryonic stem (hES) cells and induced pluripotent stem (iPS) cells to Brazilian researchers by early 2010.

In a predominantly Catholic country, the new stem cell initiative has not come easily. In 2005, Brazil's Congress passed the Biosafety Act, which allows the extraction of stem cells from surplus or nonviable human embryos stored for 3 years or more at in vitro fertilization clinics. But Catholic groups immediately challenged the legislation, claiming that embryos should have a constitutional right to life. A coalition of scientific groups, including the Brazilian Society for the Advancement of Science, and patients' advocacy organizations fought back. In May 2008, the Supreme Federal Court upheld the act.

Leading the stem cell cause was Mayana Zatz, who works on muscular dystrophies at USP. Together with patients' groups, she helped fill the Supreme Federal Court galleries with people in wheelchairs and their relatives. Eduardo Campos, then the minister of science and technology, also got involved.

The Department of Science and Technology within the Ministry of Health has identified stem cell research as one of its priorities. Since 2005, the ministry has spent $24.7 million—about one-tenth of its biomedical research budget—on stem cell research, funding some 40 labs. In October of last year, it selected eight labs to become Cell Technology Centers. LaNCE is the only center devoted exclusively to pluripotent stem cells, both hES and iPS.

So far, the government's investment has paid off with several key advances. In March 2008, Rehen's group succeeded in scaling up the culture of hES cells in bioreactors, spinning jars in which cells are grown attached to tiny beads while being continuously bathed in cell growth medium. Currently, most hES cells are cultured in tissue plates, a process that must be repeated many times over.

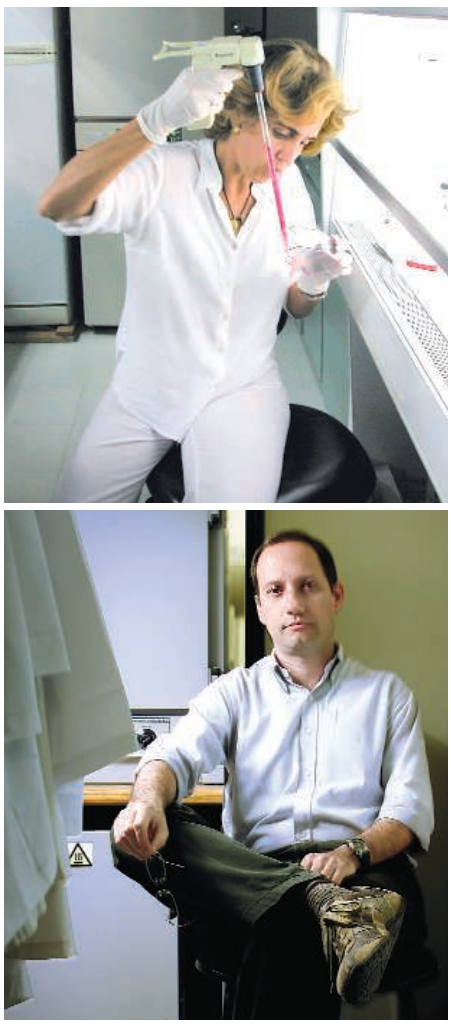

Leading lights. Lygia Pereira and Stevens Rehen are guiding efforts to create a national stem cell bank in Brazil.

"Large-scale culture of hES cells is necessary for any country that has a hES cell bank," says Jeanne Loring of the Center for Regenerative Medicine at the Scripps Research Institute in San Diego, California. "This is the first South American group to my knowledge that has achieved this, and given the short time frame in which hESC research has been supported in Brazil, this is an achievement that Stevens should be proud of."

"It was kind of obvious to try bioreactors in scaling up the production of stem cells," says Rehen, who adds that "our system was 100% developed in Brazil, although adapting already available techniques." The system, which was developed in collaboration with UFRJ chemical engineer Leda Castilho, has already boosted production more than 70-fold at half the cost of plate cultures.

Seven months after Rehen's feat, in October 2008, Pereira in São Paulo derived the first hES cell line in Brazil, branded BR-1, from surplus embryos. Since then, her lab has differentiated these cells into muscle, neuronal, and pancreatic tissues.

Rehen's lab followed that last January with the first derivation in Brazil of iPS cells. Like hES cells, iPS cells have the potential to differentiate into all body tissues but can be made without the controversial step of producing and subsequently destroying embryos. Rehen used a modification of the protocol developed by Shinya Yamanaka at the University of Kyoto in Japan, who induced differentiated cells into a pluripotent state by inserting four genes.

With the $2 million in funding for LaNCE, Pereira will keep deriving hES cell lines from surplus embryos in her São Paulo lab, while Rehen will mass-produce them in Rio. They are also committed to training Brazilian investigators on hES cell techniques free of charge.

By the beginning of 2010, they hope to have the capacity to produce 30 million pluripotent cells a month, certified free of chromosomal abnormalities and mycoplasm contamination. LaNCE plans to double the production after 450 square meters of refitted lab space become available.

"If this works, it will be fantastic," says stem cell researcher Zatz. "We do need specialized core facilities like those available in the U.S. and Europe, providing research goods for labs all over the country. But we also need steady long-term financing. Three years is not nearly enough."

Reaction from outside the country has been enthusiastic. "I truly applaud the Brazilian government for their investment in stem cell technology," says Marie Csete, chief scientific officer at the California Institute for Regenerative Medicine in San Francisco. She and Loring would like to see the group derive iPS cell lines from the many ethnically diverse populations in Brazil to test whether drugs work the same way in different groups. In addition, she says, "iPS cells from patients in Brazil can be used to establish 'disease in a dish' models that will be available to screen drugs from the novel drug libraries in [their] country." **–MARCELO LEITE**

Marcelo Leite is a writer in São Paulo, Brazil.

CREDITS (TOP TO BOTTOM): COURTESY OF LYGIA V. PEREIRA; DARYAN DORNELLES/*REVISTA ÉPOCA*

Published by AAAS

SCIENCE CAREERS

Support for Tenure-Track Jobs in Biomedical Sciences

Many universities have cut back on hiring during the recession, making faculty openings scarcer than usual. To offset the chill, the U.S. National Institutes of Health (NIH) has announced a plan that it hopes will create up to 117 new tenure-track positions for young scientists starting this fall. "We heard about spectacular postdocs having trouble finding positions because there were so many searches being canceled," says Jeremy Berg, director of the National Institute of General Medical Sciences, one of 14 centers and institutes receiving applications. The awards will provide lab start-up packages for 2 years, funded out of NIH's $10.4 billion share of the stimulus bill.

The P30 mechanism used for the competitive grant program—labeled "Biomedical Research Core Centers to Enhance Research Resources"—is, Berg admits, "unfortunately a bit obscure." But it's in place. Devising a new mechanism, he says, would have taken too long to permit two full years of support within the recovery act's time frame—the money must be spent by the end of fiscal 2010. Confusion about the program proved to be so great that on 27 March—3 days after the announcement was issued—NIH took it down, promising to post a new notice soon. "It's just [a matter of] clarifying the language," Berg says.

The $100 million program, Berg admits, is "not a huge part of the stimulus package." Its modest size, he says, reflects an effort to avoid the problems that followed the end of NIH's budget doubling in 2003, when universities could not sustain all the jobs they had created.

"Our challenge was to find something that was going to restart searches without creating a feeding frenzy," Berg says, "a level that's sufficient to be helpful but not sufficient to cause institutions to create positions that they can't really support in the long run." In selecting winners, he adds, NIH will be looking for evidence of institutional commitment to continuing the new positions after the awards expire.

A slowdown in faculty retirements, coupled with tight state budgets and endowment losses, has led to a decline in the number of entry-level faculty positions available, administrators say. Rather than delay recruitment and lose a cohort of talented researchers, says Berg, NIH leaders want "to get things moving now."

The prospect of support for start-up packages this fall is likely to spark renewed hiring, according to Jennifer Preece, dean of the College of Information Studies at the University of Maryland, College Park—one of the universities that canceled searches this year. She says the program could help get new positions authorized. "If the decision is available by September," she says, "the provost would be more likely to allow us to hire for next year."

–BERYL LIEFF BENDERLY

Beryl Lieff Benderly is a columnist for ScienceCareers.org.

From *Science*'s Online Daily News Site

Power walking. Researchers have developed an extremely tiny generator that can produce electricity from the mechanical energy produced when our bodies move. The device, described at the American Chemical Society's National Meeting in Salt Lake City, relies on flexible zinc oxide nanowires sprouting like bristles from a metal electrode and sandwiched inside a rigid polymer binding. When pressed, the polymer bends the zinc oxide filaments, which generate an electrical current through a process known as the piezoelectric effect. With further development, the nanogenerator could allow people to power personal electronic devices from the physical exertions of a day at the office.

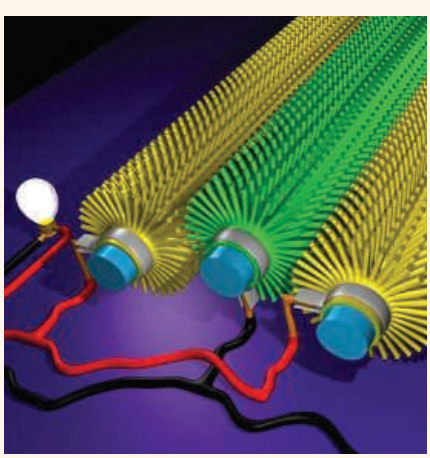

Preferences ↔ choices. Economists generally assume that people make choices based on their preferences. And we do. But psychologists have long argued that the relationship goes both ways. Just as our preferences influence our choices, so too can choices influence preferences. A new study published online last week in *The Journal of Neuroscience* backs both sides in the debate and identifies a component of the brain's reward circuitry that seems to keep track of changing preferences.

Sharp-eyed shooters. Video games, long maligned for promoting violence, may also have a good side: improving eyesight. Gory "first-person shooter" games, in which players must act quickly to kill their virtual opponents, seem to have lasting effects on a key aspect of vision called contrast sensitivity. A new study published by *Nature Neuroscience* indicates that gamers have an increased ability to detect objects in dim lighting or against a busy background.

ScienceNOW.org

Flying on fish oil. Athletes aren't the only ones who improve their performance by doping. On its 3000-km trek from its summer home in the Canadian Arctic to the South American coast, the tiny sandpiper stops off at the Bay of Fundy to gorge on mud shrimp, 1-cm-long crustaceans loaded with omega-3 fatty acids. To test whether the fatty acids alone could improve avian fitness, a team of scientists fed 40 quails, a sedentary species, a combination of omega-3 fatty acids from fish oil. To the researchers' surprise, the quail's oxidative capacity—their muscles' efficiency at using fuel—shot up 58% to 90%, they reported online last week in *The Journal of Experimental Biology*. Human endurance athletes might not enjoy the same natural doping effect, however: They metabolize less fat than do their feathered counterparts.

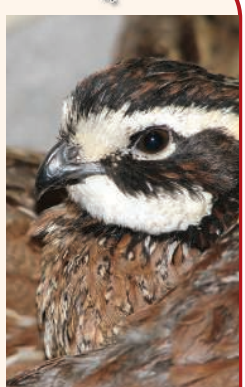

Read the full postings, comments, and more on **sciencenow.sciencemag.org**.

CREDITS (TOP TO BOTTOM): JEAN-MICHEL WEBER; Z. L. WANG AND X. D. WANG/GEORGIA INSTITUTE OF TECHNOLOGY

Published by AAAS

On the Origin of Flowering Plants

IN 1879, CHARLES DARWIN PENNED A LETTER to British botanist Joseph Dalton Hooker, lamenting an "abominable mystery" that threw a wrench into his theory of evolution: How did flowering plants diversify and spread so rapidly across the globe? From rice paddies to orange groves, alpine meadows to formal gardens, prairies to oak-hickory forests, the 300,000 species of angiosperms alive today shape most terrestrial landscapes and much of human life and culture. Their blooms color and scent our world; their fruits, roots, and seeds feed us; and their biomass provides clothing, building materials, and fuel. And yet this takeover, which took place about 100 million years ago, apparently happened in a blink of geological time, just a few tens of millions of years.

The father of evolution couldn't quite fathom it. Darwin had an "abhorrence that evolution could be both rapid and potentially even saltational," writes William Friedman in the January *American Journal of Botany*, which is devoted to this "abominable mystery." Throughout his life, Darwin pestered botanists for their thoughts on the matter, but they couldn't give him much help.

Now, 130 years later, evolutionary biologists are still pestering botanists for clues about what has made this plant group so successful, as well as when, where, and how flowers got started—and from which ancestor. Today, researchers have analytical tools, fossils, genomic data, and insights that Darwin could never have imagined, all of which make these mysteries less abominable. Over the past 40 years, techniques for assessing the relationships between organisms have greatly improved, and gene sequences, as well as morphology, now help researchers sort out which angiosperms arose early and which arose late. New fossil finds and new ways to study them—with synchrotron radiation, for example—provide a clearer view of the detailed anatomy of ancient plants. And researchers from various fields are figuring out genomic changes that might explain the amazing success of this fast-evolving group.

These approaches have given researchers a much better sense of what early flowers were like and the relationships among them. But one of Darwin's mysteries remains: the nature and identity of the angiosperm ancestor itself. When flowering plants show up in the fossil record, they appear with a bang, with no obvious series of intermediates, as Darwin noted. Researchers still don't know which seed- and pollen-bearing organs eventually evolved into the comparable flower parts. "We're a bit mystified," says botanist Michael Donoghue of Yale University. "It doesn't appear that we can locate a close relative of the flowering plants."

Seeking the first flower

One of two major living groups of seed plants, angiosperms have "covered" seeds that develop encased in a protective tissue called a carpel (picture a bean pod). That's in contrast to the nonflowering gymnosperms, such as conifers, which bear naked seeds on scales. An angiosperm's carpel sits at the center of the flower, typically surrounded by pollen-laden stamens. In most flowers, the carpel and stamens are surrounded by petals and an outer row of leaflike sepals. Seeds have a double coating as well as endosperm, tissue surrounding the embryo that serves as its food supply.

Darwin was perplexed by the diversity of flowering plants; they were too numerous and too varied, and there were too few fossils to sort out which were more primitive. Throughout much of the 20th century, magnolia relatives with relatively large flowers were leading candidates for the most primitive living flowers, although a few researchers looked to small herbs instead.

In the late 1990s, molecular systematics came to the rescue, with several reports presenting a fairly consistent picture of the lower branches of the angiosperm tree. An obscure shrub found only in New Caledonia emerged as a crucial window to the past. *Amborella trichopoda*, with its 6-millimeter greenish-yellow flowers, lives deep in the cloud forests there. In multiple gene-based assessments, including an analysis in 2007 of 81 genes from chloroplast genomes belonging to 64 species, *Amborella* sits at the base of the angiosperm family tree, the sister group of all the rest of the angiosperms.

Given that placement, *Amborella*'s tiny flowers may hint at what early blossoms were like. It's one of "the most similar living flower[s]" to the world's first flower, says James Doyle of the University of California, Davis. The petals and sepals of its single-sex flowers are indistinguishable and vary in number; so too do the numbers of seed-producing carpels on female flowers and pollen-generating stamens on male flowers. The organs are spirally arranged, and carpels, rather than being closed by fused tissue as in roses and almost all familiar flowers, are sealed by a secretion.

Most genetic analyses showed that water lilies were the next branch up the angiosperm tree, followed by a group represented by star anise, which also has a primitive look about it, says Doyle, "though each of these has deviations from the ancestral type."

Fossil records

Although some fossil pollen dates back 135 million years, no credible earlier fossil evidence exists. In Darwin's day, and for many decades afterward, paleobotanists primarily found leaves or pollen but almost no fossil flowers. They had the wrong search image, says Else Marie Friis of the Swedish Museum of Natural History in

THE YEAR OF DARWIN

This essay is the fourth in a monthly series. For more on evolutionary topics online, see the Origins blog at **blogs.sciencemag.org/origins.** For more on flower origins, listen to a podcast by author Elizabeth Pennisi at **www.sciencemag.org/multimedia/podcast.**

Published by AAAS

Stockholm. "When we started, the search profile was bigger, a magnolia [flower]," she recalls. But 30 years ago, she and others discovered tiny ancient flowers by sieving through sand and clay sediments. With this technique, they have now collected hundreds of millimeter-size flowers, some preserved in three dimensions, from Portugal and other locations with Cretaceous deposits 70 million to 120 million years old.

This fossil diversity shows that angiosperms were thriving, with several groups well-established, by 100 million years ago. In some, the flower parts are whorled like those of modern flowers; in others they are spiraled, considered by some researchers as the more primitive arrangement. Some flower fossils have prescribed numbers of petals, another modern feature, whereas in others the petal count varies.

In 1998, Chinese geologist Ge Sun of Jilin University in Changchun, China, came across what seemed to be a much older flower. The fossil, called *Archaefructus*, was an aquatic plant that looked to be 144 million years old. By 2002, Sun and David Dilcher of the Florida Museum of Natural History (FLMNH) in Gainesville had described an entire plant, from roots to flowers, entombed on a slab of rock unearthed in Liaoning in northeastern China.

In one sense, *Archaefructus* wasn't much to look at. "It's a flowering plant before there were flowers," Dilcher notes. It lacked petals and sepals, but it did have an enclosed carpel. When Kevin Nixon and colleagues at Cornell University compared its traits with those same traits in 173 living plants, *Archaefructus* came out as a sister to living angiosperms and closer to the common ancestor than even *Amborella*.

Archaefructus's distinction was short-lived, however. Within months, better dating of the sediments in which it was found yielded younger dates, putting this first flower squarely with other early fossil flower parts, about 125 million years old. Also, a 2009 phylogenetic analysis of 67 taxa by Doyle and Peter Endress of the University of Zurich, Switzerland, placed the fossil in with water lilies rather than at the base of the angiosperms, although this conclusion is contested.

Out of the past. Tiny *Amborella* sits at the bottom of the angiosperm family tree.

CREDITS (TOP TO BOTTOM): COURTESY OF STEPHEN MCCABE, UC SANTA CRUZ; PHOTO BY JENNIFER SVITKO, COURTESY OF WILLIAM L. CREPET, CORNELL UNIVERSITY

> "We are realizing that this huge diversity is probably the result of one innovation piled on top of another innovation."
>
> —Peter Crane, University of Chicago

These fossils often spark debate because specimens tend to be imperfectly preserved and leave room for interpretation. To help remedy that, Friis and her colleagues have begun to examine flowers using synchrotron radiation to generate a 3D image of their inner structures, allowing the fossil to remain intact while Friis peers inside it from many angles (*Science*, 7 December 2007, p. 1546). "We can get fantastic resolution," says Friis. "It's really exciting." But so far, the flowers Friis finds are too diverse to trace back to a particular ancestor. "From these fossils, we cannot say what is the basic form," she says.

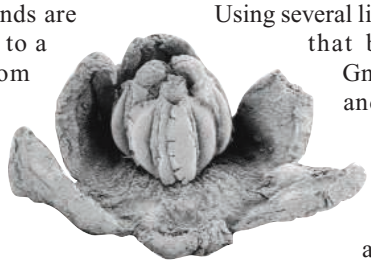

Larger than life. Although merely 2.2 millimeters in diameter, this 3D fossil flower shows that grasses date back to 94 million years ago.

Before flowers

Although they have yet to find the oldest fossil flowers, researchers assume that the ancestral angiosperm evolved from one of the nonflowering seed plants or gymnosperms, whose heyday was 200 million years ago. Modern gymnosperms include conifers, ginkgoes, and the cycads, with their stout trunks and large fronds. Before angiosperms came along, these plants were much more diverse and included cycadlike species, such as the extinct Bennettitales, and many woody plants called Gnetales, of which a few representatives, including the joint firs, survive today (see family tree, p. 31). Also common in the Jurassic were seed ferns, a group now long gone; their most famous member is *Caytonia*, which seems to have precarpel-like structures. These groups' perceived relevance to flower evolution and their relationships to angiosperms have ping-ponged between camps, depending on how the evolutionary trees were constructed.

In the mid-1980s, Peter Crane, now at the University of Chicago in Illinois, proposed a solution, the anthophyte hypothesis. Using several lines of evidence and noting that both Bennettitales and Gnetales organize their male and female organs together in what could be construed as a preflower, he considered them, along with angiosperms, as comprising a single angiosperm entity called anthophytes. For the next decade, most family trees based on morphology sup-

Published by AAAS

Flowers, food, fuel. Darwin marveled at the diversity of angiosperms. Given that they represent nine in 10 land plants, it's no surprise that they serve as mainstays of both our welfare and sense of beauty. Clockwise from left: aspens, orchids, grasses, sunflowers, tulips, apples, walnuts.

ported this idea. Crane and others carefully dissected and described fossils of these groups, looking for the precursors to carpels, the seed's double coat, and other distinctive angiosperm traits.

But they have run into problems. "We do not really know how to compare them because the structures are very different-looking; figuring out what's homologous is quite a difficult thing," says Crane. He and his colleagues argue, for example, that the seeds in the Bennettitales have two coverings, which may be a link to angiosperms. But in the January *American Journal of Botany*, Gar Rothwell of Ohio University, Athens, and two colleagues disagree, saying that what Crane calls the outer layer is the only layer, and find fault with the hypothesis in general.

To make matters worse for anthophyte proponents, gene-based evolutionary trees break up this grouping, pulling the Gnetales off any angiosperm branch and placing them among or next to the other gymnosperms. "The molecular work points in one direction; the paleobotanical work points you in another direction," Crane says.

And if the molecular work is correct, then the field doesn't know in which direction to turn, because in most analyses the genetic data don't place any living plant close to angiosperms. The angiosperms group together, the living gymnosperms group together, and there's nothing in between. "The nonangiosperm ancestor just isn't there," says paleobotanist William Crepet of Cornell. "I'm starting to worry that we will never know, that it transformed without intermediates."

Seeds of success

The angiosperm's ancestor may be missing, but what is very clear—and was quite annoying to Darwin—is that the angiosperm prototype so readily proved a winner. Seed ferns and other gymnosperms arose about 370 million years ago and dominated the planet for 250 million years. Then in a few tens of millions of years, angiosperms edged them out. Today, almost nine in 10 land plants are angiosperms.

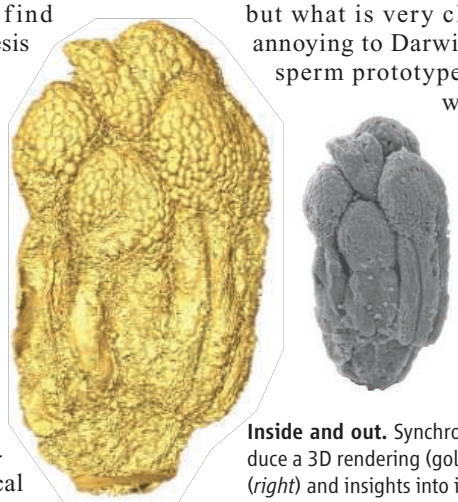

Inside and out. Synchrotron radiation helped produce a 3D rendering (gold) of this fossil male flower (*right*) and insights into its internal structure.

The exact timing of the angiosperms' explosion and expansion is under debate, as is the cause. At least one estimate based on the rate at which gene sequences change—that is, the ticking of the molecular clock—pushes angiosperm evolution back to 215 million years ago. "There appears to be a gap in the fossil record," says Donoghue, who also notes that molecular dating methods "are still in their infancy" and, thus, could be misleading. He and others think that flowering plants lingered in obscurity for tens of millions of years before radiating toward their current diversity.

Whatever the timing, there was something special about the angiosperm radiation. During the 1980s and again in 1997, Cornell's Karl Niklas compiled a database showing the first and last occurrences of fossil plants. When he and Crepet used that and more recent information to look at species' appearances and disappearances, they found that new angiosperms appeared in bursts through time, whereas other plants, such as gymnosperms, radiated rapidly only at first. Moreover, angiosperms proved less likely to disappear, somehow resisting extinction, says Crepet.

Once the angiosperms arrived, how did they diversify and spread so quickly? Darwin suspected that coevolution with insect pollinators helped drive diversification, though

such a causal relationship is not settled. Later, animals that ate fruit and dispersed seeds likely helped evolving species expand quickly into new territory. Some think the answer lies in genes: duplications that gave the angiosperm genome opportunities to try out new floral shapes, new chemical attractants, and so forth. This flexibility enabled angiosperms to exploit new niches and set them up for long-term evolutionary success. "My own view is that in the past, we have looked for one feature," says Crane. Now, "we are realizing that this huge diversity is probably the result of one innovation piled on top of another innovation."

The latest insights into diversification come from gene studies. From 2001 to 2006, Pamela Soltis of the FLMNH and Claude dePamphilis of Pennsylvania State University, University Park, participated in the Floral Genome Project, which searched for genes in 15 angiosperms. Now as a follow-up, the Ancestral Angiosperm Genome Project looks at gene activity in five early angiosperms and a cycad, a gymnosperm.

DePamphilis and his colleagues matched all the genes in each species against one another to determine the number of duplicates. They then looked at the number of differences in the sequences of each gene pair to get a sense of how long ago the duplication occurred. In most early angiosperms, including water lilies and magnolias, they saw many simultaneous duplications—but not in *Amborella*, they reported in the January 2009 *American Journal of Botany*, confirming earlier reports. The data suggest that a key genome duplication happened after the lineage leading to *Amborella* split off but before water lilies evolved. "We're beginning to get the idea that polyploidization may have been a driving force in creating many new genes that drive floral development," dePamphilis says.

Others have noted that a duplication occurred in the evolution of grasses, and the Floral Genome Project confirms that yet another duplication paved the way for eudicots, the group that includes apples, roses, beans, tomatoes, and sunflowers. "There are some real 'hot spots' in angiosperm evolutionary history," says dePamphilis, who is working to fully sequence the genome of *Amborella* with his colleagues.

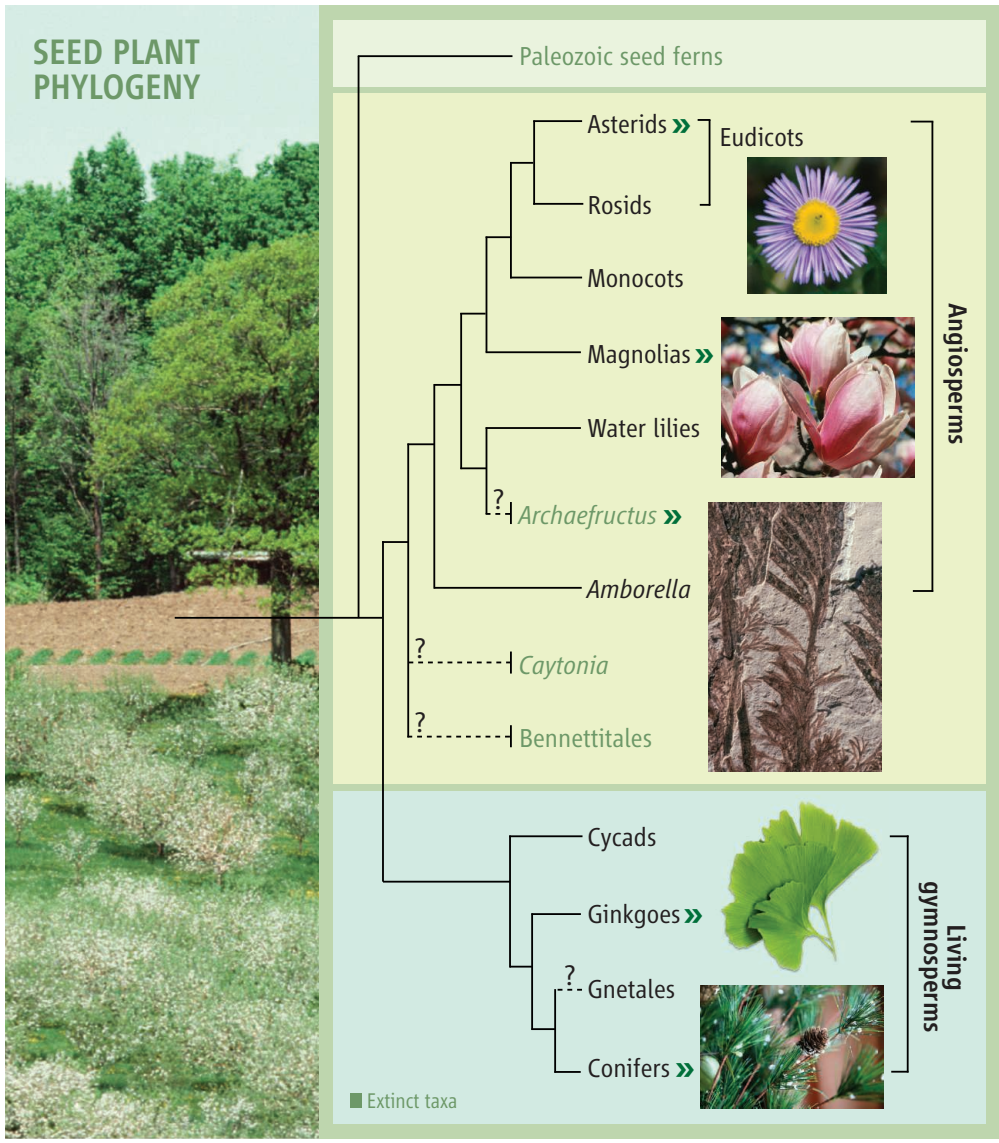

Shifting branches. As this simplified family tree shows, gene studies have helped clarify the relationships of many living angiosperms, but fitting in extinct species is still a challenge, and some nodes are hotly debated.

CREDITS: (*ARCHAEFRUCTUS* IMAGE) DAVID DILCHER; (ALL OTHER IMAGES) PHOTOS.COM

The Floral Genome Project also looked to see whether the genetic programs guiding flower development were consistent throughout the angiosperms. "We found that there are fundamental aspects that are conserved in the earliest lineages," says Soltis. "But there are differences in how the genes are deployed."

Take the avocado, a species on the lower branches of the angiosperm tree. In most angiosperms, the flower parts are arranged in concentric circles, or whorls, around the carpels, with stamens innermost, then petals, and finally sepals. Each tissue has its own distinct pattern of gene expression, but not in the avocado. Genes that in *Arabidopsis* are active only in, say, the developing petals spill over in avocado to the sepals. Thus in the more primitive plants, petals and sepals are not as well-defined as they are in *Arabidopsis*. This sloppiness may have made development flexible enough to undergo many small changes in expression patterns and functions that helped yield the great diversity in floral forms.

In his letter to Hooker, Darwin wrote that he would like "to see this whole problem solved." A decade ago, Crepet thought Darwin would have gotten his wish by now. That hasn't happened, but Crepet is optimistic that he and his colleagues are on the right track, as analyses of various kinds of data become more sophisticated. "We are less likely to go around in circles in the next 10 years," he says. "I believe a solution to the problem is within reach. … The mystery is solvable."

–ELIZABETH PENNISI

PROFILE: KEN GOLDEN

Cold Equations

Far from his cozy office in landlocked Utah, a mathematician grapples with the secrets of polar sea ice

The fire alarm woke Ken Golden up at 2:37 a.m. "My first thought was, why are they having a fire drill now?" he says. But as he walked down the hall of the *Aurora Australis* and into the frigid Antarctic night, he smelled smoke. As the 54 scientists and passengers mustered on the helicopter deck, he could see thick smoke belching out of the ship's smokestacks.

"Pretty soon I heard a muffled explosion, deep inside the ship," Golden says. "We later found out that there was a massive fireball that some of the brave crew had missed being caught in by less than 30 seconds.

"Eventually, the first mate came out to talk with us. In his Scottish accent, in a very calm and confident voice, he announced, 'Please don't be alarmed, but we have an uncontrolled fire in the engine room.' Fifteen minutes later, he came back and said, 'Please don't be alarmed, but we are lowering the lifeboats.' Right then I'm thinking: I prove theorems for a living! What have I gotten myself into? What am I doing down here?" Golden says.

What he was doing—and has continued to do in the 11 years since—was taking mathematics to places it had never been before. Golden, an applied mathematician at the University of Utah in Salt Lake City, is convinced that mathematics can answer some of the unresolved questions of climate change. As chair of the 2009 Mathematics Awareness Month (www.mathaware.org), which is happening this month and is focusing on climate change, Golden has found himself turning into a public spokesperson for this viewpoint. He has given talks about sea ice and climate change in venues that include university seminars and congressional luncheon briefings. Considering his rich trove of Antarctic and Arctic stories and the relish with which he tells them, it seems like a part he was born to play.

"Embracing the misery index, that's certainly not unique among polar scientists," says Donald Perovich of the U.S. Army Cold Regions Research and Engineering Laboratory (CRREL) in Hanover, New Hampshire. "But there's something about Ken's style. You're out there in a storm in Antarctica, or knee-deep in ice water in Barrow, and he's saying, 'Let's go and take another 200 meters of measurements.' Or 'Let's consider these variables.' Or 'I've got something I really want to show you.' That's his enthusiasm, and it's very rare."

"Ken has a boundless enthusiasm for the subject matter, and it's infectious," says Tony Worby of the Australian Antarctic Division, who was deputy voyage leader on the fire-shortened expedition in 1998 and also led a cruise in 2007 that Golden participated in. "He's very popular with the support crew. When he wanted to be out on the ice at 3 a.m. to do tracer experiments, he was never short of volunteers to help him."

An icy passion

"Enthusiasm" is a word that comes up in nearly every discussion about Golden. It starts with his zest for adrenaline-pumping adventure, from skiing to driving his 1987 Mustang GT (recently sold) to watching the Blue Angels at an air show. Golden has been a skiing buff since elementary school and moved to Utah in 1991 because, he says, "there is no place like it in the world in terms of the quality of the snow."

Golden's passion for sea ice started in 1976, when he was in his final year of high school and worked on a senior project with H. Jay Zwally of the NASA Goddard Space Flight Center in Greenbelt, Maryland. Zwally is still heavily involved in polar research, as the project scientist for NASA's ICESat mission. It was Zwally who gave Golden some of the best advice of his life: Go to Dartmouth, work with Stephen Ackley, and "learn all the mathematics that you can."

Golden traveled to Antarctica for the first time in 1980 as a field assistant for Ackley, a geophysicist who was then at CRREL. "He was looking at how sea ice behaves when you use ground-penetrating radar on it," Ackley says. "The ice is anisotropic, because it has inclusions—pockets of brine—that are conducting. Ken showed that the electromagnetic reflection looks different along the long axis of the inclusions than perpendicular to it. He published a paper in the *Journal of Geophysical Research* about this—a unique thing for an undergraduate."

As a graduate student at the Courant Institute of Mathematical Sciences in New York City, a postdoc at Rutgers University, and an assistant professor at Princeton University, Golden delved into the mathematics of composite materials. He didn't really intend to do any more research on sea ice. "It's one of those weird coincidences, though," he says. "Almost everything I got involved in turned out to be relevant for sea ice when I reentered that world in the 1990s: transport in composite materials, percolation models, diffusion processes. It's given me a leg up, in terms of how I approach these things."

Ackley invited Golden to return to the Antarctic in 1994, on an expedition called ANZFLUX. "He was probably thinking what a hoot it would be to bring an honest-

CREDIT: ADAM GULLY

Published by AAAS

Ice bound. Golden and the research vessel *Aurora Australis* on an Antarctic expedition in 2007.

CREDIT: K. GOLDEN *ET AL.*, *GEOPHYSICAL RESEARCH LETTERS*, 16 AUGUST 2007

to-goodness professor of mathematics to the Antarctic and see what they see," Golden says.

Golden's rule

If so, it worked. On that trip, Golden was struck by the Jekyll-and-Hyde nature of sea ice. When temperatures are just below freezing, the ice becomes permeable, allowing warm water to percolate up through it. Algae trapped in the ice start blooming like mad. At slightly colder temperatures, the heat flow stops and the algae shut down.

To Golden, the sudden change from impermeability to permeability (and vice versa) looked like a phase transition. He called it the "rule of fives," because it happens at about –5°C, when the brine fraction of the sea ice is about 5%. He believed that at this critical temperature and brine fraction, the isolated brine pockets connect up and form brine channels, making the ice permeable. But could he prove it? And what was the significance of 5%?

Golden remembered an old paper from 1971 about silver powder imbedded in a polymer matrix, a material developed to coat stealth airplanes. What if you replaced the polymer with ice crystals and the silver particles with brine inclusions of the right size? "I just took a ruler and measured those things, figured out the corresponding ratios, plugged it into their model, and came out with [a phase transition at] 5%," Golden says. "It all fit together beautifully."

Ironically, Golden started writing about this idea on his third trip to Antarctica—the one with the fire. After the fire was brought under control, the *Aurora Australis* drifted in the pack ice without power for 2 days, until the crew finally managed to start the backup engine and the ship slowly limped back to Hobart. Golden began writing a paper en route. It ultimately appeared in *Science* and marked the beginning of a rational explanation of fluid flow through sea ice.

One skeptic was Hajo Eicken, a geophysicist at the University of Alaska, Fairbanks, who describes the composite-powder model as "too simplistic." However, Eicken and Golden started collaborating 6 years ago, and together they have developed a much more realistic model based on three-dimensional imagery of actual brine networks. In work that has not been published yet, they substantially confirm the "rule of fives" but show that the percolation threshold is different in each of the three directions and also depends on the type of ice.

Climatic wild cards

For many years, sea ice languished as a somewhat esoteric field of study. No longer. Over the past decade, sea ice has emerged as the most visible and perhaps the most poorly understood barometer of global climate change.

The depth of scientists' ignorance became apparent in 2007, when the area of the summer ice pack in the Arctic dropped 40% from its historical average. The ice pack scarcely recovered in 2008. Not even the most pessimistic climate models foresaw such a precipitous drop.

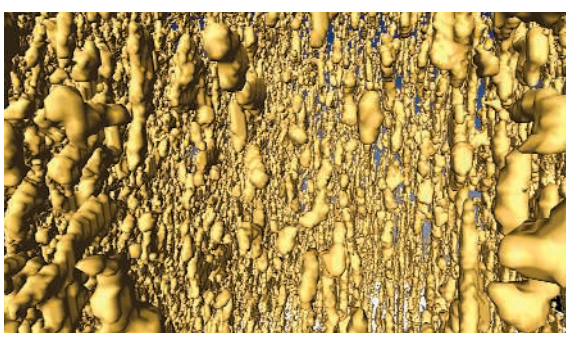

Riddled. CT scan of brine channels in lab-grown ice shows the permeable structure that makes sea ice so vexing for modelers.

"The amount of retreat in the summer of 2007 was just shocking," Perovich says. "It's a mystery, and as in any mystery there is a long list of suspects. Some people argue for preconditioning: As the ice gets thinner, it is more sensitive to warm summers than it would be if the ice were thicker. Some people argue for changes in atmospheric circulation, or export of more perennial ice to lower latitudes, or convection of heat through the Bering Strait. Then there's my favorite, the ice-albedo feedback."

The ice-albedo feedback comes into play as snow-covered ice is replaced by open water or is covered by seasonal melt ponds. The water absorbs more of the sun's heat, accelerating the ice's melting. All computerized climate models include the effect, but to some extent they all rely upon guesswork. No one at present can predict the extent, the timing, or the warming effect of the melt ponds.

"Right now, the large-scale models used in climate prediction have problems," says Ackley. "There are several processes that aren't done well." From melt ponds in the Arctic (which form only if the underlying ice is impermeable) to the growth of algae in the Antarctic, many of these processes start up or shut down when the "rule of five" phase transition tells them to. Without them, an important link in the polar climate chain cannot be closed.

Golden thinks the mathematics of composite materials can also be applied to the ice pack as a whole. "When I look at these satellite images, I see a time-evolving, two-phase composite material. I am quite sure that I can bring new methods and ways of thinking to these problems, based on my bread and butter as a mathematician." Recently, he has begun working with Elizabeth Hunke of Los Alamos National Laboratory and Cecilia Bitz of the University of Washington, Seattle, on updating the sea-ice module of the Community Climate System Model. "The salinity in sea ice is one of the things that global climate models have not incorporated yet, and we're starting to do that now," Hunke says.

Golden also looks forward to more journeys to high latitudes. A year after the fire cruise of 1998, he was back on the same ship, with the same crew. In 2007, he sailed on the *Aurora Australis* again—this time as the leader of his own experiment, studying the relationship between electrical conductivity and fluid permeability in sea ice.

"Would I have chosen to be on a burning ship in Antarctica? Obviously not," he says. "But having been through it, I wouldn't trade that experience for anything." In particular, it taught him the most important lesson for anyone doing research in Antarctica: adaptability. "There's always something that happens in Antarctica," he smiles. "I've never been on an expedition that went according to plan."

–DANA MACKENZIE

Dana Mackenzie is a writer in Santa Cruz, California.

Published by AAAS

Political oversight. Senator Barbara Mikulski with Ed Weiler during a 2006 visit to NASA Goddard SFC.

U.S. SPACE SCIENCE

Trouble on the Final Frontier

NASA's scientific missions have enjoyed spectacular success. But significant cost overruns and launch delays jeopardize future missions

The $273 million Orbital Carbon Observatory's plunge into the Southern Ocean shortly after launch last month was a sobering reminder of the unforgiving nature of space exploration. But the ability to put a spacecraft safely into orbit is the least of the pressing issues facing NASA's $4.5 billion science program. A bigger challenge than the rare but dramatic rocket failure is finding the money to pay for an ambitious, complex, and unique set of missions.

The squeeze on NASA's science budget arrives as researchers in a host of disciplines (see graphic, p. 35) begin planning the next generation of missions. No one—lawmaker, NASA manager, or senior scientist—seems to have an answer to the ballooning cost of space science projects. "There's no simple fix, or the situation would have been resolved long ago," said a frustrated Representative Gabrielle Giffords (D–AZ), the new chair of the House of Representatives science committee's space panel, during a 5 March hearing that covered both science and space-flight overruns.

The community is anxiously awaiting word on who will be the next NASA administrator. Last year on the campaign trail, President Barack Obama promised to increase the monitoring of global climate from space and support a new generation of robotic probes to other planets without throttling back on preparations for returning humans to the moon. The president's preliminary 2010 budget request, released in February and lacking details, proposes a modest boost to funding for both science and human space flight efforts as part of the agency's overall $18.7 billion budget.

But those increases do not begin to cover what NASA's science program needs just to keep pace with the demands of researchers. The agency's science honcho, Edward Weiler, says he needs $900 million more every year just to keep up with current earth science projects. "There is no greater thing than starting a new, sexy science mission," he says. "We all love it. The thing that prevents me is I've also got new, sexy missions started 5 years ago that are costing more than they were supposed to."

Back to the future

Complaints about overruns in the science program extend back to at least 1980. Back then, however, NASA's entire budget equaled that of its science budget today. And today, there's a much longer line of telescopes, planetary robots, and Earth-monitoring satellites waiting to be designed, built, and launched.

That queue, ironically, is due in part to the success enjoyed by scientists in plotting their future. Since the 1960s, astronomers have created a consensus decadal plan for the next generation of telescopes. Earlier this decade, the other three disciplines that depend heavily on NASA dollars—earth sciences, solar system exploration, and solar studies—followed suit. Providing the space agency with a clear set of missions and their costs has helped scientists make their case with members of Congress and NASA bureaucrats. "I'm a slave to the decadals," says Weiler.

But that community process relies on accurate cost estimates. And when the costs soar, the process breaks down. The most infamous example is the James Webb Space Telescope, which astronomers pegged at $1 billion, not including operations and launch, in a 2001 report. The true cost likely will top $4 billion by its launch in 2013, forcing NASA to slow down work on a slew of other astronomy and astrophysics missions.

Weiler headed the space program from 1998 to 2004 before becoming director of Goddard Space Flight Center in nearby Greenbelt, Maryland. Last April, he was called back downtown to run the program after S. Alan Stern quit in a funding dispute with then-Administrator Michael Griffin, who left NASA in January. Stern made cutting costs his mantra, and he played hardball with project managers and contractors. But Stern also failed to win advocates for his cause and departed after only 12 months on the job.

"When I walked into this office, there were a lot of promises made out there, and communities were pretty happy," Weiler said in a recent interview at NASA headquarters. But within days, he says, a team of independent cost reviewers gave him the bad news. "Over a 10-year period there were $6 billion of promises made [in planetary sciences] that could not be met. And so I was put in the position of being the bad guy."

In the past, human space flight often tapped science to pay for its own shortfalls. This time around, however, the problem is within the science program—too many missions costing too much money. For example, technical difficulties led to a $400 million cost overrun on the Mars Science Laboratory (MSL), which forced Weiler to postpone its launch by 2 years. The decision pushed back other planned Mars flights.

Mars wasn't the only trouble spot. Few missions in either the solar studies or the earth sciences program were on budget and schedule. The Solar Dynamic Observatory (SDO), a Goddard effort to investigate the sun's magnetic field, is close to 2 years behind schedule and its initial estimated budget has tripled. The Glory spacecraft being prepared to study aerosols and black carbon in Earth's atmosphere was more than 50% over its original $266 million price tag, and its 2008 launch has been postponed until at least the middle of 2009.

Such problems have triggered a round of finger-pointing. In 2007, nearly 100 earth scientists warned that the global monitoring

Online
sciencemag.org
For an interview with Ed Weiler, go to www.sciencemag.org/cgi/content/full/324/5923/34/DC1.

CREDIT: NASA

Published by AAAS

system for understanding climate change was "at risk of collapse" because of NASA's failure to promptly move ahead with its projects. Last month, solar scientists complained that nearly all of their proposed decadal missions have been delayed or deferred.

Weiler, in turn, blames the science community for its unrealistically low initial projections. "Scientists cannot do cost estimation," he says. He notes that their numbers typically come from NASA centers, which assume that a low estimate will make the project more politically viable. "I won't call it lying or cheating," says Weiler. "It's optimism."

Such criticism doesn't sit well with those who took part in the decadal studies, most of which were completed during Weiler's first stint as science chief. They defend their efforts and resent what they see as his Monday-morning quarterbacking. "We got independent cost estimates as well as numbers from NASA—and added 10% to 20% as a fudge factor," says Louis Lanzerotti, a physicist at the New Jersey Institute of Technology in Newark and a member of the 2003 decadal panel for solar studies. "We had tremendous cost awareness." Lanzerotti says his team worked hard "to make sure our report was credible."

Joseph Alexander, a former director and current officer of the Space Studies Board at the National Academies, which oversaw the reports, says estimates have gotten better since the infamous James Webb episode. But he believes that even the solar decadal—the last of the four to be completed—"still didn't have a rigorous process." The next round of decadal studies will feature a much more rigorous cost analysis, he says, aided by engineers and managers with extensive experience in putting spacecraft into orbit. At the same time, none of the missions chosen for the previous decadal study will be grandfathered into the new study. "Anything not in the works gets thrown back in the hopper to be recompeted," he warns.

No quick fix

Even as the decadal panels try harder, so too must NASA, according to independent reports presented at the 5 March congressional hearing. The Aerospace Corporation, a nonprofit organization in El Segundo, California, found that only five of 40 NASA missions—mostly to do science—came in on time and on schedule, and that more than a quarter were at least 40% costlier than anticipated. Spacecraft grew an average of 40% heavier by final design. (Weight is a critical factor in boosting the cost of a mission.) And when one project goes over budget, "the resulting domino effect impacts all missions that follow," noted Aerospace Corporation Vice President of Civil and Commercial Operations Gary Pulliam at the hearing.

The Government Accountability Office (GAO) reported similar results. The congressional watchdog found that costs for 18 projects, the bulk of them science missions, grew by an average of 13% within 3 years—one rose by 50%—and were delayed by nearly a year. The study faulted NASA for moving a program into development before it has a stable design and for assuming that new projects will save money by drawing on the technology of previous missions. "Time and costs were consistently underestimated," says GAO's Cristina Chaplain.

Acting NASA chief Chris Scolese confessed to the House panel that the agency's ability to pinpoint cost and schedule issues have been "less than desired in the past" and described early estimates as "at best, educated guesses." But extending the lifetime of successful missions is also a factor, he said, because it shrinks the pot of money available for new efforts. In the agency's defense, Scolese said NASA had no control over overruns and delays on half of the 10 projects cited in another GAO report. SDO, for example, has had to compete with commercial and military customers for an Atlas launcher. NASA officials say there was no way to predict the sudden paucity of launchers.

The root of the problem, say several scientists who declined to be quoted for fear of retribution, is an iron triangle among NASA centers, lawmakers, and contractors. "There is a lot of fat at the centers," says one researcher with years of experience on NASA science missions. Adds another: "Industry, academia, and the centers all know that NASA headquarters folds on the issue of cost overruns."

Weiler disputes that assessment. "If you think we don't get mean with contractors, go talk to some of the CEOs who've gotten an earful from me," he says. And he did kill more than a half-dozen projects in their early phases during his previous tenure as science chief. But the big savings would come from canceling missions under construction, a step that requires taking on that iron triangle. Goddard's SDO, for example, has won consistent backing from Senator Barbara Mikulski (D–MD) despite the cost increases, and the large and influential California delegation protects efforts such as MSL based at NASA's Jet Propulsion Laboratory in Pasadena. The desire to preserve high-tech jobs is especially strong during economic downturns.

Weiler suggests that such increases come with the territory. "Can we forget that Hubble overran 300%?" he asks. "It's the greatest success in NASA history, but I could give you a list of prominent people in the community who wanted Hubble killed during its development. I won't, because it turns out many of them made a career off the Hubble data."

Many space scientists agree with Weiler that most of NASA's greatest science accomplishments suffered cost overruns and that such increases are unavoidable for unique missions. But will a new NASA chief try to shake up the current system in search of a better approach? That's what scientists planning to choose what projects matter most to them for the coming decade are anxious to find out.

–ANDREW LAWLER

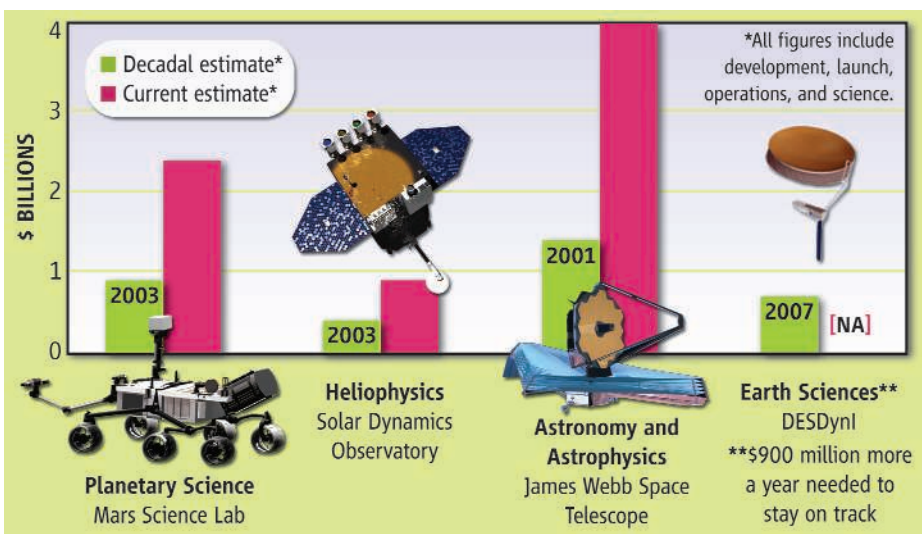

Prices taking flight. The cost of major missions for each of four disciplines has vastly exceeded estimates contained in the most recent decadal study for those fields.

CREDITS: NASA; SOURCE: NASA/NRC

LETTERS

edited by Jennifer Sills

Taste of Astronomy Lacked International Flavor

IN HIS SHORT HISTORY OF ASTRONOMY ("ASTRONOMY'S GREATEST HITS," NEWS FOCUS, 16 January, p. 326), T. Folger amply demonstrated Anglo-Saxon parochialism. Almost all major discoveries mentioned in his text are attributed to those from Britain or the United States. Why didn't Folger name great scientists from other nations? He could have included a host of scientists from the francophone world alone, including Nicolas-Claude Fabri de Peiresc (*1*) and Jean-Baptiste Cysat, who recorded, in 1610 and 1619, the first observations of a binary star; Urbain Jean Joseph Le Verrier (*2*), who by simple calculation predicted the location of the as-yet-unknown planet Neptune; Michel Major (*3*) and Didier Queloz, who discovered the first exoplanets in 1995; and René Doyon, Christian Marois, and David Lafrenière (*4*), who, in 2008, were the first to photograph exoplanets (three at a time). I'm sure scientists of other nationalities have made contributions that deserved mention in the News Focus story as well.

PIERRE COUTURE

Saint-Cyprien-de-Napierville, QC, Canada. E-mail: pa_couture@sympatico.ca

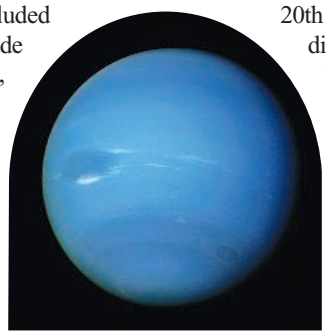

Neptune. The French astronomer Urbain Jean Joseph Le Verrier, using mathematical calculations, predicted the existence of Neptune before it was discovered.

References

1. G. Bigourdan, *Comptes Rendus* **162**, 489 (1916).
2. W. Sheehan, N. Kollerstrom, C. B. Waff, "The case of the pilfered planet: Did the British steal Neptune?" *Sci. Am.* (November 2004).
3. M. Mayor, D. Queloz, *Nature* **378**, 355 (1995).
4. C. Marois *et al.*, *Science* **322**, 1348 (2008).

Response

CRAMMING 400 YEARS OF "GREATEST HITS" into four pages inevitably slighted worthy astronomers—those whom Couture names, as well as Abbé Lemaître, Joseph von Fraunhofer, and many others. Our admittedly idiosyncratic selection did include non–Anglo-Saxons Galileo, Christian Huygens, Giovanni Schiaparelli, Maarten Schmidt, Aleksander Wolszczan, and (implicitly) members of modern international teams who gather data with orbiting observatories.

ROBERT COONTZ

Creating a Common Climate Language

THE NATIONAL RESEARCH COUNCIL HAS OBserved that climate science is progressing well, but the use of science in decision-making lags far behind (*1*). Given the high stakes involved, it is imperative that we improve the exchange of information between scientists and public stakeholders. Here, we suggest three steps that would advance the public's decision-making capacity.

First, we urge scientists and science journal editors to create a single, readily understood frame of reference for two critical concepts in climate science—atmospheric concentrations of greenhouse gases and rising global temperatures—by using a standard unit of measure and a single temperature baseline. Specifically, because total anthropogenic forcing is the relevant policy measure (*2*, *3*), we strongly recommend referencing atmospheric concentrations of all long-lived greenhouse gases as CO_2-equivalent (CO_2e), not only CO_2. CO_2e is the concentration of CO_2 that would cause the same level of radiative forcing as a given mixture of CO_2 and other greenhouse gases.

Moreover, because understanding total anthropogenic warming is important for assessing risk, we recommend referencing a standardized pre-industrial temperature baseline. Adopting these two references as elements of our common language will help reduce confusion that has been inadvertently caused by reporting results that appear to be similar [such as 397 parts per million CO_2 compared with 455 parts per million CO_2e in 2005 (*4*) and 2°C above pre-industrial compared with the late 20th century] but that have dramatically different implications with regard to understanding where we stand on the path toward real danger.

Adopting these conventions will improve science communication and help stakeholders simplify appropriately, but we must also improve communication effectiveness beyond what any scientist or journal editor can be expected to do. Therefore, we urge the broader science, communication, and funding community to support large-scale projects to translate scientific assessments into simpler, more useful terms. We support Fischhoff's (*5*) call for an interdisciplinary approach that includes the expertise of climate scientists, decision scientists, behavioral scientists, and communication practitioners.

The first priority should be to explain where humanity stands on a scale of risk that includes CO_2e, global temperatures, and climate impacts. As Schellnhuber recently observed, the Intergovernmental Panel on Climate Change (IPCC) format "is inherently tuned for burying crucial insights under heaps of facts, figures, and error bars" (*6*). For example, the key warming projections figure, SPM.5 (*4*), obscures the risk of overshooting the multimodel mean. The average warming for scenario B1 is roughly 3°C above pre-industrial levels, but the range of potential warming is roughly 2° to 4°C. It is misleading, therefore, to say that B1 avoids breaching 3°C; there is, in fact, a 50% probability that it will. Stakeholders urgently need such information, so we recommend that large-scale efforts to improve translation and relevance be given the highest priority.

CREDIT: NASA

Published by AAAS


Island megafauna
42

Better catalysts for fuel cells
48

Understanding society's response options and the tradeoffs they involve is just as important as recognizing climate risks. Unfortunately, politicized debate has overshadowed scientific understanding in public discourse. Therefore, our third recommendation is to translate the scientific basis for the range of potential solutions into terms that nonscientists can readily understand and use.

At this critical moment, scientific understanding has outstripped our society's capacity to use that knowledge by a wide margin. This situation must be resolved quickly to give policymakers—and the public—the broadest range of options. Therefore, the science community should adopt a common language and standard baselines to help nonexperts see the problem. Beyond this, the science and communications community should support a concerted effort to close the information gap by communicating climate knowledge in ways that nonscientists will find useful.

THOMAS E. BOWMAN,[1]* EDWARD MAIBACH,[2] MICHAEL E. MANN,[3] SUSANNE C. MOSER,[4] RICHARD C. J. SOMERVILLE[5]

[1]Climate Solutions Project, Bowman Global Change, Signal Hill, CA 90755, USA. [2]Center for Climate Change Communication, Department of Communication, George Mason University, Fairfax, VA 22030, USA. [3]Department of Meteorology, Pennsylvania State University, University Park, PA 16802, USA. [4]Susanne Moser Research and Consulting, Santa Cruz, CA 95060, USA. [5]Scripps Institution of Oceanography, University of California, San Diego, La Jolla, CA 92093, USA.

*To whom correspondence should be addressed. E-mail: tom@bowmanglobalchange.com

References

1. National Research Council, "Evaluating progress of the U.S. Climate Change Science Program: Methods and preliminary results" (National Academy Press, Washington, DC, 2007).
2. Commission of the European Communities, "Limiting global climate change to 2 degrees Celsius: The way ahead for 2020 and beyond" (Brussels, 2007); http://eur-lex.europa.eu/LexUriServ/LexUriServ.do?uri=COM:2007:0002:FIN:EN:PDF.
3. R. Allen *et al.*, "2007 Bali climate declaration by scientists" (Climate Change Research Centre, University of New South Wales, Sydney, Australia, 2007); www.ccrc.unsw.edu.au/news/2007/Bali.html.
4. Intergovernmental Panel on Climate Change, Summary for Policymakers (SPM), in *Climate Change 2007: The Physical Science Basis: Contribution of Working Group I to the Fourth Assessment Report of the Intergovernmental Panel on Climate Change*, S. Solomon *et al.*, Eds. (Cambridge Univ. Press, New York, 2007).
5. B. Fischhoff, *Env. Sci. Technol. Online* **41**, 7207 (2007).
6. H. J. Schellnhuber, *Proc. Natl. Acad. Sci. U.S.A.* **105**, 14239 (2008).

Effects of Increased Urbanization

IN HIS NEWS OF THE WEEK STORY "DEBATE continues over rainforest fate—with a climate twist" (23 January, p. 448), E. Stokstad is correct in saying that "preserving tropical forest would yield multiple benefits: storing more carbon, rather than releasing it from burning, and maintaining habitat." However, Wright and Muller-Landau (*1*), authors of the 2006 paper Stokstad cites, might be mistaken about the effects of increased urbanization. As people move to urban areas, deforestation may decrease, but consumption in other areas (related to increased use of Internet, mobile telephones, cars, and airplanes) will increase. Only when all facets of environmental sustainability (including pollution, overpopulation, resource depletion, and mass consumption) are taken into consideration can we fully assess the sustainability of a certain action.

ROGER CHAO

The Office of Environmental Sustainability, Monash University, Clayton, VIC 3800, Australia. E-mail: rogersteppe@gmail.com

Reference

1. S. J. Wright, H. C. Muller-Landau, *Biotropica* 38, 287 (2006).

Rheumatic Fever: Neglected Again

WE APPRECIATE M. ENSERINK'S NEWS OF the Week story ("Some neglected diseases are more neglected than others," 6 February, p. 700) on the Moran *et al.* study analyzing the current state of research into so-called "neglected diseases" (*1*). We would like to highlight one neglected disease that was neglected once again: rheumatic fever (RF).

RF and its sequel, rheumatic heart disease (RHD), are almost exclusively restricted to developing countries, with a mortality comparable to that of rotavirus, and about 50% of that of malaria (*2*). According to the George Institute report, only 0.07% of global funding is directed toward RF, much less the treatment and prevention of RHD. This limited allocation for RF illustrates the misdirection of global health funding. Although the complications of RF/RHD are potentially lethal, they are entirely preventable with antibiotic prophylaxis, which has been shown to be cost-effective in individuals with prior group A streptococcal infection (*3*). Despite the limited scientific understanding of RF/RHD, some developing countries have been able to control the disease, simply by investing heavily in existing technologies and programs (*4*). In Enserink's words, global investment in RF/RHD would "pay off quickly."

Although Moran *et al*. note a consensus on preventative vaccine development for RF/RHD, they fail to document two other critical areas of research—epidemiologic surveillance and disease control. Although several promising initiatives for RF/RHD surveillance and control have been recently published (*5*), funding opportunities for such programs are still rather scant. We encourage the international donor community to critically examine their funding priorities regarding RF/RHD. We also suggest that future surveys by the George Institute researchers include epidemiological and treatment programs, which are crucial to the eradication of neglected diseases.

DAVID A. WATKINS,[1] LIESL J. ZUHLKE,[2] MARK E. ENGEL,[1] BONGANI M. MAYOSI[1]*

[1]Department of Medicine, Groote Schuur Hospital and University of Cape Town, Cape Town 7925, South Africa. [2]Western Cape Paediatric Cardiac Services, Red Cross War Memorial Children's Hospital, Cape Town 7700, South Africa.

*To whom correspondence should be addressed. E-mail: bongani.mayosi@uct.ac.za

References

1. M. Moran *et al.*, *PLoS Med.* **6**, e30 (2009).
2. J. R. Carapetis, A. C. Steer, E. K. Mulholland, M. Weber, *Lancet Infect. Dis.* **5**, 685 (2005).
3. K. A. Robertson, J. A. Volmink, B. M. Mayosi, *BMC Cardiovasc. Disord.* **5**, 11 (2005).
4. P. Nordet, R. Lopez, A. Duenas, L. Sarmiento, *Cardiovasc. J. Afr.* **19**, 135 (2008).
5. B. Mayosi *et al.*, *S. Afr. Med. J.* **96**, 246 (2006).

Letters to the Editor

Letters (~300 words) discuss material published in *Science* in the previous 3 months or issues of general interest. They can be submitted through the Web (www.submit2science.org) or by regular mail (1200 New York Ave., NW, Washington, DC 20005, USA). Letters are not acknowledged upon receipt, nor are authors generally consulted before publication. Whether published in full or in part, letters are subject to editing for clarity and space.

COMMUNICATION

Signs of Meaning

Andrew Robinson

Writing
Theory and History of the Technology of Civilization

by Barry B. Powell

Wiley-Blackwell, Malden, MA, 2009. 296 pp. $99.95, £50, €60. ISBN 9781405162562.

"AOCCDRNIG TO RSCHEEARCH AT CMABRIGDE UINERVTISY, IT DEOSN'T MTTAER IN WAHT OREDR THE LTTEERS IN A WROD ARE, THE OLNY IPRMOETNT TIHNG IS TAHT THE FRIST AND LSAT LTTEER BE AT THE RGHIT PCLAE." Thus Barry B. Powell, near the end of *Writing*, playfully reminds the reader of the complex interplay between the shape of a word and its phonetic representation.

On the book's first page, Powell takes aim at what he regards as three long-established misunderstandings that bedevil the study of writing: that the purpose, origin, and function of writing are to represent speech; that writing originated in pictures; and that writing systems necessarily evolve over centuries of use toward more efficient phonetic representation, as in alphabets.

Egyptian hieroglyphs, for example, clearly do not fit the first claim because they do not indicate vowels. Egyptologists have to supply those when transliterating hieroglyphs to make pronounceable words in the presumed ancient Egyptian language: the pharaonic name Ramses is actually written with just three consonantal hieroglyphs that represent *r*, *ms*, and *s*. As to the second claim, although some of the earliest written signs (protocuneiform from the late fourth millennium BCE in Mesopotamia) do look like pictures—a human head, a fish, barley, and so on—most are indeed abstract. As for evolution, one has only to contemplate Chinese writing, which became progressively less phonetic from its relatively simple origins in the Shang civilization of the second millennium BCE and by the 18th century consisted of almost 50,000 characters.

Although far from a textbook, *Writing* presents the basics of Mesopotamian cuneiform, Egyptian hieroglyphs, Chinese characters, Aegean writing systems such as Cretan Linear B, and the fiendishly complicated Mayan glyphs (which have been deciphered only in the past few decades). The most important chapters concern West Semitic writing from the Near East (such as the Phoenician script) and the Greek alphabet, Powell's special field as a classicist. He is best known for his provocative thesis that the Greek alphabet was invented circa 800 BCE by one man, probably Homer, in order to write down oral epic poetry (*1*).

Archaic bookkeeping. Protocuneiform clay tablets from Uruk in Mesopotamia, circa 3200 BCE, preserve the earliest known writing.

CREDIT: GIANNI DAGLI ORTI/CORBIS

Here Powell strongly argues against another popular view: that to create their alphabet the ancient Greeks borrowed the Phoenician script, which has only consonantal letters, and added to it letters for the Greek vowels. He notes, "It is inaccurate to say that the inventor of the Greek alphabet 'added vowels' to a previously vowelless script, when the concept 'vowel' depends on how the Greek alphabet functions and not on objective features of human speech." Spectrograms of ordinary speech do not distinguish vowels from consonants: there is a continuous wave. The letters of the alphabet are what gives us the compelling idea that speech can be atomized into particles of sound. Nor are words the discrete acoustic entities we like to think. Powell reminds us that when the classicist Milman Parry (in his famous 1930s studies) asked illiterate Balkan singers to sing just one "word" of their songs, they would deliver an entire line, several lines, or even a complete song.

On the origins of writing in Mesopotamia, Powell takes pains to distinguish what he calls semasiography from lexigraphy. In semasiography (such as petroglyphs, protocuneiform, airport signage, and mathematical notation), the signs are not attached to necessary forms of speech, whereas in lexigraphy (such as cuneiform or the alphabet), they are. No one really knows how semasiography gave rise to lexigraphy. Powell favors Denise Schmandt-Besserat's theory that the semasiographic clay "tokens" found in large numbers in Mesopotamian sites from about 8000 BCE until the emergence of protocuneiform circa 3300 BCE were instrumental precursors of lexigraphy (*2*). He incorrectly suggests, however, that the tokens "gradually disappear" around 3400 BCE, whereas, as Schmandt-Besserat admits, they continue until 1500 BCE, long after the emergence of lexigraphy. Rather than precursors, the intriguing tokens are more likely to have been a parallel system of accounting that tells us nothing definite about the emergence of writing.

The book is in places partial and contentious, with a number of unsubstantiated assertions—such as its misrepresentation, following Maurice Pope (*3*), of the scientist Thomas Young's crucial contributions to Jean-François Champollion's decipherment of Egyptian hieroglyphs. Surprisingly, Powell does not mention John DeFrancis's comparable book (*4*), which has the advantage of being written by a Chinese specialist. No doubt Powell is right to generalize that "The Chinese will learn to use the alphabet, but alphabet users will not learn to use Chinese" because of its bewildering signary. But he goes too far in his undervaluing of the important role, emphasized by DeFrancis, of phoneticism in reading and writing Chinese characters. Despite these shortcomings, *Writing* is stimulating and impressive (if too

The reviewer, the author of *Lost Languages: The Enigma of the World's Undeciphered Scripts*, is at Wolfson College, Cambridge CB3 9BB, UK. E-mail: ar471@cam.ac.uk

Published by AAAS

densely written for the nonspecialist), a worthy successor to the pioneering book by Semitic specialist I. J. Gelb (*5*).

References

1. B. B. Powell, *Homer and the Origin of the Greek Alphabet* (Cambridge Univ. Press, Cambridge, 1991).
2. D. Schmandt-Besserat, *Before Writing* (Univ. Texas Press, Austin, 1992).
3. M. Pope, *The Story of Decipherment: From Egyptian Hieroglyphs to Maya Script* (Thames and Hudson, New York, ed. 2, 1999).
4. J. DeFrancis, *Visible Speech: The Diverse Oneness of Writing Systems* (Univ. Hawaii Press, Honolulu, 1989).
5. I. J. Gelb, *A Study of Writing: The Foundations of Grammatology* (Univ. Chicago Press, Chicago, ed. 2, 1963).

10.1126/science.1173405

LANGUAGE

Social Motives for Syntax

N. J. Enfield

Origins of Human Communication

by Michael Tomasello

MIT Press, Cambridge, MA, 2008. 407 pp. $36, £23.95. ISBN 9780262201773.

As surprising as it may sound, most cognitive-science research on language has been avowedly disinterested in communication. One dominant philosophy, grounded in the work of linguist Noam Chomsky, sees language as primarily an instrument of thought, not action. On this view, the key event in the evolution of language was a mutation resulting in an organlike faculty in the human mind, with selective advantage in the realm of reasoning. This faculty happened also to be useful for generating complex communicative behavior, though perhaps in the same way that a foot happens to be good for playing soccer: it did not evolve under the selective pressure of that function.

Michael Tomasello (a developmental psychologist at the Max Planck Institute for Evolutionary Anthropology) offers a distinctly contrasting perspective in *Origins of Human Communication*. Following ordinary-language philosophers from Ludwig Wittgenstein through J. L. Austin, Paul Grice, and John Searle, Tomasello sees language as a means for doing things, not a device for processing or merely externalizing thoughts. Here, to communicate is to act on others in the social realm (*1*, *2*). For language to have this function presumes not only a conspecific with a comprehending mind but also a willingness to cooperate. Take the simple example of a request: I say, "Please pass the salt." If all goes well, this utterance has an effect on your mind that in turn causes a compliant pattern of behavior: you pass me the salt.

Requests form one of three classes of social action on which Tomasello builds his account of human communication. The others are informing-helping (e.g., when one person points to keys that another just dropped) and sharing (e.g., when two people's attitudes toward a third person align in the course of a gossip session). He summarizes research showing that all three social motives are fully evident in the communicative behavior of prelinguistic infants and all but absent among our closest relatives, the great apes. Humans have a special combination of cooperative instincts, prosocial motives, high-level intention attribution, and moral propensities (*3*). Tomasello contends that without this unique psychological wherewithal in the domain of social cognition, language as we know it could never have evolved.

Tomasello's work represents a long-standing and now rapidly growing view that language is not restricted to abstract structures of grammatical patterning but includes gestures and other bodily movements of the kinds that typically accompany speech (*4*, *5*). In this book, Tomasello does more than merely include gestures: he gives them pride of place. Gestures, he argues, are necessary for the development of language in both phylogeny and ontogeny. What is new here is not the idea itself but the fascinating battery of experiments by Tomasello and colleagues garnered in support of it. The research settles some long-standing controversies in developmental psychology by showing that 9-month-olds use gestures for multiple, often sophisticated social functions, including the three basic social motives. These favorable conclusions on the social cognitive sophistication of human infants contrast with the findings on primates Tomasello summarizes. The research he discusses defines limits of chimpanzees' capacities in experimental settings (to the certain chagrin of many field-working primatologists). Lacking humanlike prosocial motives, chimps show only rudimentary strategies for making requests and little or no evidence of the helping and sharing behavior that comes so naturally to human infants.

Many traditional linguists find a focus on gesture in accounting for the origin of language unsatisfying. The problem is that while gesture provides a key link in the chain of events, other critical links remain missing. Gestures lack the highly structured complexity of grammar: How to get from one to the other? [Such statements of incredulity are of course the enemy of gradualist evolutionary accounts (*6*).] Linguists in the 1990s expressed a similar worry in response to Robin Dunbar's socially grounded theory of language evolution (*7*). When Dunbar proposed that language evolved in response to the pressure of maintaining social relations in ever-larger groups—functionally analogous to (but much more efficacious than) what primates do with grooming—linguists complained that they could not see how to get from "mere grooming" to the dazzling complexities of syntax. As a linguist, Tomasello is qualified to address this concern and advance Dunbar's cause significantly (although surprisingly he makes no reference to Dunbar's work).

Tomasello's solution is an ingenious linking of requesting, informing, and sharing with three distinct levels of complexity in the grammatical possibilities that any language will furnish. He dubs these "simple syntax" (strongly dependent on immediate context), "serious syntax" (for making unambiguous reference across contexts), and "fancy syntax" (for organizing long and complex narratives). But this is essentially as far as his links to grammar go, promissory notes notwithstanding. Precisely because the author is a linguist, this omission is a missed opportunity to complete the argument, to connect the dots that lead from basic social actions ultimately to the radically varying, historically developed complex linguistic systems that are found around the world. I fear that without the story being told through to the end, many linguists will remain incredulous.

With this book, Tomasello makes a powerful and highly readable case for the social foundations of human communication (in line with a fundamental shift in current thinking on the nature of language) and of the underlying cognition that makes language possible. In this naturalistic account, language is an adaptation that gradually emerged, in step with the evolution of a special kind of social mind.

References

1. J. R. Krebs, R. Dawkins, in *Behavioural Ecology: An Evolutionary Approach*, J. R. Krebs, N. B. Davies, Eds. (Blackwell, London, ed. 2, 1984), pp. 380–405.
2. J. M. Atkinson, J. Heritage, Eds., *Structures of Social Action* (Cambridge Univ. Press, Cambridge, 1984).
3. N. J. Enfield, S. C. Levinson, Eds., *Roots of Human Sociality: Culture, Cognition, and Interaction* (Berg, London, 2006).
4. D. McNeill, *Psychol. Rev.* **92**, 350 (1985).
5. A. Kendon, *Gesture: Visible Action as Utterance* (Cambridge Univ. Press, Cambridge, 2004).
6. R. Dawkins, *The Blind Watchmaker: Why the Evidence of Evolution Reveals a Universe Without Design* (Norton, New York, 1986).
7. R. Dunbar, *Behav. Brain Sci.* **16**, 681 (1993).

10.1126/science.1172660

The reviewer is at the Language and Cognition Group, Max Planck Institute for Psycholinguistics, 6512 HW, Nijmegen, Netherlands. E-mail: Nick.Enfield@mpi.nl

ECOLOGY

Will Threat of Biological Invasions Unite the European Union?

New data on the extent of biological invasions pose major regulatory and political challenges to European institutions.

Philip E. Hulme,[1]* Petr Pyšek,[2] Wolfgang Nentwig,[3] Montserrat Vilà[4]

Europe is the source of many of the world's worst invasive species, including Austrian pine (*Pinus nigra*), Norway maple (*Acer platanoides*), Spanish slug (*Arion lusitanicus*), German wasp (*Vespula germanica*), Scotch broom (*Cytisus scoparius*), and English starling (*Sturnus vulgaris*). However, the perspective of Europe as the source rather than recipient of invasive species is in urgent need of revision in light of the Delivering Alien Invasive Species Inventories for Europe (DAISIE) project (www.europe-aliens.org). This continent-wide assessment of the scale and impact of biological invasions reveals that Europe's maritime and land borders have been breached by >11,000 alien species. Over half of these are terrestrial plants. Aquatic and terrestrial invertebrates account for >30% of species, whereas only ~5% are vertebrates. Compared with estimates from little more than a decade ago, the new data on aliens identify more than five times as many bird species, a threefold increase in mammal species, and twice as many plants established in Europe (*1*). Europe is home to numerous species from other continents, e.g., Canada goose (*Branta canadensis*), American bullfrog (*Lithobates catesbeianus*), Argentine ant (*Linepithema humile*), Egyptian goose (*Alopochen aegyptiacus*), Indian strawberry (*Duchesnea indica*), Chinese mitten crab (*Eriocheir sinensis*), Japanese oyster (*Crassostrea gigas*), and New Zealand flatworm (*Arthurdendyus triangulatus*).

Even the crudest estimate of total known monetary impact of alien species in Europe is close to €10 billion (about U.S. $13 billion) annually (*2*). This figure is an underestimate, as potential economic and environmental impacts are unknown for almost 90% of the alien species found in Europe (*3*). Alien species predate, hybridize with, parasitize, and out-compete a wide range of native European taxa and, as a result, reduce biodiversity, threaten endangered species, and alter ecosystems (*4*).

To date, the European Union's (EU's) response to the problems of alien species has been driven by commitments to international agreements such as the World Trade Organization Agreement on the Application of Sanitary and Phytosanitary Measures (SPS) and the Convention on Biological Diversity (CBD). Yet these commitments have not always been supported by action. Under the CBD, EU member states rate implementation of Article 8h "to prevent the introduction of, control or eradicate those alien species which threaten ecosystems, habitats or species" as a significantly lower priority than nations outside Europe (*4*) and only two EU states (France and Spain) have ratified the International Convention for the Control and Management of Ships' Ballast Water and Sediments. More recently, signatories to the CBD have agreed to achieve a significant reduction of the current rate of biodiversity loss by 2010, and this includes providing evidence of actions to reduce the number and cost of biological invasions (*5*). In response, Europe has committed itself to using the cumulative number of alien species in its territory as one indicator of progress toward the 2010 goals (*6*). Yet, progress to date has been poor, with average annual rates of alien species establishment in Europe having progressively increased over the last century for many taxa (see figure, above).

Therefore, the European Commission has put forward a proposal to the European Council and Parliament for an EU strategy on invasive species (*2*). The strategy emphasizes prevention as the most cost-effective way forward and presents three new policy options: maximize the use of existing legal instruments; adapt existing legislation through specific amendments; or establish a comprehensive, dedicated legal framework to address biological invasions.

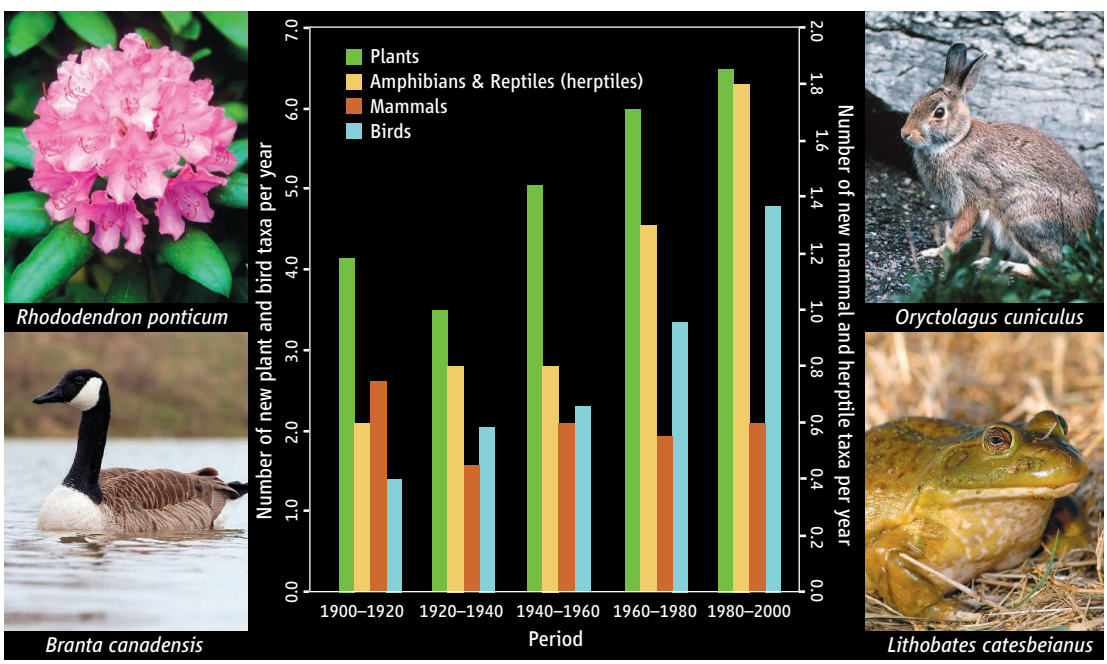

Alien taxa newly recorded as established in Europe per annum (*1*).

[1]The Bio-Protection Research Centre, Lincoln University, Post Office Box 84, Canterbury, New Zealand. [2]Institute of Botany, Academy of Sciences of the Czech Republic, CZ-252 43 Průhonice, and Department of Ecology, Charles University, CZ-128 01 Vinicná 7, Prague, Czech Republic. [3]Institute of Ecology and Evolution, University of Bern, Baltzerstrasse 6, CH-3012 Bern, Switzerland. [4]Estación Biológica de Doñana (EBD-CSIC), Avinguda Américo Vespucio, E-41092 Sevilla, Spain.

*Author for correspondence: philip.hulme@lincoln.ac.nz

Published by AAAS

Current legislative efforts to prevent introduction of invasive alien species are most effective at targeting intentional releases or where liabilities can be readily determined, e.g., pests and pathogens on plant and animal products. However, recent introductions are increasingly unintentional (*7*). Major gaps exist in the binding international regulatory framework especially as relates to hull fouling, air transport, tourism, pets and aquarium and garden species, live bait and plant seeds, and interbasin water transfers and canals.

One way that existing legislation could be adapted is through establishment of a "blacklist" of species prohibited from import and sale in Europe that would prioritize those species that pose the most significant threats. The EU has adopted such an approach in its Council Directive 2000/29/EC to protect against introduction and spread of organisms harmful to plants or plant products. This directive could form the basis for blacklisting a wider range of invasive pests in terrestrial and aquatic environments. Yet pan-European bodies have failed to agree on the criteria for listing species. The European and Mediterranean Plant Protection Organisation (EPPO) has listed several invasive plants as pests requiring official regulation because of their perceived threat to ecosystems and recommends its member countries take measures to prevent their introduction or spread and to manage established populations (*8*). Nevertheless, when EPPO risk assessments for several invasive plant species were submitted to the European Food Safety Authority (EFSA), the request to list them as official pests in Council Directive 2000/29/EC was declined (*9*, *10*). Although EFSA acknowledged that the species were probably invasive, further quantitative information on population dynamics, environmental drivers, introduction pathways, spatial distribution, and impacts was required. Yet, such additional data may not reduce the uncertainty in assessing risks. As a result, lengthy and costly steps are likely to be necessary to officially blacklist even a single species.

A further complication with blacklisting is that a significant proportion of alien species in Europe are native elsewhere on the continent—including half of all plants, a third of arthropods, and a quarter of the vertebrate species (*1*). A number of these European species include some of the worst aliens, e.g., Spanish slug, rabbit (*Oryctolagus cuniculus*), and rhododendron (*Rhododendron ponticum*). Blacklists may therefore need a regional or national focus. Several European countries have established their own national blacklists (*2*), but each uses different listing criteria based on qualitative expert opinion that do not match EFSA's requirements and thus could be challenged.

Legally binding blacklists supported by quantitative risk assessment may assist in the prevention of future threats, but current lists are reactive and include many species already established, often quite widely, in Europe (*8*). Although only ~10% of aliens established in Europe are known to have an economic or environmental impact, this still implies that there are >1000 species requiring proactive management (*3*). Europe does not have a particularly good record in managing alien species, with only 34 species (primarily vertebrates) successfully eradicated from one or more regions (*11*). Limited resources have often resulted in a piecemeal approach targeting local management, rather than a coordinated international effort.

If Europe is serious about addressing biological invasions, and especially the 2010 target, then it should support establishment of an indicator that quantifies actual responses, e.g., number and cost of national management activities against invasive species (*12*). In contrast to prevention, the regulatory and technical tools addressing eradication, control, or management of invasive species remain poorly developed (*13*).

Many of the policy and legislative needs identified for Europe are equally relevant to the U.S.A. where the Ecological Society of America has called for establishing a federal center to manage biological invasions that would parallel centers set up to tackle the threat of human diseases (*14*). Likewise, a new agency, the European Centre for Invasive Species Management (ECISM), could be established similarly to the European Centre for Disease Prevention and Control (ECDC) (*15*). ECISM would have a mission to identify, assess, and communicate current and emerging threats to the economy and environment posed by invasive species. It would bring together different elements relating to biological invasions that are currently dispersed among various European bodies, such as the European Environment Agency (monitoring and indicators), EFSA (risk assessment), and within different Directorates-General of the European Commission (environment, transport, agriculture, maritime affairs, and so on).

ECISM would ensure a broader European perspective that better integrates regulatory, scientific, and public outreach initiatives, not only by addressing preventative measures, but also by rapid response and management. Responsibilities could include providing high-level scientific advice, building a Europe-wide surveillance system, monitoring emerging threats in Europe to support rapid response, coordinating the European networking of bodies operating in the field of biological invasions, and communicating the scientific and technical outputs to stakeholders and the general public. ECISM would have no regulatory powers but would help develop new legislation addressing biological invasions.

Would such a proposal appeal to the Council of Europe and European Parliament? The need for coordinated action has been expressed at the highest political levels in Europe (*2*). Under the Czech Presidency of the EU, addressing the European Commission proposal for an EU strategy on invasive species is seen as a priority (*16*). Yet there are challenges. The cornerstone of the EU is the single market and the regulatory environment has been designed to remove technical barriers to the free movement of goods and people (*17*). Yet levels of invasion in European countries are highly correlated with national Gross Domestic Products and reflect levels of external trade and capital investment (*18*). Politicians may view additional legislation and regulation to address biological invasions as an impediment to economic growth. Tax-payers may similarly be resistant to additional costs, especially because only 2% of the European public feel biological invasions are important threats to biodiversity (*19*). Results from DAISIE may help better inform such opinions and highlight the scale of the problem in Europe. Costs of a specific agency such as ECISM, if run on a budget similar to ECDC's, would amount to <0.5% of the annual cost of biological invasions in Europe but could bring much greater dividends to the European economy and environment.

References and Notes

1. DAISIE, *Handbook of Alien Species in Europe* (Springer, Dordrecht, 2009).
2. European Commission (EC), *Towards an EU Strategy on Invasive Species* [COM(2008) 789, EC, Brussels 2008].
3. M. Vilà *et al.*, *Front. Ecol. Environ.*, 10.1890/080083, in press.
4. P. E. Hulme, *Issues Environ. Sci. Technol.* **25**, 56 (2007).
5. A. Balmford *et al.*, *Science* **307**, 212 (2005).
6. European Environment Agency (EEA), *Halting the Loss of Biodiversity by 2010: Proposal for a First Set of Indicators to Monitor Progress in Europe* (EEA, Copenhagen, 2007).
7. P. E. Hulme *et al.*, *J. Appl. Ecol.* **45**, 403 (2008).
8. EPPO A2 List of dangerous plant pests recommended for regulation, www.eppo.org/QUARANTINE/listA2.htm.
9. EFSA Scientific Panel on Plant Health, *EFSA J.* **468**, 1 (2007).
10. EFSA Scientific Panel on Plant Health, *EFSA J.* **539**, 1 (2007).
11. P. Genovesi, *Biol. Inv.* **7**, 127 (2005).
12. M. A. McGeoc *et al.*, *Conserv. Biol.* **20**, 1635 (2006).
13. P. E. Hulme, *J. Appl. Ecol.* **43**, 835 (2006).
14. D. M. Lodge *et al.*, *Ecol. Appl.* **16**, 2035 (2006).
15. ECDC, http://ecdc.europa.eu.
16. *Work Programme and Priorities of the Czech EU Presidency* (Czech Presidency of the EU, Government of the Czech Republic); www.eu2009.cz/en.
17. European Communities, *The Single Market for Goods* (EC, Brussels, 2007); http://ec.europa.eu/enterprise/regulation/goods/docs/single_mk_info_08/2007_5598_en.pdf.
18. P. E. Hulme, *J. Appl. Ecol.* **46**, 10 (2009).
19. Gallup Organisation, *Attitudes of Europeans Towards the Issue of Biodiversity* (EC, Brussels 2007).

10.1126/science.1171111

ECOLOGY

The Forgotten Megafauna

An expanded megafauna concept elucidates how extinctions of the largest vertebrates in any ecosystem have similar effects.

Dennis M. Hansen[1] and Mauro Galetti[1,2]

Large terrestrial vertebrates—called megafauna—play key roles in ecosystem dynamics by feeding on plants and by maintaining habitat heterogeneity (*1*). A global wave of megafauna extinctions occurred 50,000 to 10,000 years ago, when many large continental mammals were lost (*2*–*5*). Classical definitions of megafauna are based on such continental mammals and are variously given as animals larger than 44 kg (*6*) or above 1000 kg (*7*). Here, we argue that the megafauna concept should be extended beyond an absolute animal size to be context-dependent. In any given ecosystem, the largest vertebrates have ecosystem impacts that are similar on a relative scale to those of the largest vertebrates in another ecosystem: One ecosystem's mesofauna is another ecosystem's megafauna.

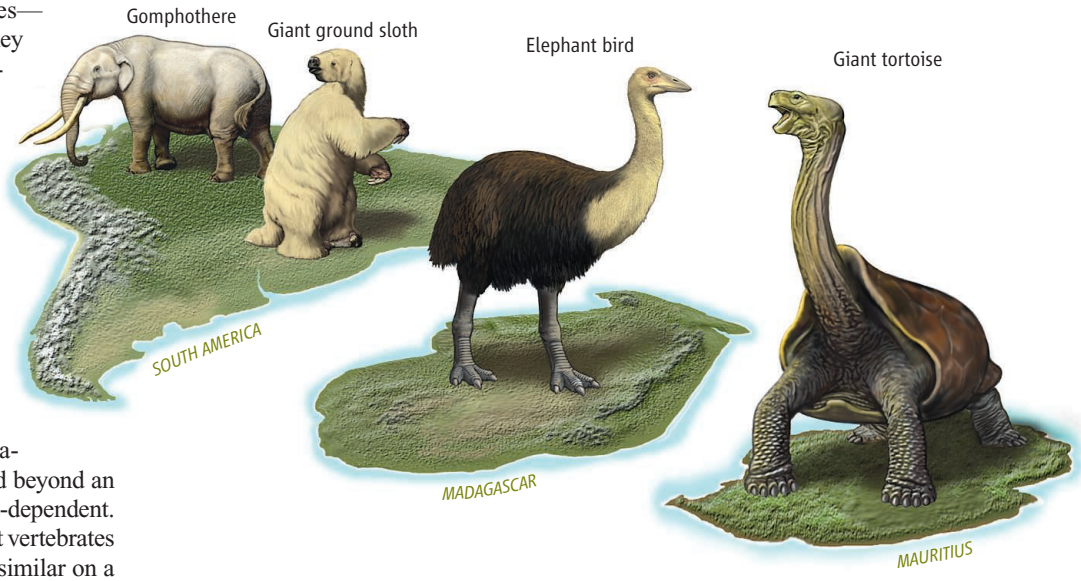

Scaling the megafauna. The magnitude of loss of frugivorous megafauna is currently most dramatic on islands, as illustrated by the smaller drawn sizes of the giant ground sloth and the gomphothere from South America, compared with the elephant bird in Madagascar and the giant tortoise of Mauritius. However, many continental regions are poised to catch up.

An ecosystem function that clearly illustrates this argument is animal-mediated seed dispersal. Here, the link between animal body mass and ecosystem function is straightforward: The larger the fruit-eating animal (frugivore), the larger the fruits it can consume. Thus, extinction-mediated "ecological shrinkage"—the loss of species interactions—in community-level seed dispersal roughly scales with frugivore body mass.

Scientists have argued that in continental Central and South America, the extinction of the classic mammalian megafauna—such as giant ground sloths and gomphotheres—caused disruption of seed dispersal for large fruits (*4*, *5*). However, on islands, the extinction of large birds and reptiles in the past two or three millennia has led to similar disruptions (*8*, *9*). In both locations the demographic and genetic consequences of large-vertebrate extinctions for plants are likely similar—for example, disruption of long-distance gene flow or changes in species composition (*10*, *11*). Yet, by the classic definitions, large insular vertebrates would not be considered megafauna.

To illustrate our point, we have examined tropical and subtropical faunas from three kinds of ecosystems: continental, continental islands, and oceanic islands. For each fauna, we compared the body masses of the largest extant frugivorous vertebrate—mammal, bird, or reptile—to the largest that has gone extinct since the late Pleistocene. On continents, the body masses of extant frugivores are an order of magnitude lower than those of extinct frugivores; in contrast, in some continental and oceanic islands, body masses of extant animals are two or even three orders of magnitude lower than those of their extinct predecessors (see the supporting online material).

For instance, the largest frugivores in South America were gomphoteres (7580 kg), whereas the largest living frugivores are the tapirs (300 kg). On the continental island of Madagascar, the role of largest frugivore has passed from the elephant bird (450 kg) to the radiated tortoise (10 kg). On Mauritius, giant tortoises weighing up to 100 kg were the largest native frugivores; today, the title goes to a fruitbat weighing only 0.54 kg. Thus, the loss of the island giants—tortoises, lizards, and flightless birds such as the dodo that were once found on many islands—has, in relative terms, led to a greater megafaunal downsizing than the extinction of even the largest gomphotheres in South America (see the figure).

Moreover, in the relatively species-poor and simple island ecosystems, cascading effects of megafaunal loss may manifest themselves faster and with more devastating results than in more complex continental ecosystems. For example, lost megafaunal seed-dispersal interactions on islands will not be compensated for by surviving frugivores, because they are too small. In continental ecosystems, there is a higher functional redundancy, with medium- and even small-sized species capable of filling at least part of the megafaunal niche (*12*).

Anthropogenic impacts are set to cause further extinctions among large vertebrates, with dramatic consequences for ecosystem dynamics (*11*). If all currently threatened vertebrate frugivores were to go extinct, the relative ecological shrinkage in many continental ecosystems would equal that of islands. For instance, if all threatened frugivores in South America were to go extinct, the largest remaining frugivore would be the howler monkey, weighing 9 kg—a factor of 700 less than the giant ground sloth. Even some islands

[1]Department of Biology, 371 Serra Mall, Stanford University, Stanford, CA 94305, USA. [2]UNESP-São Paulo State University, Department of Ecology, Rio Claro, São Paulo, Brazil 13506-900. E-mail: dmhansen@stanford.edu

Published by AAAS

stand to suffer further losses; in Mauritius, the largest nonthreatened native frugivore is the gray white-eye, a bird weighing a mere 0.009 kg (see the supporting online material).

An extended megafauna concept has the potential to promote synergy between otherwise disparate research and conservation foci, and to facilitate broader syntheses of ecosystem-level effects of extinctions of the largest vertebrates and the resulting ecological shrinkage. It is high time to more fully understand and ameliorate the recent and ongoing losses of all "the hugest, and fiercest, and strangest forms" (*13*).

References and Notes

1. R. Dirzo, A. Miranda, in *Plant-Animal Interactions: Evolutionary Ecology in Tropical and Temperate Regions*, P. W. Price, T. M. Lewinshon, G. W. Fernandes, W. W. Benson, Eds. (Wiley, New York, 1991), pp. 273–287.
2. P. L. Koch, A. D. Barnosky, *Ann. Rev. Ecol. Evol. Syst.* **37**, 215 (2006).
3. A. D. Barnosky *et al.*, *Science* **306**, 70 (2004).
4. D. H. Janzen, P. S. Martin, *Science* **215**, 19 (1982).
5. P. R. Guimaraes Jr., *et al.*, *PLoS ONE* **3**, e1745 (2008).
6. P. S. Martin, R. G. Klein, *Quaternary Extinctions: A Prehistoric Revolution* (Univ. of Arizona Press, Tucson, 1995).
7. R. N. Owen-Smith, *Megaherbivores: The Influence of Very Large Body Size on Ecology* (Cambridge Univ. Press, New York, 1988).
8. H. J. Meehan *et al.*, *J. Biogeogr.* **29**, 695 (2002).
9. D. M. Hansen *et al.*, *PLoS ONE* **3**, e2111 (2008).
10. R. G. Colevatti *et al.*, *Mol. Ecol.* **12**, 105 (2003).
11. S. J. Wright *et al.*, *Biotropica* **39**, 289 (2007).
12. W. Hallwachs, in *Frugivores and Seed Dispersal*, A. Estrada, T. H. Fleming, Eds. (Kluwer, Boston, 1986), pp. 285–304.
13. A. R. Wallace, *The Geographical Distribution of Animals* (Harper, New York, 1876).

14. Supported by the Velux Foundation (D.M.H.), Fundação de Amparo à Pesquisa do Estado de São Paulo (M.G.), and Conselho Nacional de Desenvolvimento Científico e Tecnológico (M.G.).

Supporting Online Material

www.sciencemag.org/cgi/content/full/324/5923/42/DC1
Fig. S1
Table S1
References

10.1126/science.1172393

COMPUTER SCIENCE

Automating Science

Computers with intelligence can design and run experiments, but learning from the results to generate subsequent experiments requires even more intelligence.

David Waltz[1] and Bruce G. Buchanan[2]

The idea of automating aspects of scientific activity dates back to the roots of computer science, if not to Francis Bacon. Some of the earliest programs automated the processes of creating ballistic tables, cracking cyphers, collecting laboratory data, etc., by carrying out a set of instructions from start to finish. Starting with DENDRAL in the 1960s (*1*), artificial intelligence programs such as Prospector (*2*), Bacon (*3*), and Fahrenheit (*4*) automated some of the planning, analysis, and discovery portions of the scientific enterprise. However, most of these programs were still designed to run a calculation to completion, produce an answer, and then stop. They did not fully "close the loop" in the sense of examining the results of their actions, deciding what to try next, potentially cycling forever.

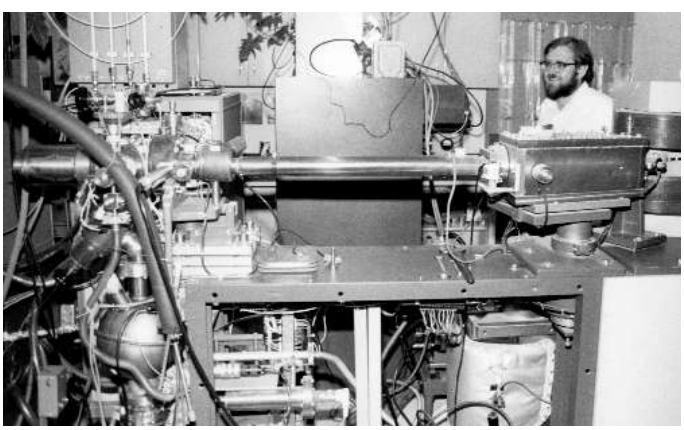

Semiautomated. Scientists at Stanford's Instrumentation Research Laboratory (circa 1970) linked a gas chromatograph and high-resolution mass spectrometer to computers to automate studies of biological fluids, meteorites, and other materials. Stanford's DENDRAL Project experimented with automated interpretation of the data and experiment planning to specify nuclear magnetic resonance or infrared data that would resolve ambiguities in the mass spectral data.

Two reports on pages 85 and 81 of this issue push the boundaries of automatic scientific experimentation and discovery. King *et al*. (*5*) describe a robotic system for running biological experiments, evaluating their results, and deciding what experiments to try next. Schmidt and Lipson (*6*) describe their work on discovering compact equations that characterize complex nonlinear dynamical systems, derived from visual observation of such systems. As these reports show, it is possible for one computer program to step through the activities needed to conduct a continuously looping procedure that starts with a question, carries out experiments to answer the question, evaluates the results, and reformulates new questions.

The main goals of automation in science have been to increase productivity by increasing efficiency (e.g., with rapid throughput), to improve quality (e.g., by reducing error), and to cope with scale, allowing scientific treatment of topics that were previously impossible to address. Tycho Brahe spent a lifetime recording observations that allowed Johannes Kepler to formulate Kepler's laws of planetary motion; today, computer-controlled data collection is commonplace and necessary for both experimental and observational science. Automating many activities beyond data collection offers even more benefits.

In the near term, a useful metaphor is to consider computers as intelligent assistants. Some assistants gather data and attend to such tasks as noise filtering, data smoothing, outlier rejection, and data storage. Other assistants are specialists at statistical analysis, still others at bench work. This metaphor has driven many research projects over the past several decades and has led to many of the most successful applications of computers.

An early articulation of this metaphor is Joshua Lederberg's effort at Stanford University School of Medicine to develop an automated biomedical laboratory to examine the soil of Mars for traces of life, as part of the 1975 Viking mission deployed by the U.S. National Aeronautics and Space Administration. The robot assistant Lederberg designed, with engineer Elliott Levinthal, consisted of a conveyor belt that scooped up samples of Martian soil and deposited them within a computer-controlled mass spectrometer. Each soil sample was bombarded with electrons, producing a fragmentation pattern that sorted the charged particles (ions) according to their mass. This pattern was transmitted to Earth, where scientists could analyze it for

CREDIT: ROBERT K. LINDSAY

[1]Center for Computational Learning Systems, Columbia University, New York, NY 10115, USA. [2]Computer Science Department, University of Pittsburgh, Pittsburgh, PA 15260, USA. E-mail: buchanan@cs.pitt.edu; waltz@ccls.columbia.edu

evidence of organic compounds and microbial life. In addition, part of Lederberg's vision for this instrumentation was also to close the loop by performing the analysis onboard the spacecraft to inform a next round of experiments without waiting for Earth-based instructions. This was, in part, the motivation for the DENDRAL project at Stanford in which an intelligent assistant hypothesized the molecular structure of organic molecules on the basis of mass spectrometry data (see the figure).

Intelligent assistants are currently numerous and well integrated into the activities of science and industry. In the longer term, however, new kinds of computer programs are needed to cope with the sheer volume of data that can be collected automatically (*7*–*9*) and with the volume of relevant information available in the literature.

Closing the loop from experiment design and data collection to hypothesis formation and revision, and from there to new experiments, will be one important way to cope with the volume of data. A new wave of programs will test the efficacy of using computers in closed-loop fashion and will explore the questions of which activities can be automated, and which ones we would even want to automate. Even for the relatively straightforward task of data collection, there are myriad questions to answer before streaming data from a laboratory instrument into a computer, including why particular data are being collected, which variables should be measured, and which instrument will measure them. If no such instrument exists, can it be designed and built?

Beyond coping with the volume of data, however, computers need to be called into service to cope with the volume of information and background knowledge relevant to any scientific question. Search engines and automated libraries will return more articles in response to a query than anyone has time to read. (For example, Google returns about 200,000 hits for the phrase "laboratory automation" and 10 million hits for the pair of terms "science" + "automation".) Programs that have the intelligence to read and interpret the online information for us will contribute to the next level of closing the loop. This is already an active area of computer science research (*10*).

For any such program to select the most cost-effective and informative hypotheses, prune hypotheses that cannot be realized experimentally, avoid repeating unsuccessful experiments that have already been tried by others, etc., it must include a rich model of the entire process of the loop, as well as knowledge of the specific scientific area being automated. This will increasingly involve a substantial modeling effort, as is already required for planning and interpreting experiments in systems biology or weather and climate.

For the foreseeable future, the prospect of using automated systems as assistants holds vast promise as these assistants are becoming not only faster but much broader in their capabilities—more knowledgeable, more creative, and more self-reflective. Human-machine partnering systems that match the tasks to what each partner does best can potentially increase the rate of scientific progress dramatically, in the process revolutionizing the practice of science and changing what scientists need to know.

References and Notes

1. R. K. Lindsay, B. G. Buchanan, E. A. Feigenbaum, J. Lederberg, *Applications of Artificial Intelligence for Organic Chemistry: The DENDRAL Project* (McGraw-Hill, New York, 1980).
2. R. O. Duda, J. Gaschnig, P. E. Hart, in *Expert Systems in the Microelectronic Age*, D. Michie, Ed. (Edinburgh Univ. Press, Edinburgh, 1979), pp. 153–167.
3. P. Langley, *Cognit. Sci.* **5**, 31 (1981).
4. J. M. Żytkow, J. Zhu, A. Hussam, in *Proceedings of the 8th National Conference on Artificial Intelligence* (AAAI Press, Menlo Park, CA, 1990), pp. 889–894 (www.aaai.org/Papers/AAAI/1990/AAAI90-133.pdf).
5. R. D. King *et al.*, *Science* **324**, 85 (2009).
6. M. Schmidt, H. Lipson, *Science* **324**, 81 (2009).
7. C. Anderson, *Wired* 16.07, June 2008 (www.wired.com/science/discoveries/magazine/16-07/pb_theory).
8. A. Srinivasan, S. H. Muggleton, M. J. E. Sternberg, R. D. King, *Artif. Intell.* **85**, 277 (1996).
9. S. Muggleton, *Nature* **440**, 409 (2006).
10. Machine Reading: Papers from the 2007 AAAI Spring Symposium (www.aaai.org/Library/Symposia/Spring/ss07-06.php).

11. Supported in part by NSF grant 0738341 (B.G.B.) and NIH grant 5 U54 CA 121852-03 C11, and by Consolidated Edison Corp. grant CU08-8987 (D.W.).

10.1126/science.1172781

CHEMISTRY

Rethinking Water Splitting

A metal complex splits water into hydrogen and oxygen through an unusual series of steps.

Richard Eisenberg

Department of Chemistry, University of Rochester, Rochester, NY 14627, USA. E-mail: eisenberg@chem.rochester.edu

Projections of global energy needs for sustainable development suggest a nearly 50% increase by 2030 (a mere 21 years hence) (*1*). This increase can be met satisfactorily by only one kind of alternative energy—the Sun. One approach to convert solar energy into a fuel is to use it to split water into H_2 and O_2. A number of strategies for the visible light–driven splitting of water are being pursued with varying levels of success. On page 74 of this issue, Kohl *et al.* (*2*) describe a very different reaction system for water splitting that uses light but also has thermally driven steps. The basis of this approach, in which key steps involve ligand modification, shows that reactions that harvest solar energy can be found among the unlikeliest of compounds.

Research in solar energy conversion follows three principal strategies. The first is the direct conversion of light into electrical energy, as in the photovoltaic (PV) devices that are currently being produced and installed around the world. Challenges here include increasing the efficiency and durability of such devices while reducing their cost to make them competitive with cheaper but environmentally problematic coal-fired power plants. The Energy Information Administration of the U.S. Department of Energy projects that global use of coal for electricity will grow relative to other sources in the next 21 years (*1*). Considerable research on dye-sensitized solar cells (*3*, *4*) has made them an interesting alternative to traditional silicon-based PVs, with demonstration units being deployed. Efforts also continue for new PV devices based on thin-film designs that use either amorphous silicon, cadmium telluride, copper indium gallium selenide, or organic charge-transfer compounds on flexible supports that can be manufactured on a massive scale (*5*, *6*).

The second strategy is to use nature's photosynthetic apparatus to produce biofuels from plants or waste agricultural by-products. Some of these approaches, such as corn-to-ethanol, are marginal in terms of economic and climate-change benefits (*7*). Other biomass sources, such as switchgrasses and agricultural by-products, may be economically more viable and have a sufficiently high positive net energy balance. To be feasible, methods must be developed for the facile catalytic

or enzymatic breakdown of cellulose into its individual sugar units and the rapid conversion of those units into liquid fuels.

The third approach involves artificial (laboratory-designed) photosynthesis. Here, the splitting of water is the major reaction under study (*4*). The key photosynthetic steps in such a system are charge-transfer (CT) excitation, electron-hole separation by electron transfer reactions, charge accumulation, and catalysis. In a simplified diagram of such a system (see the figure, panel A), photoexcitation and charge transfer move an electron to a more reducing electrochemical level, leaving behind an oxidizing or electron-accepting hole. In the nonphotochemical electron transfer steps that follow, electrons move downhill and holes rise to drive the chemistry that occurs at catalytic centers

Because the electrons and holes separate in this scheme, water splitting can be divided into its two half-cell reactions that either consume or generate electrons, and each reaction can be investigated and optimized independently. In such studies, a sacrificial electron donor or acceptor is used to balance the half reaction (sacrificial in this context means that the compound decomposes once it donates or loses an electron). Research successes have been reported for both half-reactions. Although H_2 has been generated photochemically (*8*–*10*), the efficiency and durability of molecularly designed systems are far from effective levels for practical use. The formation of O_2 is even more difficult, because the reaction involves the loss of four electrons and four H^+ units in multiple steps that must be carefully choreographed to maintain charge balance and avoid going through high-energy oxygen intermediates (*11*–*13*).

The ruthenium (Ru) complex for water splitting reported by Kohl *et al.* builds upon several disparate observations they have made that are unrelated to other studies for H_2 and O_2 generation. The first is the reversible protonation of a "pincer" ligand arm that was bound to a ruthenium(II) ion; the facility of this usually difficult process is made possible through aromatization and dearomatization of the central ring of the pincer ligand (*14*). A pincer ligand coordinates to a metal through three points of attachment; the first and third are on opposite sides of the metal, or trans to each other, and the central or middle attachment is at 90°, or cis, to the other two. The added proton becomes a captive source of H^+ that can react with a ruthenium-bound hydride to yield H_2 by a hetero coupling reaction ($H^+ + H^- \rightarrow H_2$).

The second observation is that H_2O can add to a Ru pincer hydride complex by protonating the ligand arm (not the metal) and coordinating OH^- to the Ru metal center. Such addition reactions often change the oxidation state of the metal, but in this case, Ru remains in the 2+ oxidation state. The third observation is a reaction of the Ru pincer complex having hydride and hydroxide ligands—RuH(OH)(pincer)—with another H_2O molecule (see the figure, panel B). This reaction proceeds upon heating by initial H_2 liberation through hetero coupling and subsequent addition of H_2O as described above to form the dihydroxide complex *trans*-Ru(OH)$_2$(pincer).

The fourth observation is that in a photochemical step, *trans*-Ru(OH)$_2$(pincer) eliminates the higher-energy product hydrogen peroxide (H_2O_2) intramolecularly. Rapid disproportionation of 2 H_2O_2 molecules into O_2 and 2 H_2O completes the process of splitting water. Although the detailed mechanism of O_2 formation in more conventional water-splitting efforts, as well as in natural photosynthesis, remains a matter of ongoing study, it does not proceed via H_2O_2, which is a high-energy species (*11*, *13*).

The Kohl *et al.* system is notable in that the normally redox active metal ion maintains the same oxidation state throughout the course of the overall reaction. The heterolytic coupling step that forms H_2 is most unusual in how it involves the pincer ligand, but it connects to recent studies of H_2 formation in model hydrogenase compounds that are also thought to form hydrogen by hetero coupling of H^+ and a formal hydride H^- (*15*, *16*).

The water-splitting scheme that Kohl *et al*. describe presents challenges. It is not yet catalytic, and it has an uncertain energy balance depending on how the thermal steps are driven. Also, the system is not very durable because the phosphine arm of the pincer becomes oxygenated. However, the fact that a relatively simple molecular system can accomplish water splitting with steps not conceived of or brought together by other studies on water splitting is stimulating and thought-provoking.

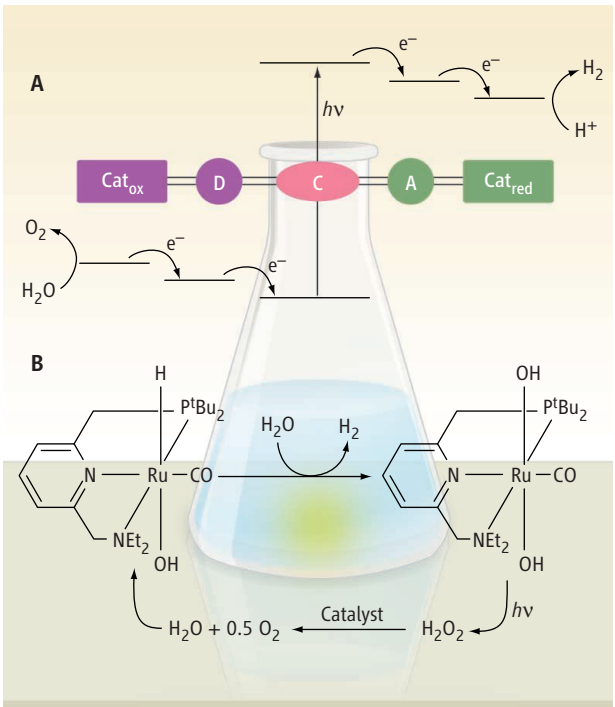

Two ways to split water. (**A**) In a simplified photosynthetic scheme, the absorption of a photon with energy *hν* by a chromophore C process generates a photoexcited electron and a hole state. Charge transfer of the electron is facilitated by the electron acceptor A and of the hole by the electron donor D. Proton reduction and hydrogen evolution occurs at Cat_{red}, which accepts electrons, and water oxidation and oxygen evolution occurs at Cat_{ox}, which accepts holes. The vertical scale qualitatively represents the electrochemical potential that drives the reactions. (**B**) The scheme of Kohn *et al*. departs from this scheme in a thermally driven reaction that generates hydrogen, and a subsequent photolytic step creates oxygen through decomposition of a hydrogen peroxide product. ᵗBu, tert-butyl; Et, ethyl.

References

1. Energy Information Administration, *International Energy Outlook 2008*; www.eia.doe.gov/oiaf/ieo (U.S. Department of Energy, Washington, DC, 2008).
2. S. Kohl *et al*., *Science* **324**, 74 (2009).
3. M. Grätzel, *Inorg. Chem.* **44**, 6841 (2005).
4. J. H. Alstrum-Acevedo, M. K. Brennaman, T. J. Meyer, *Inorg. Chem.* **44**, 6802 (2005).
5. M. D. Archer, *Series on Photoconversion of Solar Energy*, M. D. Archer, A. J. Nozik, Eds. (World Scientific, Singapore, 2008), vol. 3, pp. 1–29.
6. J. Wohlgemuth, *Kirk-Othmer Encyclopedia of Chemical Technology* (Wiley, New York, ed. 5, 2007), vol. 23, pp. 32–52.
7. W. Schultz, *Chem. Eng. News*. **85**, 12 (2007).
8. A. J. Esswein, D. G. Nocera, *Chem. Rev.* **107**, 4022 (2007).
9. P. Du, K. Knowles, R. Eisenberg, *J. Am. Chem. Soc.* **130**, 12576 (2008).
10. A. Fihri *et al*., *Angew. Chem. Int. Ed.* **47**, 564 (2008).
11. F. Liu *et al*., *Inorg. Chem.* **47**, 1727 (2008).
12. V. L. Pecoraro, W.-Y. Hsieh, *Inorg. Chem.* **47**, 1765 (2008).
13. R. Eisenberg, H. B. Gray, *Inorg. Chem.* **47**, 1697 (2008).
14. J. Zhang, G. Leitus, Y. Ben-David, D. Milstein, *J. Am. Chem. Soc.* **127**, 10840 (2005).
15. F. Gloaguen, T. B. Rauchfuss, *Chem. Soc. Rev.* **38**, 100 (2009).
16. G. M. Jacobsen *et al*., *Energy Environ. Sci.* **1**, 167 (2008).

10.1126/science.1172247

MATERIALS SCIENCE

Building a Better Nano-Biped

Controlled and coupled chemical reactions provide the basis for an autonomous DNA walker.

William Sherman

Among the many molecular motors that occur in nature, perhaps the most striking ones are the bipedal walkers such as the kinesin and dynein proteins (*1*). These molecules, together with the microtubules upon which they walk, provide cells with mechanisms to transport macromolecules and organelles through the viscous internal environment of the cell. On page 67 of this issue, Omabegho *et al.* (*2*) present a remarkable DNA-based walking system that promises to open the door to a wide assortment of experiments and applications in nanotechnology.

Splitting off from attempts to adapt naturally occurring protein motors to nanotechnology applications (*3*, *4*), DNA-based walkers have generally used one of two underlying mechanisms. Some walkers have used special DNA sequences that cut the nucleic acid footholds, forcing the walker to reach forward for new footholds (*5*, *6*). Such walkers are difficult to steer, however, as they move toward any foothold that is within reach. Other walkers have used a strand displacement system developed by Yurke *et al.* where two strands that are imperfectly hybridized via Watson-Crick base-pairing can be separated by the introduction of a perfect match for one of the strands (*7*). This is particularly advantageous because all the reactions are directed by DNA base sequences, and thus multiple versions of the walkers can be designed to function independently, without interference while operating in the same environment (*8*).

This strategy has proven remarkably fruitful. It led first to nonautomated walkers, where an operator would add strands of DNA to the system to direct the movement (*9*, *10*). Then it led to automated but random walkers (*11*). Recently, the first automated, directed walker was produced by Green *et al.* (*12*). In their system the footholds overlap in such a way that when the leading foot lands, it catalyzes the detachment of the trailing foot. The admirable economy of their design comes at a price: There is no portion of the track that is not used as a foothold. This makes it difficult to make the track rigid for generating the linear motion that is the hallmark of an effective walking system.

Omabegho *et al.* have created a system where, as each foot lands, it sends a signal to the trailing foot that catalyzes its release. One of the strands of DNA that carries that signal is tethered onto the track at the midpoint between the leading foot that is sending the signal, and the trailing foot that is receiving it. This tethering targets the signal so it can only reach the desired foothold, and thus provides directionality to the walk (see the figure, panels A to D). As only some portions of the track are used as footholds, the rest of the track has been constructed from rigid, modular components that can easily be extended or incorporated into larger and more complex assemblies.

Omabegho *et al.* have made several adjustments that make it easier to verify proper operation of the walker. To the end of each foothold, they have attached psoralen molecules that, when exposed to ultraviolet light, can form a covalent connection between the two strands of a DNA double helix. Whereas the other double helices in the structure will melt apart or "denature" when heated or treated with suitable chemicals, the strands cross-linked via psoralen will stay connected, and the resulting structures will move with a characteristically slow speed through a gel run under denaturing conditions. This method allows observation of which foothold the walker is standing on.

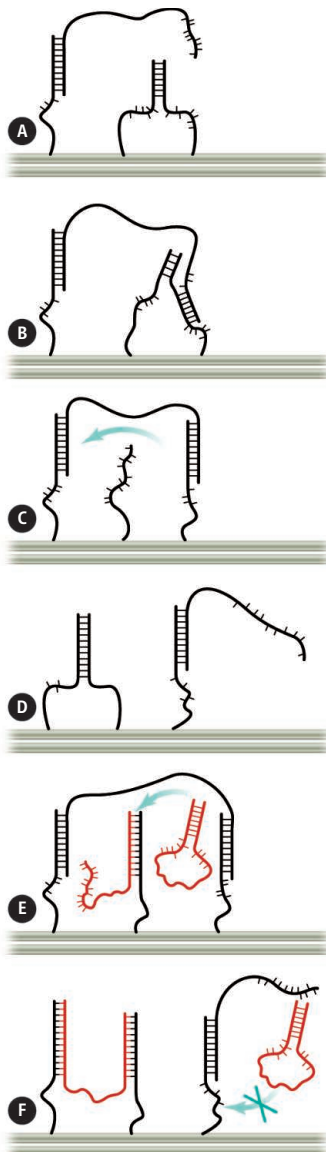

Strolling out. Coordinating the feet of a nanowalker: a simplified view of the walker taking one step. (**A**) The walker has one foot on the track and the other foot dangling free. (**B**) The dangling foot diffuses over to the next foothold and starts hybridizing to it. This releases one end of the signaling strand, which is then free (**C**) to diffuse back to the trailing foot, which it then detaches from the track (**D**). In the actual experiment of Omabegho *et al.* (*2*), the signaling strand must first open up a hairpin strand of DNA from solution (**E**), which then releases the trailing foot (**F**).

For additional control, the signaling system has been broken up into two parts. When it is released, the signal strand tethered to the track hybridizes to a DNA "hairpin" strand floating in solution; that strand in turn catalyzes the release of the trailing foot (panels E and F). One might expect these hairpin strands to catalyze the undesired detachment of feet from the track, but Omabegho *et al.* show that this occurs only very slowly over the course of an hour-long experiment. The folded hairpin structure is opened efficiently by the signaling strand only when it has a free, single-stranded end (*13*).

The track alternates between two footholds with distinct base sequences. The walker can take two and a half steps across the four footholds in the current system. For a longer track, the same sequences could be repeated, and the walker should continue its progress. Unfortunately, with the current design, the walker successfully takes a complete step forward only about 74% of the time; extended walks will require designs with improved consistency.

The system provides a detailed view of the progress of the walker. By withholding hairpin strands or making minor sequence variations in the track, the walker can be frozen in any of four different states over the course of two and a half steps. Psoralen cross-linking and radioactive labeling then allow the observation of the disposition of each of the main interacting strands

Center for Functional Nanomaterials, Brookhaven National Laboratory, Upton, NY 11973, USA. E-mail: wsherman@bnl.gov

Published by AAAS

in the system in each state.

Omabegho *et al*. have constructed an automated molecular walker with an unprecedented level of control and versatility. The movement of the walker is regulated by the presence of hairpin strands in solution. This opens up possibilities for the walker, or sets of similar walkers with different sequences, to interface with DNA-based computational circuits such as those designed by Seelig *et al*. (*14*). Indeed, the system is already smart enough to walk until it reaches the end of the track and then stop there. This is a valuable tool for working with nanoscale systems of unpredictable size. The present nanowalker will no doubt provide a launching point for the development of many complex nanomachines and nanosystems.

References

1. A. Gennerich, R. Vale, *Curr. Opin. Cell Biol.* **21**, 59 (2009).
2. T. Omabegho, R. Sha, N. C. Seeman, *Science* **324**, 67 (2009).
3. H. Hess *et al*., *Nano Lett.* **5**, 629 (2005).
4. S. Sahu, T. H. Thomas, H. Labean, J. H. Reif, *Nano Lett.* **8**, 3870 (2008).
5. R. Pei *et al*., *J. Am. Chem. Soc.* **128**, 12693 (2006).
6. Y. Tian, Y. He, Y. Q. Chen, P. Yin, C. D. Mao, *Angew. Chem. Int. Ed*. **44**, 4355 (2005).
7. B. Yurke *et al*., *Nature* **406**, 605 (2000).
8. S. Liao, N. C. Seeman, *Science* **306**, 2072 (2004).
9. W. B. Sherman, N. C. Seeman, *Nano Lett.* **4**, 1203 (2004).
10. J. S. Shin, N. A. Pierce, *J. Am. Chem. Soc.* **126**, 10834 (2004).
11. P. Yin, H. Choi, C. Calvert, N. A. Pierce, *Nature* **451**, 318 (2008).
12. S. Green, J. Bath, A. J. Turberfield, *Phys. Rev. Lett.* **101**, 238,101 (2008).
13. M. T. Kumara, D. Nykypanchuk, W. B. Sherman, *Nano Lett.* **8**, 1971 (2008).
14. G. Seelig, D. Soloveichik, D. Y. Zhang, E. Winfree, *Science* **314**, 1585 (2006).

10.1126/science.1172136

DEVELOPMENT BIOLOGY

Turnover After the Fallout

Human cardiac muscle cells slowly renew into adulthood, a potential that may be therapeutically exploited.

Charles E. Murry[1] and Richard T. Lee[2]

Heart disease is the leading cause of death worldwide. One reason is that the heart is one of the least regenerative organs in the human body. When cardiac muscle is lost—for example, through myocardial infarction (heart attack)—the heart heals principally though formation of scar tissue (*1*). As a result, contractile function declines, and patients often progress to heart failure. Absence of regeneration in the heart has been attributed to the inability of muscle cells (myocytes) to undergo cell division, coupled with the absence of a muscle-producing stem cell population in the heart. Although the heart cannot effect whole-scale tissue regeneration, there is mounting evidence that some myocyte repopulation may occur. On page 98 in this issue, Bergmann *et al*. (*2*) provide strong evidence that cardiac myocytes can repopulate in the human heart, and they exploit one of the worst man-made environmental disasters to address this question.

During human fetal life, there is extensive proliferation of cardiomyocytes. From birth to adulthood, heart mass increases by about 30- to 50-fold (*3*). The nonmyocyte populations in the heart, such as vascular and connective tissue cells, contribute many new cells during postnatal growth. By contrast, cardiomyocyte proliferation slows dramatically around the time of birth, and most of the postnatal increase in cardiomyocyte mass comes from hypertrophy (increase in cell size) rather than cell division (*4*). But lack of cell division is not due to the absence of DNA synthesis. Over the first decade of life, cardiomyocytes often undergo a final round of DNA synthesis and nuclear division without cell division, resulting in ~25% of human cardiomyocytes being binucleated (*5*). Cardiomyocytes also retain the ability to undergo DNA synthesis without nuclear division. As a result, most cardiomyocyte nuclei are polyploid, containing twice or even higher multiples of the normal content of DNA. Nuclear ploidy increases over the first decade of life, after which increased ploidy appears to be driven principally by the heart's workload (*6*).

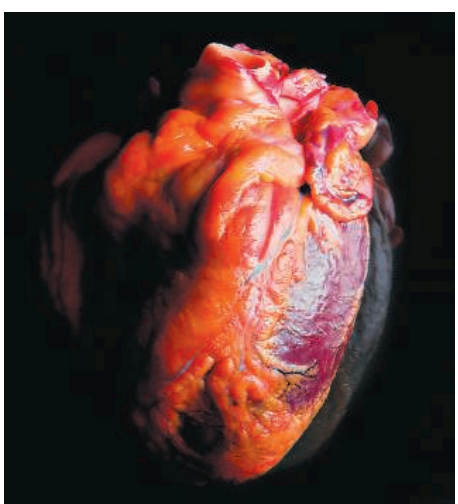

CREDIT: MARK ALBERHASKY/ALAMY

Heart regeneration. Cardiomyoctes turn over at an estimated rate of ~1% per year at age 20, declining to 0.4% per year at age 75, according to Bergmann *et al.* At age 50, 55% of human cardiomyocytes remain from birth, while 45% were generated afterward.

Slow cell turnover is a challenging process to study, and assays for labile populations, such as short-term DNA labeling, typically show near-background levels in the heart. To define the kinetics of cardiomyocyte turnover in human hearts, Bergmann *et al*. used a clever system based on radiocarbon dating of DNA. The DNA of all plant and animal cells incorporated high concentrations of carbon-14 released into the atmosphere by aboveground nuclear testing during the Cold War, and this unfortunate episode provides a unique opportunity to test cell population dynamics in human tissues. For people born before the tests, which began in the years following World War II and continued until the Limited Nuclear Test Ban Treaty in 1963, postnatal cell turnover incorporated carbon-14 into the DNA of cells that divided after the carbon-14 pulse from nuclear testing; for those born during or after the tests, cell turnover should decrease the carbon-14 concentrations. By comparing the age of the cardiomyocyte DNA to the patient's chronological age, one can estimate the extent to which the cardiomyocyte population has turned over.

Bergmann *et al*. applied this approach to DNA from unsorted nuclei (myocytes plus nonmyocytes), and showed that the mean age of the whole heart's DNA was substantially younger than the patient. Fluorescent staining of troponin—a contractile protein that the authors discovered also exists in cardiomyocyte nuclei—permitted separation of the mixed

[1]Departments of Pathology and Bioengineering, Center for Cardiovascular Biology, Institute for Stem Cell and Regenerative Medicine, University of Washington, Seattle, WA 98109, USA. [2]Cardiovascular Division, Department of Medicine, Brigham and Women's Hospital, Harvard Medical School, Partners Research Facility, Cambridge, MA 02139, USA. E-mail: murry@u.washington.edu, rlee@partners.org

nuclei for radiocarbon dating. As expected, DNA from the nonmyocyte nuclei was substantially younger than the patient, probably indicating steady turnover of endothelial cells and/or fibroblasts. Importantly, the cardiomyocyte nuclear DNA also was younger than the patient's chronological age, indicating substantial postnatal DNA synthesis. In patients born before the Cold War, the concentration of carbon-14 in their cardiomyocyte DNA exceeded the atmospheric concentration of carbon-14 at the time of their birth, whereas patients born during or after the atmospheric testing had a lower concentration of carbon-14. These findings convincingly establish that human cardiomyocytes synthesize DNA after birth. Binucleation of cardiomyocytes is essentially complete by age 10 (*5*), and patients who were adults at the time nuclear tests began still incorporated carbon-14 into their cardiomyocyte DNA.

Polyploidy was a more difficult issue to rule out. To definitively address this, Bergmann *et al*. painstakingly sorted cardiomyocyte nuclei by DNA content, and carbon dated only nuclei that had a single complement of chromosomes—that is, were diploid rather than polyploid. This subset of cardiomyocyte nuclei still had younger DNA than the patient's age. These data indicate that postnatal human cardiomyocytes synthesize DNA in a manner that cannot be explained by multinucleation or polyploidy, leaving birth of new cardiomyocytes as the most likely explanation.

Bergmann *et al*. also suggest, through mathematical modeling, that cardiomyocyte renewal is an age-dependent process, with rates of ~1% per year at age 20, declining to 0.4% per year at age 75. With this model, most cardiomyocytes will not be exchanged over the course of a normal human life span. For example, at age 50, 55% of cardiomyocytes would be present from birth and 45% would have been generated after birth. By contrast, nonmyocytes in the heart turn over at an estimated rate of 18% per year and have a mean age of only 4 years. It is interesting to compare these data with those obtained through conventional studies of DNA synthesis in mouse hearts. A 4-hour thymidine-labeling experiment showed DNA synthesis in 0.0005% of adult ventricle cardiomyocyte nuclei (*7*, *8*). Although this is barely above background, calculation [0.0005% × 365 days × (24 hours/4 hours)] yields a renewal rate of 1.1% of cardiomyocytes per year. This closely matches the findings of Bergmann *et al*. in the young adult human heart, suggesting that these mouse data may reflect human cell turnover.

The study by Bergmann *et al*. reveals that human cardiomyocytes are long-lived cells and difficult to replace, dispelling previous suggestions of widespread human cardiomyocyte repopulation. On the other hand, even though cardiomyocyte turnover is low in the adult heart, the fact that it occurs at all suggests that it can potentially be therapeutically exploited. This raises several issues. Having defined the population dynamics for normal hearts in homeostasis, what is the heart's response to injury? Cardiovascular diseases such as infarction or pressure overload will likely increase cardiomyocyte repopulation, but this must be tested experimentally. Another question is the origins of new cardiomyocytes—do they come from preexisting cardiomyocytes, or are they generated from stem cells? Thus far, genetic fate-mapping experiments in mice indicate that cardiomyocytes can be replaced following cardiac injury from a progenitor population, although, like many adult progenitor cells, cardiomyocyte progenitors may not be continuously differentiating into mature cardiomyocytes at a high rate during normal life (*9*). If we can identify these progenitors and the pathways that control their activation and differentiation, or factors promoting cell cycle reentry in existing cardiomyocytes, it may be possible to bolster cardiomyocyte repopulation and prevent the progression of heart failure.

References

1. M. A. Laflamme, C. E. Murry, *Nat. Biotechnol.* **23**, 845 (2005).
2. O. Bergmann *et al.*, *Science* **324**, 98 (2009).
3. P. Gruenwald, H. N. Minh, *Am. J. Clin. Pathol.* **34**, 247 (1960).
4. P. Ahuja *et al.*, *Physiol. Rev.* **87**, 521 (2007).
5. G. Olivetti *et al.*, *J. Mol. Cell. Cardiol.* **28**, 1463 (1996).
6. C. P. Adler, H. Friedburg, *J. Mol. Cell. Cardiol.* **18**, 39 (1986).
7. M. H. Soonpaa, L. J. Field, *Am. J. Physiol.* **272**, H220 (1997).
8. H. Nakajima *et al.*, *Circ. Res.* **94**, 1606 (2004).
9. P. C. Hsieh *et al.*, *Nat. Med.* **13**, 970 (2007).

10.1126/science.1172255

CHEMISTRY

Just a Dream—or Future Reality?

Hubert A. Gasteiger[1] and Nenad M Marković[2]

Advances in catalyst development offer hope for commercially viable hydrogen fuel cells.

Over the past decade, vast resources have been devoted to developing proton exchange membrane (PEM) fuel cells that use hydrogen fuel and oxygen from the air to produce electricity, for example, for automotive propulsion. Vehicle test data suggest that the 2009 U.S. Department of Energy targets for hydrogen storage—a 250-mile range and a refueling time of less than 5 min—can be met with high-pressure hydrogen storage tanks (*1*). Now, the main challenge is the design of cheap and stable fuel cell catalysts for the oxygen reduction reaction. On page 71 of this issue, Lefèvre *et al*. (*2*) report a breakthrough in the performance of oxygen reduction catalysts based on non–precious metals.

Oxygen reduction catalysts used in current fuel cell prototypes are platinum nanoparticles supported on carbon black (Pt/C), but cost and supply constraints for large-scale applications require a factor of >4 increase in catalytic activity per mass of precious metal (*3*). Drawing inspiration from nature, non–precious metal catalysts using abundant transition metals have long been explored (*4*, *5*), but to be viable, their activity would have to approach that of traditional—but more expensive—Pt/C catalysts.

Most current work on non–precious metal oxygen reduction catalysts focuses on nitrogen-coordinated iron in a carbon matrix (referred to as Fe/N/C). The nature of the active sites remains elusive, but graphene-coordinated FeN_4 or FeN_2 moieties were proposed (*6*–*8*). However, vastly differing syntheses produced virtually identical catalyst activities (*9*) and PEM fuel cell performance remained 150 to 200 mV below that of Pt/C—too big a gap for practical use. The results reported by Lefèvre *et al*. thus seem like a dream come true, showing that non–precious metal catalysts can match the performance of state-of-the-art Pt/C catalysts.

This paradigm shift in PEM fuel cell development is even more exciting when examined in terms of turnover frequency, which quantifies the number of electrons produced per active site per second at a defined operating condition. Turnover frequencies of previous non–precious metal catalysts—assuming that

[1]Electrochemical Energy Laboratory, Department of Mechanical Engineering, Massachusetts Institute of Technology, Cambridge, MA 02139, USA. [2]Materials Science Division, Argonne National Laboratory, Argonne, IL 60439, USA. E-mail: hubert.gasteiger@gmail.com; markovic@anl.gov

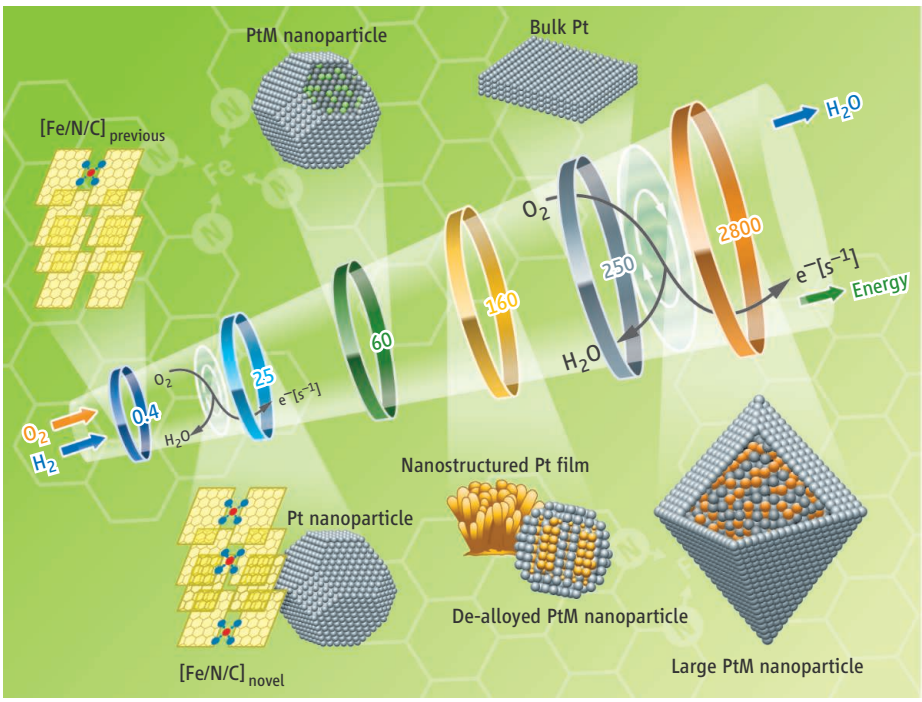

Toward higher turnover frequencies. Turnover frequencies for the electrochemical conversion of oxygen to energy and water (e^- O_2 + $2H^+$ + $2e^- \rightarrow H_2O$, the cathode reaction in a PEM fuel cell) for different oxygen reduction catalysts (operating conditions: 80°C, 100 kPa_{abs} H_2 and O_2, at 0.8 V versus the reversible hydrogen electrode). Previous generations of Fe/N/C catalysts had much lower turnover frequencies than the novel Fe/N/C catalyst reported by Lefèvre *et al*. Turnover frequencies must be much higher for Pt-based catalysts than for Fe/N/C catalysts because of cost and supply issues. Turnover frequencies were extracted from the references below and calculated as shown before (*3*, *10*), assuming ~70 mV tafel slopes for Pt catalysts.

each iron atom produces an active site—are 0.4 s^{-1} (*10*), compared with 25 s^{-1} for Pt/C (*3*) (see the figure). Because of the lower active-site density of non–precious metal catalysts and constraints on the maximum electrode catalyst loading, the turnover frequencies for non–precious metal catalysts must be similar to those of current Pt/C catalysts to be viable for applications (*2*). Lefèvre *et al.* now report turnover frequencies for their Fe/N/C catalyst that match those of Pt/C (25 s^{-1}, see the figure). Thus, the dream of using non–precious metal catalysts in PEM fuel cells is becoming a reality, with potentially revolutionary impact on fuel cell technologies.

In parallel with the non–precious metal approach, Pt-based oxygen reduction electrocatalysis has also seen important advances. Because of inherent cost and supply constraints, Pt-based catalysts must have high mass activities, given by the product of turnover frequency and metal dispersion, D (the fraction of surface atoms in a nanoparticle). Because D is already as high as 0.35 for state-of-the-art Pt/C, viable Pt-based catalysts must have turnover frequencies that are higher by about one order of magnitude 10 times those needed for non–precious metal catalysts.

Four main strategies aim to increase the turnover frequency of Pt-based catalysts (see the figure). The traditional approach involves PtM alloy nanoparticles (where M is another transition metal), but maximum turnover frequencies are only ~60 s^{-1} (*3*). Another strategy, the "de-alloying" of PtM nanoparticles, leads to particles with a PtM core and a Pt shell, with turnover frequencies of ~160 s^{-1} (*11*, *12*). Similar values are obtained for ~10 monolayer-thick Pt films on nanostructured supports (*13*). Both strategies offer large Pt dispersions while approaching turnover frequencies of bulk Pt surfaces, resulting in mass activities for de-alloyed PtM that are four times those of current Pt/C (*12*). Finally, turnover frequencies of ~2800 s^{-1} were reported for $Pt_3Ni(111)$ surfaces (*14*), which—if grown into 30-nm-diameter octahedra ($D \approx 0.03$)—should yield 10 times the mass activity of current Pt/C. The synthesis of such particles was shown recently (*15*).

High mass activities can also be achieved by depositing Pt monolayers on large non–precious metal cores, realizing high Pt dispersions ($D \approx 1$) and bulk Pt–like turnover frequencies (*16*). However, the low but finite solubility of Pt is a concern in this case. On the other hand, recent studies show that large nanostructured materials such as nanostructured Pt films and large PtM nanoparticles much reduce the current problem of Pt dissolution from voltage cycling (*13*, *17*).

Little is currently known about the stability of novel non–precious metal oxygen reduction catalysts and their ability to survive in hostile electrochemical environments. Thus, the next challenge for non–precious metal catalysts will be to overcome the twofold loss in current density at constant potential over 100 hours reported by Lefèvre *et al.*, either related to electrode design or to the catalyst itself. Little is known about the molecular processes that might lead to Fe-N bond breaking, and our insight into the stability of the active sites is based only on trial and error. However, recent durability data on Co/N/C-based catalysts are promising (*18*), and the fact that nitrogen-coordinated transition metals are used successfully by nature gives hope that detailed studies will lead to more durable catalysts.

Four years ago, neither Fe/N/C-based catalysts with Pt/C-like turnover frequencies, nor de-alloyed PtM catalysts with fourfold higher mass activity than Pt/C, nor surfaces with 100-fold higher turnover frequencies than Pt/C were known. Despite a number of remaining challenges, these recent successes bring us closer to completing our quest to put PEM fuel cell technology on the road.

References and Notes

1. K. Wipke, S. Sprik, J. Kurtz, J. Garbak, in *Handbook of Fuel Cells: Fundamentals, Technology, and Applications*, W. Vielstich, H. A. Gasteiger, H. Yokokawa, Eds. (Wiley, Chichester, UK, 2009), vol. 6, pp. 893–904.
2. M. Lefèvre, E. Proietti, F. Jaouen, J.-P. Dodelet, *Science* **324**, 71 (2009).
3. H. A. Gasteiger, S. Kocha, B. Sompalli, F. T. Wagner, *Appl. Catal. B* **56**, 9 (2005).
4. S. Gupta, D. Tryk, I. Bae, W. Aldred, E. Yeager, *J. Appl. Electrochem.* **19**, 19 (1989).
5. J. P. Collman *et al.*, *J. Am. Chem. Soc.* **102**, 6027 (1980).
6. A. L. Bouwkamp-Wijnoltz *et al.*, *J. Phys. Chem. B* **106**, 12993 (2002).
7. M. Lefèvre, J. P. Dodelet, P. Bertrand, *J. Phys. Chem. B* **109**, 16718 (2005).
8. U. I. Koslowski, I. Abs-Wurmbach, S. Fiechter, P. Bogdanoff, *J. Phys. Chem. C* **112**, 15356 (2008).
9. A. Garsuch, A. Bonakdarpour, G. Liu, R. Yang, J. R. Dahn, in *Handbook of Fuel Cells: Fundamentals, Technology, and Applications*, W. Vielstich, H. A. Gasteiger, H. Yokokawa, Eds. (Wiley, Chichester, UK, 2009), vol. 5, pp. 71–80.
10. F. Jaouen, J.-P. Dodelet, *Electrochim. Acta* **52**, 5975 (2007).
11. S. Koh, P. Strasser, *J. Am. Chem. Soc.* **129**, 12624 (2007).
12. K. C. Neyerlin, R. Srivastava, C. Yu, P. Strasser, *J. Power Sources* **186**, 261 (2009).
13. M. K. Debe, A. K. Schmoeckel, G. D. Vernstrom, R. Atanasoski, *J. Power Sources* **161**, 1002 (2006).
14. V. R. Stamenkovic *et al.*, *Science* **315**, 493 (2007); published online 10 January 2007 (10.1126/science.1135941).
15. R. R. Adzic *et al.*, *Top. Catal.* **46**, 249 (2007).
16. J.-M. Qiu, J.-P. Wang, *Adv. Mater.* **19**, 1703 (2007).
17. Y. Shao-Horn *et al.*, *Top. Catal.* **46**, 285 (2007).
18. R. Bashyam, P. Zelenay, *Nature* **443**, 63 (2006).

19. N.M.M. acknowledges support by the U.S. Department of Energy, Office of Science, Office of Basic Energy Sciences, under contract no. DE-AC02-06CH11357.

10.1126/science.1172083

The Bent Hawaiian-Emperor Hotspot Track: Inheriting the Mantle Wind

John Tarduno,[1,2*] Hans-Peter Bunge,[3] Norm Sleep,[4] Ulrich Hansen[5]

Bends in volcanic hotspot lineaments, best represented by the large elbow in the Hawaiian-Emperor chain, were thought to directly record changes in plate motion. Several lines of geophysical inquiry now suggest that a change in the locus of upwelling in the mantle induced by mantle dynamics causes bends in hotspot tracks. Inverse modeling suggests that although deep flow near the core-mantle boundary may have played a role in the Hawaiian-Emperor bend, capture of a plume by a ridge, followed by changes in sub-Pacific mantle flow, can better explain the observations. Thus, hotspot tracks can reveal patterns of past mantle circulation.

The Hawaiian-Emperor track (Fig. 1) is the archetype used to illustrate plate motion over a hotspot. In the classic view, volcanism on the surface recorded regular plate motion over a plume deep within Earth's mantle that produced a fixed region of melting near the surface (hotspot). The great bend separating the northwestern-trending Hawaiian chain from the north-south–oriented Emperor Seamounts was thought to trace a ~60°change in absolute plate motion. However, a paleomagnetic test based on ocean drilling in 2001 revealed that the islands and seamounts had formed at different latitudes (*1*). The Emperor trend seamounts thus record motion of the upwelling in the mantle.

Why didn't the community accept hotspot mobility earlier? The elegant and captivating geometry of the fixed hotspot idea (*2*) compelled a search for alternatives to emerging contradictory findings. It had been recognized in reconstructing plate motions that a fixed Hawaiian hotspot was inconsistent with fixed hotspots in the Indo-Atlantic realm (*3*). However, early reconstructions relied on a critical plate circuit link through the then poorly understood Antarctic and southernmost Pacific region. The possibility of undocumented plate motions provided an option that avoided hotspot drift. Paleomagnetic data from a single Pacific site also indicated hotspot motion, but they could be interpreted as a record of polar wander (*4*), the rotation of the entire solid Earth in response to shifts in its mass heterogeneities. In addition, although plumes could easily have been envisioned as swaying in the mantle, the geodynamic details were wanting.

Two premises embedded in the dynamic equations of how the mantle moves preclude stationary hotspots. The first is the principle of mass conservation: Any plate movement at the surface must be balanced by motion deeper in the mantle. The second premise is that the mantle can be taken as a highly viscous fluid—a nominal viscosity of 10^{21} Pa·s is suggested from studies of postglacial rebound (*5*). The large mantle viscosity implies that velocity gradients are small and that inertial forces pale in comparison to viscous ones; thus, the mantle transmits stresses nearly instantaneously. Given both premises, any plate motion change must go along with changes in the internal mantle flow. Hager and O'Connell (*6*) used this insight to infer deep mantle motion from the surface plate tectonic pattern in the decade following the first use of a hotspot reference frame.

Subsequent advances in seismic tomography and past plate motion modeling allowed modeling of the temporal evolution of the mantle back in time. Steinberger and O'Connell (*7*) produced a synoptic view of past mantle circulation that suggested southward motion of the Hawaiian hotspot, consistent with paleomagnetic data (*8*). Geophysical cruise results and paleomagnetic studies resolved potential gaps in plate circuits [e.g., (*9*, *10*)], and global paleomagnetic tests excluded polar wander (*11*–*13*). These developments have set the stage for a reassessment of mantle processes that could be recorded by large bends in hotspot tracks.

An Alternative Hawaiian-Emperor Track

To visualize the implications of hotspot motion, we consider what the Hawaiian-Emperor track

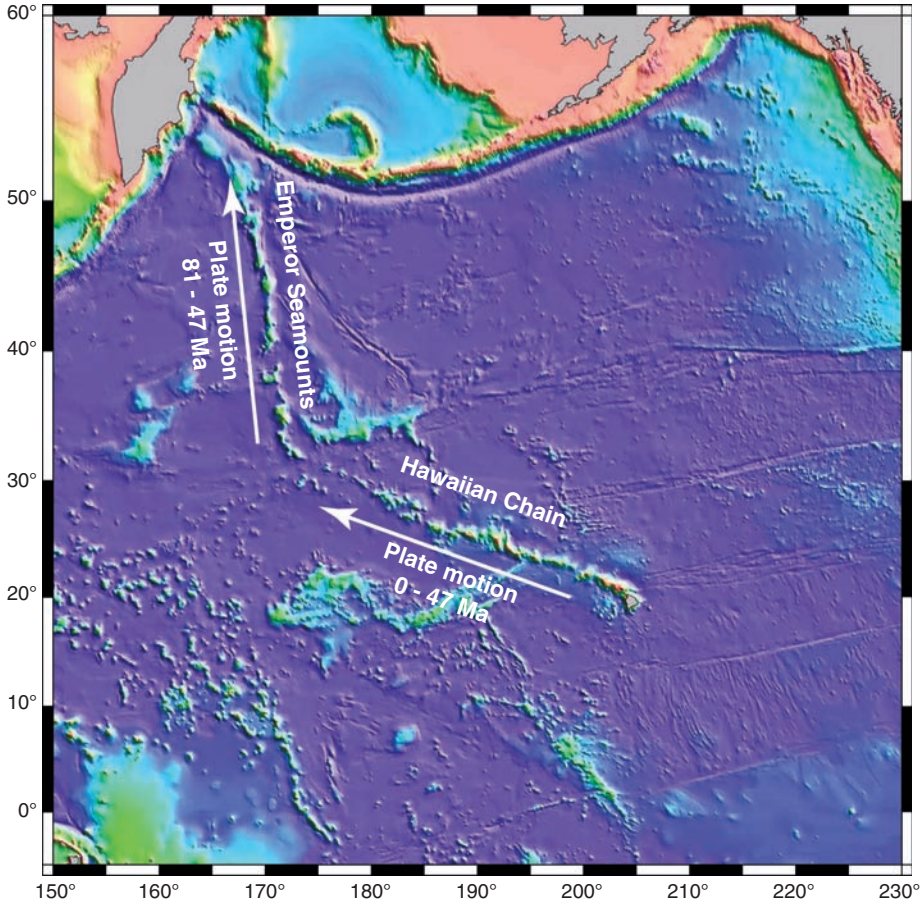

Fig. 1. Bathymetry of the northwest Pacific Ocean basin. The traditional interpretation is highlighted: The Hawaiian volcanic chain records absolute Pacific plate motion to the northwest, whereas the Emperor Seamounts reflect a more northerly plate direction.

[1]Department of Earth and Environmental Sciences, University of Rochester, Rochester, NY 14627, USA. [2]Department of Physics and Astronomy, University of Rochester, Rochester, NY 14627, USA. [3]Department of Earth and Environmental Sciences, Ludwig-Maximilians Universität, München, 80333 München, Germany. [4]Department of Geophysics, Stanford University, Stanford, CA 94305, USA. [5]Institut für Geophysik, Universität Münster, 48149 Münster, Germany.

*To whom correspondence should be addressed. E-mail: john@earth.rochester.edu

might have looked like had the Hawaii hotspot actually been fixed relative to the deep mantle. To do this, we use plate circuits and assume that volcanic chains in the Indo-Atlantic realm reflect fixed hotspots. These predictions are thus still not free of the fixed hotspot hypothesis, but paleomagnetic studies suggest that the hotspots in the Indo-Atlantic have not moved much since the Late-Cretaceous-Paleogene, when the Emperor Seamounts were formed (*14*).

The plate circuit that traverses the Indo-Atlantic and Pacific realms via Antarctica (*9*, *14*) yields a hypothetical trace that is similar to the Hawaiian chain for the last ~30 million years (Fig. 2, A to C). For older times, differences build. The Hawaiian-Emperor bend of the extant track is replaced by a gentle ~30° of curvature in the hypothetical trace (Fig. 2D). This moderate curvature is similar to that seen in the Louisville chain, the other hotspot track from the Pacific Ocean basin with a long, clear age progression (*15*) that is not confused by lithospheric structure. Moreover, the hypothetical trace resembles an oceanic fracture zone, a feature of Earth's surface known to record plate motion over tens of millions of years (*16*). As is the case with fracture zones, we can fit the trace with several small circle segments, the junction of each representing a change in plate motion. The bend in the actual track might represent one of these junction times in the hypothetical trace.

An alternative plate circuit involves transfer from Antarctica to Australia, and then through Lord Howe Rise (Fig. 2, B and C). In the predictions arising from use of this circuit, a somewhat sharper bend remains, which could imply a larger plate motion change (*17*). Both plate circuits pass paleomagnetic consistency tests (*14*); we cannot distinguish between them with the resolution of the available data. However, while avoiding the Antarctic-Pacific connection, the second circuit relies on a contentious assumption: Lord Howe Rise is locked to the Campbell Plateau between 84 and 47 million years ago (Ma). Moreover, when a revised history of Antarctic-Australian spreading history (*18*) is incorporated into the circuit through Lord Howe Rise, the predictions for the locations of the Hawaiian-Emperor chain (Fig. 2C) converge to those derived from the Antarctic connection (*19*). Both plate circuits indicate that the large present-day latitudinal trace of the Emperors is mainly due to hotspot drift, consistent with the paleomagnetic determinations from ocean drilling (*1*, *8*).

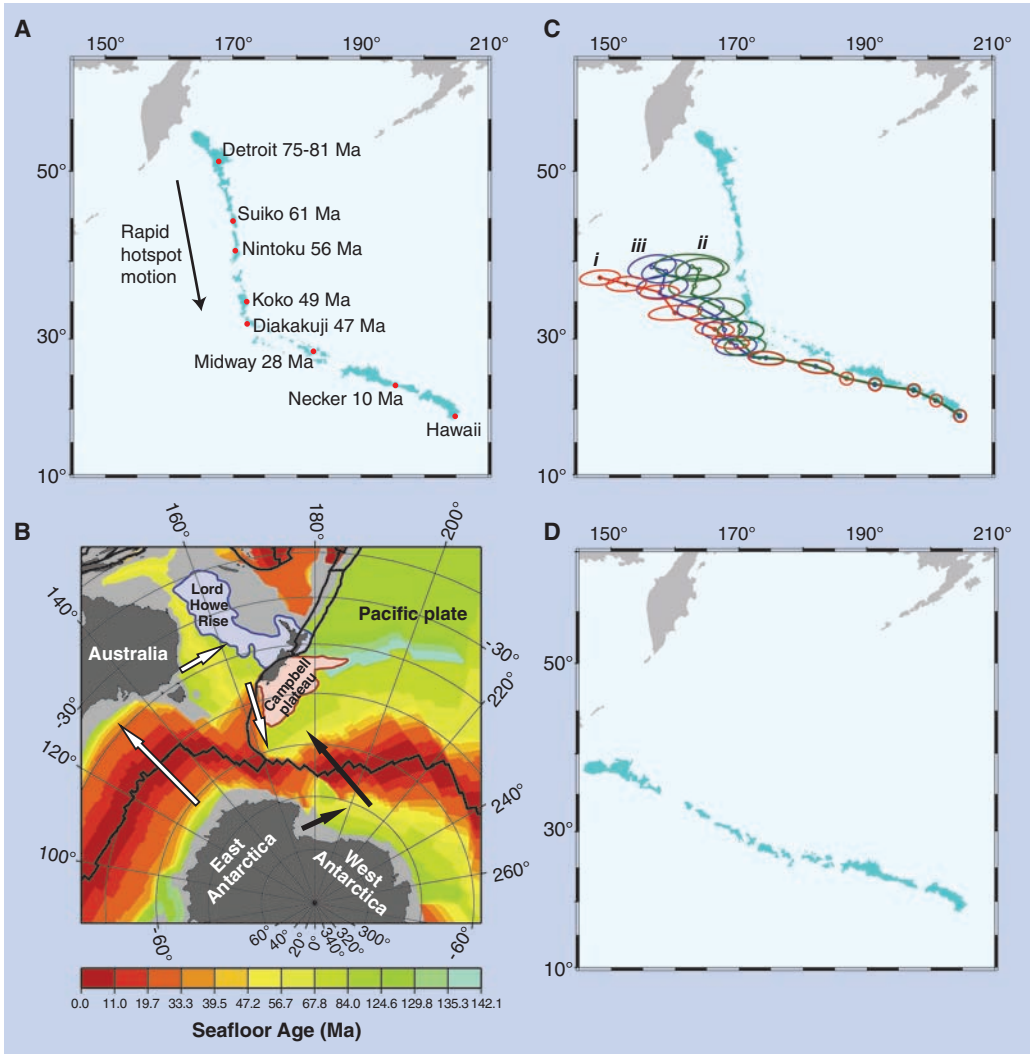

Fig. 2. Alternative Hawaiian-Emperor traces. (**A**) Present-day track with ages and episode of rapid hotspot motion highlighted. (**B**) Differences in how plate circuits connect the Indo-Atlantic realm to the Pacific for Late Cretaceous to middle Eocene times [from (*14*)]. In the standard reconstruction [e.g., (*9*)], the connection is through East-West Antarctica (black arrows); in a more recent circuit, the connection is through Australia and the Lord Howe Rise (white arrows) (*17*). (**C**) Predicted tracks from plate circuits [see (*14*) and (*19*) for ages and uncertainty analysis]: (i) East-West Antarctica circuit (red); (ii) Australia-Lord Howe Rise circuit (green); (iii) Australia-Lord Howe Rise circuit modified with a revised Antarctic-Australia spreading history [from (*17*)] (blue). Note that path (iii) converges to path (i). (**D**) Trace that would have been produced had the Hawaiian hotspot been fixed in the deep mantle (*16*). Predictions based on East-West Antarctica circuit.

Candidate Processes

Two models have been proposed to explain hotspots. One is a "top-down" plate-driven process in which rifting of the lithosphere stimulates shallow mantle melting (*20*). The second is a "bottom-up" model in which an upwelling or plume (*2*) rises in the mantle from a thermal boundary layer (the transition zone at ~700 km or as deep as the core-mantle boundary). Seismic data are still inconclusive, but we favor and thus explore the mantle plume explanation for Hawaiian volcanism in which a long-lived, narrow upwelling from the deepest mantle episodically constructs volcanic islands and seamounts. The Hawaiian hotspot's large volume flux (~350 m^3 s^{-1}) (*21*), spatial pattern, and longevity are best explained by the mantle plume hypothesis. Some studies of alternative mechanisms (e.g., a propagating crack) show that they are inadequate (*21*), whereas other modeling has shown that deep mantle plumes contribute substantially to the mantle energy budget (*22*). Below, we identify five physical processes that could have caused hotspot motion and the Hawaiian-Emperor bend. We use 47 Ma as the best age for the bend; an older age of 50 million years has been proposed (*23*), but this relies on a relocation of the bend 200 km north of the typic feature on the sea floor (*16*).

1) Ridge interaction and asthenospheric flow. Plumes will impinge at the base of the lithosphere; ponded material can flow in a type of

upside-down drainage toward a ridge (*24*). Plate reconstructions (*25*, *26*) and geochemical data (*27*) indicate that a ridge lay north of Detroit Seamount during its construction. Hence the hotspot, perhaps once located to the south, may have been "pinned" by the more northerly ridge (Fig. 3A). The mid-ocean ridge basalt signature seen in Detroit Seamount lavas is not seen in the younger Suiko Seamount (*27*). Thus, we infer that this shallow flow influenced the formation of only the northernmost seamounts (i.e., Detroit Seamount and Meiji Guyot) of the Emperor track (*1*).

2) Ridge upwelling and deeper mantle flow. Upper mantle flow is more rapid near mid-ocean ridges, and numerical modeling suggests that considerable tilts of the deeper plume conduits toward ridges might begin at depths of 1200 to 1500 km (Fig. 3B). Scaling arguments (*28*) limit the distance over which plumes and ridges interact to about 1500 km. Plate reconstructions show that a number of ridges have crossed the Pacific since 140 Ma at velocities of several centimeters per year (*29*). Thus, this ridge migration could have captured mantle plumes through flow directed at the ridge. If the ridge moves beyond that distance, a captured plume would presumably return to its original location over a deep mantle source.

3) Advection of the plume conduit and entrainment in the mantle wind. As a plume rises through the mantle, the plume conduit can be tilted as mantle convection continues over time (Fig. 3C), moving where it interacts with the shallow mantle and crust, giving rise to drift observed at the surface (*7*). Models of this process have been successful in explaining the first-order paleomagnetic observations (*1*). The apparent velocity of the hotspot can be twice that of the mantle circulation component. If the tilt becomes too great, the conduit may lose consistency. However, in most models, the tilted thermal plumes do not break up into a series of diapirs. Rather, small-scale convection near the plume conduit can entrain material from the surrounding mantle (*30*). This process readily disrupts tilted isoviscous plumes, but laboratory and theoretical studies suggest that tilted plumes with strongly temperature-dependent viscosities and fluxes appropriate to the mantle remain intact and do not entrain much surrounding material (*31*, *32*).

4) Movement of the plume base: influence of a superplume. Hawaii is an outlier relative to the cluster of hotspots in the South Pacific, a region that was anomalous in the Cretaceous when the Mid-Pacific Mountains and other seamounts formed (*11*, *33*). Modeling shows that the base of a plume tends to move toward a broad upwelling (*34*) (Fig. 3D). This process might be especially important if the plume arises from a tabular upwelling; the plume source could conceivably move along-strike of the larger upwelling. Lateral heterogeneity in D″ implies that some regions, such as "cusps" where dense material has been entrained, might serve to anchor the plume source (*35*). Together, these processes could account for differences in the motion histories between plumes and the temporal character of movement exhibited by a single plume such as Hawaii .

5) Mantle convection coupled to plate motion change. The paleomagnetic data from the Emperor Seamounts imply that there was a major change in the nature or vigor of mantle convection in the Pacific at 47 Ma, because the present-day latitude of the hotspot and paleolatitude estimates of islands, atolls, and seamounts back to the bend are similar (*1*). Plate motion–driving forces for this change include initiation of subduction in the Izu-Bonin arc and ridge subduction in the northwestern Pacific (*18*), events that may have commenced at (or before) 50 Ma (*23*). However, it is also possible that other far-field plate tectonic changes could have a cumulative effect that is not adequately captured by the current generation of plate and mantle flow models.

Scales of Hotspot Motion and Mantle Convection

In further assessing the physical processes that potentially created the bend, we consider first the background mantle motion. Geochemistry (*36*), seismic tomography (*37*, *38*), the geoid (*39*), the distribution of hotspots (*40*), and the history of subduction (*41*) suggest a flow pattern organized with two major upwellings under the Pacific and Africa, separated by a great circle of downwelling surrounding the Pacific. Although fluid

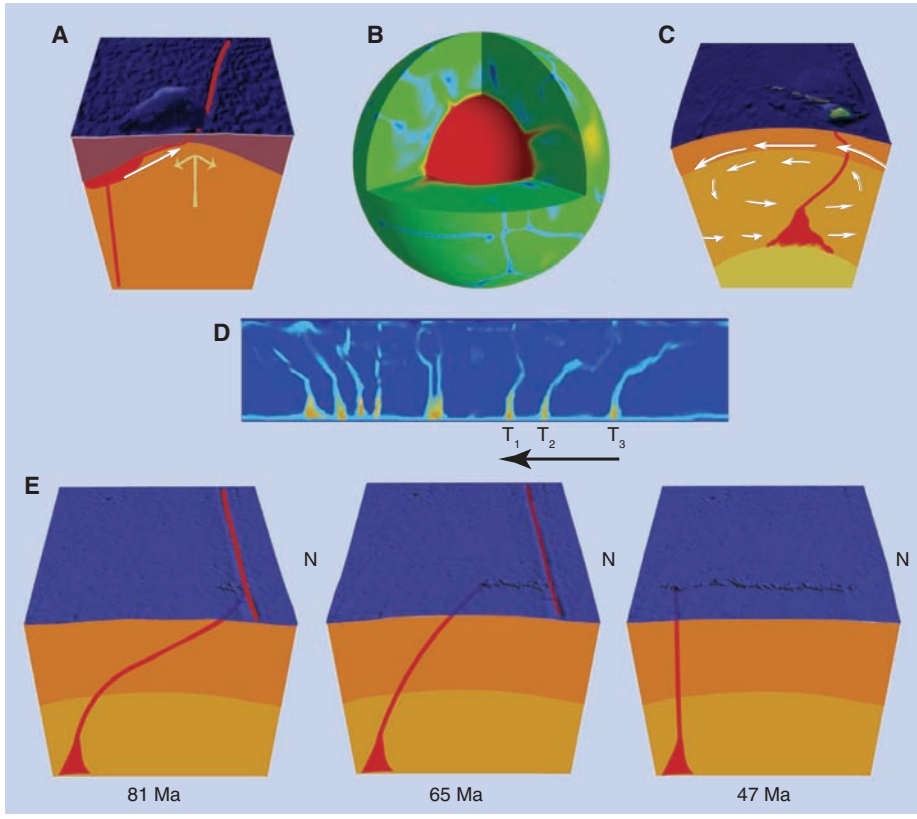

Fig. 3. Hotspot drift related to shallow (**A**), mid-mantle (**B** and **C**), and deep-mantle (**D**) processes. (A) Hotspot volcanism is channeled to a nearby ridge by asthenospheric flow (schematic) (see (*1*, *24*) for discussion). (B) Superadiabatic temperatures for a three-dimensional spherical mantle convection model with depth-dependent viscosity and bottom heating [from (*42*)]. The uppermost 200 km of the mantle is removed to show the temperature distribution beneath the thermal boundary layer. Large horizontal flow velocities in the asthenosphere, directed at an upwelling (ridge), result in a strongly tilted plume conduit. (C) Advection of plume conduits, tilted by mantle flow (schematic). See (*1*, *7*, *17*) for model results for Hawaii and other hotspots. (D) Movement of the base of a plume influence by a large-scale upwelling following (*34*). A composite snapshot of the model is shown, displaying the evolution of the temperature field in a convecting mantle. Material properties are assumed to depend on pressure and temperature. The coefficient of thermal expansivity decreases by a factor of 10 from top to bottom; the viscosity increases sharply with pressure and decreases with temperature. The Rayleigh number, based on surface values of viscosity and expansivity, was set to 10^7. The original experiment was conducted in a wide box (aspect ratio 36) to minimize edge effects. Here, the box has been truncated to highlight the phenomenon of plume movement. T1, T2, and T3 represent subsequent position of a hotspot as its base moves toward a central upwelling. (**E**) Schematic of one plume capture and release scenario for the Hawaiian-Emperor chain. The plume is bent between 1200- and 1500-km depth toward the mantle upwelling associated with the Pacific-Kula ridge system at 81 Ma; upwelling abates thereafter, allowing the plume to return to its original position relative to the deep mantle by 47 Ma.

dynamic theory of an isoviscous mantle predicts shorter convective length scales on the order of the mantle depth, modeling (*42*) and analytic studies (*43*) indicate that the larger-scale structure is a robust property of mantle flow having a low-viscosity channel, or asthenosphere.

The asthenosphere decouples plate movement from deeper mantle motion. Modeling shows that the decoupling is proportional to the inverse of the natural logarithm of the viscosity contrast between the upper and the lower mantle (*44*). Overall, the rate of mantle wind scales with slab descent rate (*45*). Mantle circulation simulations (*46*) predict deep mantle flow velocities on the order of 1 cm/year for mantle viscosity contrasts of 10 to 100 (*47*). Thus, it is possible to reconcile both times of near-hotspot fixity and times of hotspot movement with vigorous plate motion [e.g., (*48*)]. The longest spatial scale of convection implies that hotspots might move as groups (*11*). In fact, when paleomagnetic data from the Indo-Atlantic region are referenced to hotspots of that area, and paleomagnetic data from the Pacific are tied to its hotspots, there is a discrepancy (*11*–*13*, *16*). This was once thought to be a sign of polar wander (*49*), even though such polar shifts are small in mantle convection models with an asthenosphere (*50*). The difference is now recognized as a signal of hotspot motion and large-scale ($l = 2$) mantle convection (*11*, *51*).

Mantle circulation models also predict that deep mantle motion in the Late Cretaceous, when plate velocities were about twice as fast as they are today, did not exceed 2 cm/year. Rapid hotspot movement, comparable to the rates seen for Hawaii at the time between 81 and 47 Ma (>4 cm/year), is thus unlikely to originate solely from deep mantle processes. Fast-velocity episodes could instead arise in the shallow mantle, where flow velocities are large. Hotspot bends, and changes between periods of fast and slow plume motion, may then signal the switch between flow regimes in the shallow and the deeper mantle, respectively.

Models involving plume capture by a ridge are of special relevance for the Hawaiian-Emperor chain because the large shallow mantle flow rates are concomitant with the high hotspot drift rates (*1*). When spreading rates are slow, such as in the Atlantic, the mantle flow may be so weak that hotspots can cross ridges (*48*). In the faster-spreading Pacific ridges, mantle wind can produce more plume tilt.

Moreover, plume capture is consistent with two key traits of the chain and Pacific basin tectonic history. First, the scaling considerations yield a limit on the lateral extent of fast plume motion of about 15°; that is the maximum distance from which a captured plume could return to its original location. Drift models based on paleomagnetic data from the Emperor Seamounts (*1*) suggest that the rapid phase of Hawaiian hotspot motion covered 11° to 15° of latitude. Second, the Hawaiian hotspot was close to a fast-spreading ridge [full rate estimated as 180 mm year^{-1} (*21*)] at 75 to 81 Ma, but spreading ceased sometime between 56 Ma and the age of the bend (*52*). Ridge transforms and jumps [e.g., (*26*)] will complicate patterns of upwelling. The Emperor Seamounts may record an interval tens of millions of years long when the large-scale mantle upwelling associated with the Kula–Pacific ridge system north of the Hawaiian hotspot waned. This progressive change, possibly with other tectonic events on the paleo-Pacific margin [e.g., (*18*)], would have reduced any northward sub-Pacific mantle flow, allowing the captured plume to return to its original position in a dominant southward flow (*1*, *7*). Since this shift, the hotspot has been far from ridge influences and relatively stable, reflecting deeper and more sluggish mantle flow.

Further Resolution

Mantle flow models are about to achieve the numerical resolution needed (100 million to 1 billion grid points) to represent the vigor of global mantle flow, allowing further testing of plume capture. Incorporation of constraints from mineral physics [e.g., (*53*)] is improving models, and assimilation of refined seismic tomography and plate-motion histories is helping to overcome the limitations of unknown initial conditions (*54*). New observations can help. The Hawaiian-Emperor chain is well suited for paleomagnetic tests because its track is narrow. In other cases, such as Cretaceous hotspots on the Indian plate, locations are uncertain because of the >1000-km spatial scale of magmatism (commonly attributed to mantle plume heads). Drilling of the Emperor Seamounts was designed to test whether the Hawaiian hotspot had moved (*1*). Deeper drilling is needed to obtain the paleolatitude resolution required to investigate temporal variations in hotspot drift (*16*). Intrabasin hotspot motion can be assessed by drilling the Louisville hotspot track (*15*). The motion histories of Indo-Atlantic hotspots with narrow tracks can be evaluated by paleomagnetic analyses of continental rocks; when compared with Pacific data, these histories provide a means to gauge motion of hotspot groups. These efforts should ultimately allow the community to use hotspot tracks and their bends as measures of past mantle flow.

References and Notes

1. J. A. Tarduno *et al.*, *Science* **301**, 1064 (2003).
2. W. J. Morgan, *Geol. Soc. Am. Mem.* **132**, 7 (1972).
3. P. Molnar, T. Atwater, *Nature* **246**, 288 (1973).
4. W. J. Morgan, in *The Sea*, C. Emiliani, Ed. (Wiley, New York, 1981), vol. 7, pp. 443–487.
5. J. X. Mitrovica, *J. Geophys. Res.* **101**, 555 (1996).
6. B. H. Hager, R. J. O'Connell, *J. Geophys. Res.* **84**, 1031 (1979).
7. B. Steinberger, R. J. O'Connell, *Geophys. J. Int.* **132**, 412 (1998).
8. J. A. Tarduno, R. D. Cottrell, *Earth Planet. Sci. Lett.* **153**, 171 (1997).
9. S. C. Cande, C. A. Raymond, J. Stock, W. F. Haxby, *Science* **270**, 947 (1995).
10. V. DiVenere, D. V. Kent, *Earth Planet. Sci. Lett.* **170**, 105 (1999).
11. J. A. Tarduno, J. Gee, *Nature* **378**, 477 (1995).
12. J. A. Tarduno, A. V. Smirnov, *Earth Planet. Sci. Lett.* **184**, 549 (2001).
13. T. H. Torsvik, R. Van der Voo, T. F. Redfield, *Earth Planet. Sci. Lett.* **202**, 185 (2002).
14. P. V. Doubrovine, J. A. Tarduno, *J. Geophys. Res.* **113**, B07104 (2008).
15. A. A. Koppers, R. A. Duncan, B. Steinberger, *Geochem. Geophys. Geosyst.* **5**, Q06L02 (2004).
16. J. A. Tarduno, *Chem. Geol.* **241**, 234 (2007).
17. B. Steinberger, R. Sutherland, R. J. O'Connell, *Nature* **430**, 167 (2004).
18. J. M. Whittaker *et al.*, *Science* **318**, 83 (2007).
19. P. V. Doubrovine, J. A. Tarduno, *J. Geophys. Res.* **113**, B12101 (2008).
20. D. L. Anderson, *Geophys. Res. Lett.* **27**, 3623 (2000).
21. N. H. Sleep, in *Plates, Plumes and Planetary Processes*, G. R. Foulger, D. M. Jurdy, Eds. (GSA Spec. Pap. 430, Geological Society of America, Boulder, CO, 2007), pp. 29–45.
22. H.-P. Bunge, *Phys Earth Planet Int.* **153**, 3 (2005).
23. W. D. Sharp, D. A. Clague, *Science* **313**, 1281 (2006).
24. N. H. Sleep, *J. Geophys. Res.* **101**, 28065 (1996).
25. R. D. Cottrell, J. A. Tarduno, *Tectonophysics* **362**, 321 (2003).
26. I. O. Norton, in *Plates, Plumes and Planetary Processes*, G. R. Foulger, D. M. Jurdy, Eds. (GSA Spec. Pap. 430, Geological Society of America, Boulder, CO, 2007), pp. 451–470.
27. R. A. Keller, M. R. Fisk, W. M. White, *Nature* **405**, 673 (2000).
28. N. Ribe, *J. Geophys. Res.* **101**, 16,195 (1996).
29. R. D. Müller, M. Sdrolias, C. Gaina, W. R. Roest, *Geochem. Geophys. Geosyst.* **9**, Q04006 (2008).
30. M. A. Richards, R. W. Griffiths, *Nature* **342**, 900 (1989).
31. R. C. Kerr, C. Meriaux, *Geochem. Geophys. Geosyst.* **5**, Q12009 (2004).
32. N. H. Sleep, *Geochem. Geophys. Geosyst.* **8**, Q11005 (2007).
33. J. A. Tarduno, W. W. Sager, *Science* **269**, 956 (1995).
34. U. Hansen, D. A. Yuen, S. E. Kroening, T. B. Larsen, *Phys Earth Planet Int.* **77**, 205 (1993).
35. A. M. Jellinek, M. Manga, *Nature* **418**, 760 (2002).
36. B. Dupré, C. J. Allègre, *Nature* **303**, 142 (1983).
37. R. Montelli *et al.*, *Science* **303**, 338 (2004).
38. N. A. Simmons, A. M. Forte, S. P. Grand, *Earth Planet. Sci. Lett.* **246**, 109 (2006).
39. C. Reigber *et al.*, *J. Geodynamics* **39**, 1 (2005).
40. M. A. Richards, B. H. Hager, N. H. Sleep, *J. Geophys. Res.* **93**, 790 (1988).
41. M. A. Richards, D. C. Engebretson, *Nature* **355**, 437 (1992).
42. H.-P. Bunge, M. A. Richards, J. R. Baumgardner, *J. Geophys. Res.* **102**, 11,991 (1997).
43. A. Lenardic, M. A. Richards, F. H. Busse, *J. Geophys. Res.* **111**, B07404 (2006).
44. M. A. Richards, in *Glacial Isostasy, Sea Level and Mantle Rheology*, R. Sabadini, K. Lambeck, E. Boschi, Eds. (NATO ASI Ser. C, vol. 334, Kluwer, Norwell, MA, 1991), pp. 571–587.
45. N. H. Sleep, *C. R. Geosci.* **335**, 9 (2003).
46. H.-P. Bunge, M. A. Richards, J. R. Baumgardner, *Philos. Trans. R. Soc. Ser. A* **360**, 2545 (2002).
47. B. H. Hager, *J. Geophys. Res.* **89**, 6003 (1984).
48. J. P. Lowman, S. D. King, C. W. Gable, *Geochem. Geophys. Geosyst.* **5**, Q01L01 (2004).
49. J. Besse, V. Courtillot, *J. Geophys. Res.* **107**, 2300 (2002).
50. M. A. Richards, H. P. Bunge, Y. Ricard, J. R. Baumgardner, *Geophys. Res. Lett.* **26**, 1777 (1999).
51. V. Courtillot, A. Davaille, J. Besse, J. Stock, *Earth Planet. Sci. Lett.* **205**, 295 (2003).
52. I. O. Norton, *Tectonics* **14**, 1080 (1995).
53. A. Piazzoni, G. Steinle-Neumann, H.-P. Bunge, D. Dolejš, *Geochem. Geophys. Geosyst.* **8**, Q11010 (2007).
54. H. P. Bunge, C. R. Hagelberg, B. J. Travis, *Geophys. J. Int.* **152**, 280 (2003).

55. We thank R. Cottrell and P. Doubrovine for discussions. This work was supported by the NSF.

10.1126/science.1161256

Conditional Mutagenesis in *Drosophila*

Ching Man Choi,[1,2,3]* Sven Vilain,[1,2,3]* Marion Langen,[1,2,4] Sofie Van Kelst,[1,2] Natalie De Geest,[1,2] Jiekun Yan,[1,2] Patrik Verstreken,[1,2,3,4] Bassem A. Hassan[1,2,3,4]†

Most genes have diverse functions in development. Therefore, mutating genes in a spatially and temporally controlled fashion, by generating groups of mutant cells or clones in an otherwise normal animal, is important for analysis of gene function at different life stages. Current clonal methods in the fruit fly *Drosophila* require mitotic recombination and thus cell division (*1*), thereby precluding the study of gene function during late stages of differentiation or in adult animals, except if using rare temperature-sensitive alleles. In contrast, the conditional knock-out (cKO) method in the mouse allows tissue-specific gene deletion without the use of cell division and permits the assessment of a gene's function in diploid but not polyploid cells at any time (*2*). Furthermore, because cell division is not required, mutant cells do not need to be siblings. Lastly, cKO permits the combination of different mutant alleles for the same gene.

To develop cKO in *Drosophila*, we used the *atonal* (*ato*) gene, which is expressed in both mitotic and postmitotic cells. *ato* mutants display measurable phenotypes, including failure of neural cells to differentiate and express characteristic marker genes (*3*). First, we used ends-out homologous recombination, which uses sequence homology to replace genomic DNA (*4*), to exchange *ato* with the *white* eye color marker (ato^{w}). ato^{w} is flanked by *attP* integrase sites, creating a ΦC31 integrase-exchangeable cassette (fig. S1, C to F). This allows the replacement of the marker with sequences flanked by complementary *attB* sites. Next, ΦC31 (*5*) is used to replace ato^{w} with full-length wild-type *ato* (ato^{ato}), rescuing the mutant phenotype (fig. S1, H and I), or with the transcriptional activator Gal4 (ato^{Gal4}), creating a reporter of *ato* expression (fig. S1J). We name this approach integrase-mediated approach for gene knock-out (IMAGO).

To create *ato* cKO constructs, we replaced the ato^{w} with wild-type *ato*, flanked by type-3 flippase recognition targets (FRTs, F3) and followed by the Gal4 coding sequence (ato^{FAFG4}; Fig. 1A). FRTs allow flippase (FLP)-mediated deletion, and Gal4 enables marking clones with the green fluorescent protein controlled by upstream activating sequences (UAS::GFP). Thus, in cells in which *ato* is deleted, GFP is expressed. ato^{FAFG4} rescued *ato* mutants (Fig. 1B) and, when deleted via an eye-specific FLP, produced *ato* mutant phenotype (Fig. 1B'').

We tested ato^{FAFG4} in dividing sensory organ precursors (SOP) of the leg (Fig. 1C) and nondividing photoreceptor neurons (PRs) in the retina (Fig. 1, D and E). None of the emerging SOP (blue) expresses GFP. Therefore, SOP do not develop from *ato* mutant cells (green). In addition, as previously shown, large *ato* mutant eye clones fail to express a differentiation marker (red; Fig. 1, D and D''). The fly retina is a tissue where nonsibling PRs interact. All retinal cells express Ato before differentiation, but the requirement for *ato* in single postmitotic PRs is unknown. In single-cell IMAGO clones (Fig. 1E), mutant cells (green) never become R8 (blue) as expected but differentiate as non-R8 PRs (red) if neighbored by a wild-type R8 (blue) and send axons toward the brain (Fig. 1, E' and E'').

Generation of IMAGO alleles required 6 to 8 months, in line with the time required for other types of mutations. Although it may prove more challenging for complex loci, the problem should be surmountable by using recombination-mediated genetic engineering (*6*). Like other clonal techniques, IMAGO relies on existing FLP tools, making its efficiency limited by that of these tools. IMAGO offers two advantages. First, mutant cells are induced in a diploid tissue at any time. For example, specific neuronal circuits can be mutated to study animal behavior or cellular degeneration without developmental effects. Second, the mutant gene can be replaced by any sequence.

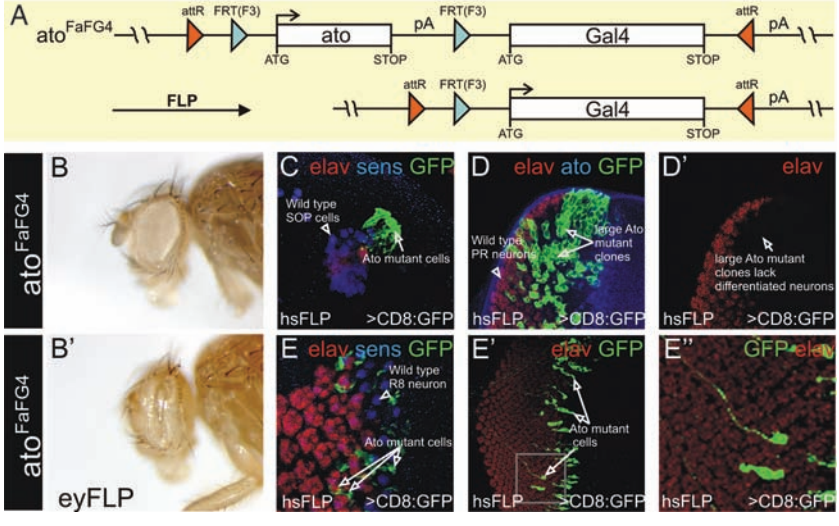

Fig. 1. (**A**) Schematic of *ato* cKO using IMAGO. Genomic (**B**) rescue and (**B'**) FLP-mediated induction of *ato* mutant eyes. (**C** to **E**) GFP-marked *ato* mutant clones in SOP and PRs. Ato mutant SOP fail to differentiate (C), as do large *ato* mutant clones in the eye (D and D'). Single *ato* mutant PR differentiate as non-R8 (E to E''). (**E'**) A basal section through the disc in (E) and (**E''**) enlargement of (E'), indicating non-R8 axons (arrows).

References and Notes

1. J. E. Rooke, N. A. Theodosiou, T. Xu, *Methods Mol. Biol.* **137**, 15 (2000).
2. R. Kuhn, F. Schwenk, M. Aguet, K. Rajewsky, *Science* **269**, 1427 (1995).
3. A. P. Jarman, Y. Sun, L. Y. Jan, Y. N. Jan, *Development* **121**, 2019 (1995).
4. W. J. Gong, K. G. Golic, *Proc. Natl. Acad. Sci. U.S.A.* **100**, 2556 (2003).
5. J. R. Bateman, A. M. Lee, C. T. Wu, *Genetics* **173**, 769 (2006).
6. K. J. T. Venken, Y. He, R. A. Hoskins, H. J. Bellen, *Science* **314**, 1747 (2006); published online 29 November 2006 (10.1126/science.1134426).
7. We thank A. Jarman, H. Bellen, M. Calos, J. Bischof, K. Basler, J. Bateman, T. Wu, A. Roebroeck, as well as the Developmental Studies Hybridoma Bank (DSHB) and the Bloomington Stock Center, for sharing flies and reagents. We thank X. Quan, S. Aerts, J. Kasprowicz, and S. Kuenen for useful discussion and technical assistance. This work was supported by VIB (B.A.H., P.V.), and Impuls, CREA, and GOA (Geconcerteerd Onderzoeks Acties) grants from K. U. Leuven and FWO (Fonds Wetenschaplijke Onderzoek) grants G.0542.08N and G.0543.08N to B.A.H. as well as Research fund K. U. Leuven, and a Marie Curie Excellence grant (MEXT-CT-2006-042267) to P.V. S.V. was partially supported by a K.U. Leuven Methusalem grant from the Flemish government. pSTAR GenBank accession number is FJ710212.

Supporting Online Material

www.sciencemag.org/cgi/content/full/324/5923/54/DC1
Materials and Methods
Fig. S1
References and Notes

10 November 2008; accepted 12 February 2009
10.1126/science.1168275

[1]Department of Molecular and Developmental Genetics, VIB 3000 Leuven, Belgium. [2]Center for Human Genetics, K. U. (Katholieke Universiteit) Leuven School of Medicine, 3000 Leuven, Belgium. [3]Doctoral program in Molecular and Developmental Genetics, K. U. Leuven Group Biomedicine, 3000 Leuven, Belgium. [4]Doctoral program in Molecular and Cognitive Neuroscience, K. U. Leuven Group Biomedicine, 3000 Leuven, Belgium.

*These authors contributed equally to this work.
†To whom correspondence should be addressed. E-mail: Bassem.Hassan@med.kuleuven.be

Sequencing and Analyses of All Known Human Rhinovirus Genomes Reveal Structure and Evolution

Ann C. Palmenberg,[1]* David Spiro,[2]* Ryan Kuzmickas,[2] Shiliang Wang,[2] Appolinaire Djikeng,[2] Jennifer A. Rathe,[3] Claire M. Fraser-Liggett,[4] Stephen B. Liggett[3]†

Infection by human rhinovirus (HRV) is a major cause of upper and lower respiratory tract disease worldwide and displays considerable phenotypic variation. We examined diversity by completing the genome sequences for all known serotypes (n = 99). Superimposition of capsid crystal structure and optimal-energy RNA configurations established alignments and phylogeny. These revealed conserved motifs; clade-specific diversity, including a potential newly identified species (HRV-D); mutations in field isolates; and recombination. In analogy with poliovirus, a hypervariable 5′ untranslated region tract may affect virulence. A configuration consistent with nonscanning internal ribosome entry was found in all HRVs and may account for rapid translation. The data density from complete sequences of the reference HRVs provided high resolution for this degree of modeling and serves as a platform for full genome-based epidemiologic studies and antiviral or vaccine development.

Human rhinovirus (HRV), the disease agent for the common cold, is responsible for ~50% of asthma exacerbations and is one of the factors that can direct the infant immune system toward an asthmatic phenotype (*1*–*4*). Direct and indirect costs from the common cold and related complications in asthmatics amount to an estimated ~$60 billion per year in the United States (*5*, *6*). HRVs are single-stranded, positive-sense RNA enteroviruses in the *Picornaviridae* family and have been cataloged primarily by capsid serotyping relative to a historical repository of 99 strains, obtained from clinical specimens. HRVs are classified by their use of either intercellular adhesion molecule–1 (ICAM-1) (88 major viruses) or low-density lipoprotein receptor (LDLR) (11 minor viruses) as their receptor for cell entry (*7*). They have also been characterized by composite sensitivities across a panel of potential therapeutics (*8*) that have been used to parse the strains into two related drug-reactivity groups. The partial sequences of viral capsid-coding regions, noncoding regions, and a limited number of complete genomes have resulted in a division of the original 99 strains into two species: HRV-A (containing 74 serotypes) and HRV-B (containing 25 serotypes).

Recently, a number of previously unknown HRV-like sequences were detected in patients with influenza-like illnesses associated with severe respiratory compromise (*9*–*11*). The newly identified viruses have not been cultured, but their sequences indicate that they likely represent a third (HRV-C) species. The lack of whole-genome sequence data for the full cohort of HRVs has made it difficult to understand basic molecular and evolutionary characteristics of the viruses and has hampered investigations of the epidemiology of upper respiratory tract infections and asthma epidemics. To define the extent and nature of HRV diversity and their evolution, we sequenced the genomes for every previously undetermined HRV in the reference repository, completing the full set of 99 serotypes, as well as 10 additional field samples.

Genome sequences and alignments. Modifications (*12*) were made to the sequence-independent, single-primer amplification (SISPA) method (*13*) to determine the complete genomes of 70 HRVs from the reference repository, as well as 10 nasal-wash samples from patients with HRV upper respiratory tract infections. We sequenced these viruses to an average of sixfold coverage for each of the ~7-kb genomes. To provide phylogenetic accuracy for these organisms with relatively small genomes and (often) high degrees of sequence similarity, a stringent approach was taken for aligning the sequences. The initial sequence fits for the polyproteins were performed on the basis of superimposition of the amino acid sequences within virion crystal structure maps (*14*) and supplemented with additional structure data from other viral proteins. In a stepwise manner, profile hidden Markov models (HMM) augmented the founder set with the remaining sequences (*13*). The published sequences (including redundant determinations) for the remaining serotypes were added so that the final collection consisted of 138 full-length HRV genomes, including at least one representative for each of the 99 original strains, 10 field samples, and 7 HRV-C strains (table S1). The genome-length RNA and polyprotein alignments for all considered sequences are provided in tables S2 and S3. Regardless of species, all HRVs were found to have similar average base compositions. They are rich in A (31 to 34%) and U (25 to 30%) but low in G (19 to 22%) and C (18 to 22%). The third codon positions have the highest composition skew. An identity matrix for the polyproteins (fig. S1) shows that the average amino acid identity between pairs of HRV-C strains is slightly more diverse (78% identity, range 68% to 95%) than among the HRV-A (80%, range 64% to 99%) or HRV-B (83%, range 75% to 97%). The lack of broader diversity suggests that all HRVs are in a stable status for maintaining selection for certain traits, yet still have mutational flexibility for escape from immune responses.

Picornaviruses encode a single open reading frame (ORF) representing about 90% of the RNA length. Translation produces a polyprotein (~215 kD for HRV), subsequently cleaved in a viral protease–dependent cascade to form the 11 to 12 mature viral proteins required to initiate and sustain an infection (fig. S2A). Local and global RNA structures play established roles in HRV biology; however, the extent, character, and relatedness of serotype-specific 5′- and 3′UTR (untranslated region) variation are unknown. The role of this variability has thus not been related to function by modeling techniques or in vivo approaches. Our alignment methods included optimal energy RNA structure considerations (*15*) and were therefore sensitive to potential differences among the HRVs in the 5′- and 3′UTRs.

HRV RNA structures. All enteroviruses encode 5′-terminal cloverleaf-like motifs (CLs) that bind viral and cellular proteins for the initiation of RNA synthesis and also help convert infecting genomes from translation to replication templates. The HRV CLs [80 to 84 bases (b)] were predicted in every sequence with minimal structural variation among the species (representative structures are shown in Fig. 1A and additional structures in fig. S3). Immediately 3′ to the CL, all HRVs were found to share an unusual pyrimidine-rich spacer segment with short oligo(C) and oligo(U) units interspersed with As (blue boxes, Fig. 1A and fig. S3A). The HRV-A have the shortest tracts (11 to 22 b) and HRV-B the longest (22 to 50 b). Nearly every HRV displayed a unique sequence in this region, and we identified unexpected variation even among isolates of the same serotype (Fig. 1A and fig. S3A). The equivalent genome location in poliovirus (10 b) interacts with poly(C)-binding protein 2 and is involved in the determination of the polio neurovirulent potential. The analogous regions in aphthoviruses or cardioviruses have homopolymeric poly(C) or poly(UC) tracts, the deletion of which markedly attenuates the virus through an RNA-activated protein kinase activation–dependent mechanism (*16*). If the HRV 5′ spacer tracts are functional analogs to those of these other picornaviruses, then it is possible that the pathogenic potential of an individual HRV may also be encoded, in part, by this region.

Picornaviruses use internal ribosome entry sites (IRESs) to mediate translation initiation of their

[1]Institute for Molecular Virology, University of Wisconsin, Madison, WI 53706, USA. [2]. Craig Venter Institute, Rockville, MD 20850, USA. [3]Cardiopulmonary Genomics Program, University of Maryland School of Medicine, Baltimore, MD 21201, USA. [4]Institute for Genome Sciences, University of Maryland School of Medicine, Baltimore, MD 21201, USA.

*These authors contributed equally to this work.
†To whom correspondence should be addressed. E-mail: sligg001@umaryland.edu

polyprotein ORFs. The IRESs of all enteroviruses (termed type 1 IRESs) are thought to bind 40*S* ribosomal subunits internally within their 5′UTR and to then scan additional nucleotides to find the proper initiator AUG (*17*). Our modeling of the known serotypes confirms that all HRV IRESs start just 3′ to the pyrimidine-rich spacer tract. We found that the internal IRES sequences are highly conserved, with an average nucleotide identity of 82%. Indeed, this region of the genome has the greatest degree of identity among all HRV (fig. S2B), exceeding 95% for regional motifs within the IRES. However, we also observed that the dominant IRES sequence conservation did not extend completely to the initiator AUG and that for the 18 to 40 bases 5′- to this codon, the region scanned by ribosomes, there was little species-specific conservation (<60% nucleotide identity). Despite this, our folding predictions configured every one of these regions into virtually the same RNA motif, which suggests that this structure is conserved even when the underlying nucleotides are not (Fig. 1B and fig. S3B).

Near the bottom of a long [15 to 20 base pair (bp)] minimum energy unbranched stem, the ORF AUG was invariably paired with a conserved upstream noncoding AUG (green boxes, Fig. 1B), marking the 3′ boundary of the IRES, and the normal launch point for 40*S* scanning. Every HRV genome fold maintains this pairing. We predict that HRVs use the proximity of these AUGs to orient the 40*S* for direct transfer to the proper codon, without the need for scanning through the intervening nucleotides. The sequence and length variation between the AUGs was consistent with the idea that ribosomes would bypass this region entirely if they jump from one AUG to the other. This IRES folding is essentially a bait-and-switch mechanism, which we predict may enhance HRV translation competitiveness. This paired AUG motif is unique to HRV and is not found in other enteroviruses (e.g., poliovirus).

The HRV 3′UTRs (40 to 60 b) begin with the ORF termination codon and extend to the genetically encoded poly(A) tail. The ORF terminators themselves (solid red boxes in Fig. 1C and fig. S3D) included UAG, UAA, and UGA codons. The codon selection often differed among isolates from the same serotype. Multiple additional terminators (tan boxes), in and out of the ORF, were identified that punctuated each segment (3 to 9 per UTR). Despite large differences (>40%) in nucleotide identity (Fig. 1C), it was noted that all HRVs maintain a 13- to 16-bp unbranched stem, covering 67 to 88% of the 3′UTR, immediately abutting the poly(A) tail (see also fig. S3D). Some 3′ stems have small interior loops, but nearly all, except for the unusual sequences of clade-D, present 5-base terminal loops, anchored with apical U-G or U-A pairs. Inevitably, the 3′ sides of these terminal loops display UAG or UGA terminator codons, which may or may not synchronize with the local ORF. The function of these 3′ stems is unknown, but such conservation is usually indicative of a putative protein recognition motif (such as translation termination factors) or, alternatively, an RNA:RNA tertiary interaction between the terminal-loop segment and a different (unknown) region of the genome.

Phylogenetic relationships of the HRV. Multiple methods were used to compute and compare phylogenetic trees for the aligned RNA and protein data. Figure 2 is a neighbor-joining consensus tree (*18*), which considered the 5′- and 3′UTRs and the first and second codon positions for the RNA genomes. All major nodes of the tree topology were stable over a range of calculation parameters, regardless of whether they invoked minimum evolution, parsimony, unweighted pair group method with arithmetic mean, or maximum likelihood (ML) methods. (See fig. S6A for ML tree with bootstrap, likelihood ratio tests, and comparison to the neighbor-joining tree.) Statistical comparisons were performed between the ML tree generated from the full genomes and the ML constrained-topology trees generated from capsid sequences that have been used as a surrogate for serotypes (fig. S6, A to C) (*13*), with the null hypothesis that topologies of these limited-sequence trees were the same as that of the full genome-based tree. The approximately unbiased (AU) test calculated from the multiscale bootstrap *P* values for the capsid VP1 and VP0 trees were $<10^{-69}$, strongly rejecting the null hypothesis. In a similar manner, ML constrained-topology trees generated from IRES and 3D-polymerase sequences were not consistent with the full genome tree (fig. S6, A and B). Additional statistical tests also confirmed these results from the AU (fig. S6, B and C) for all four of the constrained-topology trees. Taken together, these results suggest that trees based on sequences from small, albeit biologically important, regions of the HRV genome have a limited capacity to reflect the evolutionary relationships and underlying diversity of HRVs. The tree shown in Fig. 2 also accurately represents parallel calculations on the aligned polyprotein dataset (p-distances differed by <2%). All aligned full-length sequences contributed to the tree calculations, but published sequences (noted with asterisks on Fig. 2) are shown only as needed, to complete the cohort of reference serotypes. (Were the redundant published sequences illustrated, without exception they would lie on the same-serotype branches, with p-distances <0.5%.) The outer rings of this figure designate major (M: ICAM-1) or minor (m: LDLR) receptor preferences, and also each

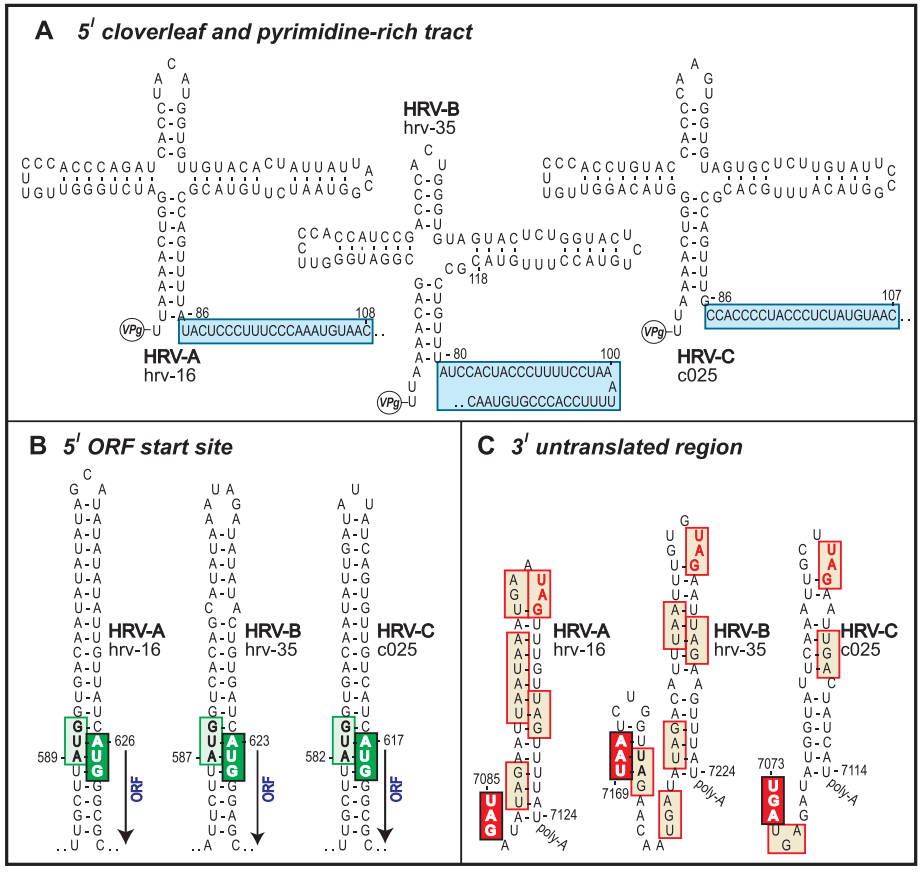

Fig. 1. Genome-wide optimal energy RNA configurations for select motifs representative of each HRV species. (**A**) All HRVs display characteristic 5′UTR CL elements with minimal predicted structural variation (blue boxes). (**B**) The alignments and predicted structures of the IRES of HRVs reveal a bait-and-switch arrangement for initiation of translation. A stem-pairing AUG (light green box) is found for each species, but a highly variable region of intervening sequence near the initiator AUG (dark green box) was noted. (**C**) HRV 3′UTRs have a unique unbranched stem motif before the poly-A tail. The left-most codon (red box, white text) is the ORF terminator. Other boxes highlight additional terminators (tan boxes), including a characteristic codon (tan box, red text) found in the apical loop.

strain's small-molecule drug reactivity group ("1" or "2") (*8*). The tree is shown rooted with three outgroup sequences from the *Human Enterovirus C* species (poliovirus 1m, coxsackieviruses a13 and a21), but the use of five additional outgroups had no effect on overall tree topology or HRV p-distances (fig. S6). The field samples (i.e., f01 to f10) were assigned tentative serotype names on the basis of capsid similarity relative to the known reference strains. Although some of the full genomes from these samples proved close to their repository cognates, a divergence in sequence for several strains was noted.

According to our tree(s), HRV-A and HRV-C share a common ancestor, which is a sister group to the HRV-B. Although the HRV-C clade currently has only seven full sequences, its genetic origin is clearly different from the reference set, and our phylogeny indicates that these represent a third HRV species, as has been recommended to the International Committee on Taxonomy of Viruses (*19*). The HRV-C have yet to be cultured or assessed for immunological cross-reactivity, but the sequence space occupied by the available samples suggests that there may be many additional HRV-C strains awaiting discovery. Distance extrapolations relative to the new full reference cohort predict that HRV-C may have an even broader range of serotypes than the original 99, of which each confers only limited immunologic cross-protection to another.

A separate phylogenic finding was the unexpected basal divergence within HRV-A of a small (n = 3) group of distinct strains, denoted clade D (*20*). Although the major basis for discriminating clade D from other HRV-A lies in their general, genome-length sequence divergence, these particular isolates have RNA elements—such as the cis-acting replication element, the 3′UTR terminal loop feature (see above and fig. S3), and local insertions/deletions and sequence motifs—that are somewhat atypical of other HRV-A strains. Some of the distinguishing characteristics are highlighted in fig. S4. Among all other major A clades, and major B clades, none have p-distances (>10%) that segregate them so distinctly. We are cautious in proposing clade D as a fourth species (HRV-D), but the phylogenetic evidence (Fig. 2) and sequence characteristics (figs. S3 and S4) are highly suggestive. Other early topological divisions within HRV-A separate a major clade composed of 10 serotypes (counterclockwise, hrv-20 through hrv-12) from a second grouping composed of ~12 miniclades representing 61 serotypes (counterclockwise, hrv-89-f09 through hrv-100). These particular relationships were not readily apparent when only partial genome sequences were examined (*21*, *22*). Fig. S6 shows a comparison of results from trees constructed with whole genomes, VP4/VP2, and VP1 sequence. Neither of the trees derived from these shorter sequences revealed the miniclades, clade D, or multiple other features. We thus contend that comparison of full-genome data, the context wherein evolutionary events occur, most likely provides the defining relationships among the HRVs, allows a more comprehensive assessment of strain diversity, and allows for more accurate historical extrapolations. The phylogenetic diversity we describe at the whole-genome level is consistent with the clinical heterogeneity of HRV infections in humans (*1*, *3*, *4*), although mapping specific clinical characteristics (i.e., incubation period, severity, respiratory compromise, and pro-asthmatic phenotypes) to responsible genomic regions will require additional field isolates from a large number of patients with multiple traits. Given the genome-wide diversity we have documented (e.g., 5′ spacer elements, ORF start, protease, 3′UTRs), clinically relevant relationships may well depend on comparisons from multiple genome regions.

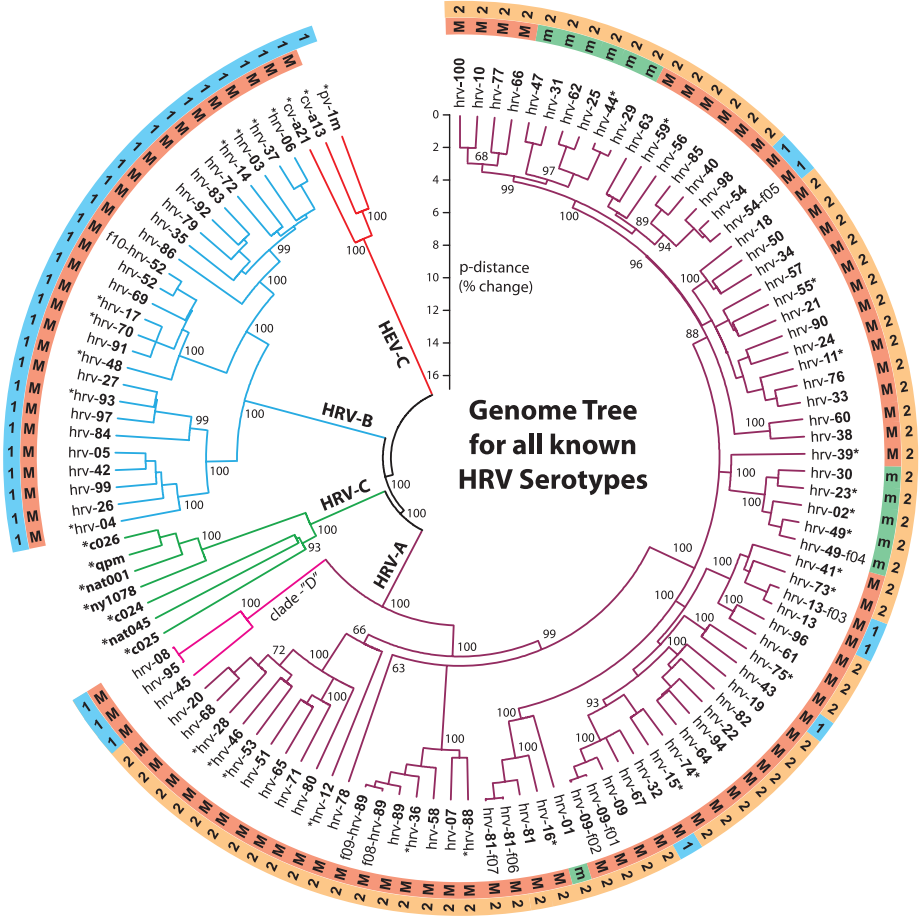

Fig. 2. A neighbor-joining (NJ) phylogenetic tree showing relationships between all known HRV serotypes created on the basis of full genome sequences. The HEV-C sequences (poliovirus 1M, coxsackievirus a13, and coxsackievirus a21) were used as outgroups. Branch lengths are proportional to similarity (p-distance). Key nodes on this tree are annotated with NJ bootstrap values (percentage of 2000 sampled trees). Asterisks in the strain names identify sequences obtained from published data (table S1). All other taxa are from this study. Letters in the outer rings designate whether that virus uses the major (M) ICAM-1 receptor or the minor (m) LDLR receptor (*7*) and whether its relative reactivity was more like group "1" or group "2" (if known) toward a panel of small-molecule antiviral compounds (*8*).

Recombination in HRV. Results from earlier sequencing of a subset of HRV reference genomes concluded that RNA recombination was not a major mechanism for HRV diversity (*23*, *24*) and asserted that known isolates were independently segregating entities. We have reevaluated the potential for recombination by scanning the full reference set and the new field strains with a suite of recombination detection programs (*25*) relying on phylogenetic distance and sequence similarity. Stringent criteria ($P < 0.00001$ from two or more analyses modes) identified 23 genomes with probable origins resulting from at least 12 independent recombination events. Figure 3A shows representative data indicating that hrv-46 arose by recombination between hrv-53 (major parent) and hrv-80 (minor parent). Within the hrv-46 genome, nucleotides 32 to 3222 are most similar to hrv-80, whereas the rest of the genome (nucleotides 3223 to 7200) is common to hrv-53. The result is consistent with this trio's computed phylogenetic relationship (Fig. 2), placing the major parent (hrv-53) and the daughter (hrv-46) in the same clade and the minor parent (hrv-80) in a different, nearby clade. Results for all 23 identified recombination scenarios are summarized in Table 1. [See also (*13*) and table S4.] Of the recombination locales suggested by these events, the majority (10 of 12) involve the 5′UTR or the adjacent capsid genes, which seemingly have been collectively rearranged to produce at least 20 separate progeny strains. Among the

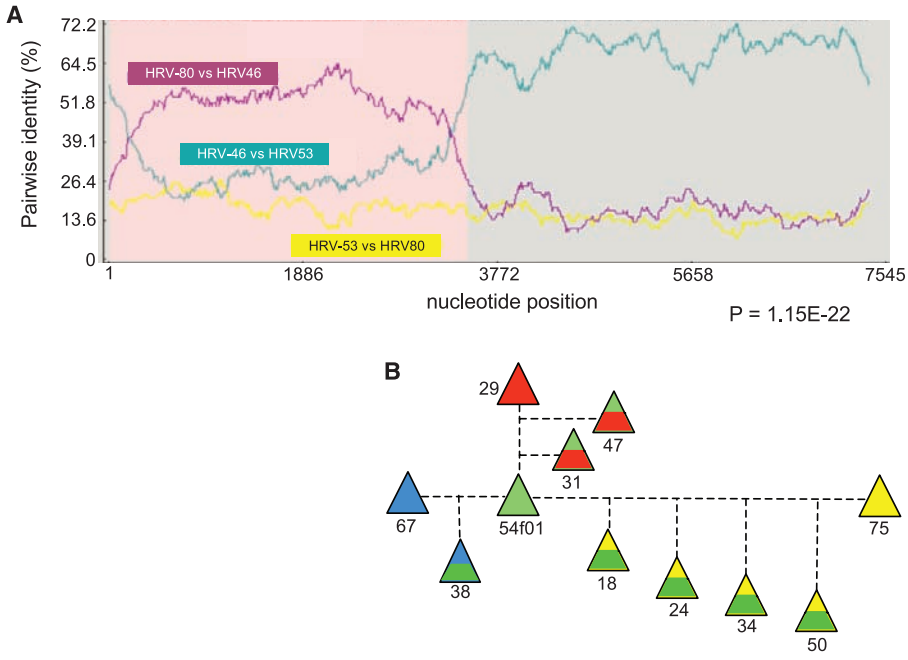

Fig. 3. Recombination of HRVs creates additional serotypes. (**A**) Representative results showing that hrv-46 arose from a recombination of hrv-53 (major parent) and hrv-80 (minor parent). Shown are normalized pairwise identities between each parent and the daughter hrv (purple and green) and the two parents (yellow). As indicated, hrv-46 nucleotides 32 to 3222 are from hrv-80, and nucleotides 3223 to 7200 are from hrv-53. (**B**) Recombination with an ancestor of hrv-54-f05 has resulted in seven serotype progeny. Each parental hrv is shown as a solid color. The contribution of each parent is proportional to the area of its color in the offspring. See Table 1 and table S4 for nucleotide boundaries and results from other recombination events.

Table 1. Recombination events in HRV serotypes. The *P* value listed is the lowest obtained. See table S4 for full data and *P* values.

Major parent	Minor parent	Recombinant	Genome region	*P*
hrv-45	hrv-21	hrv-8	5′UTR	1.094×10^{-21}
hrv-45	hrv-21	hrv-95	5′UTR	1.094×10^{-21}
hrv-65	hrv-21	hrv-80	5′UTR, VP4	6.129×10^{-23}
hrv-51	hrv-11	hrv-20	5′UTR, VP4	8.402×10^{-26}
hrv-51	hrv-11	hrv-68	5′UTR, VP4	8.402×10^{-26}
hrv-28	hrv-62	hrv-71	5′UTR	8.484×10^{-15}
hrv-54-f05	hrv-75	hrv-18	5′UTR, VP4, VP2, VP3, VP1	3.737×10^{-7}
hrv-54-f05	hrv-75	hrv-24	5UTR, VP4, VP2, VP3, VP1	3.737×10^{-7}
hrv-54-f05	hrv-75	hrv-50	5′UTR, VP4, VP2, VP3, VP1, P2A	3.737×10^{-7}
hrv-54-f05	hrv-75	hrv-34	VP4, VP2, VP3, VP1	3.737×10^{-7}
hrv-54-f05	hrv-67	hrv-38	VP2, VP3, VP1, P2A, P2B, P2C, P3A	1.561×10^{-29}
hrv-54	hrv-67	hrv-60	VP2, VP3, VP1, P2A, P2B, P2C, P3A	1.561×10^{-29}
hrv-53	hrv-80	hrv-46	5′UTR, VP4, VP2, VP3, VP1	1.291×10^{-62}
hrv-13-f03	HRV41	hrv-73	5′UTR, VP4, VP2, VP3, VP1	9.419×10^{-12}
hrv-30	hrv-59	hrv-39	5′UTR, VP4, VP2, VP3, VP1	2.963×10^{-12}
hrv-68	hrv-20	hrv-28	VP4, VP2, VP3, VP1, P2A, P2B, P2C	6.839×10^{-12}
hrv-100	hrv-10	hrv-56	P2A, P2B, P2C, P3A, P3B, P3C, P3D	4.230×10^{-17}
hrv-29	hrv-54-f05	hrv-31	P3C, P3D	7.934×10^{-13}
hrv-29	hrv-54-f05	hrv-47	P3C, P3D	1.232×10^{-10}
hrv-42	hrv-97	hrv-4	5′UTR, VP4	8.233×10^{-35}
hrv-84	hrv-37	hrv-27	5′UTR, VP4	1.500×10^{-10}
hrv-84	hrv-37	hrv-93	5′UTR, VP4	1.500×10^{-10}
hrv-84	hrv-37	hrv-97	5′UTR, VP4	1.500×10^{-10}

138 full-length sequences, hrv-54 (or its ancestor) was apparently the most active in recombination. Field strain hrv-54-f05 links closely to three separate events (see Fig. 3B), contributing to at least seven different serotype progeny. In confirmation studies, we used a progressive alignment method for the HRV genomes (*13*), then repeated the suite of recombination detection programs. Of the 23 recombination events from the HMM alignment (Table 1), 19 were also found after the progressive alignment, although in some cases different major and/or minor parents were selected from within the same closely related clade (table S4).

Although the sequence fingerprints clearly trace these ancestral patterns, nevertheless all extant progeny also showed evidence of subsequent sequence divergence within the exchanged regions. Recombination was not identified between isolates from different species (i.e., HRV-A and HRV-B), but receptor binding preferences between ICAM and LDLR apparently presented no barriers to exchange. Major group hrv-54 and minor group hrv-29, for example, both contributed to the common ancestor of the minor group viruses, hrv-31 and hrv-47. These results, particularly for HRVs with different receptor preferences and those from distant clades, such as the parents hrv-21 and hrv-65, suggest that coinfection of the host with multiple parental strains is not uncommon and may lead to variant progeny with different biological properties. Our field isolates also deviated from the reference sequences in a manner that was not confined to any specific portion of the genome. In fact, field strain deviation relative to the reference isolates (for example, hrv-52-f01 versus hrv-52 differ by 838 nucleotides) was frequently greater than that observed between pairs of characterized serotypes (hrv-44 and hrv-29 differ by 385 nucleotides). Indeed, field samples of the same serotype collected from the same geographical region within 1 year showed marked variability (tables S2, S3, and S5). The propensity for such variation could underlie the marginal efficacy, or lack of efficacy, of anti-HRV therapeutics in clinical trials (*26*, *27*). Given our reference set of full genomes, along with the means to rapidly sequence full genomes from field samples, new strategies may become apparent to engineer clade-specific agents by targeting their commonalities.

Conclusions. Our data complete and define the full set of genome-length sequences in the canonical reference repository of 99 HRV-A and HRV-B serotypes. Alignment and examination of these genomes confirmed species-specific sequence and RNA structural elements that differentiate the HRV-A and HRV-B from newly described HRV-C and further suggest that the HRV-A serotypes harbor a distinct, uncharacteristic clade, which may represent a fourth species (HRV-D). Local sequence variation, particularly in the 5′UTR, characterized each isolate within regions associated with the pathogenic potential for other picornaviruses. Parallel RNA structure comparisons defined several 5′ and 3′ elements as common to all isolates and unique to the HRV. Motifs like the AUG-presenting 5′ ORF initiation stem, or the UAG-presenting 3′ stem, may

contribute to HRV-specific IRES translation mechanisms, ORF termination, or polymerase recognition. We also found embedded within multiple sequences, including recent field isolates, clear evidence for repeated, historical genome recombination. Coinfection with multiple HRVs is known to occur (*28*), and we now know that this can lead to strains that may have distinct biologic properties and clinical characteristics. The required host environment for HRV recombination is not known, but with complete genome sequences from additional patient isolates such factors may become apparent. Our repository data set provides a baseline framework for the analysis of additional HRVs that may be in communities, including the HRV-Cs, and will enable larger-scale studies of basic molecular and evolutionary characteristics and assignment of disease phenotypes to specific genome regions. The clustering of small clades, the recombinations, and the mutations found in all regions of these genomes suggest that future HRV epidemiologic studies might benefit from full genome sequencing rather than the more limited serotyping. With such an approach, correlations may be more informative in inferring pathogenic potential and in designing antiviral agents and vaccines.

References and Notes

1. J. M. Gwaltney Jr., J. O. Hendley, G. Simon, W. S. Jordan Jr., *N. Engl. J. Med.* **275**, 1261 (1966).
2. S. L. Johnston *et al.*, *Am. J. Respir. Crit. Care Med.* **154**, 654 (1996).
3. K. G. Nicholson, J. Kent, D. C. Ireland, *Br. Med. J.* **307**, 982 (1993).
4. D. J. Jackson *et al.*, *Am. J. Respir. Crit. Care Med.* **178**, 667 (2008).
5. A. M. Fendrick, A. S. Monto, B. Nightengale, M. Sarnes, *Arch. Intern. Med.* **163**, 487 (2003).
6. K. B. Weiss, S. D. Sullivan, *J. Allergy Clin. Immunol.* **107**, 3 (2001).
7. M. Vlasak *et al.*, *J. Virol.* **79**, 7389 (2005).
8. K. Andries *et al.*, *J. Virol.* **64**, 1117 (1990).
9. S. R. Dominguez *et al.*, *J. Clin. Virol.* **43**, 219 (2008).
10. P. McErlean *et al.*, *PLoS ONE* **3**, e1847 (2008).
11. S. K. Lau *et al.*, *J. Clin. Microbiol.* **45**, 3655 (2007).
12. A. Djikeng *et al.*, *BMC Genomics* **9**, 5 (2008).
13. Materials and methods are available as supporting material on *Science* Online.
14. A. C. Palmenberg, J.-Y. Sgro, in *Molecular Biology of Picornaviruses*, B. L. Semler, E. Wimmer, Eds. (ASM Press, New York, 2001).
15. A. C. Palmenberg, J.-Y. Sgro, *Semin. Virol.* **8**, 231 (1997).
16. L. R. Martin, G. M. Duke, J. E. Osorio, D. J. Hall, A. C. Palmenberg, *J. Virol.* **70**, 2027 (1996).
17. R. J. Jackson, in *Translational Control*, W. B. Hershey, M. B. Mathews, N. Sonenberg, Eds. (Cold Spring Harbor Laboratory Press, Cold Spring Harbor, NY, 1996).
18. K. Tamura, J. Dudley, M. Nei, S. Kumar, *Mol. Biol. Evol.* **24**, 1596 (2007).
19. On the basis of these data, the International Committee on Taxonomy of Viruses Picornavirus Study Group recently proposed to recognize them as a new species (*29*).
20. hrv-08 and hrv-95 are designated as two different serotypes by ATCC but differ by 67 nucleotides, perhaps indicating a misidentification in the repository.
21. R. M. Ledford *et al.*, *J. Virol.* **78**, 3663 (2004).
22. C. Savolainen, S. Blomqvist, M. N. Mulders, T. Hovi, *J. Gen. Virol.* **83**, 333 (2002).
23. A. L. Kistler *et al.*, *Virol. J.* **4**, 40 (2007).
24. P. Simmonds, *J. Virol.* **80**, 11124 (2006).
25. D. Martin, E. Rybicki, *Bioinformatics* **16**, 562 (2000).
26. R. Fleischer, K. Laessig, *Clin. Infect. Dis.* **37**, 1722 (2003).
27. D. L. Barnard, *Curr. Pharm. Des.* **12**, 1379 (2006).
28. C. Savolainen, M. N. Mulders, T. Hovi, *Virus Res.* **85**, 41 (2002).
29. N. Knowles, personal communication.

30. Funded by the University of Maryland School of Medicine internal funds and by NIH grant U19-AI070503. We thank A. Wolf and J.-Y. Sgro for implementation of the tree topology tests. The accession numbers for the hrv strains are FJ445111 to FJ445190 (see table S1).

Supporting Online Material

www.sciencemag.org/cgi/content/full/1165557/DC1
Materials and Methods
Figs. S1 to S6
Tables S1 to S5
References

5 September 2008; accepted 4 February 2009
Published online 12 February 2009;
10.1126/science.1165557
Include this information when citing this paper.

REPORTS

Photodegradable Hydrogels for Dynamic Tuning of Physical and Chemical Properties

April M. Kloxin,[1] Andrea M. Kasko,[1,2]* Chelsea N. Salinas,[1] Kristi S. Anseth[1,2]†

We report a strategy to create photodegradable poly(ethylene glycol)–based hydrogels through rapid polymerization of cytocompatible macromers for remote manipulation of gel properties in situ. Postgelation control of the gel properties was demonstrated to introduce temporal changes, creation of arbitrarily shaped features, and on-demand pendant functionality release. Channels photodegraded within a hydrogel containing encapsulated cells allow cell migration. Temporal variation of the biochemical gel composition was used to influence chondrogenic differentiation of encapsulated stem cells. Photodegradable gels that allow real-time manipulation of material properties or chemistry provide dynamic environments with the scope to answer fundamental questions about material regulation of live cell function and may affect an array of applications from design of drug delivery vehicles to tissue engineering systems.

Hydrogels are hydrophilic polymers swollen by water that are insoluble owing to physical or chemical cross-links. These water-swollen gels are used extensively as biomaterials for complex device fabrication (*1*), cell culture for tissue regeneration (*2*), and targeted drug release (*3*). Often, sophisticated control of the gel structure in space and time is required to elucidate the dynamic relationship between biomaterial properties and their influence on biological function (*4*, *5*). For example, progenitor cells are often expanded and differentiated in hydrogel microenvironments, and researchers have demonstrated how the initial gel properties, including mechanics (*6*, *7*) and chemical functionality (*8*), influence cellular fate. In regenerative medicine, the structure and composition of gels are also regulated temporally, through hydrolytic (*9*) and enzymatic (*10*–*12*) degradation mechanisms, to promote cell secretory properties and encourage the development of tissue-like structures in vitro and in vivo. A major challenge is determining which biochemical and biophysical features must be presented in a gel culture environment.

Hydrogel structure and functionality have evolved from the direct encapsulation of cells in simple homogeneous materials to those with highly regulated structures spanning multiple size scales [e.g., through self-assembly (*13*) or microengineering (*14*)]. These hydrogel structures are further modified locally by cells with the synthetic incorporation of bioresponsive functionalities (*15*) or externally by advanced patterning to create spatially varying functionalities. For example, the chemical patterning of a gel by the addition of a second, interpenetrating network or peptide tether has been demonstrated by diffusing chemical moieties into a gel and covalently linking these functionalities to the network by photocoupling (*16*) or reaction with a photolytically uncaged reactive group (*17*). Although these are important advances, such processes do not allow modulation of the gel chemistry in real time or photodegradation of the gel structure. Few synthetic materials provide a cellular microenvironment in which physical or chemical cues are initially present and subsequently regulated on demand. We have synthesized monomers capable of polymerizing in the presence of cells to produce photolytically degradable hydrogels whose physical or chemical properties are tunable temporally and spatially with light. The desired gel property for altering cell function or fabricating a

[1]Department of Chemical and Biological Engineering, University of Colorado, 424 UCB ECCH 111, Boulder, CO 80309, USA. [2]Howard Hughes Medical Institute, University of Colorado, 424 UCB ECCH 111, Boulder, CO 80309, USA.

*Present address: Department of Bioengineering, University of California, Los Angeles, CA, 90095–1600, USA.
†To whom correspondence should be addressed. E-mail: Kristi.Anseth@colorado.edu

device is thus externally triggered and directed with irradiation by photolytic cleavage and removal of the macromolecules that compose the gel.

The photodegradable functionality, a nitrobenzyl ether-derived moiety, was selected based on its photolytic efficiency, susceptibility to two-photon photolysis, and previous use in live cell culture and imaging (*18*, *19*). Similar photolabile functionalities have been used in multistep gel-modification processes (*20*). A base photodegradable monomer was synthesized by acrylation of the photolabile moiety by a pendant hydroxyl group [photodegradable acrylate (PDA)] (Fig. 1A) and was subsequently attached with a pendant carboxylic acid to poly(ethylene glycol) (PEG)–*bis*-amine to create a photocleavable cross-linking diacrylate macromer (Compound 1, Fig. 1B) from which PEG-based photodegradable hydrogels (Fig. 1C) were synthesized. This approach, in which the photolabile moiety is incorporated within the network backbone, is fundamentally different from strategies in which reactive groups or biomolecules are asymmetrically caged or capped by a photolabile group (*20*). Here, the hydrogel itself is cleaved upon light exposure, decreasing the local network cross-link density and resulting in macroscopic property changes such as stiffness, water content, diffusivity, or complete erosion, all in the presence of cells.

The photodegradable cross-linker, Compound 1, was copolymerized with PEG monoacrylate (PEGA) in phosphate-buffered saline (PBS) by redox-initiated free radical polymerization to create photodegradable hydrogels. Upon irradiation, these hydrogels release modified PEG, and after complete degradation they release modified poly(acrylate) chains, as shown in Fig. 1C. The bulk photodegradation of these hydrogels, ensured by flood irradiation through a small thickness of material, was characterized within a parallel-plate rheometer (*21*). The storage modulus (G') is proportional to the hydrogel cross-linking density (ρ_x) (*22*, *23*), allowing calculation of the characteristic photolabile group degradation time (τ) when normalized to its initial value (G'_o) via $G'/G'_o = \rho_x/\rho_{xo} = \exp(-2t/\tau)$. At an irradiation intensity of 10 mW/cm^2 at 365 nm, typical irradiation conditions for hydrogel photopolymerizations in the presence of cells (*24*), the hydrogel completely degrades in 10 min ($\tau \sim 280$ s) (Fig. 1D). As expected from photolysis kinetics (supporting online text), doubling the intensity halves the time to complete degradation ($\tau \sim 140$ s) (Fig. 1D), whereas irradiation at 405 nm increases the degradation time inversely with the relative molar absorptivity ($\tau \sim 930$ s) (Fig. 1D). When the irradiation is ceased, the degradation is arrested; degradation is recommenced upon further irradiation (Fig. 1E). The degradation rate and extent and the resulting material properties such as stiffness thus can be predictably manipulated with light intensity and wavelength.

Precise control of gel cross-linking density was used to examine the influence of gel structure on cell spreading. Specifically, human mesenchymal stem cells (hMSCs) were encapsulated within a densely cross-linked gel where they exhibit a rounded morphology (Fig. 1F). When the gel cross-linking density was reduced through photodegradation, cell spreading was observed (Fig. 1G), whereas the cell viability was maintained (fig. S4). Thus, cell morphology can be manipulated by irradiation and degradation of these hydrogels at any time in culture. Although this control can be useful for allowing cell spreading or extracellular matrix (ECM) elaboration, this molecular-scale degradation does not allow for bulk cell migration or long-range cell-cell interactions, which require fabrication of micron-scale channels by gel erosion.

To study gel erosion, degradation was first confined to the irradiation surface by selecting an irradiation wavelength that corresponds to a high photolabile group molar absorptivity (fig. S1). Because the light intensity is highest within the uppermost layers of a thick gel, these top layers erode away rapidly during light exposure before degradation of underlying layers (see schematic, Fig. 2A). Irradiation of a hydrogel through a photomask degrades the material in the exposed regions and creates progressively recessed areas, whereas material in the unexposed areas remains intact (see photographic series, Fig. 2A). Profilometry reveals well-defined ridges, demonstrating reproduction of the irradiation pattern, and feature height increases linearly with exposure time (Fig. 2A). Such photolithographic techniques at highly absorbed wavelengths can be used to create surface features of varying height and width postgelation, while avoiding concomitant dimension changes in the hydrogel bulk, useful for the fabrication and subsequent manipulation of cell culture devices.

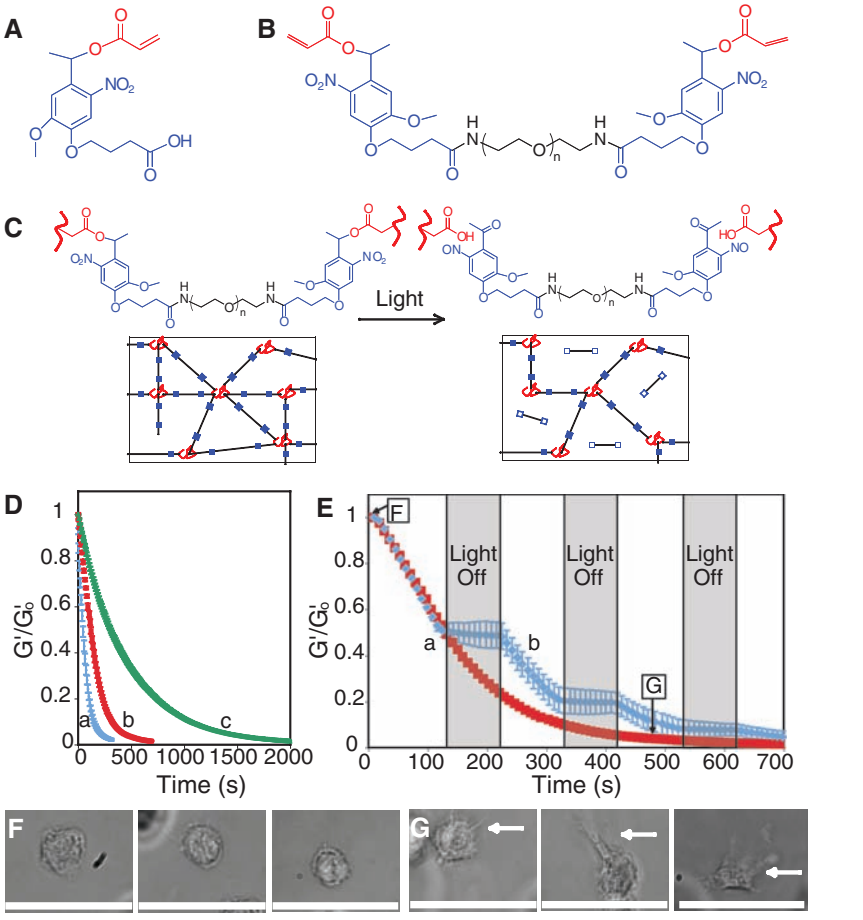

Fig. 1. Photodegradable hydrogel synthesis and degradation for tuning gel properties. (**A**) The base photodegradable acrylic monomer was used to synthesize (**B**) the photodegradable cross-linking macromer (Compound 1, $M_n \sim 4070$ g/mol), composed of PEG (black), photolabile moieties (blue), and acrylic end groups (red). (**C**) Compound 1 was copolymerized with PEGA ($M_n \sim 375$ g/mol), creating gels composed of poly(acrylate) chains (red coils) connected by PEG (black lines) with photolabile groups (solid blue boxes) (left). Upon irradiation, the photolabile moiety cleaves (open blue boxes), decreasing ρ_x and releasing modified PEG (right). (**D**) The physical structure of the hydrogel is degraded by photolysis, decreasing ρ_x and G'. The influence of irradiation on G', normalized to G'_o, was monitored with rheometry. The degradation rate was precisely controlled with irradiation intensity and wavelength: (a) 365 nm at 20 mW/cm^2, (b) 365 nm at 10 mW/cm^2, and (c) 405 nm at 25 mW/cm^2. (**E**) The gel degradation was modulated by either (a) continuous or (b) periodic irradiation with 365 nm at 10 mW/cm^2. The extents of degradation corresponding to the materials used in Fig. 1, F and G, are indicated. (**F**) hMSCs encapsulated within dense hydrogels exhibit a rounded morphology. (**G**) Irradiation (480 s, 365 nm at 10 mW/cm^2) significantly degrades the gel ($\rho_x/\rho_{xo} \sim 0.04$), promoting hMSC spreading after 3 days in culture. Scale bar, 50 μm.

Controlled creation of three-dimensional (3D) cell culture microenvironments facilitates the examination of cell-matrix and cell-cell interactions. The postgelation addition of chemical moieties, such as peptides, to hydrogels in three dimensions has been demonstrated in a multistep technique using a two-photon laser scanning microscope (LSM) (*16*, *17*). Using a photodegradable hydrogel in conjunction with a single (405 nm) (fig. S2) or two-photon (740 nm) LSM (Fig. 2B), we generated 3D features within a hydrogel by local photodegradation with scan parameters similar to those used for cell imaging and without the addition of chemical moieties. This rapid patterning (seconds to minutes) is achieved by controlled rastering of the laser focus within the hydrogel, locally degrading the polymer network and creating arbitrary 3D features on the micron scale (schematic, Fig. 2B). Interconnected channels, potentially useful for directing cell connectivity and/or migration, were created within a rhodamine-labeled photodegradable hydrogel with a two-photon LSM and visualized using brightfield and fluorescence microscopy (Fig. 2B). Other features of arbitrary shape and size for desired applications such as device fabrication can be precisely and rapidly patterned within these photodegradable hydrogels in situ using either a single or two-photon LSM with standard imaging parameters (fig. S2).

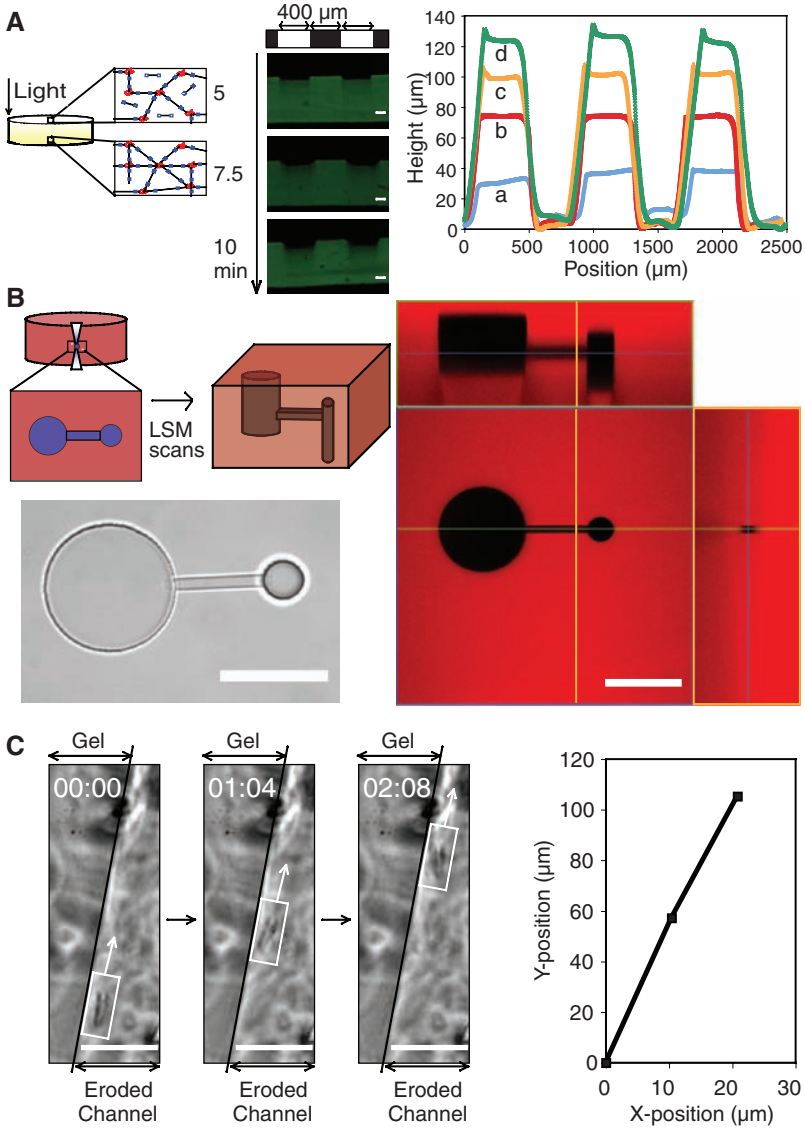

Fig. 2. 2D and 3D patterning of photodegradable hydrogels. (**A**) Thick gels demonstrate surface erosion upon irradiation (left). A gel covalently labeled with fluorescein was eroded spatially through masked flood irradiation (320 to 500 nm at 40 mW/cm^2, 400 μm line periodic photomask). Channel depth increased linearly with irradiation, and no changes in hydrogel dimensions due to increased swelling were observed (middle). Feature dimensions were quantified with profilometry: (a) 2.5, (b) 5, (c) 7.5, and (d) 10 min irradiation (right). Scale bar, 100 μm. (**B**) Interconnected 3D channels were fabricated within a photodegradable gel, covalently labeled with rhodamine B, using a two-photon LSM. A thin horizontal channel connected two offset vertical channels of different diameter, which was visualized in brightfield (bottom left) and with confocal LSM (right, intact gel is red and the created feature is black; corresponding cross sections are noted by blue, green, and orange lines). Scale bar, 100 μm. (**C**) Channels were eroded within a hydrogel encapsulating fibrosarcoma cells, releasing cells into the degraded channel and enabling migration. Migration of a cell along the edge of a channel is shown in time-lapsed brightfield images (left) and its corresponding position trace (right). Scale bar, 50 μm.

To demonstrate how erosion of these photodegradable hydrogels can be used to direct cell migration, fibrosarcoma cells were encapsulated within a hydrogel. A portion of these entrapped cells was subsequently released by degrading channels within the gel using photolithography. Cells near the periphery of the channel or released by erosion of the channel were then allowed to migrate along the channel length (Fig. 2C). With the ability to pattern microscopic to macroscopic structures in the presence of encapsulated cells, these photodegradable hydrogels provide a cell culture platform to allow unique studies of directed cell migration (*25*, *26*) and cell connectivity (*27*) by enabling real-time manipulation of the cell microenvironment. It is important to note, however, that cell migration exclusively occurs in regions of complete or near-complete gel erosion. In many cases, the culturing of cells in an environment that allows bulk migration is desirable, with subsequent direction of cell-cell interactions at a certain point in time or space. To achieve this, complementary chemistries, such as enzymatically degradable moieties, can be incorporated within these gels by, for example, Michael addition (*9*) of the photodegradable cross-linker with an enzymatically cleavable, thiol-containing peptide (*2*).

The aforementioned techniques have focused on the patterning of hydrogels for degradation of the physical network structure; however, photodegradable linkages can also be exploited to locally modify the chemical environment within a hydrogel by incorporation of tethered, but photolabile, biologically active functionalities. To demonstrate, the PDA monomer was coupled through its pendant carboxylic acid to the ubiquitous adhesion peptide sequence Arg-Gly-Asp-Ser (RGDS) (*28*), producing an asymmetric, photodegradable, biofunctional acrylic monomer (Fig. 3A). Copolymerization of this photoreleasable macromer with a nondegradable PEG diacrylate (PEGDA) yields a hydrogel with photolytic control over its chemical interaction with encapsulated cells (Fig. 3B). Upon irradiation, the modified peptide is cleaved from the polymer network and released into solution, where it quickly diffuses out of the gel (fig. S3). Peptide presentation within the microenvironment can thus be controlled with irradiation at a rate based on the photolabile group characteristic degradation time (Fig. 1D). More generally, this technique can be used for controlling the chemical structure of hydrogels in three dimensions and in time, where the peptide RGDS can be replaced with any biomolecule of interest, creating an additional tool for the modulation of ligand presentation (*4*).

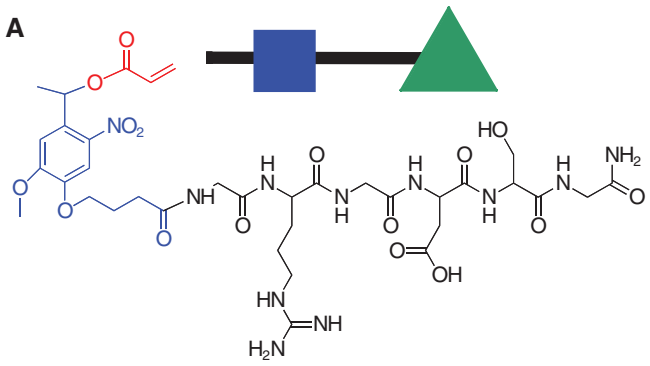

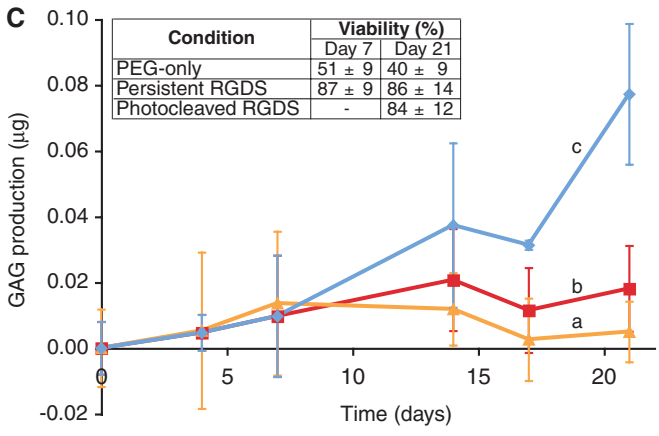

Fig. 3. Photolabile RGDS tether synthesis and use for dynamic changes in microenvironment chemistry. (**A**) A photolabile asymmetric biofunctional acrylic monomer (Compound 2) was synthesized containing the adhesion peptide RGDS (black) attached to the PDA (acrylate in red and photolabile moiety in blue). (**B**) Compound 2 was polymerized (green triangle with closed blue box) into a nondegradable gel (red poly(acrylate) coils connected by black nondegradable PEG cross-links) whose chemical composition is controlled with light exposure by photolytic release of the tethered biomolecule RGDS (bottom, green triangle with open blue box). hMSCs were encapsulated in nondegradable PEG gels (b) with or (a) without photoreleasable RGDS. The presentation of RGDS was temporally altered by (c) photocleavage of RGDS from the gel on day 10 in culture. (**C**) RGDS presentation maintains hMSC viability within PEG-based gels (inset table). RGDS photolytic removal on day 10 directs hMSC chondrogenesis, (c) increasing GAG production four-fold over (b) persistently presented RGDS or (a) PEG-only gels by day 21 ($P < 0.05$), an indicator of hMSC chondrogenesis.

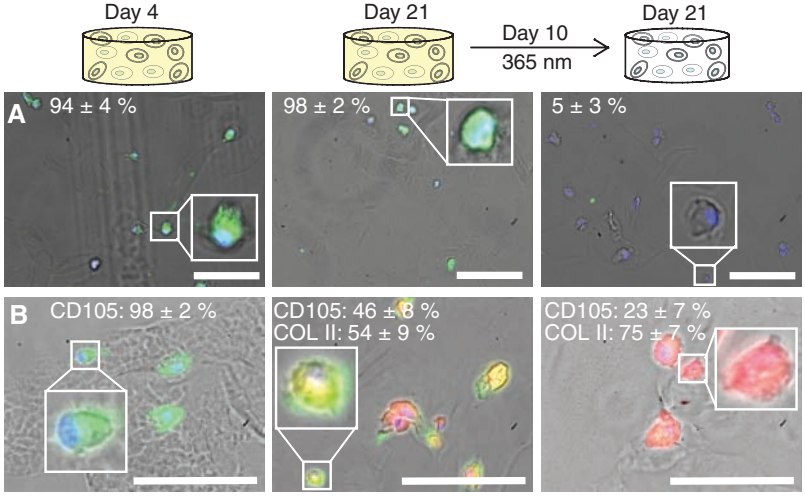

Fig. 4. Influence of dynamic microenvironment chemistry on integrin expression and differentiation. (**A**) Cells (4′,6′-diamidino-2-phenylindole–labeled nuclei, blue) cultured with persistent RGDS express the cell-surface integrin $\alpha_v\beta_3$ (fluorescein isothiocyanate–labeled, green) on day 4 (left) and day 21 (middle) in culture. Cells with photocleaved RGDS have decreased expression of the $\alpha_v\beta_3$ integrin by day 21 (right), indicating that the cells have responded to the removal of RGDS. (Representative images shown with average cell percentages noted.) (**B**) Chondrogenic differentiation of hMSCs was verified by immunostaining for the hMSC marker CD105 (FITC, green) and the chondrocyte marker COLII (tetramethyl rhodamine isothiocyanate–labeled, red). Within error, no cells initially produce COLII (day 4, left). By day 21, half of the cells presented persistently with RGDS strongly expressed CD105, and the other half produced COLII (middle). With photolytic removal of RGDS on day 10, one-fourth of the cells strongly expressed CD105 and three-fourths produced COLII (right), supporting that photolytic removal of RGDS increases chondrogenesis. (Representative images shown with average cell percentages strongly expressing the marker noted.) Scale bars, 100 μm.

To demonstrate the utility of this photolabile tether platform, hMSCs were encapsulated in nondegradable PEGDA hydrogels, both with and without the photoreleasable RGDS moiety, to examine the effect of temporal RGDS presentation on hMSC viability and chondrogenic differentiation. Control of the local biochemical environment enables promotion of chondrogenesis. Although numerous researchers have incorporated the fibronectin epitope RGD into biomaterial microenvironments to promote the survival of hMSCs (*5*, *29*, *30*), few studies investigate the importance of the persistence of this signal on the differentiation fate (*31*–*33*). Natively, hMSCs differentiating into chondrocytes initially produce the adhesion protein fibronectin, which is subsequently down-regulated between days 7 and 10, while the excreted ECM is remodeled through enzyme production (*31*, *34*). After day 10, these cells up-regulate production of glycosaminoglycans (GAGs) and type II collagen (COLII), two major components of cartilage and specific indicators of chondrogenic differentiation (*31*, *34*). To examine this temporal change in vitro, a portion of the cell-gel constructs containing the photolabile RGDS tether were irradiated on day 10 in culture to remove the fibronectin epitope RGDS from the encapsulated cell microenvironment (Fig. 3B).

The absence of RGDS in 3D cell culture yields a statistically significant decrease ($P < 0.05$) in hMSC viability within the first 7 days in PEG-only gels (see inset, Fig. 3C), in agreement with other experimental results (*29*, *30*) (supporting online text). Upon photolytic removal of RGDS from the photolabile tether gels on day 10, cell viability was unaffected; however, by day 21, a four-fold statistical increase ($P < 0.05$) in the production GAGs occurred relative to the persistently presented RGDS or PEG-only hydrogels, indicating further differentiation of the hMSCs

down the chondrogenic pathway in response to the microenvironment modification (Fig. 3C and fig. S5). To examine cell interaction with this dynamic microenvironment, fixed sections were immunostained for the expression of the $\alpha_v\beta_3$ integrin, one of the cell surface integrins by which cells interact with RGDS. Cells persistently presented with RGDS express the integrin, whereas most cells with RGDS photoreleased cease integrin expression by day 21 (Fig. 4A), indicating that the cells have locally sensed and responded to the chemical change in their environment. Additionally, to determine that the elevated GAG production is associated with chondrogenesis, sections of the cell-hydrogel constructs were immunostained for the hMSC marker CD105 (transforming growth factor–β receptor) and the chondrocyte marker COLII. As hMSCs differentiate into chondrocytes in 3D culture, a decrease in CD105 expression is observed along with onset of COLII production (*35*). The photolytic removal of RGDS on day 10 is accompanied by a decrease in CD105 expression and elevated COLII production as compared with persistently presented RGDS on day 21 (Fig. 4B), indicating increased chondrogenesis. With this photodegradable tether approach, the dynamic influence of other biomolecules on cell function can be similarly studied, expanding the ability to fabricate material environments that control cell function. Although manipulation of a single signal was examined and used to direct hMSC differentiation herein, this gel system can be readily functionalized with photolabile moieties of different light absorbances and cleavage efficiencies, enabling independent control over multiple signals through selection of irradiation wavelength and intensity.

We have demonstrated the synthesis of photodegradable macromers and their subsequent polymerization to form hydrogels whose physical, chemical, and biological properties can be tuned in situ and in the presence of cells by ultraviolet, visible, or two-photon irradiation. These photodegradable hydrogels show promise as in vitro 3D cell culture platforms in which cell-material interactions are dynamically and externally directed to elucidate how cells receive and process information from their environments. Ways to promote or suppress desired cell functions may become possible with temporal and spatial regulation of the 3D culture microenvironment, leading to applications in fields ranging from controlled drug delivery to tissue regeneration.

References and Notes

1. D. B. Weibel, W. R. DiLuzio, G. M. Whitesides, *Nat. Rev. Microbiol.* **5**, 209 (2007).
2. M. P. Lutolf, J. A. Hubbell, *Nat. Biotechnol.* **23**, 47 (2005).
3. R. Langer, N. A. Peppas, *AIChE J.* **49**, 2990 (2003).
4. M. M. Stevens, J. H. George, *Science* **310**, 1135 (2005).
5. G. Chan, D. J. Mooney, *Trends Biotechnol.* **26**, 382 (2008).
6. A. J. Engler, S. Sen, H. L. Sweeney, D. E. Discher, *Cell* **126**, 677 (2006).
7. A. J. Engler *et al.*, *J. Cell Biol.* **166**, 877 (2004).
8. P. A. Kenny, M. J. Bissell, *Int. J. Cancer* **107**, 688 (2003).
9. A. Metters, J. Hubbell, *Biomacromolecules* **6**, 290 (2005).
10. M. A. Rice, J. Sanchez-Adams, K. S. Anseth, *Biomacromolecules* **7**, 1968 (2006).
11. D. Seliktar, A. H. Zisch, M. P. Lutolf, J. L. Wrana, J. A. Hubbell, *J. Biomed. Mater. Res. Part A* **68A**, 704 (2004).
12. M. Ehrbar *et al.*, *Circ. Res.* **94**, 1124 (2004).
13. G. A. Silva *et al.*, *Science* **303**, 1352 (2004).
14. A. Khademhosseini, R. Langer, *Biomaterials* **28**, 5087 (2007).
15. R. W. Sands, D. J. Mooney, *Curr. Opin. Biotechnol.* **18**, 448 (2007).
16. M. S. Hahn, J. S. Miller, J. L. West, *Adv. Mater.* **18**, 2679 (2006).
17. J. H. Wosnick, M. S. Shoichet, *Chem. Mater.* **20**, 55 (2008).
18. Y. R. Zhao *et al.*, *J. Am. Chem. Soc.* **126**, 4653 (2004).
19. M. Alvarez *et al.*, *Adv. Mater.* **20**, 4563 (2008).
20. Y. Luo, M. S. Shoichet, *Nat. Mater.* **3**, 249 (2004).
21. S. A. Khan, I. M. Plitz, R. A. Frantz, *Rheol. Acta* **31**, 151 (1992).
22. R. J. Young, P. A. Lovell, *Introduction to Polymers* (Chapman & Hall, London, ed. 2, 1991).
23. S. J. Bryant, K. S. Anseth, in *Scaffolding in Tissue Engineering*, P. X. Ma, J. Elisseeff, Eds. (Marcel Dekker, New York, 2005), pp. 69–88.
24. S. J. Bryant, C. R. Nuttelman, K. S. Anseth, *J. Biomater. Sci. Polym. Ed.* **11**, 439 (2000).
25. P. Tayalia, C. R. Mendonca, T. Baldacchini, D. J. Mooney, E. Mazur, *Adv. Mater.* **20**, 4494 (2008).
26. G. P. Raeber, M. P. Lutolf, J. A. Hubbell, *Biophys. J.* **89**, 1374 (2005).
27. M. J. Mahoney, K. S. Anseth, *Biomaterials* **27**, 2265 (2006).
28. E. Ruoslahti, M. D. Pierschbacher, *Science* **238**, 491 (1987).
29. T. Boontheekul, D. J. Mooney, *Curr. Opin. Biotechnol.* **14**, 559 (2003).
30. G. A. Hudalla, T. S. Eng, W. L. Murphy, *Biomacromolecules* **9**, 842 (2008).
31. S. Tavella *et al.*, *J. Cell Sci.* **110**, 2261 (1997).
32. C. R. Nuttelman, M. C. Tripodi, K. S. Anseth, *Matrix Biol.* **24**, 208 (2005).
33. C. N. Salinas, K. S. Anseth, *Biomaterials* **29**, 2370 (2008).
34. A. M. DeLise, L. Fischer, R. S. Tuan, *Osteoarthritis Cartilage* **8**, 309 (2000).
35. C. N. Salinas, B. B. Cole, A. M. Kasko, K. S. Anseth, *Tissue Eng.* **13**, 1025 (2007).

36. The authors thank C. Bowman, T. Scott, and C. Kloxin for comments on early versions of this manuscript and valuable discussions; A. Aimetti for peptide synthesis training; J. McCall and S. Anderson for cell culture assistance; M. Schwartz for cell migration discussions; C. Bowman and his laboratory for use of and assistance with the rheometer and profilometer; C. Kloxin for assistance with image analysis; C. DeForest, Carl Zeiss, Inc., and the Howard Hughes Medical Institute Janelia Farms campus for assistance with and use of the Zeiss 710 two-photon confocal LSM; and the Howard Hughes Medical Institute and the NIH (grants DE12998 and DE16523) for research support. A.K. thanks the NASA Graduate Student Researchers Program fellowship and the Department of Education Graduate Assistance in Areas of National Need fellowship for support. A patent related to this work has been submitted (U.S. Patent Application No. 11/374,471).

Supporting Online Material

www.sciencemag.org/cgi/content/full/324/5923/59/DC1
Materials and Methods
SOM Text
Figs. S1 to S5
References

8 December 2008; accepted 3 February 2009
10.1126/science.1169494

Switchable Ferroelectric Diode and Photovoltaic Effect in $BiFeO_3$

T. Choi, S. Lee,* Y. J. Choi, V. Kiryukhin, S.-W. Cheong†

Unidirectional electric current flow, such as that found in a diode, is essential for modern electronics. It usually occurs at asymmetric interfaces such as p-n junctions or metal/semiconductor interfaces with Schottky barriers. We report on a diode effect associated with the direction of bulk electric polarization in $BiFeO_3$: a ferroelectric with a small optical gap edge of ~2.2 electron volts. We found that bulk electric conduction in ferroelectric monodomain $BiFeO_3$ crystals is highly nonlinear and unidirectional. This diode effect switches its direction when the electric polarization is flipped by an external voltage. A substantial visible-light photovoltaic effect is observed in $BiFeO_3$ diode structures. These results should improve understanding of charge conduction mechanisms in leaky ferroelectrics and advance the design of switchable devices combining ferroelectric, electronic, and optical functionalities.

Ferroelectrics undergo a transition from a high-symmetry structure to a low-symmetry state with a spontaneous electric polarization below a transition temperature. They usually consist of a complex microstructure of domains with different orientations of the polarization that can be switched with external electric fields (*1*). Ferroelectrics are typically highly insulating because of large band gaps (*2*), and any current leakage has been considered to be a serious problem that deteriorates their functionalities (*3*, *4*). The relationship between electronic transport characteristics and ferroelectric polarization has been little studied. This is partially due to complexity associated with ferroelectric domains. In addition, leakage often occurs through extended crystallographic defects such as grain boundaries or ferroelectric domain boundaries, so the true bulk leakage conduction may not be always dominant.

Rutgers Center for Emergent Materials and Department of Physics and Astronomy, Rutgers University, Piscataway, NJ 08854, USA.

*Present address: Neutron Science Division, Korea Atomic Energy Research Institute, Daejeon 305-353, Korea.
†To whom correspondence should be addressed. E-mail: sangc@physics.rutgers.edu

On the other hand, bulk photocurrent can be induced by high-energy light illumination even in good insulators; and directional photocurrent without external bias [that is, a photovoltaic (PV) effect] has been studied in ferroelectrics (*5*–*13*). When a ferroelectric in an open circuit is illuminated by ultraviolet light, for example, a high photovoltage, much larger than the band gap, has been observed in the direction of the electric polarization (*5*–*8*). The magnitude of this photovoltage is directly proportional to the crystal length in the polarization direction. In addition, a steady-state photocurrent can be generated in the direction of electric polarization when a ferroelectric under continuous light illumination forms a closed circuit. This PV effect in ferroelectrics is distinctly different from the typical PV effect in semiconductor p-n junctions, and was investigated in Pb-based ferroelectric oxides (*9*–*11*) and $LiNbO_3$ (*6*, *8*). However, the observed photocurrent density turns out to be minuscule—on the order of a few nanoamperes/cm^2, mainly due to poor bulk dc conduction of the ferroelectrics (*8*, *9*, *11*). Utilization of small–optical-gap ferroelectrics with good carrier transport properties and large absorption of visible light extending into the red range is therefore a promising route toward novel optoelectronic applications. It may, for example, lead to increased power conversion efficiency in solar energy applications. The origin of the PV effect in ferroelectrics is controversial and has been discussed in terms of extrinsic effects such as the excitation of electrons from asymmetric impurity potentials (*12*), interfacial effects due to polarization-dependent band bending at metal-ferroelectric interfaces (*9*), or intrinsic effects such as asymmetric induced polarization through nonlinear optical processes (*13*–*15*).

Ferroelectric $BiFeO_3$ (BFO) contains transition metal ions with unpaired *d* electrons. The presence of the *d* electrons can result in a relatively small optical gap and give rise to a high concentration of charged impurities and defects (*16*). BFO becomes ferroelectric at a critical temperature (T_c) ≈ 1100 K, below which BFO exhibits a rhombohedral *R*3*c* structure with a perovskite pseudocubic unit cell (a ≈ 3.96 Å, α ≈ 89.4°) elongated along the [111] direction that coincides with the electric polarization vector ***P***. Each of our BFO crystals contained a single ferroelectric domain (*17*, *18*). Here we describe the electronic transport properties of three thin platelike BFO crystals placed between symmetric electrodes: BFO1 (~70 μm thickness, ~2 × 2 mm^2 in-plane dimension, and ~0.6-mm-diameter circular thick Au electrodes), BFO2 (~80 μm thickness, ~2.5 × 2.5 mm^2 in-plane dimension, and ~1.6 × 1 mm^2 semitransparent Au electrodes), and BFO3 (~90 μm thickness, ~1 × 2 mm^2 in-plane dimension, and ~0.6-mm-diameter circular thick Ag or Au electrodes). The BFO plates are normal to a principal axis of the pseudocubic cell, and the "in-plane or out-of-plane" component of the polarization is defined with respect to the plate surface.

We found that in all investigated specimens, there existed substantial currents that were nonlinear with applied electric field E and also depended strongly on the direction of E. The magnitude of E here is much less than ferroelectric coercivity (fig. S1), so polarization switching does not occur during the E sweep for current density, J, versus E curves. Figure 1A shows linear-scale $J(E)$ curves of BFO1 at 300 and 350 K, which exhibit diodelike behavior. For the typical p-n junction diodes, the forward current density follows an exponential relationship with applied voltage given by $J \propto \exp(qV/\alpha k_B T)$, where q is the electron charge, V is voltage, α is a constant called the ideality factor, and k_B is the Boltzmann constant. In the range of 0.05 to 0.15 kV/cm forward bias, α is 6.3 at 300 K and 4.7 at 350 K. This large ideality factor, much larger than the ideal value of 1 in semiconductor p-n junctions, has been observed in perovskite-based oxide p-n junctions, where charge trapping at defects in the bulk seems important for transport properties (*19*). We also found that J increases drastically with increasing temperature from 200 to 350 K as evident in the semi-log plot of $J(E)$ curves in the inset of Fig. 1A. In addition, the asymmetry in the $J(E)$ curve also increases with increasing T. The rectification ratios, defined as the ratios of the positive current divided by the negative one for E = ±1.3 kV/cm, at 200, 250, 300, and 350 K, are 13, 159, 488, and 495, respectively.

The diode forward and reverse directions switch when ferroelectric polarization is uniformly reversed by large electric voltage pulses. When +150-V (an E of +17 kV/cm) pulses are applied to the top electrode of BFO3 shown in Fig. 2A, the ferroelectric polarization points down, as confirmed by piezoresponse force microscopy (PFM; see supporting online materials and methods) (Fig. 2B). The electric current through the specimen is large when the current direction is also downward; that is, the diode forward direction is from top to bottom, and along the polarization direction (Fig. 2C). When –150-V pulses are applied, ferroelectric polarization switches to the upward direction, and the diode forward direction becomes from bottom to top (still along the polarization direction). Application of +150-V pulses restores the original configuration. Therefore, the diode directions switch whenever ferroelectric polarization is reversed by external pulses, and the diode forward direction is always along the ferroelectric polarization direction (Fig. 2C). The application of the second set of +150-V pulses does not completely restore the original $J(E)$ curve, and this incomplete restoration may be due to complex factors such as incomplete polarization flipping, the formation of conducting paths, or irreversible changes in the interfacial

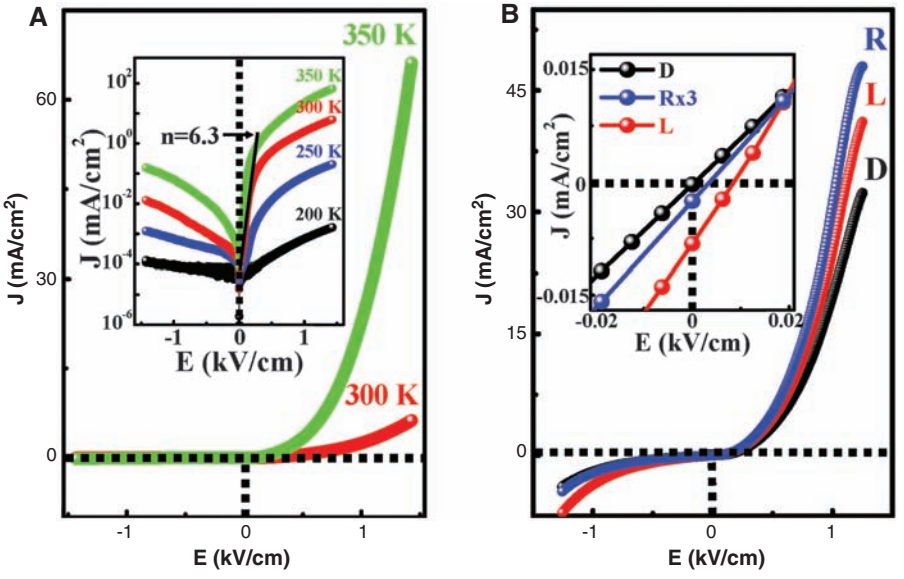

Fig. 1. (**A**) $J(E)$ curve of a symmetric Au/BFO1/Au structure in the dark at 300 and 350 K. A substantial diodelike effect is evident. The inset shows semi–log-scale $J(E)$ curves at various temperatures. All $J(E)$ measurements were performed by sweeping the voltage from the positive maximum to the negative maximum in vacuum at 200 to 350 K. The applied electric fields are far below the coercive field for polarization switching. (**B**) $J(E)$ curves of the BFO2 sample in the dark (D) and with green-light illumination on right (R) or left (L) semitransparent Au electrodes. Current for either E direction (except very near E = 0) increases with illumination on either side. The inset shows an expanded view of the $J(E)$ curves near zero bias field (E = 0). Zero-bias current flows along the reverse direction with illumination from either direction: Left-side illumination works better than right-side illumination for this particular setup, and the x and y axes for the right-side illumination are expanded by a factor of 3 to clearly show the presence of the reverse-direction current at zero bias.

regions. In the above discussion, we consider only the out-of-plane component of ferroelectric polarization because of the platelike geometry of the Ag/BFO3/Ag structure. We emphasize that even though the simultaneous $J(E)$ and PFM experiments with electric pulses were performed only on BFO3, the switchable $J(E)$ curves were observed in all specimens that we have investigated.

The observed diodelike behavior of dc conduction implies a possibility of zero-bias PV effect in BFO. Because the optical gap edge of BFO is reported to be ~2.2 eV (*20*), visible light is expected to induce substantial photocurrent. We, in fact, found a substantial PV effect in BFO with semitransparent Au electrodes illuminated with visible light [wavelength (λ) = 532-nm green light and λ = 630-nm red light], with the total power density being less than 20 mW/cm^2.

Figure 1B depicts the $J(E)$ curves of BFO2 with symmetric Au electrodes in green light as well as in the dark. Green light illuminated either left or right semitransparent Au electrodes of BFO2 (see the experimental schematic in the inset of Fig. 3). Illumination on either side induces the increase of conductance with the direction of photocurrent after the direction of the external bias. In other words, measurable photoconduction occurs with illumination. At zero bias, the photocurrent also exists and is always negative, independent from the illumination direction: negative 0.13 μA, corresponding to reverse bias direction 8.219 μA/cm^2 for the BFO2 configuration with left-side illumination; and 0.013 μA, corresponding to reverse bias direction 0.849 μA/cm^2 for the configuration with right-side illumination (Fig. 1B, inset). This bulk photocurrent in the absence of an external bias indicates that charge carriers induced by light illumination move preferentially along one direction; that is, there is a PV effect in BFO2. Figure 3 shows the time dependence of the photocurrent at zero bias in BFO2 with the turning of a green (top panel) and a red (bottom panel) light on and off. For the first 60 min, the left electrode was illuminated and for the next 60 min the right electrode was illuminated. Photoconductivity was reported in ferroelectric monodomain (111) BFO films, but any PV effect (nonzero photoconductivity at zero bias) was not discussed in the report (*21*).

In principle, thermal variation induced by visible-light illumination can contribute to the photocurrent increase shown in Fig. 1B, but the decrease of resistance due to a light-induced temperature increase cannot cause the observed negative steady photocurrent at zero bias. On the other hand, a pyroelectric current can be generated by the change of the magnitude of ferroelectric polarization because of the temperature increase caused by light illumination. However, this is a transient effect that occurs while the temperature is changing, and no steady-state photocurrent is expected from the pyroelectric effect. Thus, although the initial small spikes of photocurrent in Fig. 3 can be attributed to the pyroelectric effect, the steady-state photocurrent in Fig. 3 has a different origin. Consistently, when the light is switched on, the photocurrent increases suddenly to a transient maximum before reaching a steady state. The transient component with green light is ~6% of the steady-state photocurrent, and the time constant associated with the transient component is ~15 s. The transient component with red light is ~25% of the steady-state photocurrent and the time constant is ~60 s. The steady-state photocurrent density is ~7.35 μA/cm^2 under green light illumination on the left side. This value is much larger than the 2.6 nA/cm^2 observed under red light illumination, indicating that the photoexcited charge carriers across the bulk optical gap of ~2.5 eV contribute to the PV effect in BFO. Finally, because our BFO crystals are conducting, an equilibrium temperature gradient generated by continuous light illumination on one side of BFO can produce a steady current due to thermoelectric power voltage. However, this effect should produce an opposite-direction current when the light-illumination direction is changed from one side to the other of the BFO crystal. Our zero-bias photocurrent direction is always fixed, independent of the light-illumination conditions, which is inconsistent with the thermoelectric power scenario. On the other hand, the thermoelectric power effect may contribute to the asymmetry in the magnitude of the photocurrent with different-side light illumination, which turns out to be substantial in BFO2. Obviously, any uncontrolled asymmetry in the electrode configuration or light-illumination conditions can also contribute to the left-right asymmetry in the magnitude of the photocurrent.

A linear polarizer was placed between the light source and BFO2 to measure the effect of light polarization on the PV effect (Fig. 4, inset). The angle θ between the in-plane component of ferroelectric polarization (determined by in-plane PFM) and the electric field vector of linearly polarized light was varied by 360°. The change of the photocurrent at zero bias with θ, shown in Fig. 4 with blue circles, closely follows a sinusoidal form with a periodicity of 180°. The maximum of photocurrent was observed when the polarized-light electric field was along the in-plane ferroelectric polarization, and the current was minimal when the light electric field was perpendicular to the in-plane ferroelectric polarization. After the initial rotation experiment, the polarizer was rotated by 90°, and lighting conditions were readjusted for an optimum photocurrent. The change of photocurrent (green circles) with θ after this polarizer rotation is similar to the one before rotating the polarizer, except for a 90° phase shift of θ. This demonstrates that the reproducible angular dependence is not due to any artifact of our optical setup.

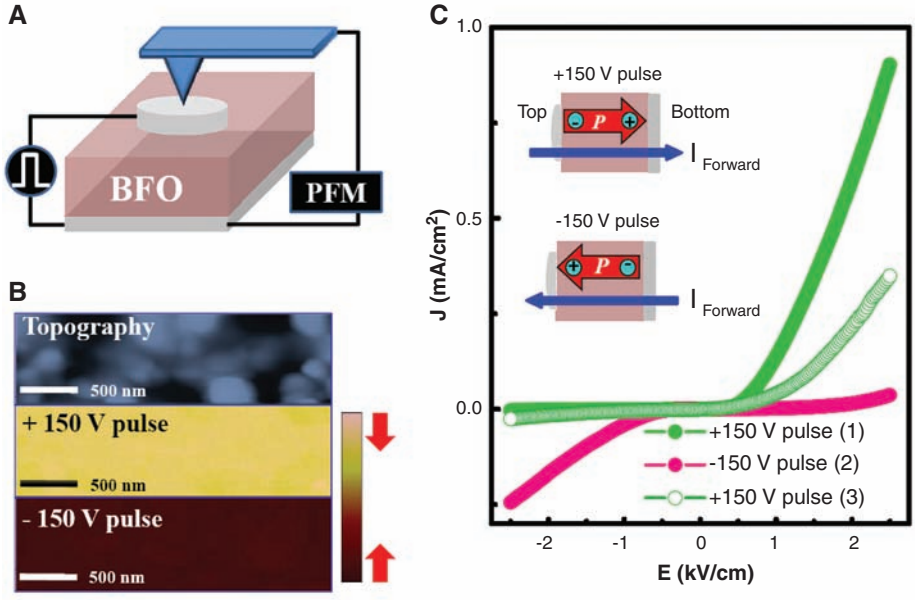

Fig. 2. (**A**) Sketch of the setup for the simultaneous PFM and $J(E)$ measurements on Ag/BFO3/Ag. One hundred electric pulses with ±150 V (E = 17 kV/cm) and a duration of 0.01 s were used to flip electric polarization. $J(E)$ was measured up to E = 2.5 kV/cm, and ac voltage of 1 V_{rms} and 17 kHz was used for PFM. (**B**) Topography image and out-of-plane PFM images after ±150-V pulses. The PFM signal is color-scaled. These images show that +150-V pulses induce a homogeneous state with downward out-of-plane polarization, and −150-V pulses induce a homogeneous state with upward polarization. (**C**) $J(E)$ curves of BFO3 after +150-V, −150-V. and +150-V pulses, in sequence. The diode forward and reverse directions switch when the direction of out-of-plane polarization (P) is reversed by ±150-V pulses. The diode forward direction turns out to be the same as the direction of electric pulses used for polarization flipping.

The above observations shed light on the origin of the PV effect in BFO. The sinusoidal behavior of the photocurrent at zero bias observed in the polarized-light rotation experiment is consistent with a nonlinear optical effect scenario (*13*). When a ferroelectric is under intense light illumination, the second-order optical response combined with a linear term is well known to induce an asymmetric polarization, which can result in an optical rectification effect (*14*, *15*). It was proposed that the asymmetric induced polarization can also give rise to a dc rectification-like effect such as a PV effect. This effect is supposed to be maximal when the polarized-light electric field is along the ferroelectric polarization and follows a sinusoidal angular dependence. This second-order optical response is an intrinsic bulk effect, and therefore it should not be sample-dependent. However, we found a noticeable variation in the magnitude of the rectification and PV effects in different samples, suggesting the importance of impurities and defects with respect to the transport mechanism. The space charge–limited conduction suggested in the diode behavior (figs. S2 and S3) is also consistent with the importance of impurities and defects. Any polarization-related asymmetry of impurity potentials can render the photocurrent sensitive to the orientation of light polarization, probably in a sinusoidal manner (*12*). Simple polarization-dependent band-bending at the metal/BFO interfaces probably does not produce the observed directional dependence. In addition, we found little difference between the effects of Ag and Au electrodes on the diode effect (fig. S4), suggesting no major contribution from the band-bending at the metal/BFO interfaces. On the other hand, the contribution of impurities and defects coupled with the band-bending or the second-order optical response to photocurrent can be influenced by the orientation of polarization.

We report here that single–ferroelectric-domain BFO crystals exhibit a diodelike effect. The forward direction of the diode is determined by the direction of the electric polarization, and the directionality of the diode can be reproducibly switched by large external electric fields. Associated with the diode effect, a substantial zero-bias PV current is induced by visible light. Further study of these effects, such as experiments involving electrodes with different conductors or controlled doping levels and spectroscopic studies of metal/BFO interfaces, will be necessary to unveil their true origin. The observation of switchable diode and photovoltaic effects in BFO reveals unusual and intriguing charge conduction behavior in leaky ferroelectrics, and should advance studies of BFO-based multifunctional devices.

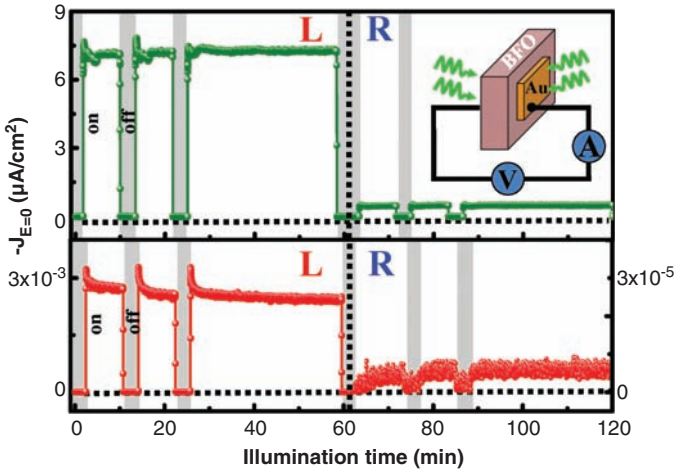

Fig. 3. The zero-bias photocurrent density as a function of time with (**top**) green light (λ = 532 nm) or (**bottom**) red light (λ = 650 nm) on or off, shining on the different sides of BFO2 (a sketch is shown in the inset). The total light power was <3 mW, and the short-circuit photocurrent was measured every 100 ms. The current with the light off decreased to <~0.1 pA. Illumination from either side results in the same-direction zero-bias photocurrent, unambiguously demonstrating the PV effect in ferroelectric BFO. The large difference in the magnitude of photocurrent between green- and red-light illumination indicates that photoexcited carriers across the bulk optical gap (~2.5 eV) dominate the PV effect. The observed right-left asymmetry may result from a thermoelectric power effect and/or uncontrolled asymmetries in the experimental configuration.

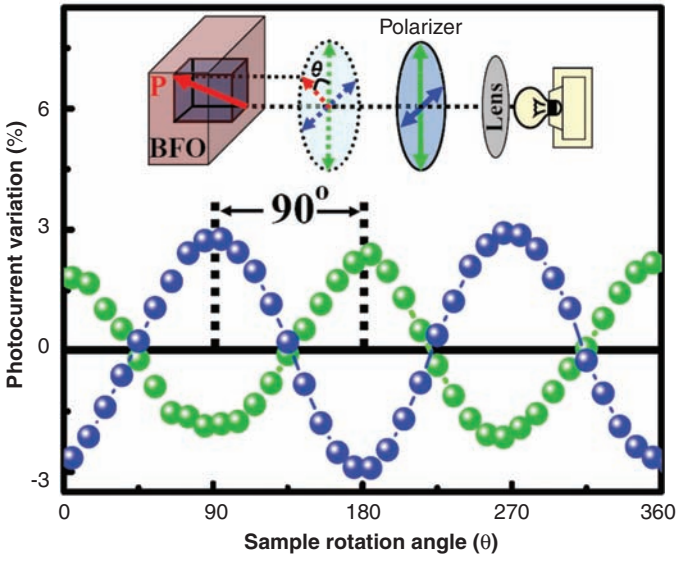

Fig. 4. The variation of photocurrent with sample rotation under illumination with a linearly polarized light. The experimental sketch is shown in the inset. The PV effect becomes maximum when the polarized-light electric field is parallel to the in-plane component of the ferroelectric polarization, and minimum when the field is perpendicular to the in-plane component.

References and Notes

1. J. F. Scott, *Ferroelectric Memories* (Springer, Heidelberg, Germany, 2000).
2. M. Dawber, K. M. Rabe, J. F. Scott, *Rev. Mod. Phys.* **77**, 1083 (2005).
3. J. F. Scott, *J. Phys. Condens. Matter* **20**, 021001 (2008).
4. J. Wang *et al.*, *Science* **299**, 1719 (2003).
5. V. M. Fridkin, B. N. Popov, *Sov. Phys. Usp.* **21**, 981 (1978).
6. A. M. Glass, D. Von der Linde, T. J. Negran, *Appl. Phys. Lett.* **25**, 233 (1974).
7. N. Noginova *et al.*, *J. Opt. Soc. Am. B* **14**, 1390 (1997).
8. G. Dalba, Y. Soldo, F. Rocca, V. M. Fridkin, Ph. Sainctavit, *Phys. Rev. Lett.* **74**, 988 (1995).
9. Y. S. Yang *et al.*, *Appl. Phys. Lett.* **76**, 774 (2000).
10. P. Poosanaas, A. Dogan, S. Thakoor, K. Uchino, *J. Appl. Phys.* **84**, 1508 (1998).
11. L. Pintilie, I. Vrejoiu, G. L. Rhun, M. Alexe, *J. Appl. Phys.* **101**, 064109 (2007).
12. V. I. Belinicher, B. I. Sturman, *Sov. Phys. Usp.* **23**, 199 (1980).
13. K. Tonooka, P. Poosanaas, K. Uchino, *Proc. SPIE* **3324**, 224 (1998).
14. M. Bass, P. A. Franken, J. F. Ward, G. Weinreich, *Phys. Rev. Lett.* **9**, 446 (1962).
15. A. Rice *et al.*, *Appl. Phys. Lett.* **64**, 1324 (1994).
16. A. J. Hauser *et al.*, *Appl. Phys. Lett.* **92**, 222901 (2008).
17. S. Lee, W. Ratcliff II, S.-W. Cheong, V. Kiryukhin, *Appl. Phys. Lett.* **92**, 192906 (2008).
18. S. Lee *et al.*, *Phys. Rev. B* **78**, 100101 (2008).
19. Y. W. Xie *et al.*, *J. Phys. Condens. Matter* **19**, 196223 (2007).
20. F. Gao *et al.*, *Appl. Phys. Lett.* **89**, 102506 (2006).
21. S. R. Basu *et al.*, *Appl. Phys. Lett.* **92**, 091905 (2008).

22. This work was funded by NSF (grants NSF-DMR-0804109 and 0704487). T.C. was partially supported by a Korea Research Foundation Grant funded by the Korean government (MOEHRD, grant KRF-2007-357-C00023).

Supporting Online Material

www.sciencemag.org/cgi/content/full/1168636/DC1
Materials and Methods
Figs. S1 to S4
References

17 November 2008; accepted 3 February 2009
Published online 19 February 2009;
10.1126/science.1168636
Include this information when citing this paper.

A Bipedal DNA Brownian Motor with Coordinated Legs

Tosan Omabegho,[1] Ruojie Sha,[2] Nadrian C. Seeman[2]*

A substantial challenge in engineering molecular motors is designing mechanisms to coordinate the motion between multiple domains of the motor so as to bias random thermal motion. For bipedal motors, this challenge takes the form of coordinating the movement of the biped's legs so that they can move in a synchronized fashion. To address this problem, we have constructed an autonomous DNA bipedal walker that coordinates the action of its two legs by cyclically catalyzing the hybridization of metastable DNA fuel strands. This process leads to a chemically ratcheted walk along a directionally polar DNA track. By covalently cross-linking aliquots of the walker to its track in successive walking states, we demonstrate that this Brownian motor can complete a full walking cycle on a track whose length could be extended for longer walks. We believe that this study helps to uncover principles behind the design of unidirectional devices that can function without intervention. This device should be able to fulfill roles that entail the performance of useful mechanical work on the nanometer scale.

Biological bipedal motors, such as kinesin (*1*), myosin (*2*), and dynein (*3*), are all examples of coordinated activity between two motor domains that lead to processive linear movement along directionally polar tracks. How such directed motion emerges from domain coordination is a major issue in the effort to create synthetic molecular motors that can cyclically bias Brownian motion by using chemical energy as input (*4*, *5*). Synthetic DNA walking devices (*6*–*11*) are useful systems to explore these questions because of DNA's programmability and structural robustness. A benchmark goal is the design and construction of controlled autonomous translocators, for example to use in synthetic molecular assembly procedures that emulate nucleic acid polymerases or the ribosome.

It was recently shown in an autonomous DNA bipedal system (*10*) that when the legs of the biped do not communicate, the motion of the biped is random, and it does not remain bound to its track. The implication from such a study and natural systems like kinesin is that coordinated motion is fundamental to the operation of molecular motors. Hence, coordination mechanisms that allow for information feedback between the domains of a device need to be devised.

We present an autonomous bipedal walker made of DNA that walks along a directionally polar DNA track. This device displays true motor behavior by coordinating the stepping cycle of its two legs as it walks along its track; it does this by having its leading leg catalyze the release of its trailing leg. The release signal, sent from the leading leg to the trailing leg, is mediated by metastable DNA fuel strand complexes (*10*–*13*) and aided by the structural asymmetry of the track. Green *et al*. recently showed how the back leg of a DNA biped could be biased for forward movement by its leading leg on a single-stranded DNA substrate that lacks a robust structure (*11*). They outline a clever leg coordination design that may in principle be capable of directed motion on a reusable track. In our experiments, we demonstrated the operation of a biped that completes a fully coordinated unidirectional stepping cycle on a linear stiff track, thereby exhibiting autonomous and directed molecular motion on a track that is consumed.

Our system is made up of 21 DNA strands. As Fig. 1A shows, the walker is a single strand of DNA containing a 5′,5′ linkage in the middle; one leg is called Leg-Even (L-E), and the other is called Leg-Odd (L-O). The walker walks upon a linear double-crossover (DX) (*14*) track, which is designed to be approximately 49 nm long and has a persistence length of ~100 nm (*15*). The track is assembled from 18 strands, four of which are metastable stem-loop structures (T1, T2, T3, and T4) that function both in the operation of the device and as structural elements in the track [supporting online material (SOM) text and fig. S1]. Two metastable hairpin fuel strands, F1 and F2, float freely in solution. To distinguish them from the stationary track stem loops, we refer to the freely floating fuel strands as hairpins.

All the reactions are designed around six "toehold" (*16*) sequences on the loop regions of the track stem loops (Fig. 1, A and B) (see SOM text for a discussion of the sequence design). There is leg-holding site d, a toehold-binding site for L-O on T1 and T3, and leg-holding site a, another toehold-binding site for L-E on both T2 and T4. There are fuel-grabbing sites c and f, which are toeholds for the activation of fuel strands F1 and F2. Fuel-grabbing site c is on T2 and T4, whereas fuel-grabbing site f is on T1 and T3. Finally, there are leg-releasing sites e and b; these are toeholds for the activated fuel molecules F1 and F2 that release walker legs L-O and L-E, respectively.

By controlling these toehold interactions kinetically, we show that the walker can take two steps autonomously from what we call resting-state 1 (RS-1) (Fig. 1C, left) to RS-3 with the simultaneous addition of fuel strands F1 and F2 (Fig. 1C, middle). We also show the one-step intermediate transition from RS-1 to RS-2 when only F1 is added (Fig. 1C, top). To demonstrate control of the system and its dependence on both fuel strands, we show that when F2 alone is added (Fig. 1C, bottom) no transition takes place and that only when F1 is further added does the walker make the transition from RS-1 to RS-3 (Fig. 1C, right). In the experimental demonstrations of the three transitions described above, the system was closed; this was achieved by changing both fuel-grabbing site f on T1 and fuel-grabbing site c on T4 to tracts containing only polythymidine, thereby rendering them both nonspecific and inactive. We also show that when the sequence of fuel-grabbing site c on T4 is restored, the walker transitions to RS-4, incorporating one more F1 molecule into the track (Fig. 1D).

Figure 2 depicts the biped's autonomous transition from RS-1 to RS-2 in 8 sequential steps. Steps 1 to 5 depict the release of L-O from T1 with the incorporation of F1 into the track. The fuel strand that releases the walker biases or rectifies the walker's forward movement by creating a more stable duplex with the stem loop that was holding the released leg (step 5). The catalyzed release of the trailing leg by the leading leg begins in step 6: The leading leg (L-O) first diffuses to and activates its target stem loop (T3) (step 7); as is shown taking place for F1 in steps 1 and 5, F2 then releases L-E from T2, and the walker transitions to RS-3 to complete the cycle (the complete sequence of steps is shown in fig. S3). Step 3 demonstrates how the activated fuel strands have limited single-stranded flexibility (*17*, *18*) and are placed three times closer (7 nm versus 21 nm) to their complementary stem loops (holding the trailing leg of the walker) than to the stem loops one site ahead. This difference in distance, 7 nm versus 21 nm, gives rise to the track's directional polarity. The two metastable topologies the walker forms with the track, when either one or two legs are attached, protect the leg-releasing sequences directly beneath each leg from being accessed by their fuel strands prematurely (SOM text and fig. S4). After one step of the walker, an overall free energy gain corresponding to 20 base pairs (bp) occurs with the incorporation of one fuel molecule into the track: 8 bp for the fuel-grabbing region and 12 bp for the leg-holding and leg-releasing region.

We tracked the progress of the walker by covalently cross-linking aliquots of it to the track as fuel was added and then visualizing the constituent strands of the products in autoradiograms produced from either super-denaturing (*19*) or nondenaturing polyacrylamide gel electrophoresis (PAGE). Each track stem loop was synthesized with a psoralen molecule on its 3′ end; consequently, the track stem loops cross-link across their duplexes when the system is exposed to ultraviolet (UV) light (Fig. 3A) (*1*, *20*). Five experiments were run in parallel: W*; T1*; T2*;

[1]School of Engineering and Applied Sciences, Harvard University, Cambridge, MA 02138, USA. [2]Department of Chemistry, New York University, New York, NY 10003, USA.

*To whom correspondence should be addressed. E-mail: ned.seeman@nyu.edu

T3*; and T4*. In each experiment, only one of the strands was radioactively labeled: W*, walker; T1*, track stem loop T1; T2*, track stem loop T2; T3*, track stem loop T3; and T4*, track stem loop T4. Figure 3B shows the cross-linking reactions that take place in the four resting states (RS-1, RS-2, RS-3, and RS-4) of the track and for each resting state, the experiments in which the walker/stem loop cross-linked products are visible.

The products of the walker cross-linked to the track stem loops will appear as two higher molecular weight bands on super-denaturing PAGE (*21*). A molecule migrates on a denaturing gel as a function of both its size and its topology (*22*). The upper band consists of the walker cross-linked to two stem loops, one on its trailing leg and one on its leading leg [walker–trailing leg–leading leg (w-t-l) product] (Fig. 3C). The lower band contains the walker cross-linked to one stem loop, either on its trailing or on its leading leg (w-t and w-l products, respectively) (Fig. 3C). The formation and global state changes of the track are visible in nondenaturing gels, and the position of the walker on the track is visible in super-denaturing gels.

After an initial annealing step in which the two halves of the track (Fig. 4A, lanes 1 to 5) were combined to assemble the whole track (SOM text and figs. S6 and S7), all five radioactive track species (W*, T1*, T2*, T3*, and T4*) colocalized on a gel to form one band (Fig. 4A, lanes 6 to 10). To show that the assembled track was consistent with state RS-1, we exposed aliquots of all five track solutions to 366 nm of light, capturing the position of the walker. A super-denaturing gel of these five mixtures shows the walker cross-linked almost entirely to T1 and T2 (Fig. 4B, lanes 1 to 5). Pictured on the left hand side of the gel, the resulting cross-linked products are w-t-l (W-T1-T2) in experiments W* (lane 1), T1* (lane 2), and T2* (lane 3); w-t (W-T1) in experiments W* and T1*; and w-l (W-T2) in experiments W* and T2*. [For an explanation of the secondary products seen in the middle of the gel, see SOM text and figs. S8 to S11]

To show that the walker transitioned from RS-1 to RS-2 with the addition of F1, we added F1 to aliquots of all five assembled track solutions. After 1 hour (*23*), the walker clearly transitioned and cross-linked to T2 and T3 (Fig. 4B, lanes 6 to 10). It is clear that both w-t-l (W-T1-T2) and w-t (W-T1) were greatly reduced in experiment T1* (compare lanes 2 and 7), and w-t-l (W-T2-T3) and w-l (W-T3) appeared in experiment T3* (compare lanes 4 and 9), which is consistent with the transition from RS-1 to RS-2. The target products W-T2-T3, W-T2, and W-T3 are pictured on the right of the gel.

To show that the walker took two steps autonomously from RS-1 to RS-3 upon the addition of F1 and F2, we added both fuel strands simultaneously. After 1 hour, a majority of the walker cross-linked to T3 and T4, which is consistent with the transition to RS-3 (Fig. 4C, lanes 6 to 10). As a control, we let aliquots of the track sit without fuel for the same hour: In this experiment, the walker remained on T1 and T2 (lanes 1 to 5), demonstrating that on the time scale of an hour it was the addition of fuel that drove the movement of the walker, and not random diffusion. Quantitation of band intensities established the stepping efficiency of the walker to be 74% for each step of the walker (SOM text, fig. S13, and table S1).

As the walker moved and the track picked up fuel molecules, the molecular weight of the walker and track increased, and its three-dimensional shape changed; as a result, its mobility decreased. These changes can be seen as mobility shifts in a nondenaturing gel (Fig. 4D). In lane 1, an aliquot of experiment W* in state RS-1 acts as a marker. When F1 alone was added, a gel shift occurred reflecting the incorporation of one fuel molecule during the transformation to RS-2 (lanes 2 to 6). When both fuel molecules were added, a larger gel shift was observed, reflecting the incorporation of two fuel molecules during the transformation to RS-3 (lanes 7 to 11). Uniform behavior is seen in all five experiments. Neither free walker nor track multimers are visible in Fig. 4D; this finding strongly suggests that the walkers began and

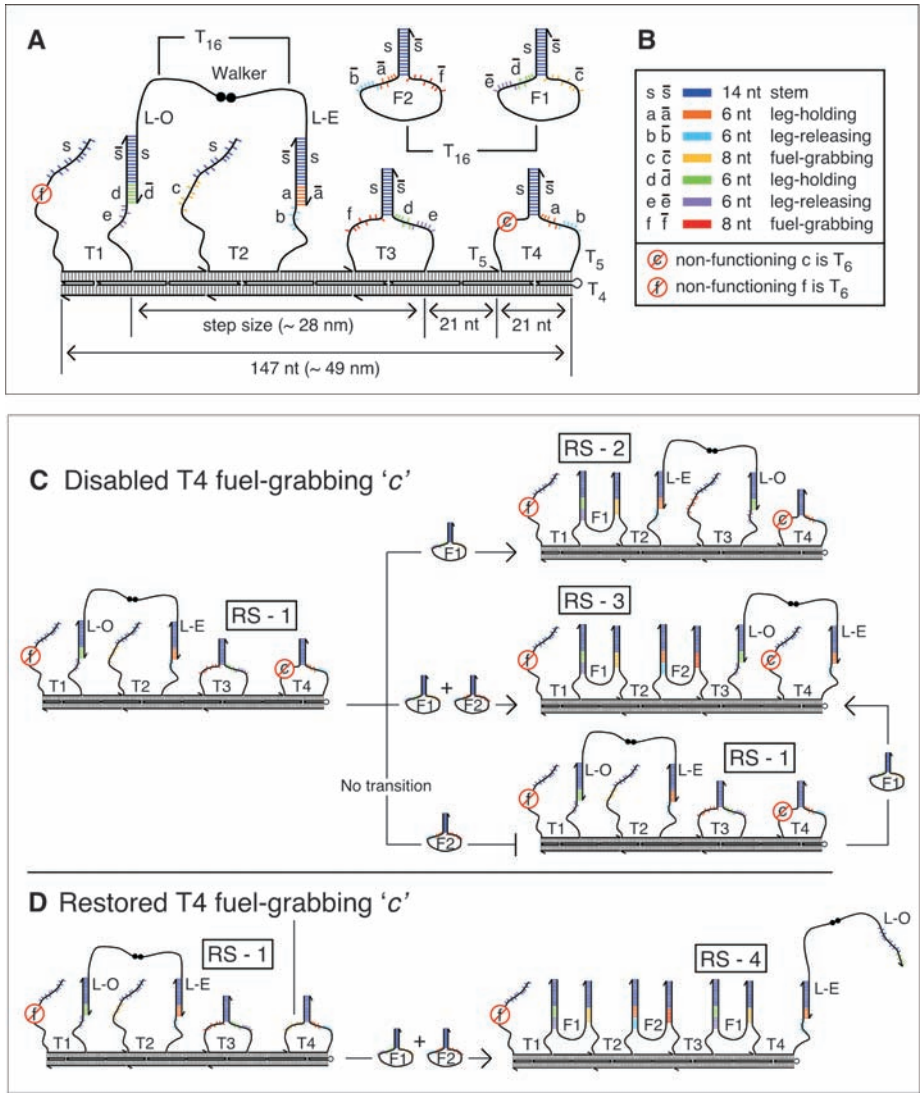

Fig. 1. (**A**) Illustration of the DX track structure with the walker on it. The walker is shown on stem loops T1 and T2. The walker's 5′,5′ linkage is denoted by two black dots and its 3′ ends by half arrows. T_{16} denotes flexible polythymidine linkers on the walker and two fuel hairpins, F1 and F2. Two T_5 regions provide flexibility at the base of the track stem loops. All the binding sites are labeled with lowercase letters, and complementary sequences are capped with a bar. The two fuel-grabbing sequences f and c on T1 and T4, respectively, are not functional. (**B**) Color-coding and the names of the binding sites. (**C**) Transitions made with a nonfunctional T4 fuel-grabbing sequence c. The walker is programmed to take two steps from RS-1 to RS-3 with the addition of F1 and F2 simultaneously (middle). A single step is made from RS-1 to RS-2 with the addition of F1 alone (top). With the addition of F2 alone, the walker does not move, and only with the further addition of F1 does the walker make the transition from RS-1 to RS-3 (bottom). (**D**) With the T4 fuel-grabbing sequence c restored, the walker transitions to RS-4, incorporating another F1 into the track, thereby kicking L-O off of T3.

ended their walks on the same track and coupled their legs by intramolecular interactions.

Further demonstrating control of the system, we added F2 alone to the track for 1 hour and found that the walker primarily remained on and cross-linked to T1 and T2 (Fig. 4E, lanes 1 to 5). When we added F1 to this solution containing the track and F2 and left it to react for another hour, the walker was found cross-linked to T3 and T4 (lanes 6 to 10), again demonstrating that it transitioned from the RS-1 structure to the RS-3 structure only when both fuel molecules were present. A nondenaturing gel (Fig. 4F) also shows that the track that sat in solution with F2 (lanes 2 to 6) colocalized with the track to which no fuel was added (lane 1) and then shifted after F1 was added to this mixture (lanes 7 to 11).

The transition to RS-4 is shown in Fig. 4, G and H. The data in this case indicate that the walker cross-linked primarily to T4 upon the addition of F1 and F2 or that the distribution of product shifted to the w-l product (Fig. 4G, lanes 6 to 10). Figure 4H shows uniform transitioning in the native state. This result further verifies that the system works as designed and that the fuel-grabbing sequences can control the walker's progress.

We have demonstrated the activity of a DNA molecular motor that uses leg coordination to achieve directed bipedal motion in a "burnt bridges" Brownian ratchet–type (*24*, *25*) mechanism whereby the stem loops on the track are consumed irreversibly during the walk. Our work suggests, as does nature, that to cycle a motor along a predefined trajectory and to break directional symmetry, coordination between at least two parts of the motor may be required. Molecular spiders (*8*, *9*) and the recently demonstrated stochastic walker (*10*) are also synthetic autonomous walking systems in which the track is consumed, but they function without leg-coordination mechanisms. In these systems, directional polarity is not built into the system but is strictly imposed

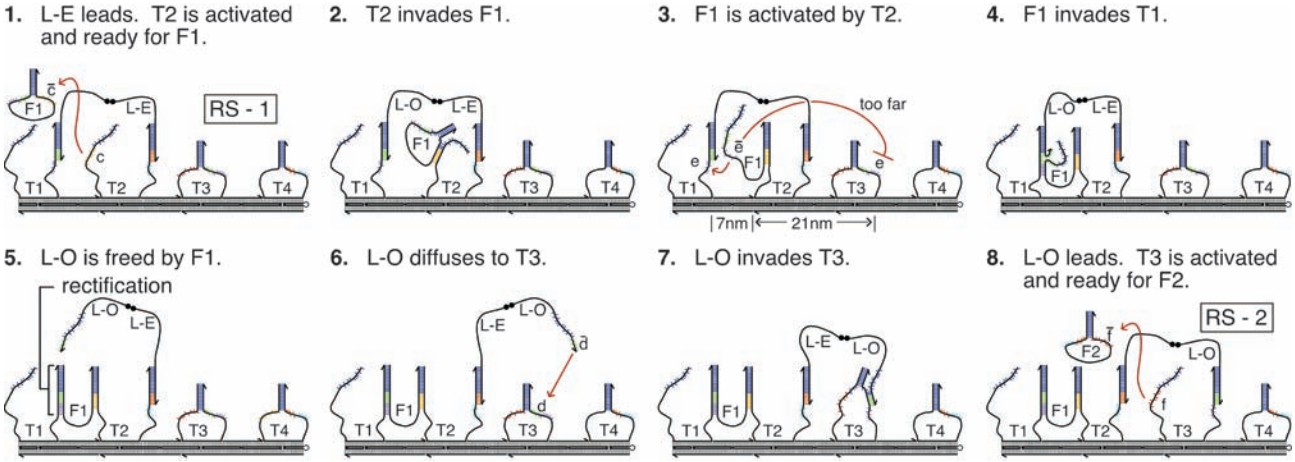

Fig. 2. Transition from RS-1 to RS-2. In eight sequential frames, this illustration depicts the biped taking one step. Illustrations 1 to 5 depict the activation of F1 by T2 and the release of L-O from T1 by F1. The freed leg L-O then begins the catalyzed release of L-E from T2 (illustrations 6 to 8). Key to directionally biasing the biped, illustration 3 shows how the activated fuel strands are spatially restricted to act on the stem loop 7 nm away rather than the stem loop 21 nm away. (The complete transition to RS-3 is shown in fig. S3.)

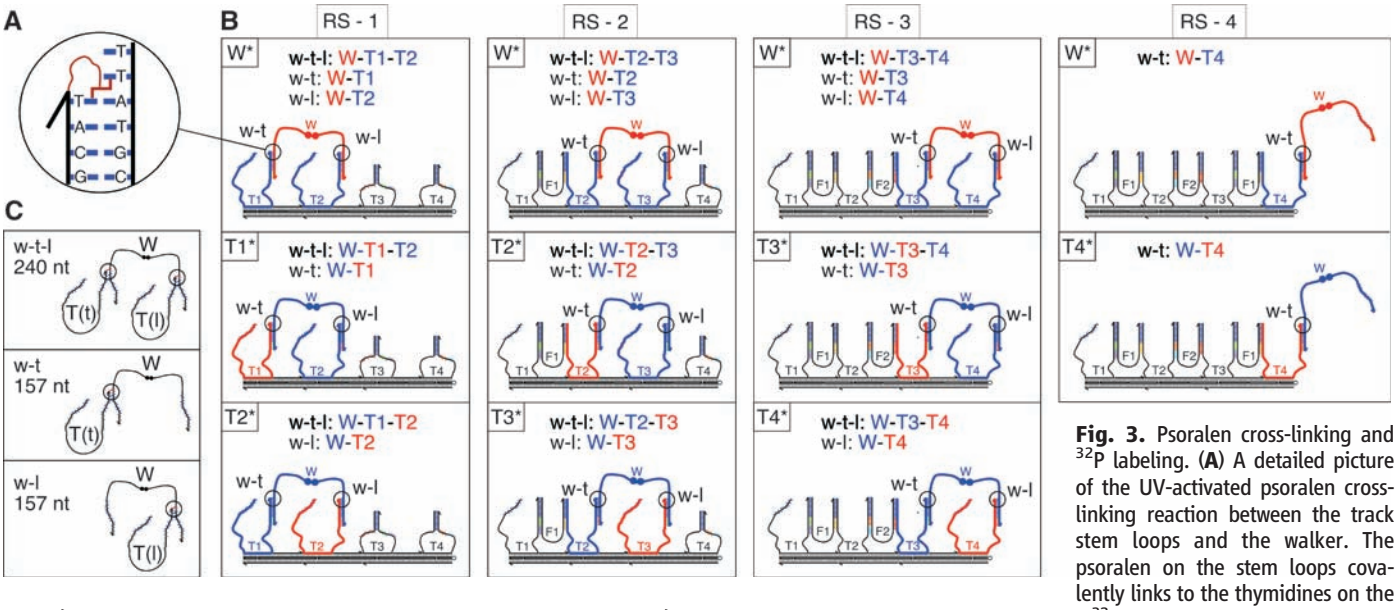

Fig. 3. Psoralen cross-linking and ^{32}P labeling. (**A**) A detailed picture of the UV-activated psoralen cross-linking reaction between the track stem loops and the walker. The psoralen on the stem loops covalently links to the thymidines on the walker's legs just outside the duplex formed by the stem loops and the walker's legs. (**B**) Visualizing the cross-link products with ^{32}P. The three cross-linked products w-t (walker linked to the stem-loop on its trailing leg), w-l (walker linked to the stem-loop on its leading leg), and w-t-l (walker linked on both its trailing and leading leg) are shown forming in each experiment (W*, T1*, T2*, T3*, and T4*) that they are visible for each resting state (RS-1, RS-2, RS-3, and RS-4) of the system. The radioactive strand is drawn in red and the nonradioactive strands that are part of the cross-linked complex are drawn in blue. The constituent components of the products formed are listed in each box. (**C**) Denatured topologies and size of the three walker–stem-loop cross-link products w-t, w-l, and w-t-l.

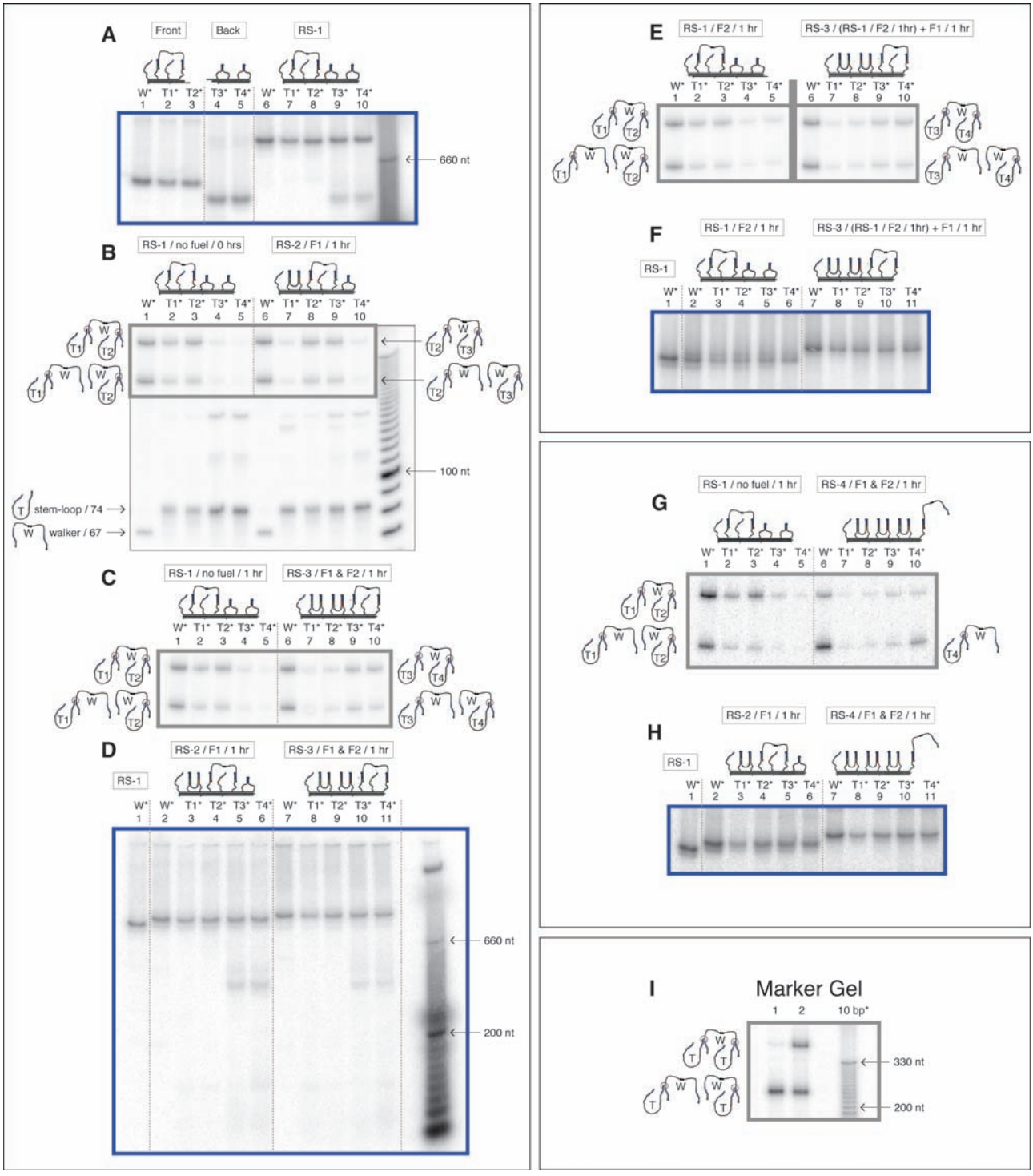

Fig. 4. Autoradiogram analysis of the walking cycle. Nondenaturing gels (all 4%) are outlined in blue, and super-denaturing gels (all 10%) are outlined in gray. Target products for the two states shown in each super-denaturing gel are drawn on the left and right hand side of each gel. (**A**) Nondenaturing gel verifying formation of the five radioactive tracks. (**B**) Super-denaturing gel showing the walker's position in RS-1 at 0 hours (lanes 1 to 5) and then in RS-2 (lanes 6 to 10) with the addition of F1 after 1 hour. (The box inside the gel outlines the walker–stem-loop cross-link products. See SOM text and figs. S8 to S11 for a detailed explanation of the secondary products seen on the super-denaturing gels as well as complete images of the super-denaturing gels.) (**C**) Super-denaturing gel verifying the transition to RS-3 (lanes 6 to 10) with the addition of F1 and F2 and no transition with no fuel added (lanes 1 to 5), both within an hour. (**D**) Nondenaturing gel verification of (B) and (C). (**E**) Composite super-denaturing gel showing the track remained in RS-1 while sitting in solution with F2 for 1 hour (lanes 1 to 5) and then transitioned to RS-3 when F1 was added to the mixture (lanes 6 to 10). [The gray line separates data from two different gels (fig. S10).] (**F**) Nondenaturing gel of (E). (**G**) Super-denaturing gel verifying the transition to RS-4 (lanes 6 to 10) with the addition of F1 and F2 and verification that the system remained in RS-1 (lanes 1 to 5) with no fuel added (lanes), both within an hour. (**H**) Nondenaturing gel verification of (G). (**I**) Marker gel showing the position of the w-t, w-l, and w-t-l products on a super-denaturing gel. (Complete pictures of the nondenaturing gels are outlined in the SOM text and fig. S12).

by track consumption. Hence, if given the choice between two directions, these walkers can go either way. In our system, directionality is a consequence of the asymmetry of the design, which is a key component of functional Brownian motors (*4*, *5*).

Through track stem-loop consumption, our mechanism allows the walker to hybridize the fuel hairpins onto the track sequentially and dynamically according to the presence of a code on the track. Such a capability in a molecular automaton is reminiscent of the ribosome and DNA or RNA polymerase (*26*). Indeed, the leg-holding sequences are uncoupled from the fuel-grabbing sequences. Thus, in principle, a track could be encoded to hybridize with an arbitrary number of fuel molecules before the walker returned to the beginning of the fuel cycle to take further steps in the same direction. This demonstration of molecular coordination is a step toward the development of more complex and autonomous synthetic molecular motor systems, whether they are made from DNA or from other polymeric materials (*5*).

References and Notes

1. K. Svoboda *et al.*, *Nature* **365**, 721 (1993).
2. A. D. Mehta, *Nature* **400**, 590 (1999).
3. R. D. Vale, *Cell* **112**, 467 (2003).
4. R. D. Astumian, *Science* **276**, 917 (1997).
5. E. R. Kay, D. A. Leigh, F. Zerbetto, *Angew. Chem. Int. Ed.* **46**, 72 (2007).
6. W. B. Sherman, N. C. Seeman, *Nano Lett.* **4**, 1203 (2004).
7. J. S. Shin, N. A. Pierce, *J. Am. Chem. Soc.* **126**, 10834 (2004).
8. Y. Tian, Y. He, Y. Chen, P. Yin, C. Mao, *Angew. Chem. Int. Ed.* **44**, 4355 (2005).
9. R. Pei *et al.*, *J. Am. Chem. Soc.* **128**, 12693 (2006).
10. P. Yin, H. M. T. Choi, C. R. Calvert, N. A. Pierce, *Nature* **451**, 318 (2008).
11. S. J. Green, J. Bath, A. J. Turberfield, *Phys. Rev. Lett.* **101**, 238101 (2008).
12. A. J. Turberfield *et al.*, *Phys. Rev. Lett.* **90**, 118102 (2003).
13. J. S. Bois *et al.*, *Nucleic Acids Res.* **33**, 4090 (2005).
14. T. J. Fu, N. C. Seeman, *Biochemistry* **32**, 3211 (1993).
15. P. Sa-Ardyen, A. V. Vologodskii, N. C. Seeman, *Biophys. J.* **84**, 3829 (2003).
16. B. Yurke, A. J. Turberfield, J. A. P. Mills, F. C. Simmel, J. L. Neumann, *Nature* **406**, 605 (2000).
17. J. B. Mills, E. Vacano, P. J. Hagerman, *J. Mol. Biol.* **285**, 245 (1999).
18. S. B. Smith, Y. J. Cui, C. Bustamante, *Science* **271**, 795 (1996).
19. S. G. Fischer, L. S. Lerman, *Cell* **16**, 191 (1979).
20. O. Gia, S. M. Magno, A. Garbesi, F. P. Colonna, M. Palumbo, *Biochemistry* **31**, 11818 (1992).
21. Material and methods are available as supporting material on *Science* Online.
22. T. J. Fu, Y. C. Tse-Dinh, N. C. Seeman, *J. Mol. Biol.* **236**, 91 (1994).
23. A 1-hour time interval was used in all of the experiments. This was an ideal time period for handling the five radioactive track versions simultaneously because all associated denaturing and nondenaturing experiments were conducted in parallel from one stock solution (*21*). Hence, detailed results about the reaction rates of the system are not available from this study.
24. J. Mai, I. M. Sokolov, A. Blumen, *Phys. Rev. E Stat. Nonlin. Soft Matter Phys.* **64**, 011102 (2001).
25. S. Saffarian *et al.*, *Science* **306**, 108 (2004).
26. E. Shapiro, Y. Benenson, *Sci. Am.* **294**, 44 (2006).

27. We thank C. Mao, H. Yan, and N. Jonoska for critical reading of the manuscript. This research has been supported by grants to N.C.S. from the National Institute of General Medical Sciences, NSF, the Army Research Office, the Office of Naval Research, the New York Nano-Bio-Molecular Information Technology Incubator program of the Department of Energy, and the W. M. Keck Foundation.

Supporting Online Material

www.sciencemag.org/cgi/content/full/324/5923/67/DC1
Materials and Methods
SOM Text
Figs. S1 to S14
Table S1
References

29 December 2008; accepted 10 February 2009
10.1126/science.1170336

Iron-Based Catalysts with Improved Oxygen Reduction Activity in Polymer Electrolyte Fuel Cells

Michel Lefèvre,* Eric Proietti,* Frédéric Jaouen, Jean-Pol Dodelet†

Iron-based catalysts for the oxygen-reduction reaction in polymer electrolyte membrane fuel cells have been poorly competitive with platinum catalysts, in part because they have a comparatively low number of active sites per unit volume. We produced microporous carbon–supported iron-based catalysts with active sites believed to contain iron cations coordinated by pyridinic nitrogen functionalities in the interstices of graphitic sheets within the micropores. We found that the greatest increase in site density was obtained when a mixture of carbon support, phenanthroline, and ferrous acetate was ball-milled and then pyrolyzed twice, first in argon, then in ammonia. The current density of a cathode made with the best iron-based electrocatalyst reported here can equal that of a platinum-based cathode with a loading of 0.4 milligram of platinum per square centimeter at a cell voltage of ≥0.9 volt.

The desired high power density from polymer electrolyte membrane fuel cells (PEMFCs) can only be achieved by speeding up the otherwise slow reaction steps at their low operating temperatures (~80°C) through catalysis. For the oxygen-reduction reaction (ORR), non–precious metal catalysts (NPMCs), which are potentially less expensive and more abundant, have been outperformed by Pt-based catalysts (*1*, *2*), which exhibit high activity as the native metal. For metals such as Co and Fe, improved performance will require a robust method for increasing the reactivity of the metal ion through ligation.

Since 1964, when Jasinski observed that cobalt phthalocyanine catalyzed the ORR (*3*), a number of approaches have been explored to create practical NPMCs. Catalysts were first obtained by adsorbing Fe-N_4 or Co-N_4 macrocycles on a carbon support and pyrolyzing the resulting material in an inert atmosphere (*4*). A breakthrough was then achieved by Yeager when it was revealed that these often-expensive macrocycles could instead be substituted by individual N and Co precursors (*5*). This approach was followed by several groups, including ours (*4*, *6*–*16*). Meanwhile, NPMC research using metal-N_4 macrocycles has also progressed (*17*–*19*).

Our previous approach in the synthesis of NPMCs for ORR has been to use NH_3 as a nitrogen precursor. The catalysts were obtained by wet impregnation of carbon black with an iron precursor such as iron(II) acetate (FeAc), followed by a heat treatment in NH_3; we refer to the products as Fe/N/C electrocatalysts. During pyrolysis at temperatures of ≥800°C, NH_3 partly gasifies the carbon support, resulting in a mass loss that depends on the duration of the heat treatment (*20*). The disordered domains of the carbon support are preferentially gasified (*21*–*23*). As a result, micropores are created in the carbon black particles. The mass loss at which maximum activity is reached [30 to 50 weight percent (wt %)] corresponds to the largest microporous surface area for the etched carbon, which suggests that these micropores (width ≤2 nm) host most of the catalytic sites (*21*).

The reaction of NH_3 with the disordered carbon domains also produces the N-bearing functionalities needed to bind iron cations to the carbon support (*24*, *25*). It has been proposed that most of the Fe/N/C catalytic sites consist of an iron cation coordinated by four pyridinic functionalities attached to the edges of two graphitic sheets, each belonging to adjacent crystallites on either side of a slit pore in the carbon support (*21*, *25*). Thus, four factors have been identified as requirements for producing active Fe-based catalysts for ORR: (i) disordered carbon content in the catalyst precursor (*20*), (ii) iron, (iii) surface nitrogen, and (iv) micropores in the catalyst.

Our present approach, which introduces a new material (pore filler) and replaces impregnation with planetary ball-milling, has elevated the catalytic activity of an Fe-based NPMC by a factor of >35 relative to the previous best reported

Institut National de la Recherche Scientifique, Énergie, Matériaux et Télécommunication, Varennes, Québec J3X 1S2, Canada.

*These authors contributed equally to this work.
†To whom correspondence should be addressed. E-mail: dodelet@emt.inrs.ca

activity for Fe-based catalysts (*11*) (and within ~10% of the best Pt-based catalysts). Furthermore, these NPMCs may also present opportunities for ORR in direct alcohol, formic acid, and alkaline fuel cells.

For NPMCs, it is meaningful to speak in terms of volumetric activity for ORR (*1*) because its product with electrode thickness predicts the kinetic current density (A cm^{-2}) of the cathode. Because of mass-transport limitations related to electrode thickness, NPMC cathodes must attain the same kinetic current density as Pt-based cathodes without exceeding a thickness of ~100 μm (*1*). This criterion defines a target for volumetric activity (A cm^{-3}) for NPMCs. [The activity is originally measured in amperes per gram of NPMC; conversion from A g^{-1}_{NPMC} to A $cm^{-3}_{electrode}$ is described in (*26*).] For NPMCs, the U.S. Department of Energy (DOE) has set a 2010 target of 130 A cm^{-3} as measured in a fuel cell at 0.8 V *iR*-free cell voltage (i.e., after correction for ohmic loss *R*), at 80°C, and at O_2 and H_2 absolute pressures of 1 bar (*27*). All volumetric activity values reported in this work correspond to these reference conditions. For the best catalysts synthesized by our group to date by impregnation of FeAc on carbon black followed by heat treatment in NH_3 at 950°C, a volumetric activity of 0.8 to 1.5 A cm^{-3} was obtained (*28*, *29*). This value is comparable to the value of 2.7 A cm^{-3} (recalculated for O_2 and H_2 pressures of 1 bar) obtained by Wood *et al*. for a Fe/N/C catalyst (*11*). All of these activities are still well below the DOE 2010 target of 130 A cm^{-3}.

The volumetric activity is the product of the catalytic site density and the activity of a single site. The latter varies with voltage and is an intrinsic property of the catalytic site. If the catalytic activity of the site is left unchanged, increased volumetric activity can only be achieved by increasing the site density. The volumetric catalytic activity may be improved by increasing the Fe content. However, doing so increases the activity proportionally only up to

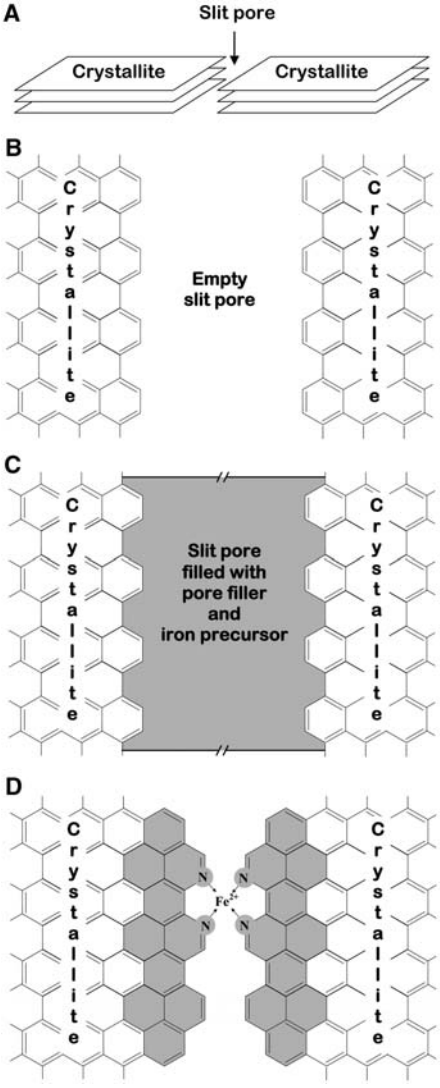

Fig. 1. Schematic representation of catalytic site formation in the micropores of the carbon support. (**A**) Simplified 3D view of a slit pore between two adjacent graphitic crystallites in the carbon support. (**B**) Plan view of an empty slit pore between two crystallites. (**C**) Plan view of a slit pore filled with pore filler and iron precursor after planetary ball-milling. (**D**) Plan view of the presumed catalytic site (incomplete) and graphitic sheet growth (shaded aromatic cycles) between two crystallites after pyrolysis.

Table 1. Catalytic activity for optimized catalysts. Volumetric activities are at 0.8 V *iR*-free cell voltage at reference conditions of 80°C and 1 bar O_2 and H_2. Black Pearls 2000 was used as the carbon support. The mass ratio of pore filler to carbon support was 1:1. Catalyst loading for all tests was ~1 mg cm^{-2}. The Nafion-to-catalyst ratio (NCR) was 2 unless otherwise noted.

Gas for first pyrolysis (1050°C)	Gas for second pyrolysis (950°C)	Pore filler	Nominal Fe content (wt %)	Catalytic activity (A cm^{-3})*
NH_3	—	PTCDA	0.2	22
NH_3	—	PTCDA	0.5	24
NH_3	—	PTCDA	1.0	30
Ar	—	Phen	0.2	2.8
Ar	—	Phen	1.0	5.5
Ar	—	Phen	4.1	1.4
Ar	NH_3	Phen	0.2	60†
Ar	NH_3	Phen	1.0	64†
Ar	NH_3	Phen	4.1	31†
Ar	NH_3	Phen	1.0	99‡ (NCR 1.5)

*Converted from the activity measured under 1.5 bar O_2 and H_2 absolute pressures to the reference pressures of 1 bar absolute pressure (*26*). †Unoptimized mass loss in second pyrolysis. ‡Optimized mass loss in first and second pyrolysis.

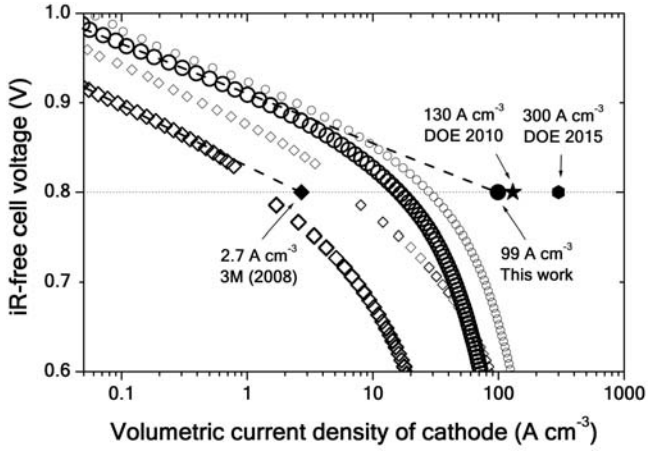

Fig. 2. Volumetric current density of best NPMC in this work. Original polarization curves were obtained from H_2-O_2 fuel cell tests at 80°C and 100% relative humidity (RH) for cathodes made with the best NPMC in this work (small open circles, P_{O_2} = P_{H_2} = 1.5 bar) and for the presumed previous best NPMC (*11*) (small open diamonds, P_{O_2} = 3.9 bar and P_{H_2} = 2.5 bar). Corrected polarization curves are based on DOE fuel cell test reference conditions (P_{O_2} = P_{H_2} = 1 bar, 80°C, 100% RH) for the best NPMC in this work (large open circles) and for the presumed previous best NPMC (*11*) (large open diamonds). A catalyst loading of ~1 mg cm^{-2} was used for all polarization curves. The actual Fe content in the catalyst from this work is 1.7 wt %, resulting in a Fe loading of 17 μg cm^{-2}. The volumetric (kinetic) current density at 0.8 V *iR*-free cell voltage for the presumed previous best NPMC (solid diamond) and the best NPMC in this work (solid circle) is the intersection of the extended Tafel slope of the corrected polarization curves (dashed lines) with the 0.8 V axis. Also included are the 2010 (star) and 2015 (hexagon) DOE performance targets for ORR on NPMCs, all at the reference conditions of P_{O_2} = P_{H_2} = 1 bar, 80°C, and 100% RH.

~0.2 nominal wt % Fe, beyond which the activity levels off and eventually decreases (*29*). Furthermore, when catalysts were prepared using he impregnation method on nonmicroporous carbon black and pyrolyzed in pure NH_3, the micropore surface area of the resulting catalysts was shown to govern the catalytic activity; the nitrogen and iron content were usually nonlimiting (*21*).

In a recent study, we impregnated FeAc onto highly microporous carbon supports followed by pyrolysis in NH_3 (*30*). An example of a highly microporous carbon black is Black Pearls 2000 with a Brunauer-Emmett-Teller (BET) surface area of 1379 $m^2\ g^{-1}$ and a micropore area of 934 $m^2\ g^{-1}$. By contrast, a typical carbon support of lower porosity such as Vulcan XC-72R has a BET surface area of 213 $m^2\ g^{-1}$ and a micropore area of 114 $m^2\ g^{-1}$. Surprisingly, the use of highly microporous carbon supports did not improve the activity relative to catalysts made with nonmicroporous carbon supports. We concluded that only the micropores created during heat treatment in NH_3 may host catalytic sites. The micropores in the as-received microporous carbon blacks do not bear the surface nitrogen necessary to form catalytic sites. Because these carbon blacks have little disordered carbon content, surface nitrogen is difficult to add during pyrolysis in NH_3.

In the present work, to capitalize on the high micropore content of microporous carbon blacks and to overcome the limitations resulting from their lack of disordered carbon, we filled these micropores with a mixture of pore filler (PF) and iron precursor (Fig. 1). Doing so created a catalyst precursor that complies with the factors required for producing active NPMCs, as described above. To overcome the limitation of solubility and/or adsorbability associated with the impregnation method, we used planetary ball-milling to fill the pores of the microporous carbon support with PF and iron precursor. Planetary ball-milling uses both friction and impact effects to force the filler materials (PF and iron precursor) into the pores of the carbon support while leaving its microstructure relatively unaffected.

For all catalysts in the present work, we used Black Pearls 2000 (Cabot; micropore surface area 934 $m^2\ g^{-1}$) as the microporous carbon black and FeAc as the iron precursor. Micropores are defined as pores having a width of ≤20 Å. We chose two pore fillers: perylene-tetracarboxylic dianhydride (PTCDA), which is nitrogen-free, and 1,10-phenanthroline (phen), which is N-bearing. For catalysts made using PTCDA, the N atoms necessary to form catalytic sites arise from its reaction with NH_3 during pyrolysis. For catalysts made with phen, the pyrolysis may be performed either in Ar or NH_3 because phen already contains nitrogen. Note that phen forms a complex with Fe^{2+}.

We first investigated the effect of the wt % of PTCDA in the catalyst precursor. Four different wt % PTCDA values (0, 25, 50, 75) were used with a constant nominal Fe loading of 0.2 wt %. Optimal volumetric activities of 1.8, 8.5, 22, and 27 A cm^{-3} were obtained, respectively. The experimental conditions and corresponding fuel cell polarization curves are given in fig. S3 (*26*). Next, a PF loading of 50 wt % (PTCDA or phen) was chosen to investigate the effect of nominal Fe loading in the catalyst precursor. Catalyst precursors made with PTCDA were pyrolyzed in NH_3 and those made with phen in Ar, both at 1050°C. Although better volumetric activities were obtained with the PTCDA series (Table 1), we investigated the effect of a subsequent 5-min pyrolysis in NH_3 for the phen series. This subsequent pyrolysis amplified the volumetric activity of the Ar-pyrolyzed phen series by a factor of ≤20. These amplified activities surpassed those of the PTCDA series. Given the notable improvement in activity of the phen-based catalysts after a second pyrolysis in NH_3, we prepared phen-based catalysts (with 1 wt % nominal Fe content) using a single pyrolysis in NH_3 at 1050°C. The volumetric activities of the latter catalysts (16 to 29 A cm^{-3}) were lower than those achieved using a two-step pyrolysis, first in Ar at 1050°C, then in NH_3 at 950°C.

Two factors were further optimized on the most active catalyst corresponding to 1 wt % nominal Fe content (64 A cm^{-3}, Table 1): (i) the mass loss during pyrolysis in NH_3, and (ii) the Nafion-to-catalyst ratio (NCR) in the cathode (Nafion is a proton-conducting perfluoro polyethylene sulfonic acid polymer made by DuPont). The optimal mass loss and NCR were found to be ~30% and ~1.5, respectively, leading to an increase in volumetric activity from 64 to 99 A cm^{-3}, which is much closer to the 2010 DOE performance target of 130 A cm^{-3} for ORR on NPMCs. (See table S2 for additional details on mass activity, mass loss during pyrolysis, micropore surface area, and nitrogen content.)

Polarization curves (both as-measured and corrected to the DOE fuel cell test reference conditions) in terms of volumetric current density for our best NPMC and for the presumed best NPMC reported to date by Wood *et al.* (*11*) are shown in Fig. 2. The DOE volumetric activity target for ORR on NPMCs is specified for 0.8 V *iR*-free cell voltage and under reference conditions. The kinetic activity (free of ohmic and mass transport losses) of the NPMCs at 0.8 V *iR*-free cell voltage cannot be directly read from the corrected polarization curves, but must instead be estimated by extrapolating the kinetically controlled Tafel slope observed at higher cell voltage. Our best NPMC shows a factor of >35 activity enhancement relative to the presumed previous best NPMC.

To compare these NPMCs for ORR in PEMFCs to precious metal catalysts, Fig. 3 shows, in terms of current density, the polarization curves of the best NPMC produced in this work (Table 1, last row) using two catalyst loadings, 1.0 and 5.3 mg cm^{-2}, compared with that of a Pt-based cathode catalyst (~0.4 mg cm^{-2} Pt) tested under the same conditions and test fuel cell. At 0.9 V *iR*-free cell voltage, where both polarization curves are within the kinetically controlled Tafel region, increasing the loading of the NPMC by a factor of ~5 increases the current density of the cell by about the same factor. At 0.9 V, the current density of the cathode with the NPMC (5.3 mg cm^{-2}) is equal to that with the Pt-based cathode. Although the NPMC loading of ~5 mg cm^{-2} is much greater than that for Pt (0.4 mg cm^{-2}), the limiting factor for the Pt loading is materials cost, unlike the low-cost NPMCs in this work (*31*). On the other hand, the limiting factor for NPMC loading is electrode thickness, which, if increased beyond ~100 μm (*1*), creates unacceptable mass transport losses at high current density, resulting in decreased power density. Indeed, Fig. 3 clearly shows how increasing the electrode thickness of the NPMC cathode raises the current density to that of the Pt-based cathode at high cell voltage,

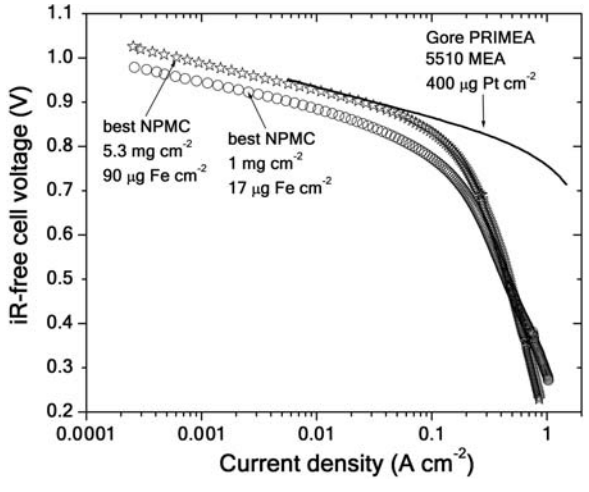

Fig. 3. Comparison of the best NPMC in this work with a Pt-based catalyst. Polarization curves from H_2-O_2 fuel cell testing ($P_{O_2} = P_{H_2}$ = 1.5 bar, 80°C, 100% RH) are shown for cathodes made with the best NPMC in this work, one with a loading of 1 mg cm^{-2} (circles) and another with a loading of 5.3 mg cm^{-2} (stars). Also shown is a ready-to-use Gore PRIMEA 5510 membrane electrode assembly (MEA; W. L. Gore & Associates) with ~0.4 mg Pt cm^{-2} at cathode and anode (black line). Flow rates for H_2 and O_2 were well above stoichiometric. The actual Fe content in our catalyst is 1.7 wt %, resulting in a Fe loading of 17 μg cm^{-2} for a catalyst loading of 1 mg cm^{-2}. Open circuit voltages are 1.03, 1.03, and 1.01 V for the MEAs using 17 and 90 μg Fe cm^{-2} and 400 μg Pt cm^{-2} at the cathode, respectively.

but creates increased mass transport losses at current densities of >0.1 A cm^{-2}. It is clear from these results that improvements in electrode mass transport properties are required to overcome this performance loss.

The results of 100-hour durability tests in fuel cells using hydrogen/oxygen and hydrogen/air as anode/cathode gases are shown in fig. S4. Relative to the stable current densities obtained by Bashyam and Zelenay (*32*) for tests performed under the same conditions (0.2 A cm^{-2} with H_2/O_2 at 0.5 V; 0.13 to 0.14 A cm^{-2} with H_2/air at 0.4 V), the initial current densities produced by the catalyst in this work (0.75 A cm^{-2} with H_2/O_2 at 0.5 V; 0.58 A cm^{-2} with H_2/air at 0.4 V) were much higher and remained higher throughout the 100-hour period, with final values of 0.33 A cm^{-2} with H_2/O_2 at 0.5 V and 0.36 A cm^{-2} with H_2/air at 0.4 V.

The best NPMC in this work has a much higher initial activity, but less stability, than those prepared by Bashyam and Zelenay according to a nonpyrolytic method based on a cobalt salt and polypyrrole deposited on carbon black (*32*). Continued research must now focus on improving the stability of these NPMCs and optimizing their cathode mass-transport properties.

References and Notes

1. H. A. Gasteiger, S. S. Kocha, B. Sompalli, F. T. Wagner, *Appl. Catal. B* **56**, 9 (2005).
2. H. A. Gasteiger, J. E. Panels, S. G. Yan, *J. Power Sources* **127**, 162 (2004).
3. R. Jasinski, *Nature* **201**, 1212 (1964).
4. J. P. Dodelet, in *N4-Macrocyclic Metal Complexes*, J. H. Zagal, F. Bedioui, J. P. Dodelet, Eds. (Springer, New York, 2006), pp. 83–147.
5. S. Gupta, D. Tryk, I. Bae, W. Aldred, E. Yeager, *J. Appl. Electrochem.* **19**, 19 (1989).
6. M. Yuasa *et al.*, *Chem. Mater.* **17**, 4278 (2005).
7. N. P. Subramanian *et al.*, *J. Power Sources* **157**, 56 (2006).
8. E. B. Easton, A. Bonakdarpour, J. R. Dahn, *Electrochem. Solid State Lett.* **9**, A463 (2006).
9. R. Z. Yang, A. Bonakdarpour, E. B. Easton, P. Stoffyn-Egli, J. R. Dahn, *J. Electrochem. Soc.* **154**, A275 (2007).
10. J. Maruyama, I. Abe, *Chem. Commun.* **2007**, 2879 (2007).
11. T. E. Wood, Z. Tan, A. K. Schmoeckel, D. O'Neill, R. Atanasoski, *J. Power Sources* **178**, 510 (2008).
12. A. Garsuch, K. MacIntyre, X. Michaud, D. A. Stevens, J. R. Dahn, *J. Electrochem. Soc.* **155**, B953 (2008).
13. T. Schilling, M. Bron, *Electrochim. Acta* **53**, 5379 (2008).
14. A. H. C. Sirk, S. A. Campbell, V. I. Birss, *J. Electrochem. Soc.* **155**, B592 (2008).
15. J. Maruyama, N. Fukui, M. Kawaguchi, I. Abe, *J. Power Sources* **182**, 489 (2008).
16. V. Nallathambi, J.-W. Lee, S. P. Kumaraguru, G. Wu, B. N. Popov, *J. Power Sources* **183**, 34 (2008).
17. U. I. Koslowski, I. Abs-Wurmbach, S. Fiechter, P. Bogdanoff, *J. Phys. Chem. C* **112**, 15356 (2008).
18. J. Maruyama, J. Okamura, K. Miyazaki, Y. Uchimoto, I. Abe, *J. Phys. Chem. C* **112**, 2784 (2008).
19. J. M. Ziegelbauer *et al.*, *J. Phys. Chem. C* **112**, 8839 (2008).
20. F. Jaouen, F. Charreteur, J. P. Dodelet, *J. Electrochem. Soc.* **153**, A689 (2006).
21. F. Jaouen, M. Lefèvre, J. P. Dodelet, M. Cai, *J. Phys. Chem. B* **110**, 5553 (2006).
22. F. Jaouen, J. P. Dodelet, *J. Phys. Chem. C* **111**, 5963 (2007).
23. F. Jaouen, A. M. Serventi, M. Lefevre, J. P. Dodelet, P. Bertrand, *J. Phys. Chem. C* **111**, 5971 (2007).
24. F. Jaouen, S. Marcotte, J. P. Dodelet, G. Lindbergh, *J. Phys. Chem. B* **107**, 1376 (2003).
25. F. Charreteur, F. Jaouen, S. Ruggeri, J. P. Dodelet, *Electrochim. Acta* **53**, 2925 (2008).
26. See supporting material on *Science* Online.
27. U. S. Department of Energy, Technical Plan: Fuel Cells, 2007 (www1.eere.energy.gov/hydrogenandfuelcells/mypp/pdfs/fuel_cells.pdf).
28. F. Charreteur, S. Ruggeri, F. Jaouen, J. P. Dodelet, *Electrochim. Acta* **53**, 6881 (2008).
29. F. Jaouen, J. P. Dodelet, *Electrochim. Acta* **52**, 5975 (2007).
30. M. Lefèvre, J.-P. Dodelet, *Electrochim. Acta* **53**, 8269 (2008).
31. Although detailed cost analysis of these Fe-based electrocatalysts was not performed, their principal elements are carbon, nitrogen, and iron and they require no expensive precursors or processing steps. Their manufacturing cost is conservatively estimated to be at least two orders of magnitude lower than that of current Pt-based ORR catalysts for PEMFCs.
32. R. Bashyam, P. Zelenay, *Nature* **443**, 63 (2006).

33. Supported by General Motors of Canada and the Natural Sciences and Engineering Council of Canada. The Cabot Corporation provided the carbon black. U.S. patent application US 61/112,844 related to this work was filed on 10 November 2008.

Supporting Online Material

www.sciencemag.org/cgi/content/full/324/5923/71/DC1
Materials and Methods
SOM Text
Figs. S1 to S4
Tables S1 and S2
References

19 December 2008; accepted 9 February 2009
10.1126/science.1170051

Consecutive Thermal H_2 and Light-Induced O_2 Evolution from Water Promoted by a Metal Complex

Stephan W. Kohl,[1] Lev Weiner,[2] Leonid Schwartsburd,[1] Leonid Konstantinovski,[2] Linda J. W. Shimon,[2] Yehoshoa Ben-David,[1] Mark A. Iron,[2] David Milstein[1]*

Discovery of an efficient artificial catalyst for the sunlight-driven splitting of water into dioxygen and dihydrogen is a major goal of renewable energy research. We describe a solution-phase reaction scheme that leads to the stoichiometric liberation of dihydrogen and dioxygen in consecutive thermal- and light-driven steps mediated by mononuclear, well-defined ruthenium complexes. The initial reaction of water at 25°C with a dearomatized ruthenium (II) [Ru(II)] pincer complex yields a monomeric aromatic Ru(II) hydrido-hydroxo complex that, on further reaction with water at 100°C, releases H_2 and forms a cis dihydroxo complex. Irradiation of this complex in the 320-to-420–nanometer range liberates oxygen and regenerates the starting hydrido-hydroxo Ru(II) complex, probably by elimination of hydrogen peroxide, which rapidly disproportionates. Isotopic labeling experiments with $H_2{}^{17}O$ and $H_2{}^{18}O$ show unequivocally that the process of oxygen–oxygen bond formation is intramolecular, establishing a previously elusive fundamental step toward dioxygen-generating homogeneous catalysis.

The design of efficient catalytic systems for splitting water into H_2 and O_2, driven by sunlight without the use of sacrificial reductants or oxidants, is among the most important challenges facing science today, underpinning the long-term potential of hydrogen as a clean, sustainable fuel (*1*, *2*). In this context, it is essential to enhance our basic understanding of the fundamental chemical steps involved in such processes (*3*–*17*). Of the two parts of the water-splitting cycle, the oxidation half-cycle to form O_2 presents the greatest challenge. Well-defined metal complexes that catalyze water oxidation to dioxygen are rare and generally require a sacrificial strong oxidant. The molecular mechanisms of such systems, including that of the intensively studied "blue dimer" *cis*,*cis*-$[(bpy)_2(H_2O)Ru^{III}ORu^{III}(OH_2)(bpy)_2]^{4+}$ (*3*, *11*, *12*), are generally thought to involve metal oxo intermediates and bimolecular steps, but clarification of the fundamental chemical principles responsible for O–O bond formation remains a considerable challenge. In addition, a major challenge faced by hydrogen and oxygen photogeneration systems based on soluble metal complexes is that for a viable system, the two half-cycles must be combined, avoiding the use of sacrificial oxidants and reductants. We present here a ruthenium-mediated reaction sequence that, in a stepwise stoichiometric manner, generates hydrogen thermally and oxygen photochemically, involves well-defined complexes, and demonstrates the feasibility of unimolecular O–O bond formation at a single metal center.

[1]Department of Organic Chemistry, The Weizmann Institute of Science, Rehovot 76100, Israel. [2]Department of Chemical Research Support, The Weizmann Institute of Science, Rehovot 76100, Israel.

*To whom correspondence should be addressed. E-mail: david.milstein@weizmann.ac.il

We have previously reported that the non-aromatic pincer Ru(II) complex **1** (Fig. 1) is a powerful catalyst for the coupling of alcohols to form esters with the liberation of H_2 (*18*) and for the dehydrogenative coupling of alcohols with amines to produce amides (*19*). We have now studied the reactivity of this complex with water. The addition of one equivalent of water to a solution of **1** in tetrahydrofuran (THF) at room temperature immediately led to ligand aromatization with quantitative formation of the *trans* hydrido-hydroxo complex **2** (Fig. 1), which we isolated and fully characterized (*20*). This compound is probably formed by a mechanism involving coordination of water at the vacant coordination site trans to the hydride ligand, followed by proton migration to the side arm. This unique water activation process involves cooperation between the metal and the ligand and no change in the metal oxidation state (*21*).

Characteristic spectroscopic features in the ^1H nuclear magnetic resonance (NMR) spectrum of **2** are the large downfield shift of the hydride ligand resonance from –26.5 parts per million (ppm) (d, $^2J_{PH}$ = 25.5 Hz) in **1** to –14.9 ppm (d, $^2J_{PH}$ = 27.5 Hz) and a doublet at –1.4 ppm ($^3J_{PH}$ = 2.3 Hz) assigned to the hydroxo ligand. If one equivalent of D_2O is used instead of H_2O, one deuterium atom is incorporated at the side-arm benzylic carbon, leading to a broad peak (because of unresolved small $^2J_{HD}$ and $^2J_{PD}$) at 2.8 ppm in the ^2H NMR spectrum; the OD group gives rise to a signal at –1.2 ppm (complex **2-*D*$_2$**, Fig. 1). These reactions are reversible. Placing the solid under vacuum or heating it in benzene solution at 65°C resulted in water elimination to quantitatively yield the starting complex **1**. Direct spectroscopic evidence for coordination of the hydroxo group to the metal center was obtained by adding one equivalent of $H_2{}^{17}O$ to **1** in THF. The oxygen atom in the labeled complex **2-*^{17}O*** exhibits a singlet at 32.43 ppm in the ^{17}O NMR spectrum (in THF). Coupling ($^2J_{OP}$, $^2J_{OC}$) of the ^{17}O atom (s = 5/2) with the adjacent ligands leads to broadening of the signal in the ^{31}P NMR spectrum at 112.14 ppm and the appearance of a more complicated signal for the carbonyl ligand in the $^{13}C\{^1H\}$NMR spectrum (δ = 209.27 ppm). The doublet in the ^1H NMR spectrum (δ = 14.78 ppm) assigned to the hydride ligand in the trans position is not affected.

Repeating the reaction in benzene by adding an excess of water to **1** resulted in formation of colorless crystals at the interface between the water and benzene layers. X-ray diffraction analysis of the isolated solid (**2.*n*H$_2$O**) shows a distorted octahedral coordination geometry at ruthenium (Fig. 2). The Ru–O–H nonlinear angle [103(3)] indicates repulsion between the oxygen lone pairs and d electrons of the complex (*22*, *23*). The crystals are composed of alternating layers of the metal complex, benzene, and water. The hydroxo groups of the complex are involved in hydrogen bonding with the water layer (figs. S4 to S6). These crystals are stable below 10°C and release the solvated water at room temperature.

Heating complex **2** (or **2.*n*H$_2$O**) in refluxing water for 3 days resulted in evolution of H_2 with concomitant formation of the green *cis* dihydroxo complex **3** (Fig. 3). The gas was collected in a burette, and hydrogen was detected by the reaction of a sample of the gas phase with $(PEt_3)_3IrCl$ to form *mer-cis*-$(PEt_3)_3Ir(H)_2Cl$ (*24*). H_2 was quantified with gas chromatography (GC) (yield: 37%). The NMR yield of the complex **3** was 45%. Some unreacted **2.*n*H$_2$O** (25%) remained, the rest being unidentified products. This reaction may proceed by electrophilic attack by water on the hydride ligand. Pure **3** was independently prepared by reaction of **2.*n*H$_2$O** with N_2O (*25*, *26*): N_2O was bubbled into a THF solution of **2.*n*H$_2$O** for 10 min at room temperature, after which the solution was stirred overnight and turned green. We isolated and fully characterized the result-

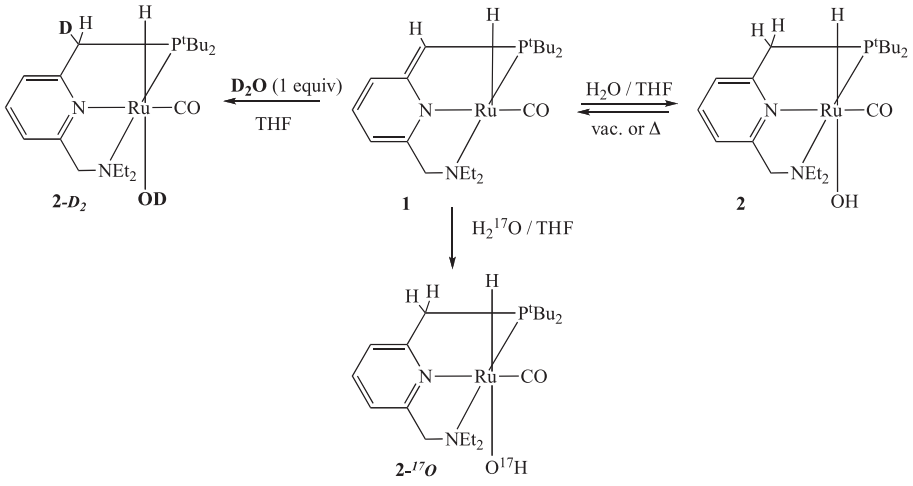

Fig. 1. Reactions of water with complex **1.** Et, ethyl.

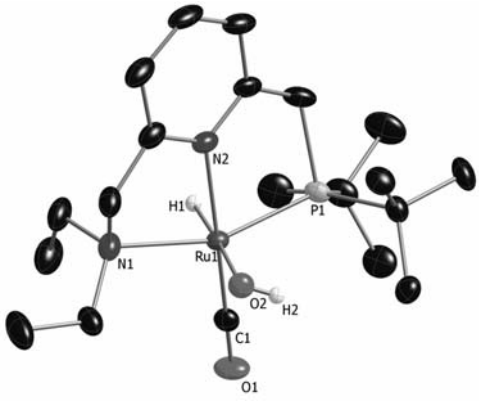

Fig. 2. Structure of the *trans* hydrido-hydroxo complex **2.*n*H$_2$O** (ellipsoids shown at 50% probability level). Hydrogen atoms are shown only for the hydride and hydroxo ligands. The water and benzene layers are omitted for clarity. Selected bond distances (in angstroms) and angles (in degrees): Ru1–H1, 1.54(3); Ru1–C1, 1.820(3); Ru1–N2, 2.097(2); Ru1–N1, 2.241(2); Ru1–O2, 2.261(2); Ru1–P1, 2.2653(8); N2–Ru1–C1, 173.02(10); N1–Ru1–P1, 159.12(7); H1–Ru1–O2, 171.9(13); N2–Ru1–O2, 86.94(8); N1–Ru1–O2, 82.44(9); Ru1–O2–H2, 103(3).

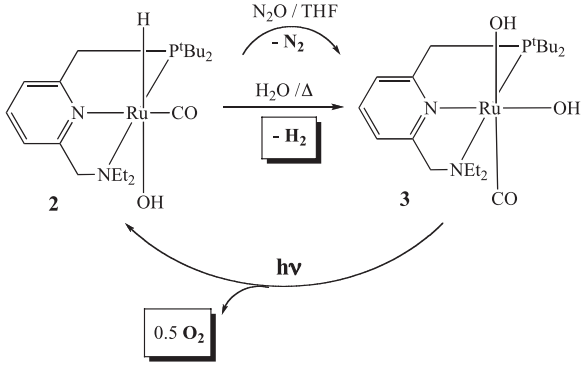

Fig. 3. Thermal activation of water by the hydrido-hydroxo complex **2** with liberation of H_2, independent synthesis of the dihydroxo complex **3** using N_2O, and O_2 formation upon photolysis of **3** regenerating complex **2.** *h*, Planck's constant; ν, frequency.

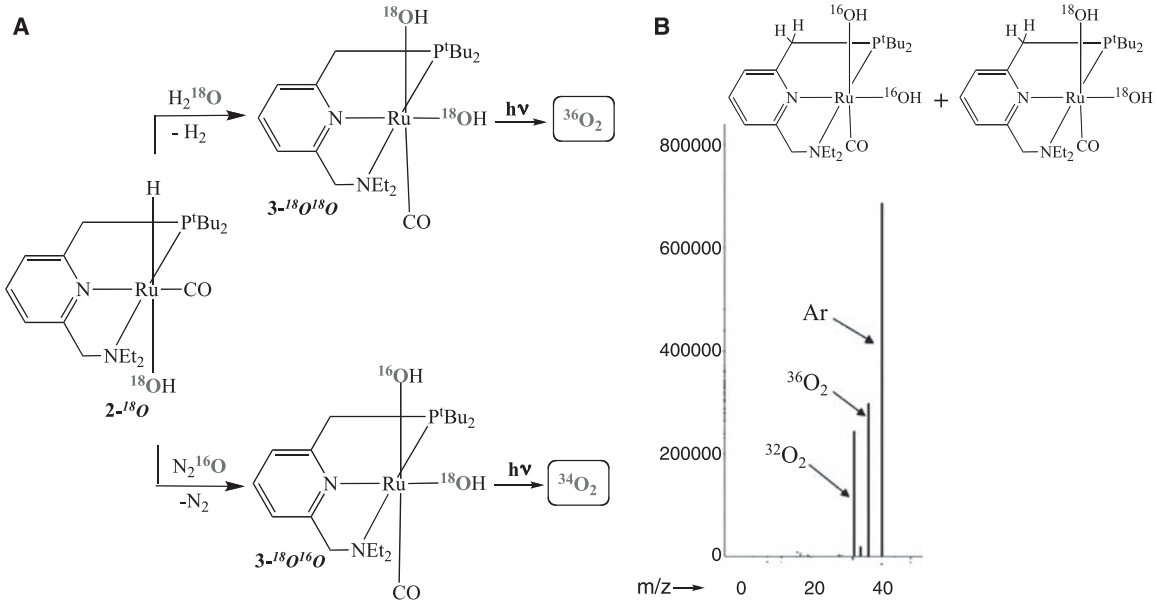

Fig. 4. Photolysis of isotopically labeled dihydroxo complexes. (**A**) Synthesis and photolysis of complexes **3-^{18}O^{18}O** and **3-^{18}O^{16}O**. (**B**) Mass spectrum of a gaseous extract from the photolytic reaction of equimolar amounts of **3-^{18}O^{18}O** and **3-^{16}O^{16}O**, showing virtually no crossover.

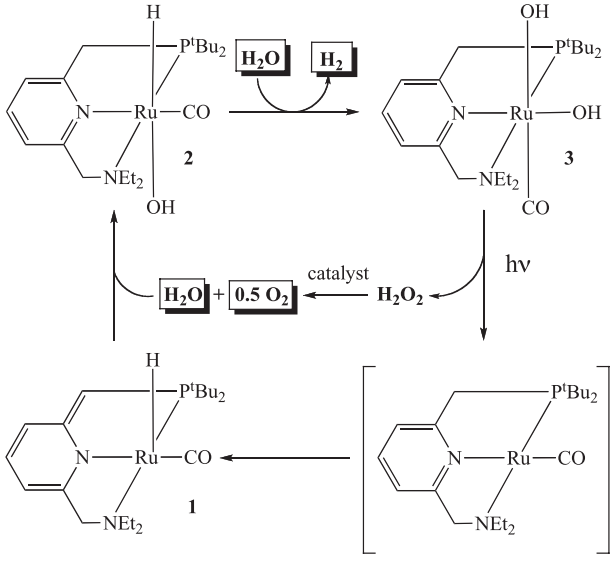

Fig. 5. Proposed mechanism for the formation of H_2 and O_2 from water.

ant green microcrystalline solid **3** (60% yield). It is stable in a THF solution up to 65°C but decomposes into unidentified products at 102°C in dioxane. The $^{31}P\{^1H\}$ NMR spectrum of **3** shows a singlet at 94.0 ppm, representing an upfield shift of 14 ppm relative to the corresponding singlet of complex **2**. The two tert-butyl (^{t}Bu) groups of P^{t}Bu$_2$ give rise to different signals in both the ^1H and $^{13}C\{^1H\}$NMR spectra, and the ethyl groups of NEt_2 are also nonequivalent, indicating C_1 symmetry and a cis dihydroxo arrangement. The hydroxo ligands give rise to a broad signal at –7.4 ppm in the ^1H NMR spectrum and absorb at 3413 cm^{-1} in the infrared (IR) spectrum. The carbonyl ligand exhibits a doublet at 207.4 ppm ($^2J_{PC}$ = 16.1 Hz) in the $^{13}C\{^1H\}$ NMR spectrum and absorbs at 1923 cm^{-1} in the IR spectrum. The main peak in the mass spectrum (electrospray ionization) at mass/charge ratio (m/z) = 453 (100) can be assigned to the cation $[M - OOH]^+$ and the peak at m/z = 469 (18) is characteristic for $[M - OH]^+$. Elemental analysis agrees with the calculated values for our posited structure.

We next studied the stability of complex **3** on exposure to light. Irradiation of THF or aqueous solutions of **3** under N_2 or Ar with a 300-W halogen lamp filtered through perspex (*27*) over 2 days resulted in a color change from green to greenish-yellow, accompanied by O_2 evolution. NMR of the solution showed that besides unreacted **3** (33%), the hydrido-hydroxo complex **2.*n*H$_2$O** (45%) was formed, in addition to some unidentified by-products (22%), most probably phosphine oxides (Fig. 3). The liberated gas was identified as dioxygen by GC–mass spectrometry (GC-MS) and by the reaction with $(PEt_3)_3IrCl$ to form the dioxygen complex $(PEt_3)_3Ir(O_2)Cl$ (*20*). This specific and very sensitive reaction was also used for quantification (*20*). The yield of the detected dioxygen formed from the reaction in water was 23% (34% based on reacted **3**). When irradiation of aqueous solutions of **3** was performed under argon flow to remove the generated O_2, clean conversion of **3** (49%, the rest being unreacted **3**) to **2.*n*H$_2$O** (49%) was observed, with no by-products being formed, indicating that the unidentified by-products are a result of reaction with the generated dioxygen.

To verify that O_2 was released from the dihydroxo complex, a labeled complex bearing two ^{18}OH groups (**3-^{18}O^{18}O**) was prepared using $H_2{}^{18}O$ (Fig. 4). The ^{18}O-H stretching vibration is shifted in the IR spectrum to lower energy by 14 wavenumbers, to 3399 cm^{-1}, whereas all NMR spectra are identical to those of **3**. Upon irradiation (*27*) of **3-^{18}O^{18}O** in H_2O, $^{36}O_2$ was formed as the major dioxygen product, as confirmed by GC-MS (Fig. 4A and fig. S3A). No exchange between **3-^{18}O^{18}O** and $H_2{}^{16}O$ was observed, indicating that no substantial Ru-OH dissociation took place.

An important question is whether the O–O bond formation process is intra- or intermolecular. To address this issue, we prepared the isotopically mixed-labeled dihydroxo complex **3-^{18}O^{16}O** by treatment of **2-^{18}O** with $N_2{}^{16}O$ (Fig. 4A). Upon photolysis, $^{34}O_2$ was formed predominantly with only small amounts of $^{32}O_2$ and $^{36}O_2$ observed (observed ratio $^{32}O_2$:$^{34}O_2$:$^{36}O_2$, 3.8:16.2:1) (fig S3B) (*20*). Moreover, we performed a crossover experiment involving photolysis of equimolar amounts of complexes **3-^{18}O^{18}O** and **3-^{16}O^{16}O**, resulting in formation of $^{36}O_2$ and $^{32}O_2$ with only a small amount of $^{34}O_2$ (observed ratio $^{32}O_2$:$^{34}O_2$:$^{36}O_2$, 13.1:1:15.6) (Fig. 4B). Thus, our results unambiguously show that the O-O

bond formation process in this system is intramolecular and involves a single metal center.

We suggest that upon photolysis, complex **3** liberates hydrogen peroxide in a reductive elimination step (*28*, *29*), which then catalytically disproportionates into O_2 and water (Fig. 5). Our labeling studies show that, if H_2O_2 is indeed an intermediate in the O_2 generation process, then O_2 is formed by two electron oxidation of H_2O_2 without scission of the O–O bond, as reported for the reaction catalyzed by the enzyme catalase (*30*).

The metal-to-ligand charge transfer (MLCT) band of **3** has an absorbance maximum in the ultraviolet-visible (UV-Vis) spectrum in water at wavelength $\lambda = 380$ nm (extinction coefficient $\varepsilon = 8157\ cm^{-1}M^{-1}$). Weaker absorptions appear at $\lambda = 459$ nm ($\varepsilon = 2045\ cm^{-1}M^{-1}$) and $\lambda = 716$ nm ($\varepsilon = 505\ cm^{-1}M^{-1}$) (fig. S2). The theoretical UV-Vis spectrum (of the NMe_2, PMe_2 model of **3**) in water was determined by time-dependent density functional theory (TDDFT) (figs S8 and S9 and table S5). When a 400-nm filter was used, the yield of produced O_2 decreased to only 8 to 10%. Together with filtration of wavelengths of $\lambda < 320$ nm by the perspex filter, this observation is in line with an effective spectral range corresponding to the MLCT band of **3** (320 to 420 nm).

Unlike the dihydroxo complex **3**, the hydrido-hydroxo complex **2** was stable toward irradiation with a 300-W halogen lamp for 2 days, with or without the perspex filter, and did not release O_2. This observation is in line with an intramolecular, mononuclear O–O bond formation mechanism.

Because the intermediacy of H_2O_2 might give rise to hydroxyl radicals, via a Fenton-type reaction (*31*), we employed the spin trap 5,5-dimethyl-1-pyrroline-1-oxide (DMPO) (*32*) to detect them. Electron paramagnetic resonance spectra did provide evidence for DMPO-OH adducts (fig. S7A). However, it is clear that these hydroxyl radicals are not substantially involved in O_2 production (as the isotopic labeling experiments would have resulted in scrambling). Thus, in the presence of the OH radical scavenger *tert*-butanol (*33*), no hydroxyl radicals were observed, whereas the amount of O_2 formed remained unchanged. Further evidence supporting hydrogen peroxide as the source of hydroxyl radicals, and that the hydroxyl radicals are not the source of the produced O_2, was obtained from experiments with the enzyme catalase, which is an extremely efficient catalyst for the disproportionation of hydrogen peroxide to O_2 and water by a non-radical mechanism. If H_2O_2 were the source of hydroxyl radicals, its interception by catalase would retard their formation. When irradiation of **3** was performed in the presence of catalase, only traces of hydroxyl radicals were observed (fig. S7C), whereas the amount of O_2 produced remained almost unchanged (actually slightly increased). Thus, we believe that H_2O_2 forms photolitically from **3** and undergoes disproportionation to O_2 and water, with only a marginal amount of it forming hydroxyl radicals, perhaps by a Fenton-type reaction. As expected, no OH radicals were detected when the hydrido-hydroxo complex ***2.nH$_2$O*** was irradiated.

Combining the separate stoichiometric reactions presented here gives rise to a stepwise cycle in which H_2 and O_2 are released in consecutive steps, and the starting Ru complex is regenerated (Fig. 5). The cycle starts with the *trans* hydrido-hydroxo complex ***2.nH$_2$O*** that reacts with water under refluxing conditions, evolving H_2 and forming the *cis* dihydroxo complex **3**. The second step is light-induced. Irradiating **3** may release hydrogen peroxide by reductive elimination, probably forming a Ru(0) intermediate, which converts to **1** by migration of a proton from the methylene group of the phosphorus side arm to the ruthenium center to form a hydride ligand with coincident dearomatization of the pyridine ring (*34*, *35*). The liberated hydrogen peroxide is then rapidly catalytically decomposed into dioxygen and water. A possible catalyst for this latter reaction is complex **1**. The addition of a very dilute THF solution of **1** to a THF solution of hydrogen peroxide at room temperature resulted in immediate O_2 evolution, as detected by GC-MS and by reaction with $(PEt_3)_3IrCl$ (*20*). In the last step of the cycle, the water reacts readily with **1** to form the starting complex **2**.

We believe that our studies indicate a distinct approach toward a complete cycle for the generation of dihydrogen and dioxygen from water catalyzed by metal complexes and show that light-induced O–O bond formation can be intramolecular and need not necessarily involve bimolecular mechanisms, dinuclear complexes, and metal oxo intermediates.

References and Notes

1. N. S. Lewis, D. G. Nocera, *Proc. Natl. Acad. Sci. U.S.A.* **103**, 15729 (2006).
2. V. Balzani, A. Credi, M. Venturi, *ChemSusChem* **1**, 26 (2008).
3. R. A. Binstead, C. W. Chronister, J. Ni, C. W. Hartshorn, T. J. Meyer, *J. Am. Chem. Soc.* **122**, 8464 (2000).
4. J. H. Alstrum-Acevedo, M. K. Brennaman, T. J. Meyer, *Inorg. Chem.* **44**, 6802 (2005).
5. T. A. Betley, Q. Wu, T. Van Voorhis, D. G. Nocera, *Inorg. Chem.* **47**, 1849 (2008).
6. J. K. Hurst, *Coord. Chem. Rev.* **249**, 313 (2005).
7. M. Yagi, M. Kaneko, *Chem. Rev.* **101**, 21 (2001).
8. W. Ruttinger, G. C. Dismukes, *Chem. Rev.* **97**, 1 (1997).
9. I. Romero *et al*., *Inorg. Chem.* **47**, 1824 (2008).
10. Z. Deng, H.-W. Tseng, R. Zong, D. Wang, R. Thummel, *Inorg. Chem.* **47**, 1835 (2008).
11. J. K. Hurst, J. L. Cape, A. E. Clark, S. Das, C. Qin, *Inorg. Chem.* **47**, 1753 (2008).
12. X. Yang, M.-H. Baik, *J. Am. Chem. Soc.* **128**, 7476 (2006).
13. J. T. Muckerman, D. E. Polyansky, T. Wada, K. Tanaka, E. Fujita, *Inorg. Chem.* **47**, 1787 (2008).
14. N. D. McDaniel, F. J. Coughlin, L. L. Tinker, S. Bernhard, *J. Am. Chem. Soc.* **130**, 210 (2008); and references therein.
15. Y. V. Geletii *et al*., *Angew. Chem. Int. Ed.* **47**, 3896 (2008); and references therein.
16. J. Limburg *et al*., *Science* **283**, 1524 (1999).
17. S. Chakraborty, T. J. Wadas, H. Hester, R. Schmehl, R. Eisenberg, *Inorg. Chem.* **44**, 6865 (2005).
18. J. Zhang, G. Leitus, Y. Ben-David, D. Milstein, *J. Am. Chem. Soc.* **127**, 10840 (2005).
19. C. Gunanathan, Y. Ben-David, D. Milstein, *Science* **317**, 790 (2007).
20. Experimental details are available as supporting material on *Science* Online.
21. DFT calculations on a model system (with PMe_2, NMe_2 groups) at the PCM(H_2O)-M06/SDB-cc-pVDZ//M06/SDD(d) level indicate that the Gibbs free energy change (ΔG) = –5.4 kcal/mol for H_2O coordination and ΔG = –5.7 kcal/mol and $\Delta G^{\ddagger}$ = 9.4 kcal/mol for the subsequent proton migration. Addition of a bridging water molecule as part of the proton-transfer transition state lowers the barrier to $\Delta G^{\ddagger} = 3.6$ kcal/mol. According to this DFT calculation, the D atom would selectively transfer to the same side of the double bond as the hydroxo ligand, but we have not yet demonstrated this experimentally.
22. P. E. M. Siegbahn, M. R. A. Blomberg, M. Svenson, *J. Phys. Chem.* **97**, 2564 (1993).
23. D. Milstein, J. C. Calabrese, I. D. Williams, *J. Am. Chem. Soc.* **108**, 6387 (1986).
24. O. Blum, D. Milstein, *J. Am. Chem. Soc.* **117**, 4582 (1995).
25. Reaction of a Ru(H)(OH) complex with N_2O was reported to yield a $Ru(OH)_2$ complex (*26*). We found that bubbling N_2O into a solution of the crystalline material ***2.nH$_2$O*** (rather then **2**) avoided the formation of impurities.
26. A. W. Kaplan, R. G. Bergman, *Organometallics* **17**, 5072 (1998).
27. We used a filter made of polymethylmethacrylate (perspex, thickness = 1 cm) during the irradiation. This material absorbs UV light at wavelengths shorter than $\lambda = 320$ nm. Irradiation without perspex gave more by-products, and dioxygen was formed in only 19% yield.
28. Photochemically induced reductive elimination of HOCl from a $Pt^{(IV)}(Cl)(OH)$ complex was suggested (*29*).
29. Y. Nakabayashi *et al*., *Chem. Eur. J.* **13**, 3980 (2007).
30. S. Kato, T. Ueno, S. Fukuzumi, Y. Watanabe, *J. Biol. Chem.* **279**, 52376 (2004).
31. C. Walling, *Acc. Chem. Res.* **8**, 125 (1975).
32. M. A. Grela, M. E. J. Coronel, A. J. Colussi, *J. Phys. Chem.* **100**, 16940 (1996).
33. J. von Sonntag, E. Mvula, K. Hildenbrand, C. von Sonntag, *Chem. Eur. J.* **10**, 440 (2004).
34. For such a proton migration process with a PNP-Ir(I) complex, see (*35*).
35. E. Ben-Ari, G. Leitus, L. J. W. Shimon, D. Milstein, *J. Am. Chem. Soc.* **128**, 15390 (2006).

36. This project was supported by the Israel Science Foundation, the Petroleum Research Fund administered by the American Chemical Society, the programme for Deutsch-Israelische Partnerschaft, and the Helen and Martin Kimmel Center for Molecular Design. S.W.K. thanks the Humboldt Foundation for a Feodor Lynen Postdoctoral Fellowship. D.M. holds the Israel Matz Professorial Chair of Organic Chemistry. We thank M. Feller for fruitful discussions, A. Tishbee and R. Kramer for performing mass spectroscopy, A. Khenkin and H. Weissman for carrying out GC-MS and GC measurements, and E. Shirman for photon flux measurements. Structural parameters for ***2.nH$_2$O*** are available free of charge from the Cambridge Crystallographic Data Centre under identification number CCDC-681749.

Supporting Online Material

www.sciencemag.org/cgi/content/full/324/5923/74/DC1
Materials and Methods
SOM Text
Figs. S1 to S9
Tables S1 to S5
References

17 November 2008; accepted 13 February 2009
10.1126/science.1168600

Persistent Positive North Atlantic Oscillation Mode Dominated the Medieval Climate Anomaly

Valérie Trouet,[1]* Jan Esper,[1,2] Nicholas E. Graham,[3,4] Andy Baker,[5] James D. Scourse,[6] David C. Frank[1]

The Medieval Climate Anomaly (MCA) was the most recent pre-industrial era warm interval of European climate, yet its driving mechanisms remain uncertain. We present here a 947-year-long multidecadal North Atlantic Oscillation (NAO) reconstruction and find a persistent positive NAO during the MCA. Supplementary reconstructions based on climate model results and proxy data indicate a clear shift to weaker NAO conditions into the Little Ice Age (LIA). Globally distributed proxy data suggest that this NAO shift is one aspect of a global MCA-LIA climate transition that probably was coupled to prevailing La Niña–like conditions amplified by an intensified Atlantic meridional overturning circulation during the MCA.

The North Atlantic Oscillation (NAO)—the main synoptic mode of atmospheric circulation and climate variability in the North Atlantic/European sector—has a substantial influence on marine and terrestrial ecosystems and regional socio-economic activity (*1*). Because the instrumental record of the NAO is relatively short (*2*), there is a need for information on its long-term variability to better understand climate variability in the more distant past and to assess NAO predictability. An array of multiproxy approaches has been applied to extend the NAO record back in time (*3*); however, these only extend to 1400 A.D. and do not span the MCA (*4*), a period (~800–1300) marked by a wide range of changes in climate globally, including apparent relative warmth over the North Atlantic/European sector and much of the extra-tropical Northern Hemisphere (*5*). The MCA is the most recent natural counterpart to modern warmth and can therefore be used to test characteristic patterns of natural versus anthropogenic forcing.

A recent tree-ring–based drought reconstruction for Morocco (1049–2002) (*6*) and a millennial-length speleothem-based precipitation proxy for Scotland (900–1993) (*7*), strategically sited and sensitive to atmospheric variations in the southern and northern nodes of the NAO dipole, provide us with a basis for extending the instrumental winter NAO index (*8*) back to the MCA (Fig. 1) (*9*). Over the 20th century, correlations between instrumental (*10*) Scotland and Morocco December-to-March precipitation and the NAO (*2*) are 0.75 and –0.64, respectively. The Morocco and Scotland reconstructions contain substantial multidecadal variability that is characterized by antiphase oscillatory behavior over the last millennium. The Scotland speleothem record is remarkably similar to Lamb's reconstruction (*4*) of England-Wales September-to-June precipitation (fig. S1), with a sharp 10% decrease in inferred precipitation between the late 13th to mid-14th centuries, a continued decline through the mid-16th to late 18th centuries, and an increasing trend toward present. Contrasting moisture conditions between the Morocco and the Scotland proxy series were particularly strong between 1050 and 1400, during the 18th century, and since the 1940s. A strong inverse relation is also found when comparing observational precipitation records (*10*) for Scotland and Morocco (Pearson correlation coefficient $r = -0.49$, $P < 0.01$ for 1940–2001).

We identified periods of opposing values in the Scotland and Morocco proxies as extremes in the residual series (NAO_{ms}), calculated as the difference between the 30-year smoothed and normalized Scotland and Morocco records (*9*). We used NAO_{ms} as a proxy for decadal-scale winter NAO variability back to 1050. NAO_{ms} reveals multidecadal variability over the 20th century similar to that seen in smoothed instrumental NAO time series (*2*, *11*), including a high-index phase from the turn of the 20th century until the 1930s, a minimum in the 1960s, and an increase since the 1970s (fig. S2). In the 19th century, coherence between the individual instrumental NAO series decreases, probably representing increasing uncertainty back in time, which is typical for both proxy and instrumental data (*12*). Interdecadal fluctuations in NAO_{ms} correspond well with the variability reflected by other NAO reconstructions (*3*, *13*, *14*) (Fig. 2 and table S1). NAO_{ms} is 350 years longer than Cook's reconstruction (*3*) and covers the latter part of the MCA (1050–1400), a period over which NAO_{ms} values were persistently positive compared with the 1500–1983 reference period.

Multidecadal fluctuations in a winter temperature-sensitive $\delta^{18}O$ record from a speleothem in the European Alps (*15*) match the fluctuations in NAO_{ms} over the full period of the record (fig. S1), which is in correspondence with the known relation between the NAO, variability in the strength of winter westerlies across Europe, and winter temperatures across northern and central Europe (*11*). In the low-frequency domain, these winter changes are similar to reconstructed European annual and summer temperatures. In addition, reconstructed European winter sea-level pressure (SLP), temperature (*16*), and precipitation (*17*) patterns, composited for positive and negative NAO_{ms} phases, correspond well with longer-term NAO signatures since 1659 (Fig. 3A). The increased pressure difference between the Azores High (+3 hPa) and the Icelandic Low (–5 hPa) during positive NAO phases results in enhanced zonal flow, with stronger westerlies transporting warm air to the

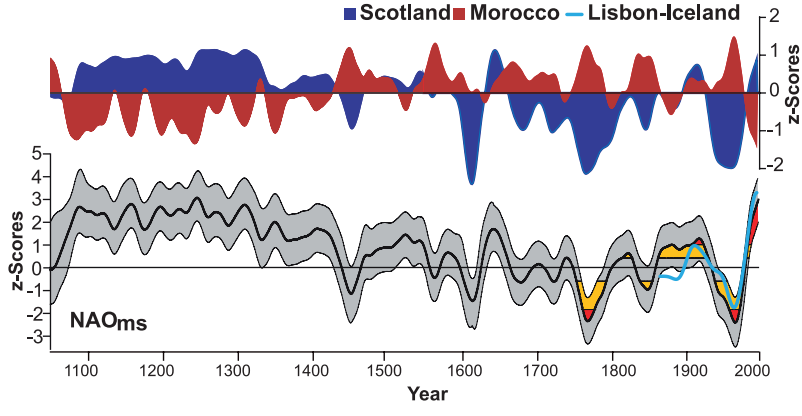

Fig. 1. Proxy-derived long-term NAO reconstruction. (**Top**) Reconstructed winter precipitation for Scotland and February-to-June Palmer Drought Severity Index (*29*) for Morocco. Records were normalized over the common period (1049–1995) and smoothed with the use of a 30-year cubic spline. (**Bottom**) Winter NAO reconstruction NAO_{ms} (black curve) is the difference of the Scotland and Morocco records. The gray area is the estimated uncertainty; yellow and red areas are the 10 and 33% highest and lowest values since 1700. The blue line represents the 30-year smoothed Lisbon-Iceland instrumental NAO index series (*11*).

[1]Swiss Federal Institute for Forest, Snow, and Landscape Research (WSL), Zürcherstrasse 111, 8903 Birmensdorf, Switzerland. [2]Oeschger Centre for Climate Change Research, Erlachstrasse 9a, 3012 Bern, Switzerland. [3]Hydrologic Research Center, 12780 High Bluff Drive, Suite 250, San Diego, CA 92130–2069, USA. [4]Scripps Institution of Oceanography, 9500 Gilman Drive, La Jolla, CA 92093–0225, USA. [5]School of Geography, Earth and Environmental Sciences, University of Birmingham, Birmingham, B15 2TT, UK. [6]School of Ocean Sciences, University of Wales Bangor, Menai Bridge, Anglesey, LL59 5AB, UK.

*To whom correspondence should be addressed. E-mail: trouet@wsl.ch

European continent. The axis of maximum moisture transport and the preferred storm track extend further to the north and east during positive NAO phases when the Azores High is strengthened, resulting in wetter winters over northwestern Europe (50-to-200–mm positive anomalies per season) and decreased precipitation over southern Europe and northwestern Africa (50-to-100–mm negative anomalies per season).

We used a proxy-model analog method [proxy surrogate reconstruction (PSR) (*18*)] to develop a more complete synoptic understanding of the changes associated with the reconstructed NAO dynamics (*9*). In PSR, data from coupled ocean-atmosphere general circulation model (CGCM) simulations are reordered to maximize temporal agreement between multiple proxy records and commensurate data drawn from the model output. The reordered model data set can be used to more fully characterize climate patterns implied by sparse and diverse proxy data. Specifically, in this study, December-to-March precipitation and temperature CGCM data are conditioned on the proxy precipitation records from Scotland (*7*) and Morocco (*6*) and a winter temperature record from the Alps (*15*).

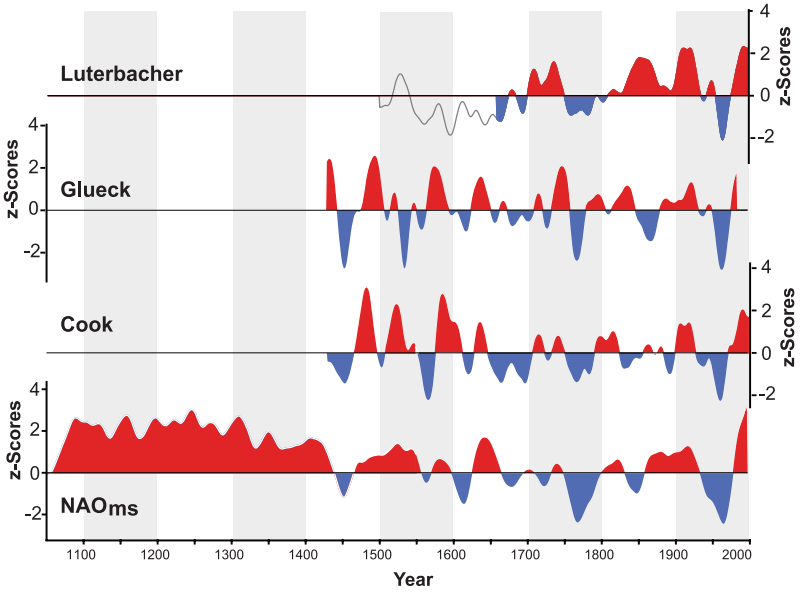

Fig. 2. Proxy-based NAO reconstructions. NAO_{ms} compared with reconstructions by Cook *et al.* (*3*), Glueck and Stockton (*13*), and Luterbacher *et al.* (*14*). All series were smoothed with the use of a 30-year spline and normalized over the 1500-to-1983 common period. The blank period in the Luterbacher reconstruction represents the period before 1659, for which only seasonal values were available.

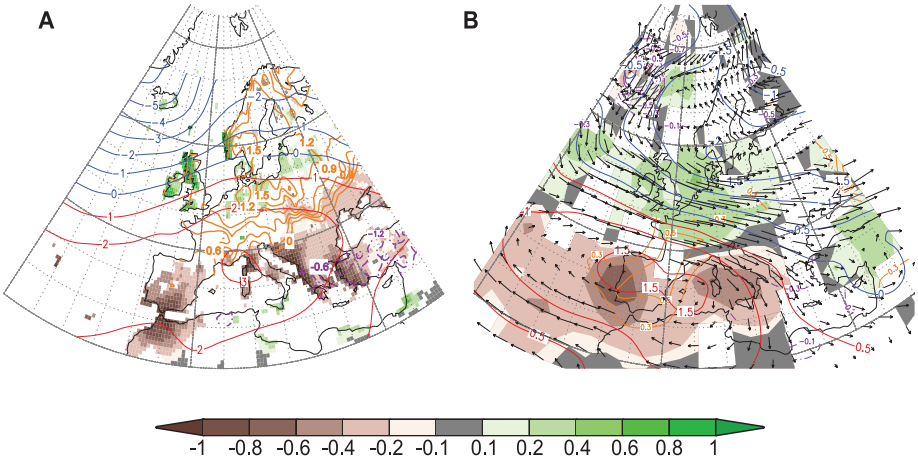

Fig. 3. Empirical and model-derived NAO patterns. Proxy and instrumental (*16*, *17*) (1659–1995) (**A**) and PSR (*18*) reconstructed [with Max Planck Institute model data (*19*)] (**B**) fields of December-to-February SLP, temperature, and precipitation were composited for positive and negative NAO phases. NAO phases were determined in (A) as the 10% most positive versus the 10% most negative NAO_{ms} winters (1659–1995) (Fig. 1) and in (B) as average values for the period 1049–1298 minus those for 1448–1923. Composite difference maps are shown for SLP (red and blue contours, in meters), temperature (orange and dashed purple contours, in degrees Celsius), and precipitation (shaded areas, in millimeters). Shaded areas and contours reflect significant ($P < 0.1$) differences, calculated with a *t* test.

Figure 3B shows composite differences between the MCA and the Little Ice Age (LIA) (averages for 1049–1298 minus those for 1448–1923) in December-to-March SLP, precipitation, and near-surface temperature from the PSR reconstruction, based on a 240-year simulation with the Max Planck Institute coupled ECHAM4-OPYC model (*19*). At the three proxy-model comparison points, the agreement between the input proxy- and model-derived series is close, with correlations of 0.94, 0.94, and 0.92 for Morocco precipitation, Alps temperature, and Scotland precipitation, respectively. Results show an SLP dipole with centers over southern Scandinavia (–2 hPa) and across Iberia (+1.5 hPa) and increased westerlies across western Europe. Considering uncertainties (supporting online text), a plausible range for the magnitude of the PSR-reconstructed MCA-LIA NAO difference is 1.5 to 6.0 hPa. For comparison, the late 20th century upward swing in the NAO was ~7.5 hPa. Increased precipitation over the northeast Atlantic extends across the British Isles and into northwestern Europe (20-to-40–mm positive anomalies per season), and decreased precipitation extends across northwestern Africa, Iberia, and south-central Europe (20-to-50–mm negative anomalies). MCA-to-LIA winter temperature differences of 0.3° to 0.5°C cover most of western Europe with the largest amplitude over Iberia and southern France. The reconstruction suggests an MCA-LIA decrease of westerlies on the order of 0.8 to 1.2 ms^{-1}, a decline of 10 to 20%. Similar patterns and magnitudes found using National Center for Atmospheric Research Community Climate System Model data (fig. S3C) (*20*) suggest that results do not depend on the particular model used in the study.

The persistently strong winter MCA NAO and its weakening during the LIA raise questions about the mechanism responsible for producing such a temporally pervasive atmospheric state over the North Atlantic, as well as MCA-LIA climate anomalies elsewhere (Fig. 4). The widespread signature of this climatic shift implies that changes in tropical sea surface temperatures (SSTs) were involved. A possible explanation is that heating of the western equatorial Pacific (*21*, *22*) and of the tropical Indian Ocean (*23*) induced decreased eastern and central tropical Pacific SSTs resulting in an initial strengthening of the NAO through tropospheric dynamics (*18*, *24*). This modeled La Niña–like state during the MCA is supported by marine proxy records (Fig. 4C and table S2) that show warm SST anomalies in the western tropical Pacific during the MCA (*25*) and cool SSTs in the central and eastern tropical Pacific (*26*).

Stronger westerlies associated with a prolonged positive NAO phase may have enhanced the Atlantic meridional overturning circulation

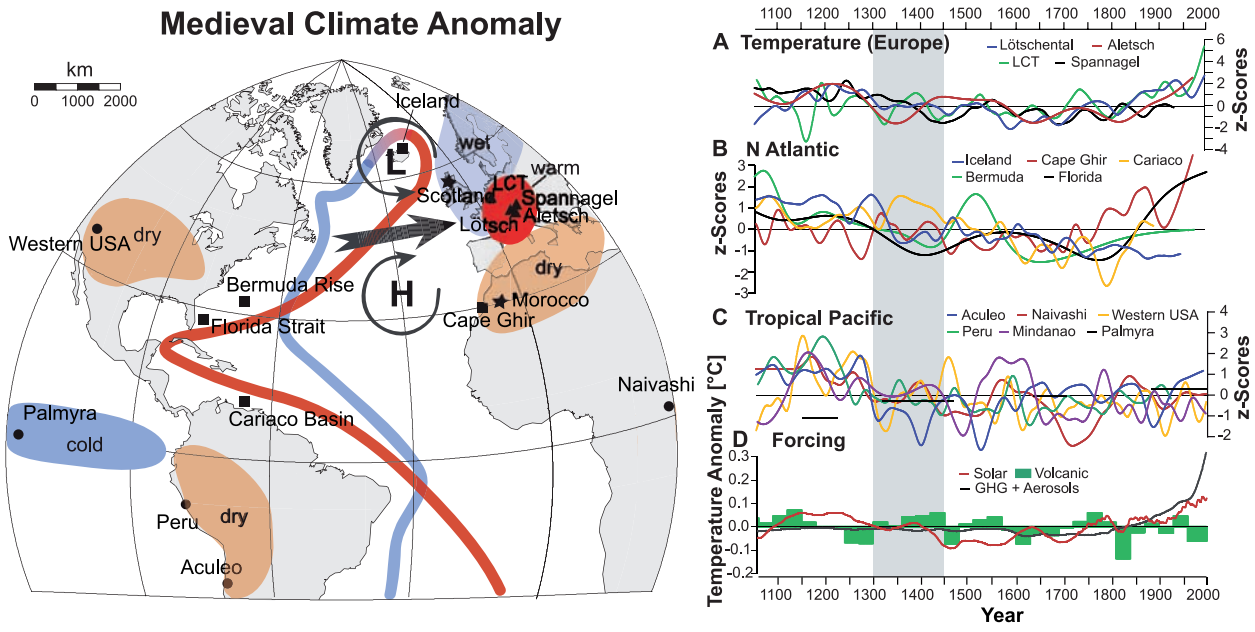

Fig. 4. Large-scale Medieval Climate Anomaly pattern. Geographical location and time series (1050–2000) of proxy records of European temperatures [(**A**), black triangles in the map at left], North Atlantic conditions [(**B**), black squares], tropical Pacific conditions [(**C**), black circles], and external forcings (**D**). Records in (A) to (C) were smoothed with a 60-year spline and normalized over the full period. References for all records are provided in table S1. The radiative forcing time series is derived from (*30*) with the volcanism time series consisting of 30-year averages. The 1300-to-1450 MCA-LIA transition period is highlighted in gray. The map indicates inferred climatic conditions and an intensified AMOC during the MCA, as derived from the proxy records. L, Icelandic Low; H, Azores High.

(AMOC) (*27*), which, in turn, generated cross-equatorial salinity and SST anomalies in the tropical Atlantic and a related northward migration of the intertropical convergence zone (*28*). An enhanced AMOC may have accommodated a constructive feedback mechanism, proxy evidence for which is provided by North Atlantic records (Fig. 4B and table S2), that reinforced the La Niña–like conditions in the tropical Pacific (*22*).

Independent of temperature indicators, the persistent positive NAO phase reconstructed for the MCA now provides a dynamical explanation of winter warmth over Europe during Medieval times (Fig. 4A). Whereas non-stationarity is a general challenge for proxy-based reconstructions, the records used here originate from locations that were shown to lie consistently within the influence of the northern and southern nodes of the NAO dipole (*3*). To help overcome the reduced degrees of freedom in the low-frequency domain that generally limit possibilities for calibration, our proxy-based reconstruction was additionally supported by physically plausible PSR-based synoptic fields. The persistent positive phase reconstructed for the MCA appears to be associated with prevailing La Niña–like conditions possibly initiated by enhanced solar irradiance and/or reduced volcanic activity (*21*) (Fig. 4D) and amplified and prolonged by enhanced AMOC. The relaxation from this particular ocean-atmosphere state into the LIA appears to be globally contemporaneous and suggests a notable and persistent reorganization of large-scale oceanic and atmospheric circulation patterns.

References and Notes

1. J. W. Hurrell, Y. Kushnir, G. Ottersen, M. Visbeck, in *Geophysical Monograph Series 134*, (American Geophysical Union, Washington, DC, 2003), pp. 1–35.
2. P. D. Jones, T. Jonsson, D. Wheeler, *Int. J. Climatol.* **17**, 1433 (1997).
3. E. R. Cook, R. D. D'Arrigo, M. E. Mann, *J. Clim.* **15**, 1754 (2002).
4. H. H. Lamb, *Palaeogeogr. Palaeoclimatol. Palaeoecol.* **1**, 13 (1965).
5. J. Esper, E. R. Cook, F. H. Schweingruber, *Science* **295**, 2250 (2002).
6. J. Esper *et al.*, *Geophys. Res. Lett.* **34**, L17702 (2007).
7. C. J. Proctor, A. Baker, W. L. Barnes, R. A. Gilmour, *Clim. Dyn.* **16**, 815 (2000).
8. The NAO is defined by an atmospheric seesaw between the Icelandic Low and the Azores High and is expressed as an index as the normalized December-to-March sea-level pressure difference between these two poles (*12*).
9. Materials and methods are available as supporting material on *Science* Online.
10. T. D. Mitchell, T. R. Carter, P. D. Jones, M. Hulme, M. New, *A Comprehensive Set of High-Resolution Grids of Monthly Climate for Europe and the Globe: The Observed Record (1901-2000) and 16 Scenarios (2001-2100)* (Working Paper 55, Tyne Centre for Climate Change Research, Univ. of East Anglia, Norwich, UK, 2004).
11. J. W. Hurrell, *Science* **269**, 676 (1995).
12. D. Frank, U. Büntgen, R. Böhm, M. Maugeri, J. Esper, *Quat. Sci. Rev.* **26**, 3298 (2007).
13. M. F. Glueck, C. W. Stockton, *Int. J. Climatol.* **21**, 1453 (2001).
14. J. Luterbacher, C. Schmutz, D. Gyalistras, E. Xoplaki, H. Wanner, *Geophys. Res. Lett.* **26**, 2745 (1999).
15. A. Mangini, C. Spotl, P. Verdes, *Earth Planet. Sci. Lett.* **235**, 741 (2005).
16. J. Luterbacher *et al.*, *Clim. Dyn.* **18**, 545 (2002).
17. A. Pauling, J. Luterbacher, C. Casty, H. Wanner, *Clim. Dyn.* **26**, 387 (2006).
18. N. E. Graham *et al.*, *Clim. Change* **83**, 241 (2007).
19. E. Roeckner, L. Bengtsson, J. Feichter, J. Lelieveld, H. Rodhe, *J. Clim.* **12**, 3004 (1999).
20. C. M. Ammann, F. Joos, D. S. Schimel, B. L. Otto-Bliesner, R. A. Tomas, *Proc. Natl. Acad. Sci. U.S.A.* **104**, 3713 (2007).
21. M. E. Mann, M. A. Cane, S. E. Zebiak, A. Clement, *J. Clim.* **18**, 447 (2005).
22. J. Emile-Geay, M. Cane, R. Seager, A. Kaplan, P. Almasi, *Paleoceanography* **22**, PA3210 (2007).
23. J. W. Hurrell, M. P. Hoerling, A. Phillips, T. Y. Xu, *Clim. Dyn.* **23**, 371 (2004).
24. M. P. Hoerling, J. W. Hurrell, T. Y. Xu, *Science* **292**, 90 (2001).
25. L. Stott *et al.*, *Nature* **431**, 56 (2004).
26. K. M. Cobb, C. D. Charles, H. Cheng, R. L. Edwards, *Nature* **424**, 271 (2003).
27. T. L. Delworth, R. J. Greatbatch, *J. Clim.* **13**, 1481 (2000).
28. A. Timmermann *et al.*, *J. Clim.* **20**, 4899 (2007).
29. W. C. Palmer, *Meteorological Drought* (Research paper 45, U.S. Department of Commerce, Washington, DC, 1965).
30. T. J. Crowley, *Science* **289**, 270 (2000).

31. J.E., D.C.F., and J.D.S. were supported by the European Commission MILLENNIUM Integrated Project (grant 017008) and J.E. and D.C.F. by the Swiss National Science Foundation through the National Centre for Competence in Climate Research (NCCR-Climate). N.E.G. is grateful for support from National Oceanic and Atmospheric Administration (grant NA06OA-R4310120), and J.D.S. acknowledges a Royal Society–Leverhulme Trust Senior Research Fellowship. We thank C. Ammann, E. R. Cook, D. Lund, J. Luterbacher, M.-A. Sicre, J. Smith, D. Stephenson, and three anonymous referees for supplying data and useful suggestions.

Supporting Online Material

www.sciencemag.org/cgi/content/full/324/5923/78/DC1
Materials and Methods
SOM Text
Figs. S1 to S5
Tables S1 and S2
References

24 September 2008; accepted 19 February 2009
10.1126/science.1166349

Distilling Free-Form Natural Laws from Experimental Data

Michael Schmidt[1] and Hod Lipson[2,3]*

For centuries, scientists have attempted to identify and document analytical laws that underlie physical phenomena in nature. Despite the prevalence of computing power, the process of finding natural laws and their corresponding equations has resisted automation. A key challenge to finding analytic relations automatically is defining algorithmically what makes a correlation in observed data important and insightful. We propose a principle for the identification of nontriviality. We demonstrated this approach by automatically searching motion-tracking data captured from various physical systems, ranging from simple harmonic oscillators to chaotic double-pendula. Without any prior knowledge about physics, kinematics, or geometry, the algorithm discovered Hamiltonians, Lagrangians, and other laws of geometric and momentum conservation. The discovery rate accelerated as laws found for simpler systems were used to bootstrap explanations for more complex systems, gradually uncovering the "alphabet" used to describe those systems.

Mathematical symmetries and invariants underlie nearly all physical laws in nature (*1*), suggesting that the search for many natural laws is inseparably a search for conserved quantities and invariant equations (*2*, *3*). Automated techniques for generating, collecting, and storing data from scientific measurements have become increasingly precise and powerful, but automated processes for distilling this data into knowledge in the form of analytical natural laws have not kept pace. Thus, there is a pressing practical need (*4*, *5*) for improved forms of scientific data mining (*6*, *7*).

The most prohibitive obstacle to overcome in order to search for conservation laws computationally is finding meaningful and nontrivial invariants. There exist an infinite number of identities that are numerically invariant but have no connection to the natural physics or dynamics of the system. We introduce a principle for identifying only the useful analytical relations that are related to the system dynamics. We then demonstrate how a search algorithm based on this principle identifies meaningful analytical links in data captured from various physical systems (Fig. 1).

Our goal is to find natural relations where they exist, with minimal restrictions on their analytical form (i.e., free-form). Many methods exist for modeling scientific data: Some use fixed-form parametric models derived from expert knowledge, and others use numerical models (such as neural networks) aimed at prediction. Still others have explored restricted model spaces using greedy monomial search (*8*, *9*). Alternatively, we seek the principal unconstrained analytical expression that explains symbolically precise conserved relations, thus helping distill data into scientific knowledge.

Symbolic regression (*10*) is an established method based on evolutionary computation (*11*) for searching the space of mathematical expressions while minimizing various error metrics [see section S4 in the supporting online material (SOM)]. Unlike traditional linear and nonlinear regression methods that fit parameters to an equation of a given form, symbolic regression searches both the parameters and the form of equations simultaneously (see SOM section S6). Initial expressions are formed by randomly combining mathematical building blocks such as algebraic operators {+, –, ÷, ×}, analytical functions (for example, sine and cosine), constants, and state variables. New equations are formed by recombining previous equations and probabilistically varying their subexpressions. The algorithm retains equations that model the experimental data better than others and abandons unpromising solutions. After equations reach a desired level of accuracy, the algorithm terminates, returning a set of equations that are most likely to correspond to the intrinsic mechanisms underlying the observed system.

Although symbolic regression is typically used to find explicit (*12*–*14*) and differential equations (*15*), this method cannot readily find conservation laws or invariant equations. Rather than trying to model a specific signal, we are trying to detect any underlying physical law that the system obeys, which may or may not be constant (e.g., a Lagrangian).

A particular challenge is requiring the law to be a function of the system's state while avoiding trivial or meaningless relations. For any system over the state space x, there are infinitely many trivial equations over x that satisfy a conserved quantity, such as $\sin^2(x_1) + \cos^2(x_1)$ or $x_1 + 4.56 - x_2 x_1 / x_2$. Additionally, there are infinitely many arbitrarily close trivial conservations, such as $4.56 + 1/(100 + x_1^2)$. To distinguish good conservation law candidates from poor ones, we need a more robust principle than simply invariance alone.

The identification of nontrivial relations is a major challenge, even for human scientists: Many published invariant quantities have turned out to be coincidental (*16*). The mere appearance of a conserved value is insufficient for a conservation

[1]Computational Biology, Cornell University, Ithaca, NY 14853, USA. [2]School of Mechanical and Aerospace Engineering, Cornell University, Ithaca, NY 14853, USA. [3]Computing and Information Science, Cornell University, Ithaca, NY 14853, USA.

*To whom correspondence should be addressed. E-mail: hod.lipson@cornell.edu

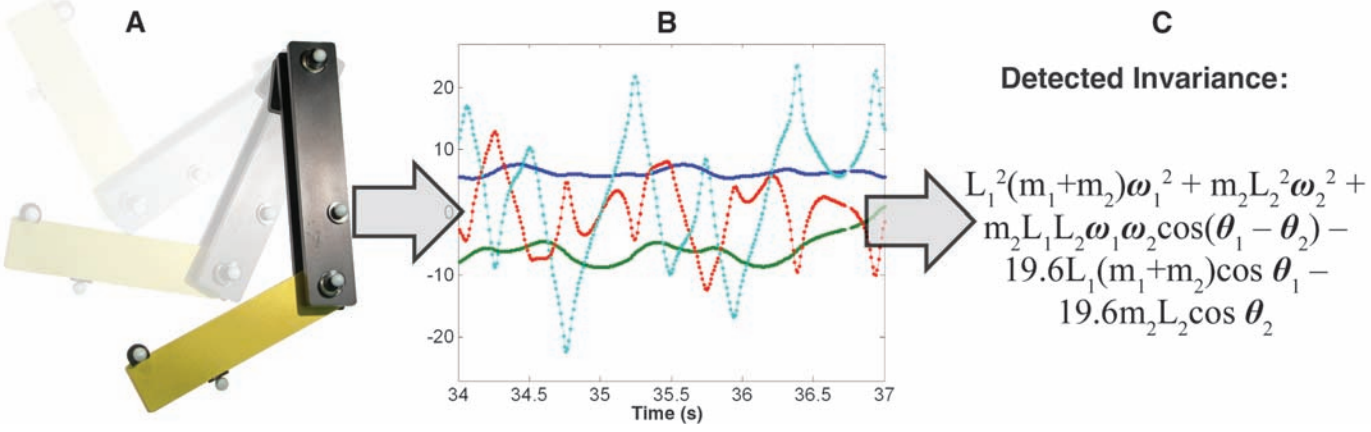

Fig. 1. Mining physical systems. We captured the angles and angular velocities of a chaotic double-pendulum (**A**) over time using motion tracking (**B**), then we automatically searched for equations that describe a single natural law relating these variables. Without any prior knowledge about physics or geometry, the algorithm found the conservation law (**C**), which turns out to be the double pendulum's Hamiltonian. Actual pendulum, data, and results are shown.

law. The key insight into identifying nontrivial conservation laws computationally is that the candidate equations should predict connections between dynamics of subcomponents of the system. More precisely, the conservation equation should be able to predict connections among derivatives of groups of variables over time, relations that we can also readily calculate from new experimental data.

One instance of such a metric is the partial derivatives between pairs of variables (see SOM section S1). For example, in a two-dimensional system we could measure variables $x(t)$ and $y(t)$ over time. The system's partial derivatives estimated from time-series data would then be $x'/y' \approx \Delta x/\Delta y$ and $y'/x' \approx \Delta y/\Delta x$ (where x' and y' represent the time derivatives of x and y). Similarly, given a candidate conservation law equation $f(x,y)$, we can derive the same values through differentiation: $(\delta f/\delta y)/(\delta f/\delta x) \approx \delta x/\delta y$ and $(\delta f/\delta x)/(\delta f/\delta y) \approx \delta y/\delta x$. We can now compare $\Delta x/\Delta y$ values from the experimental data with $\delta x/\delta y$ values from a candidate conservation expression $f(x,y)$ to measure how well it predicts intrinsic relations in the system. In higher-dimensional systems, multiple variable pairings and higher-order derivatives yield a plethora of criteria to use. See SOM sections S2 and S3 for generalization to higher-dimensional systems. Using the partial-derivative pairs, we define a new type of search criteria for measuring how well a candidate analytical expression represents a nontrivial invariance over the experimental data.

An important consequence of the partial-derivative–pair measure is that it can also identify relations that represent other nontrivial identities of the system beyond invariants and conservation laws. For example, if the system is confined to a manifold, the manifold equation can also derive accurate partial-derivative pairs. Similarly, the partial-derivative pair can identify equations such as Lagrangian equations, the energy equivalent to the equation of motion in classical mechanics, which summarize the systems dynamics but are not invariant.

One can control, to an extent, the type of law that the system might find by choosing what variables to provide to the algorithm. For example, if we only provide position coordinates, the algorithm is forced to converge on a manifold equation of the system's state space. If we provide velocities, the algorithm is biased to find energy laws. If we additionally supply accelerations, the algorithm is biased to find force identities and equations of motion. However, given these or other types of variables, other or previously unknown analytical laws may exist.

We used an algorithm (Fig. 2) to search for analytical laws in data captured from several synthetic and physical systems using various sets of system variables. We present results for a number of physical experimental systems (see SOM section S7 for a study of synthetic systems, geometric symmetries, and manifolds). A video is available online (see SOM section S14).

We collected data from standard experimental systems typically used in undergraduate physics education: an air-track oscillator and a double pendulum (Fig. 3). We used motion-tracking software to record the devices' positions over time. We then numerically calculated velocities and accelerations (see SOM section S11). All data sets are available in SOM section S15.

Without any additional information, system models, or theoretical knowledge, the search with the partial-derivative–pairs criterion produced several analytical law expressions directly from these data. For each system, the algorithm outputs a short list of ~10 equations that have maximal accuracy found for different sizes (complexities) of equations (see SOM section S8). We then inspect this list manually to select the final equation. Often the list consists of varying approximations or elaborations on a particular law equation, but it can contain qualitatively different equations, as discussed below.

We experimented on two configurations of the air track: (i) two-spring single-mass and (ii) three-spring double-mass. Similarly, we collected time-series data from a pendulum and a double pendulum (Fig. 3) with the use of motion-tracking (SOM section S12).

The single-car air track is a harmonic oscillator with slight damping from the air and its two springs. With only minimal noise and damp-

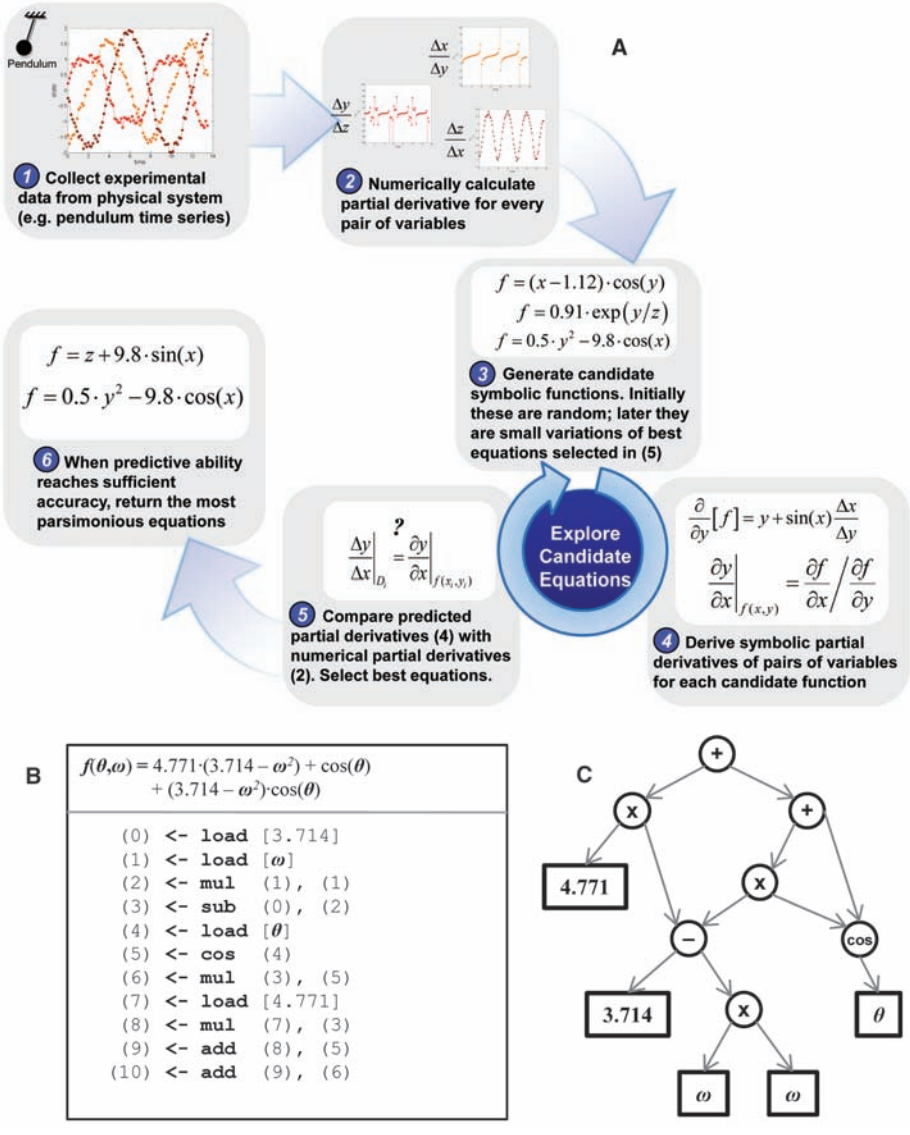

Fig. 2. Computational approach for detecting conservation laws from experimentally collected data. (**A**) First, calculate partial derivatives between variables from the data, then search for equations that may describe a physical invariance. To measure how well an equation describes an invariance, derive the same partial derivatives symbolically to compare with the data. (**B**) The representation of a symbolic equation in computer memory is a list of successive mathematical operations (see SOM section S6). (**C**) This list representation corresponds to a graph, where nodes represent mathematical building blocks and leaves represent parameters and system variables. Both (B) and (C) correspond to the same equation. The algorithm varies these structures to search the space of equations.

ing, it was the simplest physical system that we examined. The double-mass air track consisted of two coupled harmonic oscillators of different masses. There was considerable noise in this data set as a result of compression of the middle spring. The pendulum is a nonlinear oscillator that is masked by small-angle approximations. The double pendulum is a coupled nonlinear oscillator system that exhibits rich dynamics (*17*) and chaos at certain energies (*18*), making it challenging to model (*19*, *20*). Additionally, there is higher measurement noise and dampening errors due to higher velocities.

Given position and velocity data over time, the algorithm converged on the energy laws of each system (Hamiltonian and Lagrangian equations). Given acceleration data also, it produced the differential equation of motion corresponding to Newton's second law for the harmonic oscillator and pendulum systems. Given only position data for the pendulum, the algorithm converged on the equation of a circle, indicating that the pendulum is confined to a circle. The algorithm also produced several inexact expressions through small-angle approximations—for example, using x in place of $\sin(x)$ and $1 - x^2$ in place of $\cos(x)$ in the pendulum and double-pendulum systems.

An interesting approximate law for the double pendulum that emerged was conservation of angular momentum. Given only data measured while the pendulum was chaotic (at high energy), the algorithm fixated on this law. The conservation of momentum equation is simpler than other valid laws and is approximately correct for high velocities where gravity is negligible, as with the high-energy chaotic data set.

Similarly, given only data from low-velocity in-phase oscillations, the algorithm fixated on small-angle approximations and uncoupled energy terms. By combining the chaotic data with low-velocity in-phase oscillation data, the algorithm converged onto the precise energy laws after several hours of computation.

In the absence of appropriate building blocks, the algorithm developed approximations. For example, eliminating the sine and cosine operations from the set of equation building blocks caused the pendulum invariant to be expressed as $\omega^2 + k_1\theta^2 - k_2\theta^4$ (where θ is the pendulum's angle, ω is the angular velocity, and k_1 and k_2 are constants), thereby exploiting the 4th-order Taylor series expansion of the cosine function. Eliminating cosine but not sine drove the algorithm to converge on the equality $\cos(\theta) = \sin(\theta + \pi/2)$ or more complex equivalences (see SOM section S13).

Useful scientific theory is both predictive and parsimonious. Similarly, some equations may be more accurate but overfit the data, whereas others may be more parsimonious but oversimplify

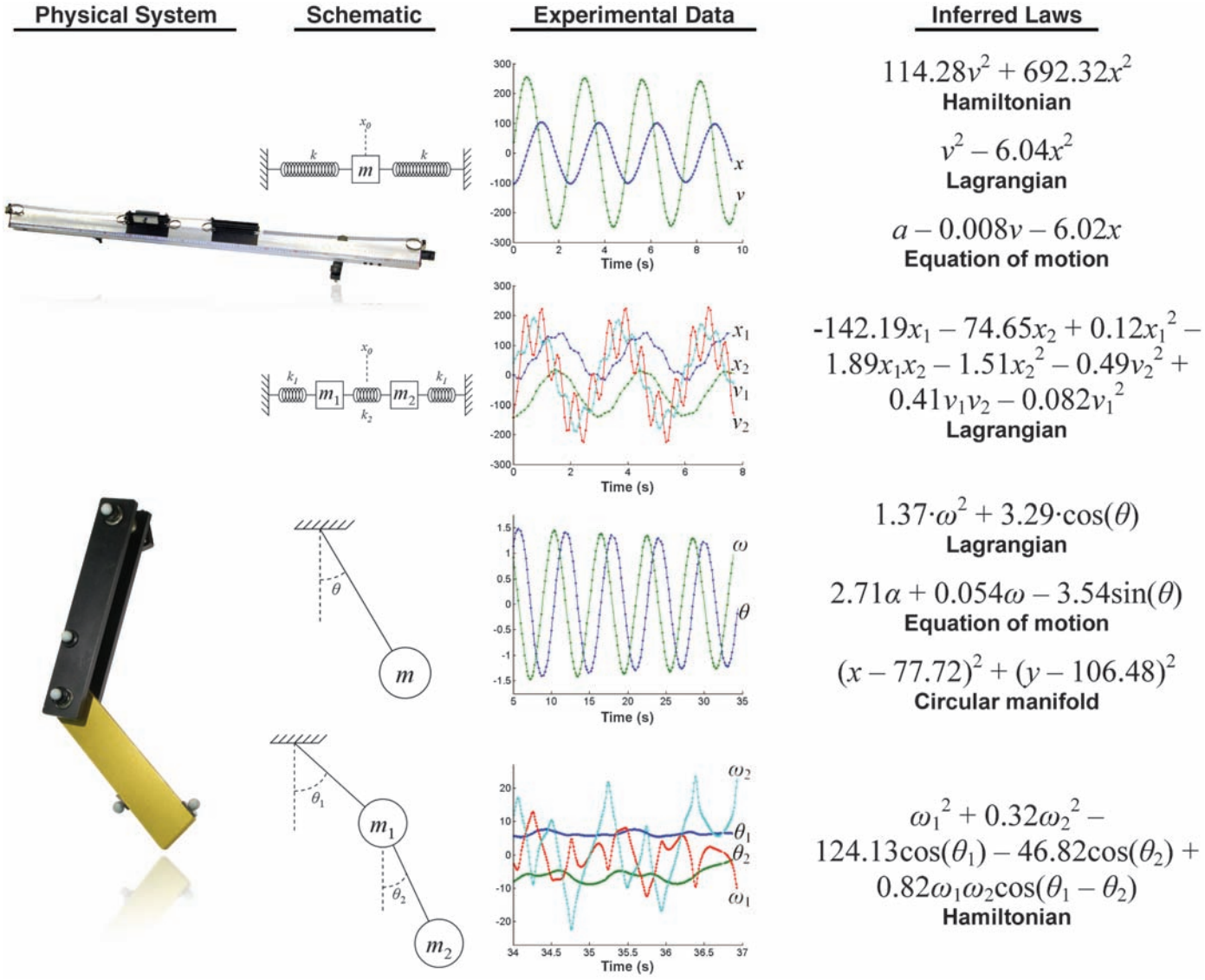

Fig. 3. Summary of laws inferred from experimental data collected from physical systems. Depending on the types of variables provided to the algorithm, it detects different types of laws. Given solely position information, the algorithm detects position manifolds; given velocities, the algorithm detects energy laws; given accelerations, it detects equations of motion and sum of forces laws (θ, angle; ω, angular velocity; α, angular acceleration).

(*21*, *22*); the right balance is difficult to specify in advance. Instead of producing a single result, the algorithm produces a small set of final candidate analytical expressions on the accuracy-parsimony Pareto front (see SOM section S8), which represents the optimal solutions as they vary over equation complexity and the maximum predictive ability. Parsimony is measured as the inverse of the number of terms in the expression, whereas the predictive accuracy is measured as error on withheld experimental data used only for validation.

The Pareto front for the double pendulum (Fig. 4A) reveals a few particularly simple equations that predict the partial-derivative pairs accurately. Predictive accuracy was measured by cross-validation with the partial-derivative–pairs criterion (see SOM section S2). The Pareto front tends to contain a cliff where predictive ability jumps rapidly at some minimum complexity. Predictive ability then improves only marginally with more complex equations (Fig. 4A). The conservation of angular momentum equation lies on the Pareto front, though it is inexact. The double pendulum's Hamiltonian lies at the point representing the simplest equation with the largest increase in predictive ability. In all of our experiments, the solution at this point has been an exact theoretical law (see SOM section S7 for additional systems).

In the worst case, the time to converge on the law equations depends exponentially on the complexity of the law expression itself and roughly quadratically on the system dimensionality (the number of variable pairings) (Fig. 4B). The algorithm's search is readily parallelizable, as many candidate functions need to be evaluated simultaneously. In a 32-core implementation, the time required ranged from a few minutes for the harmonic oscillator to 30 hours for the double pendulum. The impact of noise also couples with these factors (see SOM section S9). For comparison, the simulated double-mass air-track and simulated double-pendulum data sets (where measurements are noiseless) took ~1/10th of the computational effort to analyze. A summary of performance versus noise level is provided in SOM section S9.

Though the algorithm can present equations corresponding to physical laws in their mathematical form, we are still faced with the challenge of justifying and giving words to their meaning. One difficulty is that we cannot know with certainty the units of bulk constants in the law expressions (for example, combinations of masses, lengths, etc. embodied in the system). Second, the equation may model something that is inherently difficult to observe directly, such as total energy. Requiring equations to maintain consistent physical units still leaves room for ambiguity.

A more systematic approach to parsing the coefficients is to analyze multiple data sets from the same systems, albeit with different configurations and parameters. To demonstrate this approach, we used several virtual double pendula with randomly chosen masses and lengths to generate several synthetic data sets. We fit the free coefficients of the automatically discovered model to each data set and then invoked the equation search algorithm again to seek a relation between the coefficients and parameter sets. After arbitrarily defining $k_1 = 1$, the algorithm identified that $k_2 = m_2L_2^2/(m_1L_1^2 + m_2L_1^2)$, $k_3 = 2m_2L_2/(m_1L_1 + m_2L_1)$, $k_3 = 19.6/L_1$, and $k_4 = 19.6m_2L_2/(m_2L_1^2 + m_1L_1^2)$, where 19.6 is the only absolute constant (over all parameter variations) whose units are necessarily meters per square seconds (see SOM section S5). In the above expressions, m is mass and L is length. A similar approach can be used to identify coefficients that vary slowly over time (for example, because of damping, creeping, or ecological drift).

Computational systems such as this could play a role in modeling high-dimensional and complex phenomena (*23*, *24*) that currently stress the reach of expert-driven research. A key challenge is scaling to higher complexity. To accomplish this, scientists leverage knowledge from simpler systems to explain more complex systems. Can an algorithm do this as well?

One method to use prior knowledge is seeding the equation search by initializing the algorithm's initial set of candidate expressions with terms from equations from simpler systems. For example, the single-pendulum and the double-harmonic oscillator equations provide clues to the laws governing the more complex double pendulum. We shuffled terms of the simpler systems (for example, exchanging velocity symbols with double-pendulum velocity variables) and randomized parameters to generate many inexact initial expressions. This seeding approach does not constrain the equation search, but it biases the search to reuse terms from previous laws.

Bootstrapping the double-pendulum search in this fashion reduced the search time by nearly an order of magnitude, from 30 to 40 hours of computation to 7 to 8 hours (Fig. 4B). On the basis of this result, we conjecture that bootstrapping may be critical for detecting laws in higher-order systems that are veiled in complexity.

A statistical analysis of the subexpression frequency and complexity across populations of various physical systems revealed that the terms that are both frequently used and complex tend to be more physically meaningful, such as trigonometric terms representing potential energies, squared velocities representing kinetic energies, or linear force combinations (see SOM section S10). These terms may make up an "emergent alphabet" for describing a range of systems, which could accelerate their modeling and simplify their conceptual understanding.

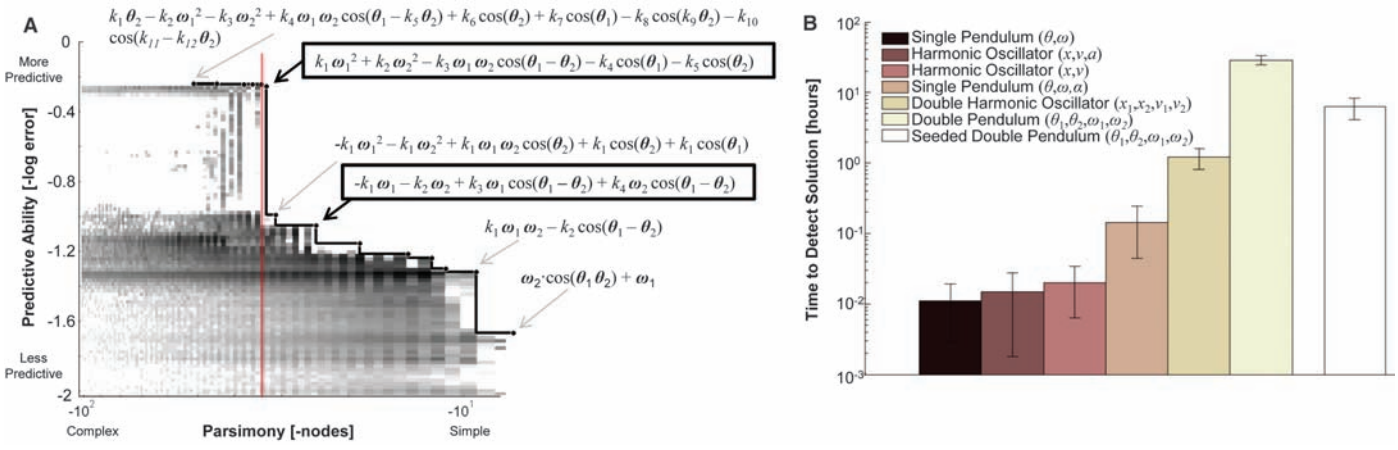

Fig. 4. Parsimony versus accuracy and computation time. (**A**) Pareto front (solid black curve) for physical laws of the double pendulum and the frequency of sampling during the law equation search (grayscale). The equation at the cliff corresponds to the exact energy conservation law of the double pendulum (highlighted in the figure). A second momentum conservation law that we encountered is also highlighted. (**B**) Computation time required to detect different physical laws for several systems. The computation time increases with the dimensionality, law equation complexity, and noise. A notable exception is the bootstrapped double pendulum, where reuse of terms from simpler systems helped reduce computational cost by almost an order of magnitude, suggesting a mechanism for scaling higher complexities.

We have demonstrated the discovery of physical laws, from scratch, directly from experimentally captured data with the use of a computational search. We used the presented approach to detect nonlinear energy conservation laws, Newtonian force laws, geometric invariants, and system manifolds in various synthetic and physically implemented systems without prior knowledge about physics, kinematics, or geometry. The concise analytical expressions that we found are amenable to human interpretation and help to reveal the physics underlying the observed phenomenon. Many applications exist for this approach, in fields ranging from systems biology to cosmology, where theoretical gaps exist despite abundance in data.

Might this process diminish the role of future scientists? Quite the contrary: Scientists may use processes such as this to help focus on interesting phenomena more rapidly and to interpret their meaning.

References and Notes

1. P. W. Anderson, *Science* **177**, 393 (1972).
2. E. Noether, *Nachr. d. König Gesellsch. d. Wiss. zu Göttingen, Math-Phys. Klasse* 235 (1918).
3. J. Hanc, S. Tuleja, M. Hancova, *Am. J. Phys.* **72**, 428 (2004).
4. D. Clery, D. Voss, *Science* **308**, 809 (2005).
5. A. Szalay, J. Gray, *Nature* **440**, 413 (2006).
6. R. E. Valdés-Pérez, *Commun. Assoc. Comput. Mach.* **42**, 37 (1999).
7. R. D. King *et al.*, *Nature* **427**, 247 (2004).
8. P. Langley, *Cogn. Sci.* **5**, 31 (1981).
9. R. M. Jones, P. Langley, *Comput. Intell.* **21**, 480 (2005).
10. J. R. Koza, *Genetic Programming: On the Programming of Computers by Means of Natural Selection*. (MIT Press, Cambridge, MA, 1992).
11. S. Forrest, *Science* **261**, 872 (1993).
12. J. Duffy, J. Engle-Warnick, *Evolutionary Computation in Economics and Finance* **100**, 61 (2002).
13. F. Cyril, B. Alberto, in *2007 IEEE Congress on Evolutionary Computation*, S. Dipti, W. Lipo, Eds. (IEEE Press, Singapore, 2007), pp. 23–30.
14. B. Elena, B. Andrei, L. Henri, in *Seventh International Symposium on Symbolic and Numeric Algorithms for Scientific Computing (SYNASC '05)* (IEEE Press, 2005), pp. 321–324.
15. J. Bongard, H. Lipson, *Proc. Natl. Acad. Sci. U.S.A.* **104**, 9943 (2007).
16. S. Nee, N. Colegrave, S. A. West, A. Grafen, *Science* **309**, 1236 (2005).
17. P. Jäckel, T. Mullin, *Proc. R. Soc. London Ser. A* **454**, 3257 (1998).
18. T. Shinbrot, C. Grebogi, J. Wisdom, J. A. Yorke, *Am. J. Phys.* **60**, 491 (1992).
19. Y. Liang, B. Feeny, *Nonlinear Dyn.* **52**, 181 (2008).
20. M. Mor, A. Wolf, O. Gottlieb, in *Proceedings of the 21st ASME Biennial Conference on Mechanical Vibration and Noise* (ASME Press, Las Vegas, NV, 2007), pp. 1–8.
21. P. Gregory, R. Denis, F. Cyril, in *Evolution Artificielle, 6th International Conference*, vol. 2936, L. Pierre, C. Pierre, F. Cyril, L. Evelyne, S. Marc, Eds. (Springer, Marseilles, France, 2003), pp. 267–277.
22. E. D. De Jong, J. B. Pollack, in *Genetic Programming and Evolvable Machines*, vol. 4 (Springer, Berlin, 2003), pp. 211–233.
23. S. H. Strogatz, *Nature* **410**, 268 (2001).
24. P. A. Marquet, *Nature* **418**, 723 (2002).

25. This research was supported in part by Integrative Graduate Education and Research Traineeship program in nonlinear systems, a U.S. NSF graduate research fellowship, and NSF Creative-IT grant 0757478 and CAREER grant 0547376. We thank M. Kurman for editorial consultation and substantive editing of the manuscript.

Supporting Online Material

www.sciencemag.org/cgi/content/full/324/5923/81/DC1
Materials and Methods
SOM Text
Figs. S1 to S7
Tables S1 to S3
References
Movie S1
Data Sets S1 to S15

15 September 2008; accepted 19 February 2009
10.1126/science.1165893

The Automation of Science

Ross D. King,[1]* Jem Rowland,[1] Stephen G. Oliver,[2] Michael Young,[3] Wayne Aubrey,[1] Emma Byrne,[1] Maria Liakata,[1] Magdalena Markham,[1] Pınar Pir,[2] Larisa N. Soldatova,[1] Andrew Sparkes,[1] Kenneth E. Whelan,[1] Amanda Clare[1]

The basis of science is the hypothetico-deductive method and the recording of experiments in sufficient detail to enable reproducibility. We report the development of Robot Scientist "Adam," which advances the automation of both. Adam has autonomously generated functional genomics hypotheses about the yeast *Saccharomyces cerevisiae* and experimentally tested these hypotheses by using laboratory automation. We have confirmed Adam's conclusions through manual experiments. To describe Adam's research, we have developed an ontology and logical language. The resulting formalization involves over 10,000 different research units in a nested treelike structure, 10 levels deep, that relates the 6.6 million biomass measurements to their logical description. This formalization describes how a machine contributed to scientific knowledge.

Computers are playing an ever-greater role in the scientific process (*1*). Their use to control the execution of experiments contributes to a vast expansion in the production of scientific data (*2*). This growth in scientific data, in turn, requires the increased use of computers for analysis and modeling. The use of computers is also changing the way that science is described and reported. Scientific knowledge is best expressed in formal logical languages (*3*). Only formal languages provide sufficient semantic clarity to ensure reproducibility and the free exchange of scientific knowledge. Despite the advantages of logic, most scientific knowledge is expressed only in natural languages. This is now changing through developments such as the Semantic Web (*4*) and ontologies (*5*).

A natural extension of the trend to ever-greater computer involvement in science is the concept of a robot scientist (*6*). This is a physically implemented laboratory automation system that exploits techniques from the field of artificial intelligence (*7*–*9*) to execute cycles of scientific experimentation. A robot scientist automatically originates hypotheses to explain observations, devises experiments to test these hypotheses, physically runs the experiments by using laboratory robotics, interprets the results, and then repeats the cycle.

High-throughput laboratory automation is transforming biology and revealing vast amounts of new scientific knowledge (*10*). Nevertheless, existing high-throughput methods are currently inadequate for areas such as systems biology. This is because, even though very large numbers of experiments can be executed, each individual experiment cannot be designed to test a hypothesis about a model. Robot scientists have the potential to overcome this fundamental limitation.

The complexity of biological systems necessitates the recording of experimental metadata in as much detail as possible. Acquiring these metadata has often proved problematic. With robot scientists, comprehensive metadata are produced as a natural by-product of the way they work. Because the experiments are conceived and executed automatically by computer, it is possible to completely capture and digitally curate all aspects of the scientific process (*11*, *12*).

To demonstrate that the robot scientist methodology can be both automated and be made effective enough to contribute to scientific knowledge, we have developed Robot Scientist "Adam" (*13*) (Fig. 1). Adam's hardware is fully automated such that it only requires a technician to periodically add laboratory consumables and to remove waste. It is designed to automate the high-throughput execution of individually designed microbial batch growth experiments in microtiter plates (*14*). Adam measures growth curves (phenotypes) of selected microbial strains (genotypes) growing in defined media (environments). Growth of cell cultures can be easily measured in high-throughput, and growth curves are sensitive to changes in genotype and environment.

We applied Adam to the identification of genes encoding orphan enzymes in *Saccharomyces cerevisiae*: enzymes catalyzing biochemical reactions thought to occur in yeast, but for which the encoding gene(s) are not known (*15*). To set up Adam for this application required (i) a comprehensive logical model encoding knowledge of *S. cerevisiae* metabolism [~1200 open

[1]Department of Computer Science, Aberystwyth University, SY23 3DB, UK. [2]Cambridge Systems Biology Centre, Department of Biochemistry, University of Cambridge, Sanger Building, 80 Tennis Court Road, Cambridge CB2 1GA, UK. [3]Institute of Biological, Environmental and Rural Sciences, Aberystwyth University, SY23 3DD, UK.

*To whom correspondence should be addressed. E-mail: rdk@aber.ac.uk

reading frames (ORFs), ~800 metabolites] (*15*), expressed in the logic programming language Prolog; (ii) a general bioinformatic database of genes and proteins involved in metabolism; (iii) software to abduce hypotheses about the genes encoding the orphan enzymes, done by using a combination of standard bioinformatic software and databases; (iv) software to deduce experiments that test the observational consequences of hypotheses (based on the model); (v) software to plan and design the experiments, which are based on the use of deletion mutants and the addition of selected metabolites to a defined growth medium; (vi) laboratory automation software to physically execute the experimental plan and to record the data and metadata in a relational database; (vii) software to analyze the data and metadata (generate growth curves and extract parameters); and (viii) software to relate the analyzed data to the hypotheses; for example, statistical methods are required to decide on significance. Once this infrastructure is in place, no human intellectual intervention is necessary to execute cycles of simple hypothesis-led experimentation. [For more details of the software, and its application to a related functional genomics problem, see (*16*) and figs. S1 and S2].

Adam formulated and tested 20 hypotheses concerning genes encoding 13 orphan enzymes (*16*) (Table 1). The weight of the experimental evidence for the hypotheses varied (based on observations of differential growth), but 12 hypotheses with no previous evidence were confirmed with $P < 0.05$ for the null hypothesis.

Because Adam's experimental evidence for its conclusions is indirect, we tested Adam's conclusions with more direct experimental methods. The enzyme 2-aminoadipate:2-oxoglutarate aminotransferase (2A2OA) catalyzes a reaction in the lysine biosynthetic pathways of fungi. Adam hypothesized that three genes (YER152C, YJL060W, and YGL202W) encode this enzyme and observed results consistent with all three hypotheses (Table 1). To test Adam's conclusions, we purified the protein products of these genes and used them in in vitro enzyme assays, which confirmed Adam's conclusions [supporting online material (SOM)] (Fig. 2).

To further test Adam's conclusions, we examined the scientific literature on the 20 genes investigated (Table 1) (*16*). This revealed the existence of strong empirical evidence for the correctness of six of the hypotheses; that is, the enzymes were not actually orphans (Table 1). The reason that Adam considered them to be orphans was due to the use of an incomplete bioinformatic database. These six genes therefore constitute a positive control for Adam's methodology. A possible error was also revealed (Table 1) (SOM).

To better understand the reasons why the identity of the genes encoding these enzymes has remained obscure for so long, we investigated their comparative genomics in detail (*16*). The likely explanation is a combination of three complicating factors: gene duplications with retention of overlapping function, enzymes that catalyze more than one related reaction, and existing functional annotations. Adam's systematic bioinformatic and quantitative phenotypic analyzes were required to unravel this web of functionality.

Use of a robot scientist enables all aspects of a scientific investigation to be formalized in logic. For the core organization of this formalization, we used the ontology of scientific experiments: EXPO (*11*, *12*). This ontology formalizes generic knowledge about experiments. For Adam, we developed LABORS, a customized version of EXPO, expressed in the description logic language OWL-DL (*17*). Application of LABORS produces experimental descriptions in the logic-

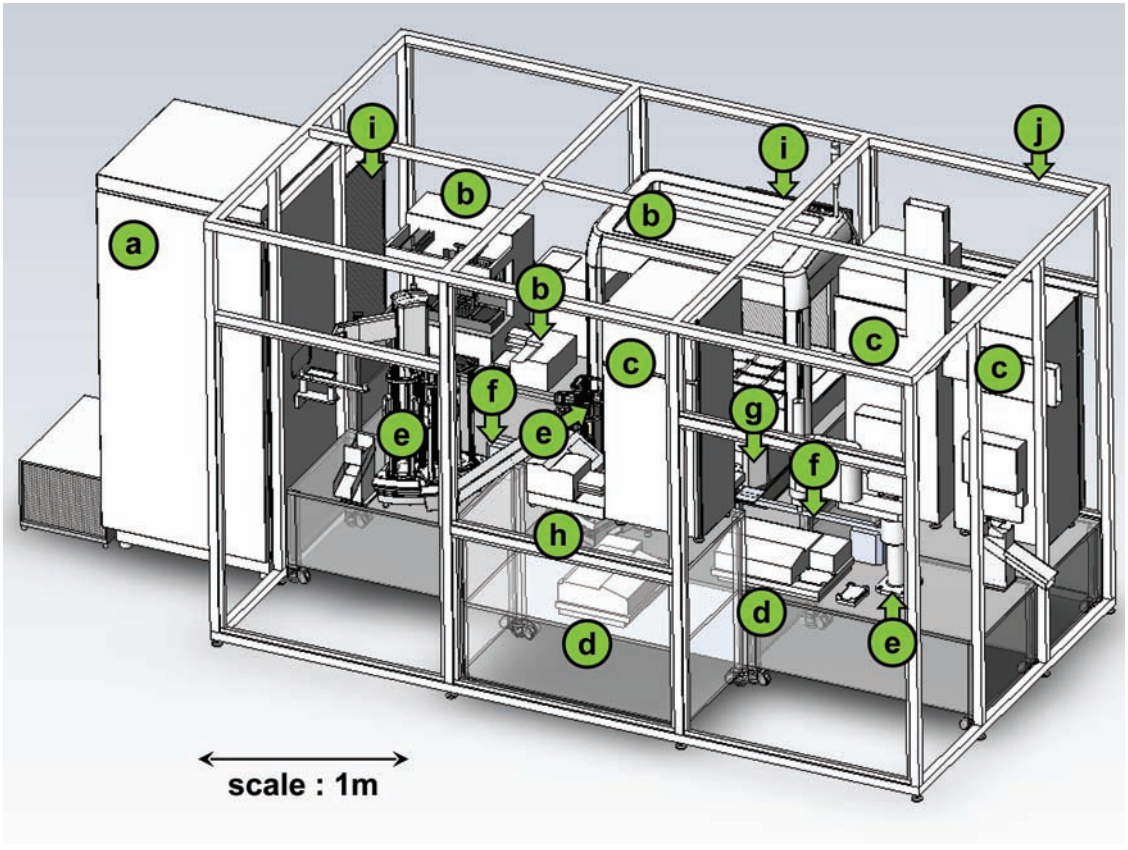

Fig. 1. The Robot Scientist Adam. The advances that distinguish Adam from other complex laboratory systems are the individual design of the experiments to test hypotheses and the utilization of complex internal cycles. Adam's basic operations are selection of specified yeast strains from a library held in a freezer, inoculation of these strains into microtiter plate wells containing rich medium, measurement of growth curves on rich medium, harvesting of a defined quantity of cells from each well, inoculation of these cells into wells containing defined media (minimal synthetic dextrose medium plus up to four added metabolites from a choice of six), and measurement of growth curves on the specified media. To achieve this functionality, Adam has the following components: a, an automated −20°C freezer; b, three liquid handlers (one of which can separately control 96 fluid channels simultaneously); c, three automated +30°C incubators; d, two automated plate readers; e, three robot arms; f, two automated plate slides; g, an automated plate centrifuge; h, an automated plate washer; i, two high-efficiency particulate air filters; and j, a rigid transparent plastic enclosure. There are also two bar code readers, seven cameras, 20 environment sensors, and four personal computers, as well as the software. Adam is capable of designing and initiating over a thousand new strain and defined-growth-medium experiments each day (from a selection of thousands of yeast strains), with each experiment lasting up to 5 days. The design enables measurement of OD_{595nm} for each experiment at least once every 30 min (more often if running at less than full capacity), allowing accurate growth curves to be recorded (typically we take over a hundred measurements a day per well), plus associated metadata. See the supporting online material for pictures and a video of Adam in action.

programming language Datalog (*18*). In the course of its investigations, Adam observed 6,657,024 optical density (OD_{595nm}) measurements (forming 26,495 growth curves). These data are held in a MySQL relational database. Use of LABORS resulted in a formalization of the scientific argumentation involving over 10,000 different research units (segments of experimental research). This has a nested treelike structure, 10 levels deep, that logically connects the experimental observations to the experimental metadata. (Fig. 3). This structure resembles the trace of a computer program and takes up 366 Mbytes (*16*). Making such experimental structures explicit renders scientific research more comprehensible, reproducible, and reusable. This paper may be considered as simply the human-friendly summary of the formalization.

Table 1. The orphan enzymes and Adam's hypotheses. The hypothesized genes are those which Adam abduced encoded an orphan enzyme. Prob. is Adam's Monte Carlo estimate of the probability of obtaining the observed discrimination accuracy or better with a random labeling of replicates. The discrimination is between the differences in growth curves observed with the addition of specified metabolites to the wild type and the deletant. Acc. is the highest accuracy for a metabolite species in discriminating between the growth curves observed with the addition of specified metabolites to the wild type and the deletant. No. is the number of metabolites tested. Existing annotation is the summary from the *Saccharomyces* Genome Database of the annotation of the ORF. Dry is the summary of whether the annotated function is the same as predicted by Adam. If a gene already has an associated function, we do not consider this to be contradictory to Adam's conclusions unless this function is capable of explaining the observed growth phenotype, for example, *BCY1*. ida indicates inferred from direct assay and iss, inferred from sequence or structural similarity (*5*). Wet is the result of our manual enzyme assays. See (*16*) for details.

Orphan enzyme	Hypothesized gene	Prob.	Acc.	No.	Existing annotation	Dry	Wet
Glucosamine-6-phosphate deaminase (3.5.99.6)	YHR163W (SOL3)	$<10^{-4}$	97	8	6-Phosphogluconolactonase, ida	–	–
Glutaminase (3.5.1.2)	YIL033C (BCY1)	$<10^{-4}$	92	11	Cyclic adenosine 3′,5′-monophosphate (cAMP)–dependent protein kinase inhibitor, ida	✗	–
L-Threonine 3-dehydrogenase (1.1.1.103)	YDL168W (SFA1)	$<10^{-4}$	83	6	Alcohol dehydrogenase, ida	–	–
Purine-nucleoside phosphorylase (2.4.2.1)	YLR209C (PNP1)	$<10^{-4}$	82	11	Purine-nucleoside phosphorylase, ida	✓	–
2-Aminoadipate transaminase (2.6.1.39)	YGL202W (ARO8)	$<10^{-4}$	80	3	Aromatic–amino acid transaminase, ida	✓	✓
5,10-Methenyltetrahydrofolate synthetase (6.3.3.2)	YER183C (FAU1)	$<10^{-4}$	80	4	5,10 Formyltetrahydrofolate cyclo-ligase, ida	✓	–
Glucosamine-6-phosphate deaminase (3.5.99.6)	YNR034W (SOL1)	$<10^{-4}$	79	2	Possible role in tRNA export	–	–
Pyridoxal kinase (2.7.1.35)	YPR121W (THI22)	$<10^{-4}$	78	1	Phosphomethylpyrimidine kinase, iss	–	–
Mannitol-1-phosphate 5-dehydrogenase (1.1.1.17)	YNR073C	$<10^{-4}$	78	6	Putative mannitol dehydrogenase, iss	–	–
1-Acylglycerol-3-phosphate O-acyltransferase (2.3.1.51)	YDL052C (SLC1)	0.0001	80	6	1-Acylglycerol-3-phosphate O-acyltransferase ida	✓	–
Glucosamine-6-phosphate deaminase (3.5.99.6)	YGR248W (SOL4)	0.0002	78	2	6-Phosphogluconolactonase, ida	–	–
Maleylacetoacetate isomerase (5.2.1.2)	YLL060C (GTT2)	0.0003	76	3	Glutathione S-transferase, ida	–	–
Serine O-acetyltransferase (2.3.1.30)	YJL218W	0.0005	78	2	Unknown function	–	–
L-Threonine 3-dehydrogenase (1.1.1.103)	YLR070C (XYL2)	0.0052	75	6	Xylitol dehydrogenase, ida	–	–
2-Aminoadipate transaminase (2.6.1.39)	YJL060W (BNA3)	0.0084	73	3	Kynurenine aminotransferase, ida	–	✓
Pyridoxal kinase (2.7.1.35)	YNR027W	0.0259	76	2	Involved in bud-site selection, iss	–	–
Polyamine oxidase (1.5.3.11)	YMR020W (FMS1)	0.0289	78	4	Polyamine oxidase, ida	✓	–
2-Aminoadipate transaminase (2.6.1.39)	YER152C	0.0332	74	3	Uncharacterized	–	✓
L-Aspartate oxidase (1.4.3.16)	YJL045W	0.1300	72	1	Succinate dehydrogenase isozyme, iss	–	–
Purine-nucleoside phosphorylase (2.4.2.1)	YLR017W (MEU1)	0.1421	72	6	Methylthioadenosine phosphorylase, ida	✓	–

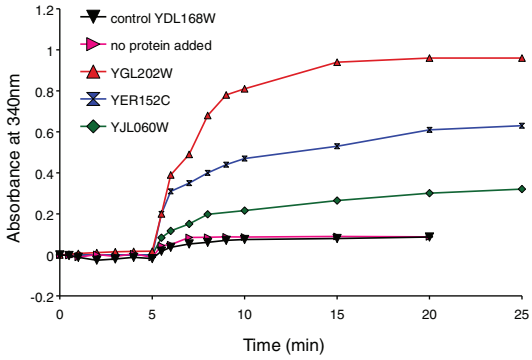

Fig. 2. Assay results for 2A2OA activity. The proteins encoded by YGL202W, YJL060W, YER152C, and YDL168W were expressed from OpenBiosystems (www.openbiosystems.com) yeast ORF clones and purified. Activity was tested in an assay of NADPH (reduced form of nicotinamide adenine dinucleotide phosphate) production based on (*22*). L-α-aminoadipic acid and 2-oxoglutarate were provided as substrates and pyridoxal phosphate as cofactor. Glutamate production was assayed by using commercially available yeast glutamate dehydrogenase, which uses NADP as cofactor and deaminates glutamate, producing ammonia and NADPH and regenerating 2-oxoglutarate (*16*). Also consistent with 2A2OA activity is experimental evidence indicating a higher activity with L-α-aminoadipic acid over either alanine or aspartate (*16*).

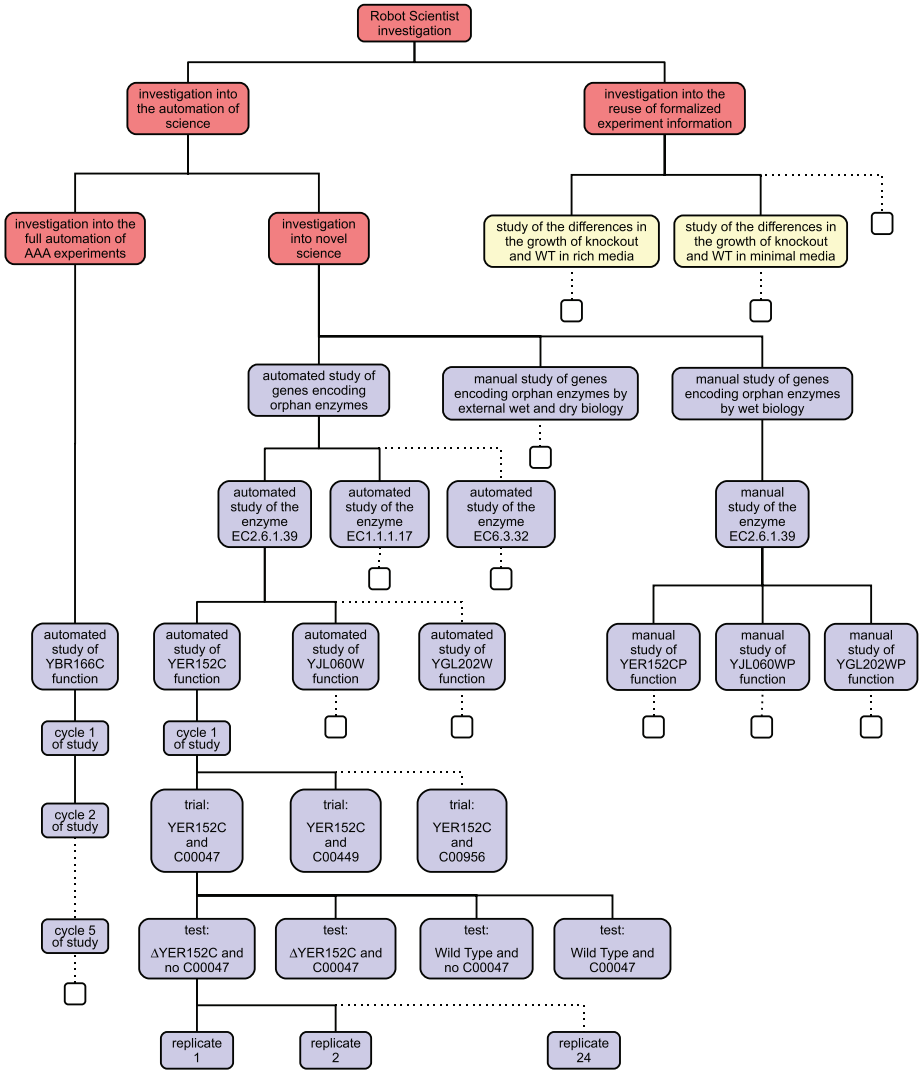

Fig. 3. Structure of the Robot Scientist investigation (a fragment). It consists of two main parts: an investigation into the automation of science and an investigation into the reuse of formalized experiment information. The top levels involve AI research (red), which requires research in functional genomics (blue) and systems biology (yellow). Each level of research unit (studies, cycles, trials, tests, and replicates) is characterized by a specific set of properties (fig. S3) (*16*). Such a nested structure is typical of many scientific experiments, where the testing of a top-level hypothesis requires the planning of many levels of supporting work. What is atypical in Adam's work is the scale and depth of the nesting.

A major motivation for the formalization of experimental knowledge is the expectation that such knowledge is more easily reused to answer other scientific questions. To test this, we investigated whether we could reuse Adam's functional genomic research (*16*). An example question investigated was the relative growth rates (μ_{max}) in rich and defined media of the deletion strains compared with those of the wild type. What was observed, in both media, was a skewed distribution, with a few deletants having a much lower μ_{max} than that of the wild type, but most having a slightly higher μ_{max}. These observations question the common assumption that wild-type *S. cerevisiae* is optimized for μ_{max} and provide quantitative test data for yeast systems biology models (*19*).

It could be argued that the scientific knowledge "discovered" by Adam is implicit in the formulation of the problem and is therefore not novel. This argument that computers cannot originate anything is known as Lady Lovelace's objection (*20*): "The Analytical Engine has no pretensions to *originate* anything. It can do *whatever we know how to order it* to perform" (her italics). We accept that the knowledge automatically generated by Adam is of a modest kind. However, this knowledge is not trivial, and in the case of the genes encoding 2A2OA, it sheds light on, and perhaps solves, a 50-year-old puzzle (*21*).

Adam is a prototype and could be greatly improved. Its hardware and software are "brittle," so although Adam is capable of running for a few days without human intervention, it is advisable to have a technician nearby in case of problems. The integration of Adam's artificial intelligence (AI) software also needs to be enhanced so that it works seamlessly. To extend Adam, we have developed software to enable external users to propose hypotheses and experiments, and we plan to automatically publish the logical descriptions of automated experiments. The idea is to develop a way of enabling teams of human and robot scientists to work together. The greatest research challenge will be to improve the scientific intelligence of the software. We have shown that a simple form of hypothesis-led discovery can be automated. What remain to be determined are the limits of automation.

References and Notes

1. *Nature* **440**, 383 (2006).
2. T. Hey, A. Trefethen, in *Grid Computing: Making the Global Infrastructure a Reality*, **36** 809 (Wiley, New York, 2003).
3. S. Toulmin, in *Encyclopaedia Britannica Deluxe Edition 2004 CD* (Encyclopaedia Britannica UK, London, 2003).
4. T. Berners-Lee, J. Hendler, O. Lassila, *Sci. Am.* **284**, 34 (May 2001).
5. M. Ashburner *et al.*, *Nat. Genet.* **25**, 25 (2000).
6. R. D. King *et al.*, *Nature* **427**, 247 (2004).
7. B. G. Buchanan, G. L. Sutherland, E. A. Feigenbaum, in *Machine Intelligence*, B. Meltzer, D. Michie, Eds. (Edinburgh Univ. Press, Edinburgh, UK, 1969), vol. 5, pp. 209–254.
8. P. Langley, H. A. Simon, G. L. Bradshaw, J. M. Zytkow, *Scientific Discovery: Computational Explorations of the Creative Process* (MIT Press, Cambridge, MA, 1987).

9. J. M. Zytkow, J. Zhu, A. Hussam, in *Proceedings of the Eighth National Conference on Artificial Intelligence (AAAI-90)*, 889 (AAAI Press, Menlo Park, CA, 1990).
10. L. Hood, J. R. Heath, M. E. Phelps, B. Lin, *Science* **306**, 640 (2004).
11. L. N. Soldatova, R. D. King, *J. R. Soc. Interface* **3**, 795 (2006).
12. L. N. Soldatova, A. Clare, A. Sparkes, R. D. King, *Bioinformatics* **22**, e464 (2006).
13. R. D. King *et al.*, The Robot Scientist Project, www.aber.ac.uk/compsci/Research/bio/robotsci/ (2008).
14. J. Warringer, E. Ericson, L. Fernandez, O. Nerman, A. Blomberg, *Proc. Natl. Acad. Sci. U.S.A.* **100**, 15724 (2003).
15. K. E. Whelan, R. D. King, *BMC Bioinformatics* **9**, 97 (2008).
16. Materials and methods are available as supporting material on *Science* Online.
17. I. Horrocks, P. F. Patel-Schneider, F. van Harmelen, *Web Semantics* **1**, 7 (2003).
18. J. D. Ullman, *Principles of Database and Knowledge-Base Systems, Vol. I: Classical Database Systems* (Computer Science, New York, 1988).
19. M. J. Herrgard *et al.*, *Nat. Biotechnol.* **26**, 1155 (2008).
20. A. Turing, *Mind* **236**, 433 (1950).
21. T. M. Zabriskie, M. D. Jackson, *Nat. Prod. Rep.* **17**, 85 (2000).
22. M. Young, *J. Exp. Bot.* **24**, 1172 (1973).

23. This work was funded by grants from the Biotechnology and Biological Sciences Research Council to R.D.K., S.G.O., and M.Y.; by a SRIF 2 award to R.D.K.; by fellowships from the Royal Commission for the Great Exhibition of 1851, the Engineering and Physical Sciences Research Council, and the Royal Academy of Engineering to A.C.; and by a RC-UK Fellowship to L.N.S. We thank D. Struttman for help with yeast and M. Benway for help with Adam.

Supporting Online Material

www.sciencemag.org/cgi/content/full/324/5923/85/DC1
Materials and Methods
Figs. S1 to S3
Table S1
References

8 September 2008; accepted 10 February 2009
10.1126/science.1165620

Priming in Systemic Plant Immunity

Ho Won Jung,[1] Timothy J. Tschaplinski,[2] Lin Wang,[3]* Jane Glazebrook,[3] Jean T. Greenberg[1]†

Plants possess inducible systemic defense responses when locally infected by pathogens. Bacterial infection results in the increased accumulation of the mobile metabolite azelaic acid, a nine-carbon dicarboxylic acid, in the vascular sap of *Arabidopsis* that confers local and systemic resistance against the pathogen *Pseudomonas syringae*. Azelaic acid primes plants to accumulate salicylic acid (SA), a known defense signal, upon infection. Mutation of the *AZELAIC ACID INDUCED 1 (AZI1)* gene, which is induced by azelaic acid, results in the specific loss of systemic immunity triggered by pathogen or azelaic acid and of the priming of SA induction in plants. Furthermore, the predicted secreted protein AZI1 is also important for generating vascular sap that confers disease resistance. Thus, azelaic acid and AZI1 are components of plant systemic immunity involved in priming defenses.

Whole plant immunity, called systemic acquired resistance (SAR), often develops after localized foliar infections by diverse pathogens. In this process, leaves distal to the localized infection become primed to activate a stronger defense response upon secondary infection (*1*). Leaves infected with SAR-inducing bacteria produce vascular sap, called petiole exudate, which confers disease resistance to previously unexposed (naïve) plants (*2*, *3*). This indicates that a mobile systemic signal(s) is involved in SAR (*4*). Although the hormone jasmonic acid (JA) accumulates to a high level in petiole exudates from leaves infected with SAR-inducing bacteria, JA does not seem to be the critical signal for SAR (*5*, *6*). Instead, SAR and the production of active exudates require the DIR1 protein, a predicted secreted protein and putative signal carrier in the lipid transfer protein family, and other proteins involved in glycerolipid biosynthesis (*2*, *3*, *7*). Additionally, SAR and exudate-induced resistance appears to require the phenolic metabolite salicylic acid (SA) (*3*, *8*) and possibly methylsalicylate (MeSA) and its methyl

[1]Department of Molecular Genetics and Cell Biology, The University of Chicago, 1103 East 57th Street EBC410, Chicago, IL 60637, USA. [2]Oak Ridge National Laboratory, Environmental Sciences Division, Oak Ridge, TN 37831–6341, USA. [3]Department of Plant Biology, Microbial and Plant Genomics Institute, University of Minnesota, 1500 Gortner Avenue, St. Paul, MN 55108, USA.

*Present address: Boyce Thompson Institute for Plant Research, Tower Road, Ithaca, NY 14853–1801, USA.
†To whom correspondence should be addressed. E-mail: jgreenbe@midway.uchicago.edu

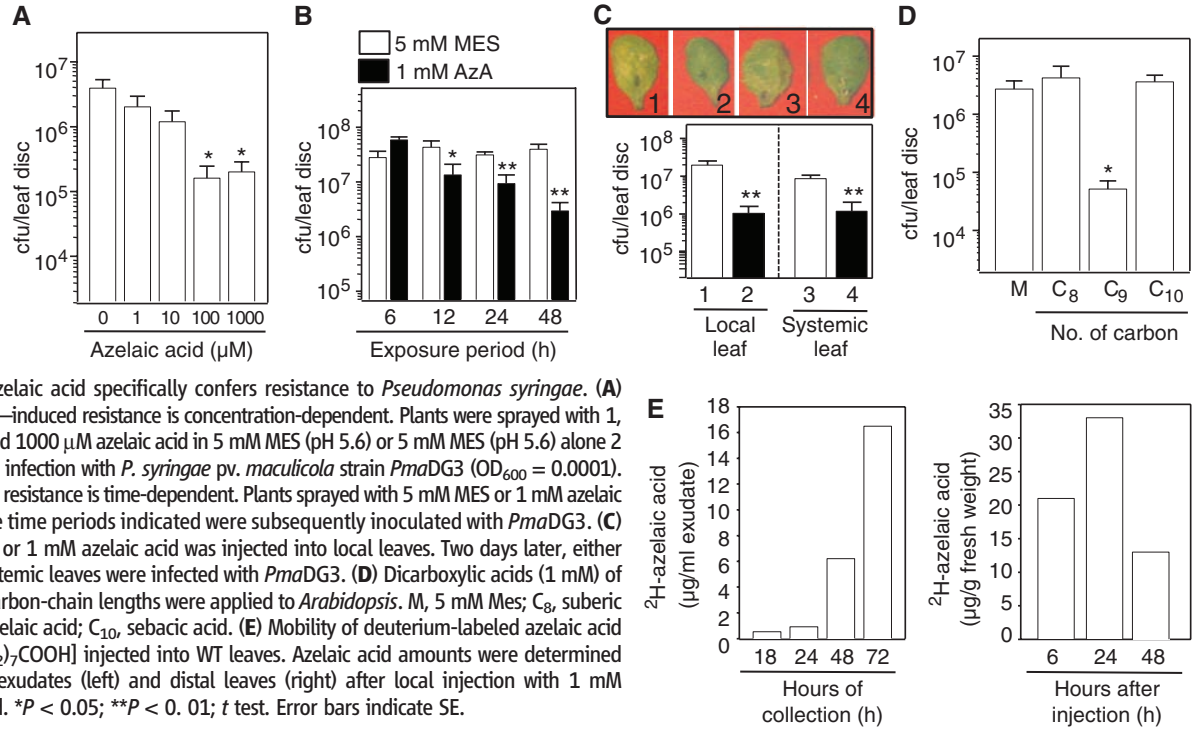

Fig. 1. Azelaic acid specifically confers resistance to *Pseudomonas syringae*. (**A**) Azelaic acid–induced resistance is concentration-dependent. Plants were sprayed with 1, 10, 100, and 1000 μM azelaic acid in 5 mM MES (pH 5.6) or 5 mM MES (pH 5.6) alone 2 days before infection with *P. syringae* pv. *maculicola* strain *Pma*DG3 (OD_{600} = 0.0001). (**B**) Induced resistance is time-dependent. Plants sprayed with 5 mM MES or 1 mM azelaic acid for the time periods indicated were subsequently inoculated with *Pma*DG3. (**C**) 5 mM MES or 1 mM azelaic acid was injected into local leaves. Two days later, either local or systemic leaves were infected with *Pma*DG3. (**D**) Dicarboxylic acids (1 mM) of different carbon-chain lengths were applied to *Arabidopsis*. M, 5 mM Mes; C_8, suberic acid; C_9, azelaic acid; C_{10}, sebacic acid. (**E**) Mobility of deuterium-labeled azelaic acid [$HOOC(CD_2)_7COOH$] injected into WT leaves. Azelaic acid amounts were determined in petiole exudates (left) and distal leaves (right) after local injection with 1 mM azelaic acid. *$P < 0.05$; **$P < 0.01$; *t* test. Error bars indicate SE.

esterase activity (which converts MeSA to SA) in distal leaves (*9*, *10*).

Effective establishment of SAR is not always correlated with elevated systemic SA accumulation, despite its necessary presence, before secondary infections (*11*). This finding implicates that there are additional signal(s) important for priming during SAR. We hypothesize that any such signal should: (i) show elevated levels in petiole exudates of tissue treated with a SAR-inducing pathogen, (ii) confer local and systemic disease resistance through a priming event, (iii) be mobile in plants, and (iv) act in a manner that depends on SA.

To identify this hypothetical signal, we obtained petiole exudates from SAR-induced plants that, unlike exudates from mock-treated plants, conferred disease resistance. We found that pathogen-induced exudates (Col-Pex), but not mock-induced exudates (Col-Mex), conferred resistance to a virulent *Pseudomonas syringae* strain (*Pma*DG3) (fig. S1). Importantly, the SAR-induced exudates did not induce disease resistance when applied to many SAR-defective mutants (fig. S2). Thus, these exudates were biologically active and induced disease resistance in a manner that requires many of the same genes important for SAR.

Because small molecules are often involved in plant signaling, we used gas chromatography coupled with mass spectrometry with electron impact ionization to scan for small molecules (70 to 550 dalton) enriched in the active (SAR-induced) versus inactive (mock-induced) exudates. In four independent experiments, the active exudates consistently had an average of 6.2-fold higher levels of the dicarboxylic acid azelaic acid ($C_9H_{16}O_4$) as compared with inactive exudates [5.1 μM (± 2.3 SEM) in mock-induced exudates versus 31.6 μM (± 10.0 SEM) in active exudates, $P = 0.042$, *t* test]. In vitro, azelaic acid showed weak antimicrobial activity against phytopathogenic bacteria but no activity against fungi (table S1).

To examine if azelaic acid induces disease resistance, we measured *Pma*DG3 growth after spraying plants with different concentrations of azelaic acid and found that more than 10 μM azelaic acid was required to confer disease resistance (Fig. 1A). Additionally, plants needed to be exposed to azelaic acid for at least 12 hours before infection, suggesting that azelaic acid does not directly inhibit *Pma*DG3 during infection (Fig. 1B). Local application of azelaic acid (1 mM) conferred both local and systemic resistance to *Pma*DG3 (Fig. 1C). The immunity-inducing properties of azelaic acid appeared to be specific, as the related C_8 and C_{10} dicarboxylic acids did not induce disease resistance (Fig. 1D). Furthermore, azelaic acid accumulated in distal systemic tissue as well as petiole exudates when it was locally applied to leaves, showing that it was mobile in plants when labeled with deuterium [$HOOC(CD_2)_7COOH$] (Fig. 1E and fig. S3).

To test which genes are necessary for azelaic acid–induced resistance, we monitored *Pma*DG3 growth in leaves of various mutants affecting SAR.

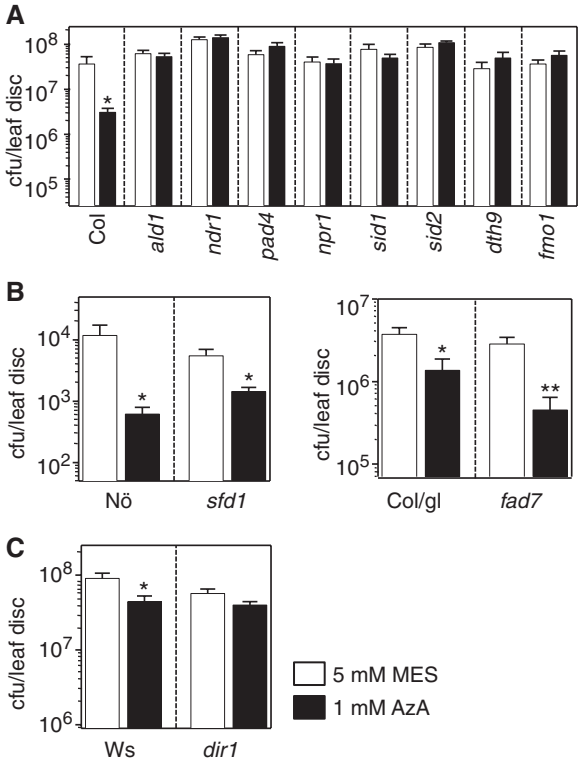

Fig. 2. Genes involved in azelaic acid–induced resistance. 1 mM azelaic acid in 5 mM MES and 5 mM MES alone were sprayed on to WT *Arabidopsis* accessions and the indicated SAR-defective SA pathway mutants (**A**) and glycerolipid mutants (**B** and **C**) 2 days before challenge inoculation with *Pma*DG3 (A and B) or *P. syringae* pv. *tomato* DC3000 (C). Bacterial growth in azelaic acid–treated plants should only be compared with those of the same genotype pre-treated with 5 mM MES, because different genotypes were grown separately. $*P < 0.05$; $**P < 0.01$; *t* test. Error bars indicate SE.

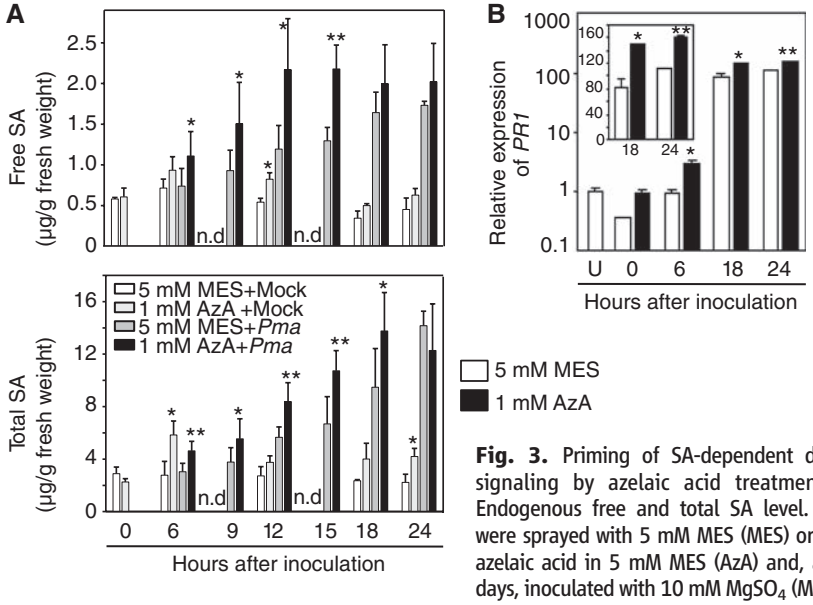

Fig. 3. Priming of SA-dependent defense signaling by azelaic acid treatment. (**A**) Endogenous free and total SA level. Plants were sprayed with 5 mM MES (MES) or 1 mM azelaic acid in 5 mM MES (AzA) and, after 2 days, inoculated with 10 mM $MgSO_4$ (Mock) or *Pma*DG3 (*Pma*). (**B**) Relative *PR1* expression in leaves treated as in (A). Expression of *PR1* is plotted on a log scale; *PR1* levels at 0 hours were not statistically different ($P = 0.065$). (Inset) Increased *PR1* levels in azelaic acid–treated plants at 18 and 24 hours after subsequent *Pma*DG3 infection. $*P < 0.05$; $**P < 0.001$; *t* test. Error bars indicate SD [number of samples analyzed per treatment (n) = 5 (A) or 3 (B)]. U, untreated; n.d., not determined.

We found that azelaic acid did not induce resistance in known SAR-defective SA pathway mutants (Fig. 2A) but did confer resistance to *sfd1* and *fad7* mutants (Fig. 2B), which lack an unidentified glycerolipid-requiring SAR signal (*3*, *7*). In contrast, the SAR-defective *dir1-1* mutant was insensitive to azelaic acid, suggesting that a DIR1-mediated signal is required for azelaic acid–induced resistance (Fig. 2C). The hormone mutants, *jar1* and *etr1*, that are not SAR-defective were responsive to azelaic acid (fig. S4).

Azelaic acid's effects may be to directly induce SA production. Although intact SA synthesis and signaling was required for azelaic acid–induced resistance, free and total SA levels were not significantly elevated up to 48 hours after treatment, compared with those of mock-treated plants (fig. S5). Alternatively, it may be that azelaic acid primes

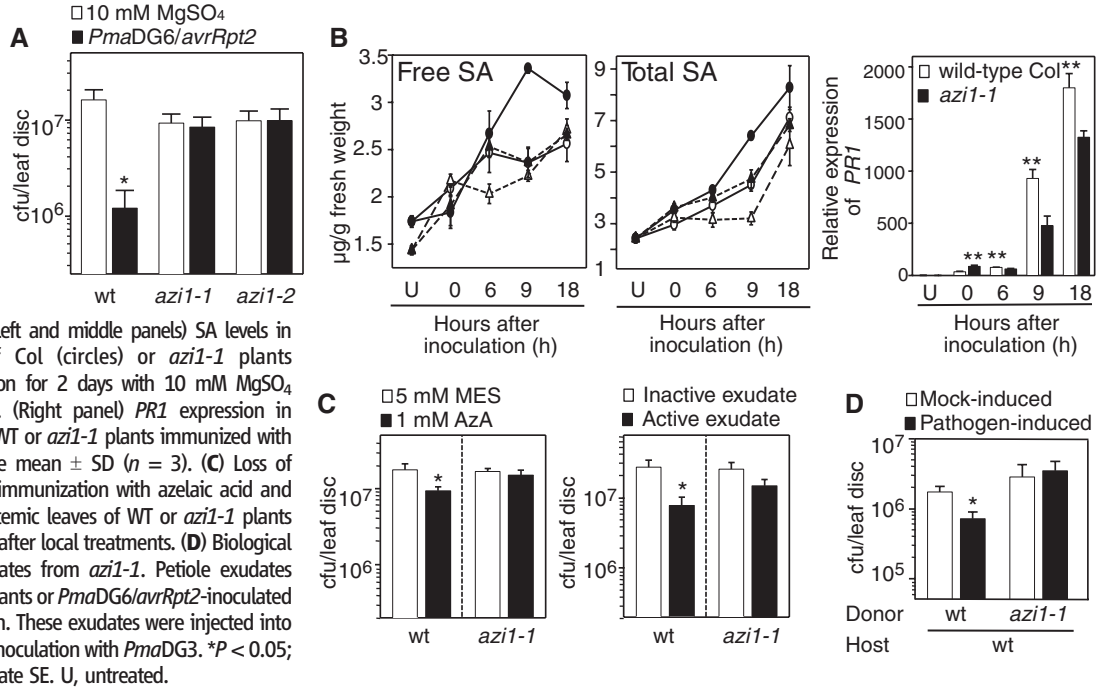

Fig. 4. Signaling defects of *azi1* mutants. (**A**) Loss of SAR as measured by *Pma*DG3 growth in immunized *azi1* plants. WT Col or *azi1* plants were immunized with 10 mM MgSO4 or *Pma*DG6/*avrRpt2* 2 days before secondary infection of distal systemic leaves with *Pma*DG3 and differences identified with a *t* test. (**B**) Reduced defense priming in distal systemic leaves of *Pma*DG6/*avrRpt2*-inoculated *azi1*. (Left and middle panels) SA levels in *Pma*DG3–infected distal leaves of Col (circles) or *azi1-1* plants (triangles) after local immunization for 2 days with 10 mM $MgSO_4$ (white) or *Pma*DG6/*avrRpt2* (black). (Right panel) *PR1* expression in *Pma*DG3–infected distal leaves of WT or *azi1-1* plants immunized with *Pma*DG6/*avrRpt2*. Data present the mean ± SD ($n = 3$). (**C**) Loss of systemic response of *azi1* to local immunization with azelaic acid and Col-Pex (active exudate). Distal systemic leaves of WT or *azi1-1* plants were infected with *Pma*DG3 2 days after local treatments. (**D**) Biological activity of pathogen-induced exudates from *azi1-1*. Petiole exudates were collected from mock-treated plants or *Pma*DG6/*avrRpt2*-inoculated plants for 72 hours after inoculation. These exudates were injected into WT plants 2 days before challenge inoculation with *Pma*DG3. *$P < 0.05$; **$P < 0.001$; *t* test. Error bars indicate SE. U, untreated.

plant cells to mount a faster and/or stronger defense response, including SA production, upon infection. Azelaic acid–treated plants that were subsequently infected had higher levels of both SA (Fig. 3A) and transcripts of the SA-associated signaling marker *PR1* compared with mock-treated plants (Fig. 3B). Thus, azelaic acid primes SA production upon infection upstream of both the SA-dependent SAR signaling pathway and the DIR1-dependent signal and downstream or independent of SFD1 and FAD7.

We examined possible effectors of azelaic acid with microarray analysis (*12*) but observed no statistically significant altered expression above twofold (table S2) of 464 defense-related genes. Thus, azelaic acid does not cause dramatic reprogramming of the plant transcriptome. However, *AZI1* (*AZELAIC ACID INDUCED 1*, At4g12470), which showed modest induction at 24 hours (1.8-fold, $P = 0.13$), was transiently and significantly induced at 3 to 6 hours by azelaic acid and active exudates (fig. S6). AZI1 encodes a predicted secreted protease inhibitor/seed storage/lipid transfer protein family protein, has no significant similarity to DIR1 (*2*), and confers disease resistance when overexpressed (*13*).

Two independent *azi1* mutants (SALK_017709 and SALK_085727, fig. S7) were found to be defective in SAR (Fig. 4A). However, *azi1* plants showed normal susceptibility to local infection with several strains of *P. syringae* (fig. S8). We observed that after local immunization with SAR-inducing bacteria, wild-type (WT) plants appeared to be primed to accumulate SA and *PR1* transcripts in distal leaves upon secondary infection (Fig. 4B). In contrast, *azi1* plants showed reduced priming during SAR (Fig. 4B), although they showed normal SA and *PR1* accumulation during local immunization (fig. S9).

SAR can be impaired because of a failure to recognize a defense/priming signal, generate the signal(s) in local infected-leaves, or translocate the signal(s) from local infected-leaves. To test if *azi1* plants fail to recognize a defense/priming signal(s), we infiltrated azelaic acid or active petiole exudate into leaves of *azi1* mutants. Two days later, we inoculated the same leaves with *Pma*DG3. *azi1* plants were resistant to subsequent local infection (fig. S10), indicating that *azi1* mutants still recognize defense/priming signal(s). To test whether AZI1 functions in long-distance signaling for systemic immunity, we examined the growth of *Pma*DG3 in systemic leaves of *azi1* plants in which azelaic acid or active petiole exudate (Col-Pex) was locally infiltrated. Azelaic acid and petioles exudates failed to induce systemic immunity in *azi1* plants, although these treatments protected WT plants against subsequent infection (Fig. 4C). Additionally, pathogen-induced exudates from *azi1* were inactive when applied to WT plants (Fig. 4D). Thus, AZI1 modulates production and/or translocation of a mobile signal(s) during SAR.

In summary, azelaic acid has the expected properties of a SAR component in that the molecule is mobile in plants, shows increased accumulation in biologically active exudates, confers pathogen resistance to local and systemic tissues, requires genes important for SA production and action to confer disease resistance, and primes SA accumulation and SA-associated gene expression. AZI1 appears to be induced by azelaic acid and regulates and/or directly translocates a SAR signal(s) from local infected tissues. The identification of previously unknown SAR components may be useful for plant protection and provides insight into how some interactions trigger systemic plant immunity.

References and Notes

1. J. A. Ryals *et al.*, *Plant Cell* **8**, 1809 (1996).
2. A. M. Maldonado, P. Doerner, R. A. Dixon, C. J. Lamb, R. K. Cameron, *Nature* **419**, 399 (2002).
3. R. Chaturvedi *et al.*, *Plant J.* **54**, 106 (2008).
4. R. A. Dean, J. Kuc, *Phytopathology* **76**, 966 (1986).
5. W. Truman, M. H. Bennett, I. Kubigsteltig, C. Turnbull, M. Grant, *Proc. Natl. Acad. Sci. U.S.A.* **104**, 1075 (2007).
6. C. M. J. Pieterse *et al.*, *Plant Cell* **10**, 1571 (1998).
7. A. Nandi, R. Welti, J. Shah, *Plant Cell* **16**, 465 (2004).
8. J. Malamy, J. P. Carr, D. F. Klessig, I. Raskin, *Science* **250**, 1002 (1990).
9. S.-W. Park, E. Kaimoyo, D. Kumar, S. Mosher, D. F. Klessig, *Science* **318**, 113 (2007).
10. A. C. Vlot *et al.*, *Plant J.* **56**, 445 (2008).
11. R. K. Cameron, N. L. Paiva, C. J. Lamb, R. A. Dixon, *Physiol. Mol. Plant Pathol.* **55**, 121 (1999).
12. M. Sato *et al.*, *Plant J.* **49**, 565 (2007).
13. C. Chassot, C. Nawrath, J.-P. Métraux, *Plant J.* **49**, 972 (2007).

14. This work was funded by NSF grants to J.T.G. (IOB-0450207) and J.G. (IOB-0419648) and by a fellowship from Korea Research Foundation to H.W.J., and T.J.T. was supported by the Office of Biological and Environmental Research of the U.S. Department of Energy. Oak Ridge National Laboratory is managed by UT-Battelle for the U.S. Department of Energy under contract DE-AC05-00OR22725. We thank J. Bergelson and L. Mets for the use of their high-performance liquid chromatographys, F. Katagiri and J. Malamy for useful discussions, R. Cameron for sharing her detailed exudate collection protocol, and N. Engle for analysis of exudates. A patent application related to this work has been filed by the University of Chicago and UT-Battelle on behalf of inventors J.T.G., H.W.J., and T.J.T. on the use of azelaic acid to confer protection in crop plants against infection.

Supporting Online Material

www.sciencemag.org/cgi/content/full/324/5923/89/DC1
SOM Text
Figs. S1 to S10
Tables S1 to S3
References

19 December 2008; accepted 9 February 2009
10.1126/science.1170025

RNA Pol II Accumulates at Promoters of Growth Genes During Developmental Arrest

L. Ryan Baugh,* John DeModena, Paul W. Sternberg†

When *Caenorhabditis elegans* larvae hatch from the egg case in the absence of food, their development is arrested (L1 arrest), and they show increased stress resistance until food becomes available. To study nutritional control of larval development, we analyzed growth and gene expression profiles during L1 arrest and recovery. Larvae that were fed responded relatively slowly to starvation compared with the rapid response of arrested larvae to feeding. Chromatin immunoprecipitation of RNA polymerase II (Pol II) followed by deep sequencing showed that during L1 arrest, Pol II continued transcribing starvation-response genes, but the enzyme accumulated on the promoters of growth and development genes. In response to feeding, promoter accumulation decreased, and elongation and messenger RNA levels increased. Therefore, accumulation of Pol II at promoters anticipates nutritionally controlled gene expression during *C. elegans* development.

Animals cope with fluctuating nutrient availability by altering resource allocation between growth and survival. For the free-living nematode *Caenorhabditis elegans*, life in the wild is characterized by feast or famine, so that organismal fitness presumably depends on developmental responses to nutrient availability. *C. elegans* L1 arrest is an acute response to starvation, in which development is suspended and environmental stress resistance is increased without morphological modification (*1*). L1 arrest offers an opportunity to identify regulatory mechanisms mediating nutritional control of gene expression and, therefore, resource allocation, in a developmental system.

We measured growth and gene expression in *C. elegans* larvae as they hatched from mature eggs and were cultured in the presence or absence of *E. coli* as food (Fig. 1A) (*2*). We also switched conditions (fed or starved) 12 hours after hatching to further dissociate the effects of development and nutrition. Using a flow cytometer (COPAS) to measure growth (*2*), we found that larvae hatched in the presence of food increased in mass within an hour (Fig. 1B). Arrested L1s also responded rapidly to feeding, increasing in mass within 2 hours and achieving the normal L1 growth rate within 3 hours.

In three independent experiments, we collected samples for gene expression analysis using a high-density oligonucleotide array (table S1). During L1 arrest, multiple energy homeostasis signaling pathways and two known regulators of metabolic gene expression (fig. S3) (*3*, *4*) were up-regulated (fig. S2). Numerous metabolic genes were modulated as expected (fig. S4) (*5*), and reporter gene analysis further validated our results (figs. S5 and S6, table S2).

Using a two-factor analysis of variance (ANOVA) to isolate the effects of nutrition and time, we found that expression of more genes was affected by nutrient availability than by development (fig. S7). At the smallest P value (10^{-16}), 20.6% (2386 genes) of the transcriptome was affected by time and 26.9% (3117 genes) by nutrition, which demonstrated the profound influence of energy homeostasis on gene regulation.

We used principal components analysis (PCA) to visualize the dynamics of the transcriptome. This PCA projects multidimensional gene expression data into the two orthogonal factors that capture the most variance; transcriptome-wide dynamics of gene expression can be visualized by the relative positions of data points in the resulting "phase plane." The clustering of starvation data points obtained after >6 hours indicates that the gene expression response to starvation was largely established within 6 hours of hatching in the absence of food (Fig. 2A), a conclusion also supported by pairwise t tests (fig. S8). In contrast, gene expression continued to change in the fed, developing larvae as indicated by the lack of clustering among data points for fed larvae. Notably, arrested L1s responded to feeding more rapidly than fed L1s responded to starvation. The dashed lines in Fig. 2A plot the transcriptome-wide effects of switching conditions. Feeding arrested L1s caused the transcriptome to change so much in 3 hours that it switched sides of the PCA graph, becoming more similar to that of fed than starved L1s (Fig. 2A). In contrast, starving fed L1s had less effect on the transcriptome; it remained more similar to fed larvae than starved. Moreover, pairwise t tests showed that feeding starved L1s for 3 hours caused 381 genes to change ($P \leq 10^{-3}$) so that only 47 differed between them and L1s hatched in the presence of food 3 hours earlier, but starving fed L1s for 3 hours caused only 56 genes to change, leaving 544 that differed between them and L1s hatched in the absence of food 3 hours earlier (fig. S9). We infer that arrested L1s are primed for rapid response to food.

We used cluster analysis to visualize the diversity and relative proportion of nutritionally regulated gene expression patterns. The genes divided cleanly into two clusters that were up-regulated during either L1 arrest or larval development (Fig. 2B). The relatively complex expression dynamics of larval development compared with those of L1 arrest are evident in the clustered expression patterns. Cluster analysis was also consistent with the observed asymmetric response to switching conditions. The expression profile of larvae fed for 12 hours and then starved for 3 hours resembled larvae fed for 15 hours rather than those starved for 3 hours. Conversely, the expression profile of larvae starved for 12 hours and then fed for 3 hours did not resemble larvae starved for 15 hours but rather larvae fed for 3 hours.

Expression analysis indicated that the response to starvation is complete within about 6 hours and that the transcriptome is in steady state thereafter (Fig. 2), possibly as a result of transcriptional quiescence during arrest. We performed chromatin immunoprecipitation of RNA Pol II followed by deep sequencing (ChIP-Seq) (*6*, *7*) to map the genomic pattern of Pol II binding. Contrary to our hypothesis, Pol II was enriched on thousands of genes during L1 arrest (Fig. 3A). Consistent with this, destabilized reporter genes for 16 transcription factors up-regulated during L1 arrest were transcribed for at least the first few days of L1 arrest,

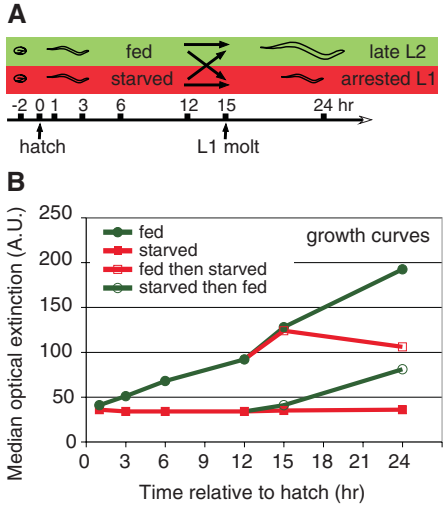

Fig. 1. (**A**) A schematic of the experimental design for growth and expression analysis. Time points sampled are indicated below, where 0 hours is precisely mid-hatch (fig. S1). Crossed arrows indicate when starved cultures were fed and when fed cultures were starved. (**B**) Optical extinction (arbitrary units) was measured as a proxy for mass for synchronous populations of about 5000 individuals at each time point, and the median is reported.

Howard Hughes Medical Institute and Division of Biology, California Institute of Technology, Pasadena, CA 91125, USA.

*Present address: Department of Biology, Duke University, Durham, NC 27708, USA.

†To whom correspondence should be addressed. E-mail: pws@caltech.edu

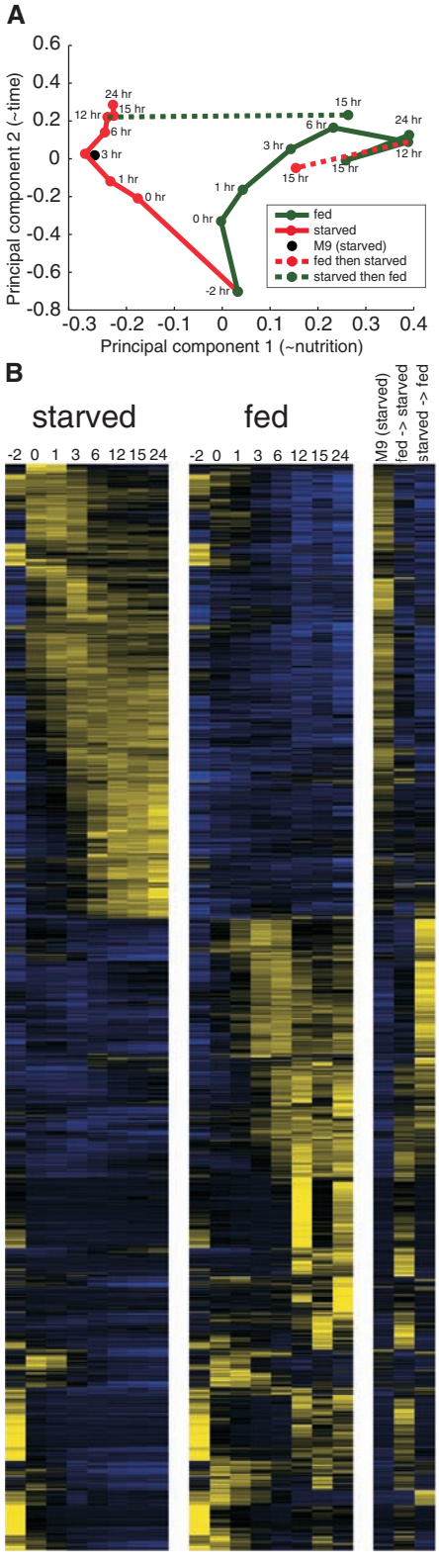

Fig. 2. **(A)** Principal components analysis reveals the dynamics of gene expression in response to starvation and feeding. Note the large and rapid response of arrested L1s to food during recovery (dashed green line). **(B)** The 3117 genes most significantly affected by nutrition (fig. S7) were *Z* transformed and hierarchically clustered by pairwise correlation. Yellow indicates relatively high levels of normalized expression; blue indicates low levels.

whereas signal from transient heat-shock induction of the reporter was undetectable after 12 hours (fig. S6). ChIP-Seq showed that the genome-wide pattern of transcription did not change between 6 and 12 hours of L1 arrest (Fig. 3A), consistent with the transcriptome's maintenance of the steady state.

The amount of elongating Pol II per gene changed rapidly in response to feeding (Fig. 3B). After just 1 hour of recovery from L1 arrest, Pol II enrichment over the coding region increased on 387 genes and decreased on 183 genes. Genes with increased elongation included numerous constituents of the ribosome and translational regulators (table S3). Genes with decreased elongation in response to feeding were enriched for effectors of aging and long-chain fatty acid metabolism (table S3), which indicated that they overlap with clusters of genes up-regulated in response to starvation (table S4). Thus, RNA Pol II ChIP-Seq from whole worms provides effective measurement of instantaneous transcriptional activity.

Genome-wide analyses of Pol II binding reveal that Pol II is concentrated in the promoters of many human, *Drosophila*, and yeast genes (*8*–*12*). We hypothesized that Pol II is recruited to the promoters of growth and development genes during L1 arrest. We performed ChIP-Seq, using three different antibodies against the C-terminal domain of Pol II, using animals in the arrested L1 state for 12 hours and after 1 hour of recovery by feeding (figs. S10 and S11). We defined a 5′ bias index for Pol II binding as the ratio of Pol II enrichment in a 200–base pair (bp) window spanning the transcription start site to enrichment over the entire coding region. To focus on genes with the most reliable Pol II distribution, we included only genes of >300 bp with Pol II enriched at least threefold over the coding region (1238 genes). We consistently saw an overall decrease in 5′ bias after 1 hour of recovery (Fig. 4A). On average, 5′ bias decreased by about 20%, and for the 178 genes (14%) with 5′ bias >2, average bias decreased by 37%. 8WG16 is the most specific of the three antibodies for nonphosphorylated Pol II (*13*), and it detected the largest difference in 5′ bias between L1 arrest and recovery.

In spite of cell-type heterogeneity, RNA Pol II accumulation was readily detected from whole worms, which indicated its prevalence. Notably, 5′ bias was detected with each antibody in spite of the different specificities of the antibodies (Fig. 4A). Promoter accumulation of Pol II has been detected in *C. elegans* embryos with the use of antibody 8WG16 (*14*), but the S2 antibody was raised against a Ser2 phosphorylated polypeptide from the C-terminal domain of Pol II, which is correlated with elongation in other systems (*15*–*17*). However, we found that S2 also bound nonphosphorylated Pol II in *C. elegans* (fig. S10).

The subset of genes with 5′ biased Pol II was particularly responsive to feeding. Pol II enrichment over the entire coding region, which reflects processive elongation, increased substantially during recovery for this set of genes (Fig. 4B). The average increase in Pol II enrichment per gene was 67% ($P < 10^{-5}$; paired-sample *t* test), with S2 showing the largest increase (110%) and 8WG16 the smallest (36%). The heat shock protein hsp70 homolog *hsp-3* illustrates nutritional control of promoter accumulation (Fig. 4C). Finally, genes affecting development and positively regulating growth rate were most significantly enriched among those with 5′ bias (Fig. 4D, and tables S3 and S5).

There are multiple potential points of regulation between Pol II recruitment and uninhibited elongation, and there is unlikely to be a single mechanism underlying Pol II promoter accumulation during L1 arrest. Nevertheless, we speculate that in many of the observed instances, Pol II had initiated elongation and was paused proximally. About half of the 178 genes with 5′ bias had peak Pol II positions just inside the transcription start site (Fig. 4E), consistent with pausing, although the distribution was not as tight as with bona fide pausing (*18*). Including all 1209 genes with 5′ bias >3, rather than only those with Pol II enriched over the coding region (and therefore expressed), accentuated the bimodality in peak Pol II positions, with the majority of peaks upstream of the start site (fig. S12). The negative elongation factor (NELF) complex promotes pausing in *D. melanogaster* (*10*, *18*–*20*), but NELF homologs have not been identified in *C. elegans*, which suggests that the postrecruitment accumulation we observe is mechanistically distinct (*21*).

Accumulation of Pol II at promoters anticipates nutritionally induced gene expression. We examined mRNA expression during L1 arrest, recovery, and growth for genes with and without 5′ biased Pol II (Fig. 4F). Consistent with pausing not necessarily being repressive (*20*, *21*), we saw

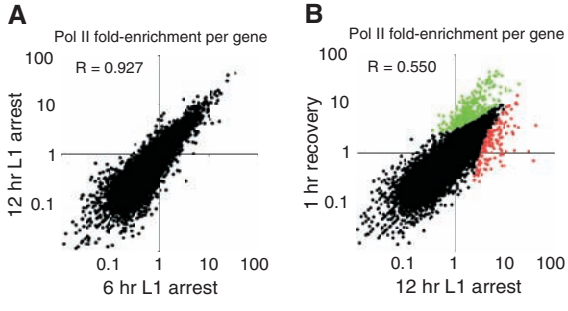

Fig. 3. **(A)** Fold enrichment of Pol II relative to input (preimmunoprecipitation) over each gene in the genome is plotted for 6 and 12 hours of L1 arrest. **(B)** The amount of elongating Pol II per gene changes dramatically within 1 hour of feeding after 12 hours of L1 arrest. The plot is the same as in (A), except genes that increase or decrease in Pol II fold enrichment by at least two units are colored green and red, respectively.

that genes with Pol II accumulation were expressed during L1 arrest. However, their average mRNA expression increased significantly during recovery, demonstrating an anticipatory role of promoter accumulation. Genes with Pol II accumulation during L1 arrest were also upregulated during L1 growth after hatching in the presence of food (Fig. 4F), which underscored their characterization as larval growth and development genes. These results support our Pol II ChIP-Seq results and demonstrate that Pol II promoter accumulation is nutritionally controlled and that a decrease in accumulation is correlated with an increase in elongation and mRNA expression.

This work demonstrates the profound influence of energy homeostasis on gene regulation during development. Analyses of growth, gene expression, and RNA Pol II binding indicate that *C. elegans* responds rapidly to feeding during recovery from developmental arrest. We suggest that this rapid response is facilitated by RNA Pol II accumulation on growth and development genes, poising them for expression. Nutritional control of Pol II promoter accumulation may be a general feature of gene regulation involving energy homeostasis.

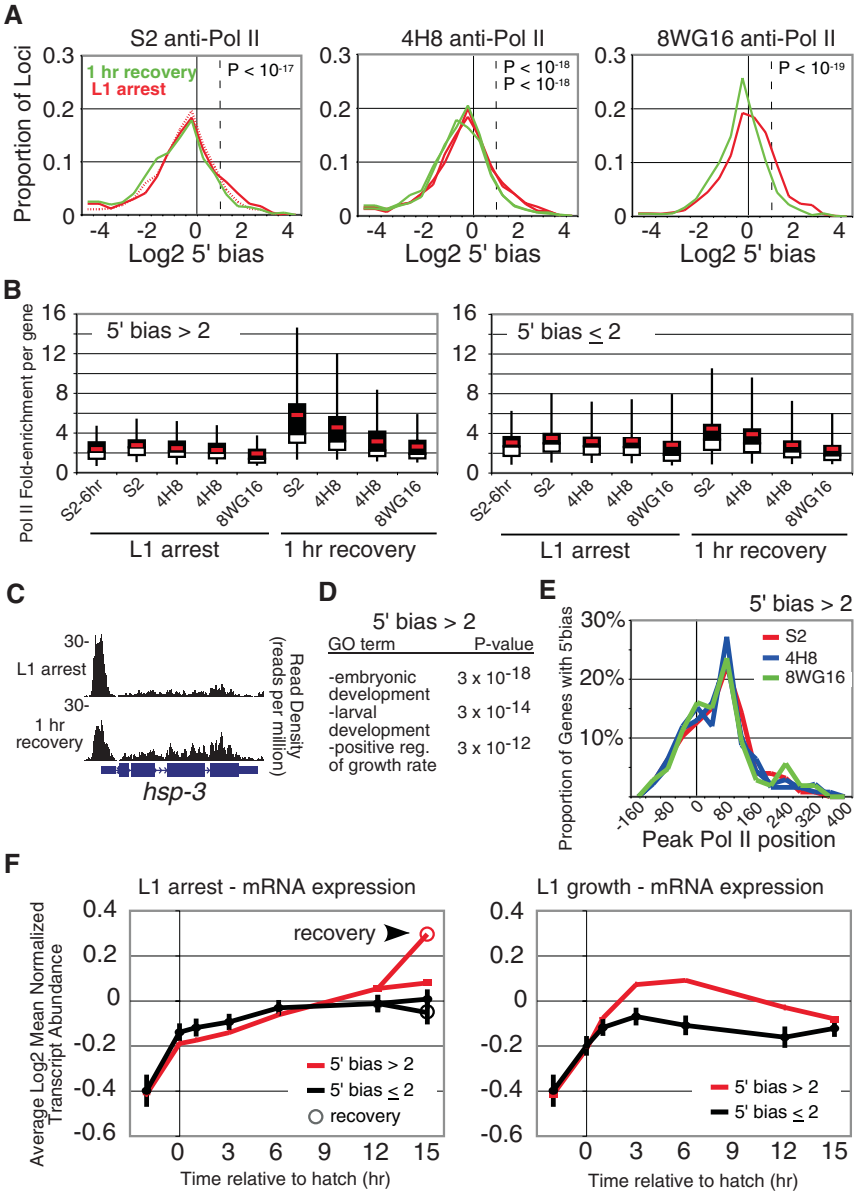

Fig. 4. (**A**) Histograms of $\log_2$ 5′ bias are plotted for three different Pol II antibodies after L1 arrest for 12 hours (red) and 1 hour of recovery (green). In the S2 graph, L1 arrest after 6 hours is plotted as a red dotted line. Biological replicates are plotted in the 4H8 graph. The vertical dashed line on each graph marks a 5′ bias of 2. *P* values resulted from a paired-sample *t* test for the difference between L1 arrest and recovery for genes with 5′ bias >2 during arrest. (**B**) Fold-enrichment of Pol II over the coding region during L1 arrest and after 1 hour of recovery is plotted for each ChIP. Starting with 1238 genes plotted in (A), 178 genes (14.4%) with average 5′ bias during L1 arrest of at least 2 are plotted in the left box plot, and the remaining 1060 are plotted in the right box plot. The box plots show the median and two quartiles of each distribution, with bars reflecting 5th and 95th percentiles and a red bar indicating the average. (**C**) Normalized read counts for each condition are plotted over the *hsp-3* gene. (**D**) The three most significantly enriched gene ontology (GO) terms and associated hypergeometric *P* values are shown for 178 genes with 5′ bias during L1 arrest. (**E**) Histograms of Pol II-binding peak positions relative to the transcription start site are plotted for each L1 arrest ChIP. Bins of 40 bp and strand-corrected peak locations were used. (**F**) Average of $\log_2$ mean normalized transcript abundance is plotted for two sets of genes: the set of 1238 plotted in (A) are in black, and a subset of them (178 genes) with 5′ bias greater than 2 are in red. (Left) Expression during L1 arrest and recovery; (right) expression during L1 growth. The bars on the black curves represent the standard deviations of 1000 averages computed for a set of 178 genes randomly selected from the 1238 genes.

References and Notes

1. L. R. Baugh, P. W. Sternberg, *Curr. Biol.* **16**, 780 (2006).
2. Materials and methods are available as supporting material on *Science* Online.
3. S. Taubert, M. R. Van Gilst, M. Hansen, K. R. Yamamoto, *Genes Dev.* **20**, 1137 (2006).
4. M. R. Van Gilst, H. Hadjivassiliou, A. Jolly, K. R. Yamamoto, *PLoS Biol.* **3**, e53 (2005).
5. M. R. Van Gilst, H. Hadjivassiliou, K. R. Yamamoto, *Proc. Natl. Acad. Sci. U.S.A.* **102**, 13496 (2005).
6. A. Barski *et al.*, *Cell* **129**, 823 (2007).
7. D. S. Johnson, A. Mortazavi, R. M. Myers, B. Wold, *Science* **316**, 1497 (2007).
8. M. G. Guenther, S. S. Levine, L. A. Boyer, R. Jaenisch, R. A. Young, *Cell* **130**, 77 (2007).
9. T. H. Kim *et al.*, *Nature* **436**, 876 (2005).
10. G. W. Muse *et al.*, *Nat. Genet.* **39**, 1507 (2007).
11. M. Radonjic *et al.*, *Mol. Cell* **18**, 171 (2005).
12. J. Zeitlinger *et al.*, *Nat. Genet.* **39**, 1512 (2007).
13. S. Q. Xie, S. Martin, P. V. Guillot, D. L. Bentley, A. Pombo, *Mol. Biol. Cell* **17**, 1723 (2006).
14. C. M. Whittle *et al.*, *PLoS Genet.* **4**, e1000187 (2008).
15. A. K. Boehm, A. Saunders, J. Werner, J. T. Lis, *Mol. Cell. Biol.* **23**, 7628 (2003).
16. H. P. Phatnani, A. L. Greenleaf, *Genes Dev.* **20**, 2922 (2006).
17. J. R. Weeks, S. E. Hardin, J. Shen, J. M. Lee, A. L. Greenleaf, *Genes Dev.* **7**, 2329 (1993).
18. C. Lee *et al.*, *Mol. Cell. Biol.* **28**, 3290 (2008).
19. C. H. Wu *et al.*, *Genes Dev.* **17**, 1402 (2003).
20. D. A. Gilchrist *et al.*, *Genes Dev.* **22**, 1921 (2008).
21. D. S. Gilmour, *Chromosoma* **118**, 1 (2009).

22. We thank L. Schaeffer, D. Trout, A. Mortazavi, J. L. Riechmann, and B. Wold for assistance and discussions. We thank E. H. Davidson for sharing his COPAS Biosorter and B. Hwang for sharing his destabilized YFP plasmid. L.R.B. was supported by the American Cancer Society. P.W.S. is an investigator with the Howard Hughes Medical Institute, which supported this work. Microarray analysis and sequencing were performed in the Millard and Muriel Jacobs Genetics and Genomics Laboratory at Caltech. Data and analysis available for download from NCBI Gene Expression Omnibus (accession GSE14009) at www.ncbi.nlm.nih.gov/geo/query/acc.cgi?acc=GSE14009.

Supporting Online Material

www.sciencemag.org/cgi/content/full/1169628/DC1
Materials and Methods
SOM Text
Figs. S1 to S14
Tables S1 to S7
References

11 December 2008; accepted 17 February 2009
Published online 26 February 2009;
10.1126/science.1169628

Nuclear Hormone Receptor Regulation of MicroRNAs Controls Developmental Progression

Axel Bethke,[1,2] Nicole Fielenbach,[1] Zhu Wang,[3] David J. Mangelsdorf,[3] Adam Antebi[1,4]*

In response to small-molecule signals such as retinoids or steroids, nuclear receptors activate gene expression to regulate development in different tissues. MicroRNAs turn off target gene expression within cells by binding complementary regions in messenger RNA transcripts, and they have been broadly implicated in development and disease. Here we show that the *Caenorhabditis elegans* nuclear receptor DAF-12 and its steroidal ligand directly activate promoters of *let-7* microRNA family members to down-regulate the microRNA target *hbl-1*, which drives progression of epidermal stem cells from second to third larval stage patterns of cell division. Conversely, the receptor without the ligand represses microRNA expression during developmental arrest. These findings identify microRNAs as components of a hormone-coupled molecular switch that shuts off earlier developmental programs to allow for later ones.

Lipophilic hormones coordinate organism-wide developmental progression in metazoans by binding to nuclear hormone receptors (NHRs), converting the presence or absence of ligand into changes in gene expression patterns (*1*). This regulation is conserved in the nematode *Caenorhabditis elegans*, where the nuclear hormone receptor DAF-12, a homolog of vertebrate liver X and vitamin D receptors, regulates developmental progression or arrest in response to the environment (*2*, *3*). In favorable environments, activation of transforming growth factor-β (TGF-β) and insulin/insulin-like growth factor (IGF) signaling cascades results in production of the DAF-12 steroidal ligands, the dafachronic acids (e.g., Δ^4-DA), which promote rapid progression through four larval stages (L1 to L4) to reproductive adults (*4*). In unfavorable environments, endocrine systems are suppressed, and DAF-12 without the ligand causes arrest at a stress-resistant, long-lived alternative third larval stage, called the dauer diapause (L3d) (*5*).

A more cell-intrinsic level of developmental control is exerted by microRNAs. MicroRNAs are ~20- to 22-nucleotide-long RNA molecules that bind to the 3′ untranslated region (3′UTR) of target messenger RNAs (mRNAs) and decrease their expression (*6*–*8*). Null mutants for several microRNA genes show tissue-selective failure of progression from one stage-specific program to the next, generally described as heterochronic phenotypes. These phenotypes are most visible in the hypodermis, where hypodermal seam cells undergo invariant asymmetric stem cell division patterns, in which one daughter cell fuses to the hypodermal syncytium, whereas the other retains stem cell character and its capacity to divide (*9*). Only during L2 do seam cells undergo one proliferative division before stem cell division, and repetition or loss of this program leads to changes in overall seam cell number in later stages. Finally, seam cell division ceases altogether by adulthood. Seam cells in animals with mutation of the microRNA *lin-4* repeat L1 programs of asymmetric cell division during L2 stage; a triple deletion of the *let-7* microRNA homologs *mir-48*, *-84*, *-241* (referred to as *let-7s*) repeat L2 programs of cell proliferation during L3 stage; and *let-7* null mutants repeat larval stage divisions and molting behavior in adults (*10*–*12*).

[1]Huffington Center on Aging, Department of Molecular and Cellular Biology, Baylor College of Medicine, One Baylor Plaza, Houston, TX 77030, USA. [2]University of Osnabrück, Fachbereich Biologie/Chemie, Barbarastrasse 11, 49069 Osnabrück, Germany. [3]Department of Pharmacology and Howard Hughes Medical Institute, University of Texas Southwestern Medical Center, 6001 Forest Park Road, Dallas, TX 75390, USA. [4]Max-Planck-Institute for Biology of Ageing, Gleulerstrasse 50a, D-50931 Cologne, Germany.

*To whom correspondence should be addressed. E-mail: aantebi@bcm.edu

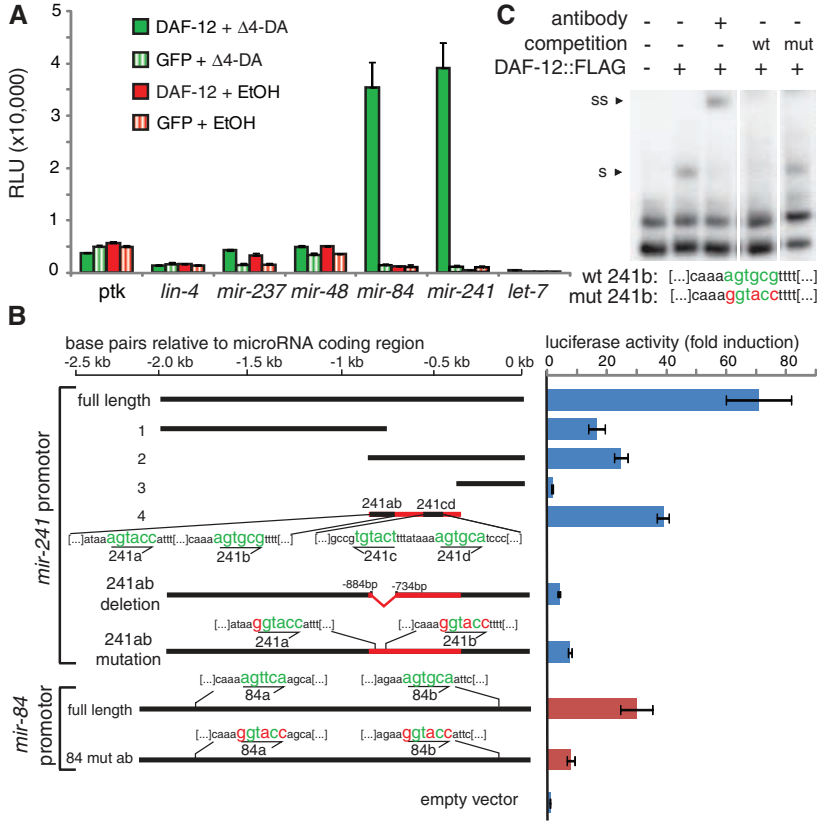

Fig. 1. DAF-12 and dafachronic acid (Δ^4-DA) activate microRNA promoters in vitro. (**A**) Activation of microRNA promoters in HEK293T cells. Promoters of *let-7* homologs, *mir-84* and *mir-241*, were strongly activated in the presence of DAF-12 and 400 nM Δ^4-DA, whereas other microRNAs were relatively unaffected. Luciferase assays were measured in triplicate and are shown with SD. EtOH, ethanol vehicle control; ptk, empty luciferase vector. (**B**) Mutation analysis of *mir-241p* and *mir-84p* reveals DAF-12–Δ^4-DA–activating elements. Deletion analysis of the *mir-241p* showed that the highest relative induction occurs with fragment 4, which contains four DAF-12 REs, 241a, b, c, and d. Deletion or point mutation of *241ab* elements (in red) abolished activation (blue bars). Similarly, point mutation of DAF-12 REs in *mir-84p*, 84a and b, reduced expression (red bars). (**C**) Gel mobility shift assay of DAF-12 and *mir-241p*. ^{32}P-radiolabeled oligomers containing the WT 241b element were shifted (s) by nuclear extracts expressing DAF-12::FLAG and supershifted (ss) in the presence of FLAG-specific antibody. Unlabeled WT 241b-oligomer prevented the shift, but addition of an oligomer with a point mutation did not.

daf-12(*rh61rh411*) null mutants exhibit a heterochronic phenotype similar to triple deletion of *let-7* family members *mir-48*,*mir-241*(*nDf51*); *mir-84*(*n4037*), resulting in extra seam cells at the L3 stage (table S1) (*2*, *11*). This observation suggested that *daf-12* might directly activate the *let-7s* microRNAs. To test this hypothesis, we fused the microRNA promoters *mir-241p* and *mir-84p* to the luciferase gene and co-transfected the reporters with DAF-12 into human cells (*13*). DAF-12 and Δ^4-DA strongly activated *mir-241p* and *mir-84p*, whereas other promoters gave little or no signal (Fig. 1A). Deletion analysis of the *mir-241p* revealed that, whereas several deletion mutations retained transcriptional activity in the presence of DAF-12 and Δ^4-DA, fragment 4 produced the highest fold induction, and its removal substantially reduced activity (Fig. 1B). This fragment contained two pairs of DAF-12 response elements (REs), as described by Shostak (*14*). In the full-length promoter context, mutation of one RE pair in *mir-241p* and two REs in *mir-84p* led to a decrease in activation of about seven- and threefold, respectively. Gel mobility shift assays confirmed in vitro binding of DAF-12 to these REs, whereas mutated versions abolished the interaction (Fig. 1C).

To examine microRNA expression in vivo, we generated transgenic worms containing the microRNA promoters fused to green fluorescent protein (GFP). Wild-type (WT) worms containing *mir-241p::GFP* gave a broad expression pattern as described (*15*). However, *daf-12* nulls showed decreased expression, most noticeably in the excretory cells (exc), as well as in muscles, pharynx, and intestine, although neuronal expression seemed less affected, which reveals the tissue selectivity of *daf-12* regulation (Fig. 2, A to D). Null mu-

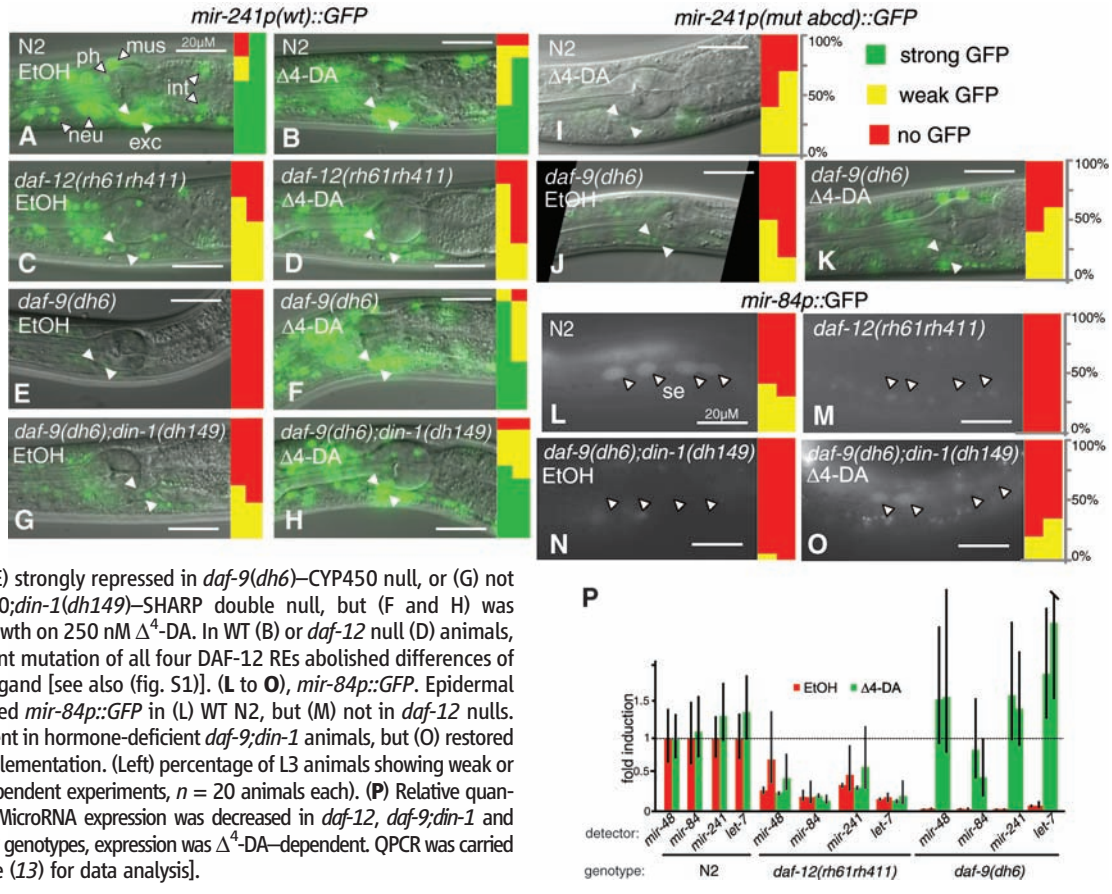

Fig. 2. DAF-12 and Δ^4-DA regulate microRNA promoters in vivo. (**A** to **K**) *mir-241p::GFP*. Images show representative L3 animals, with indicated cell types (white arrowheads and exc, excretory cell; outlined arrowheads, neu, neuron; mus, muscle; int, intestine; ph, pharynx). Bar graphs alongside the images quantify the percentage of worms with excretory cell GFP expression as either strong (green), weak (yellow), or off (red) (two independent experiments, left and right, $n = 10$ animals each). For *mir-241p::GFP* expression level in worms grown without ligand (EtOH) or with ligand (Δ4-DA). (A and B) WT (N2-type). (C) Expression was decreased in *daf-12*(*rh61rh411*)–NHR null, (E) strongly repressed in *daf-9*(*dh6*)–CYP450 null, or (G) not activated in *daf-9*(*dh6*)–CYP450;*din-1*(*dh149*)–SHARP double null, but (F and H) was rescued nearly to WT level by growth on 250 nM Δ^4-DA. In WT (B) or *daf-12* null (D) animals, Δ^4-DA had no effect. (I to K) Point mutation of all four DAF-12 REs abolished differences of tested genetic backgrounds or ligand [see also (fig. S1)]. (**L** to **O**), *mir-84p::GFP*. Epidermal seam cells (arrowheads) expressed *mir-84p::GFP* in (L) WT N2, but (M) not in *daf-12* nulls. (N) Seam cell expression was absent in hormone-deficient *daf-9;din-1* animals, but (O) restored to nearly WT levels by Δ^4-DA supplementation. (Left) percentage of L3 animals showing weak or no seam cell expression (two independent experiments, $n = 20$ animals each). (**P**) Relative quantification of microRNAs by QPCR. MicroRNA expression was decreased in *daf-12*, *daf-9;din-1* and repressed in *daf-9* mutants. In *daf-9* genotypes, expression was Δ^4-DA–dependent. QPCR was carried out using the TaqMan system [see (*13*) for data analysis].

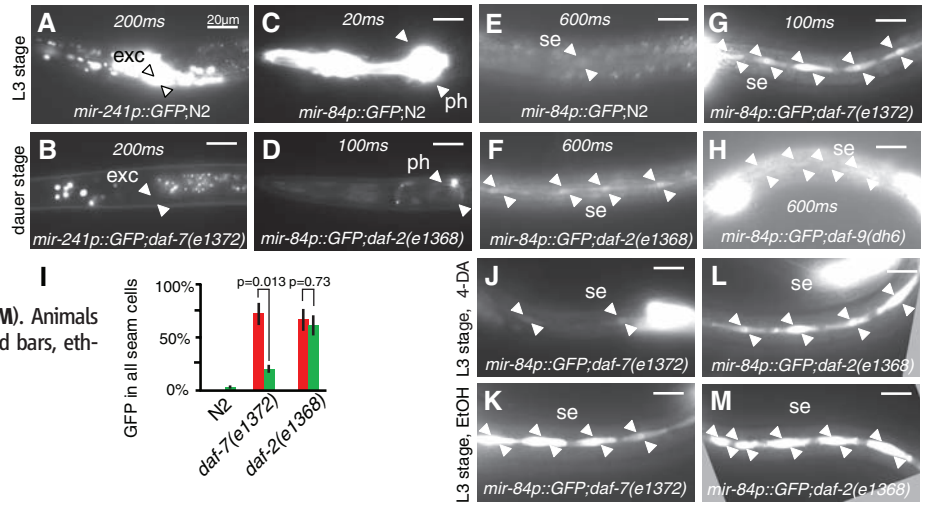

Fig. 3. MicroRNA regulation by dauer signaling pathways. *mir-241p::GFP* showed high expression in continuously growing WT (**A**), but low expression in *daf-7*(*e1372*) dauer larvae (**B**). *mir-84p::GFP* showed high expression in the pharynx of continuously growing WT (**C**) but low expression in *daf-2*(*e1368*) dauers (**D**). *mir-84p::GFP* seam cell expression (**E**) was elevated in *daf-2* and *daf-9* mutants during dauer stage (**F** and **H**) and was even higher in *daf-7* mutants during reproductive growth at 20°C (**G**). Penetrant seam expression was reversed by 500 nM Δ^4-DA in *daf-7*, but not *daf-2*, during reproductive growth (**I** to **M**). Animals were assayed during L3 and/or L3d stages, $n > 20$. Red bars, ethanol vehicle, green bars, Δ^4-DA (SEM).

tants for cytochrome P-450 (CYP450) *daf-9*(*dh6*) fail to produce dafachronic acids, and DAF-12 without the ligand interacts with its co-repressor DIN-1–SHARP to repress transcriptional targets; together they cause constitutive developmental arrest and dauer larvae formation (*16*–*18*). In these hormone-deficient larvae, *mir-241p::GFP* expression was tightly repressed in most tissues (Fig. 2E). Supplementation with Δ^4-DA rescued this arrest and brought *mir-241p::GFP* expression back to WT levels (Fig. 2F). Tight repression was also relieved in *daf-9*(*dh6*);*din-1*(*dh149*) double-null mutants lacking the corepressor, with *mir-241p::GFP* expression levels similar to *daf-12* nulls (Fig. 2, G and H). Unlike *daf-12* nulls, however, Δ^4-DA supplementation of *daf-9;din-1* worms restored *mir-241p::GFP* expression back to WT levels. Point mutation of all four *daf-12*-REs in *mir-241p* resulted in the same weak expression level in WT, *daf-12* null with ligand, as well as *daf-9* null, and *daf-9;din-1* doubles with or without ligand (Fig. 2, I to K, and fig. S1), which revealed that these REs mediate both activation and repression. Thus, DAF-12 with the ligand works through its REs to mildly activate *mir-241p* in some tissues, whereas DAF-12 without the ligand, together with DIN-1, tightly represses expression in nearly all tissues.

As reported, *mir-84p::GFP* was expressed in pharynx, somatic gonad, seam cells, vulva cells, and, occasionally, in the intestine (*15*, *19*). Seam cell expression was absent in *daf-12* null and *daf-9;din-1* null worms, and expression was increased almost to WT levels in *daf-9;din-1* animals by addition of Δ^4-DA (Fig. 2, L to O), which explains *daf-12* heterochronic phenotypes as a failure to activate the microRNAs in temporally patterned tissues. By contrast, expression in other tissues, such as the pharynx, was less affected, which shows again tissue-specific *daf-12* regulation (fig. S2). The transcriptional regulation of the *let-7s* is also reflected in the abundance of total mature microRNAs as measured by TaqMan fluorescence-based quantitative real-time polymerase chain reaction (QPCR). *daf-12* mutants and *daf-9;din-1* animals showed decreased levels compared with WT, whereas *daf-9* nulls showed tight repression of *let-7* family of microRNAs (Fig. 2P and figs. S3 to S5). As expected, expression in *daf-9*, *daf-9;din1*, but not *daf-12*, mutants was rescued by Δ^4-DA.

The dauer signaling pathways work upstream of *daf-12* to govern organismal developmental progression and Δ^4-DA production. We therefore wanted to see if *let-7s* expression was affected by dauer constitutive mutant backgrounds of *daf-7*–TGF-β, *daf-2*–insulin/IGF-I receptor, and *daf-9*–CYP450. *mir-241p::GFP* expression was nearly completely repressed in these dauer larvae, whereas *mir-84p::GFP* was down-regulated in some tissues, such as the pharynx (Fig. 3, A to D), but consistently up-regulated and more penetrant in others such as the seam (Fig. 3, E to H). Even in reproductively growing L3 larvae, seam cell expression was more penetrant in *daf-2*(*e1368*) and *daf-7*(*e1372*) mutants than in WT (Fig. 3G). Δ^4-DA supplementation largely reversed this effect in *daf-7*, but not in the *daf-2* background (Fig. 3, I to M), which suggests that insulin/IGF and TGF-β signaling distinctly regulate *mir-84p* expression in a Δ^4-DA–independent and Δ^4-DA–dependent manner.

The zinc finger protein *hbl-1* (hunchback) is responsible for L2 proliferative programs of seam cells (*11*). *hbl-1* loss leads to a loss of proliferative programs and, hence, a decreased seam cell number (table S1). *let-7s* are proposed to inhibit *hbl-1*, through microRNA-mediated repression of its 3′UTR, because *let-7s* mutants have both increased seam number and *hbl-1::GFP* expression at L3 (*11*, *20*). Given that DAF-12 activates *let-7s*, we examined interactions with *hbl-1*. Consistent with the notion that *hbl-1* inhibition is promoted by NHR signaling, *daf-12* mutants and *daf-9;din-1* double-mutants have extra seam cells, the latter reversed by Δ^4-DA (table S1). Moreover, the penetrant extra seam phenotype of the *daf-12*(*rh61*) ligand–binding domain mutant was dependent on functional *hbl-1*(+), placing *daf-12* upstream of *hbl-1* by genetic epistasis. Accordingly, we observed consistent up-regulated hypodermal expression of *hbl-1p::GFP::hbl-1*–3′UTR during L3 in *daf-12*(*rh61*), but not in WT (Fig. 4, A and B). This up-regulation was likely due to loss of UTR-mediated repression, as exchange of the *hbl-1*–3′UTR for a nonrepressed *unc-54*–3′UTR led to equal hypodermal expression levels in both WT and the *daf-12*(*rh61*) background (Fig. 4, C and D).

In this work, we show that the NHR DAF-12 directly regulates the *let-7* relatives, *mir-84* and *mir-241*, and connects organism-wide commitments to cell intrinsic programs (Fig. 4E). These studies suggest a model whereby, in unfavorable environments, down-regulated insulin/IGF-1 and TGF-β pathways suppress dafachronic acid production and DAF-12 without the ligand together with co-repressor DIN-1 repress microRNA expression in most tissues and specify developmental arrest. Conversely, in favorable environments, stimulation of insulin/IGF-1 and TGF-β growth signaling pathways results in dafachronic acid production. DAF-12 with the ligand activates *let-7* homologs, which, in turn, down-regulate their target, *hbl-1*, and allows L2 to L3 transitions in the hypodermis. The use of this NHR-microRNA–coupled molecular switch to turn off earlier programs to allow for later ones is a function likely to be conserved and may be a paradigm for understanding hormone-dependent developmental progression, stem cell differentiation, maturation, or tumor formation in metazoans. In particular, activation of new programs and inhibition of earlier ones are critical for the fidelity of distinct developmental states, which may be less apparent in more complex animals whose cell lineages are unknown. In fact, DAF-12 itself is down-regulated by *let-7* at later stages, which suggests that both feedforward and feedback loops drive transitions (*21*). In *Drosophila melanogaster*, the steroid hormone ecdysone and its cognate receptor regulate developmental progression in part via *mir-14*, but it is not known whether regulation is direct or indirect (*22*). Our studies also reveal the intricacy of NHR signaling in an organismal context. They give visible evidence that receptors with the ligand can activate their targets, whereas receptors without the ligand can repress them, with vastly different outcomes for progression or arrest. This hormone-dependent modulation of target gene expression around basal transcription mirrors that seen with the vertebrate homolog LXR (*23*). Finally, DAF-12–NHR regulation of the microRNAs is highly tissue- and stage-specific, implicating other transcription factors, coregulators, and chromatin factors in the control of microRNA expression.

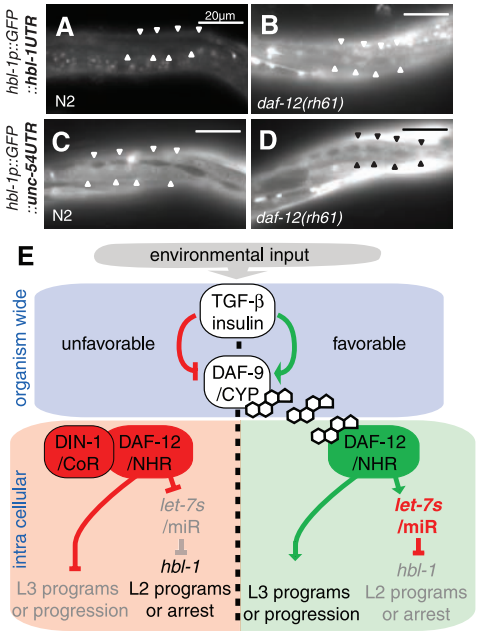

Fig. 4. *let-7s* repression target, *hbl-1*, is regulated by DAF-12. A GFP-fusion to *hbl-1* promoter and 3′UTR was repressed in the hypodermis at mid L3 (28 hours) in WT (**A**). In the *daf-12*(*rh61*) mutant, reporter signal was up-regulated in the hypodermis (arrows) and other tissues (**B**) (exposure 250 ms). A GFP-fusion to the *hbl-1* promoter, containing the *unc-54*–3′UTR lacked substantial up-regulation in the hypodermis (**C** and **D**), although body muscles showed modest reporter up-regulation (D) (exposure time 50 ms). (**E**) Model for NHR-microRNA signaling cascades (E). In response to favorable environmental signals, activated insulin/IGF and TGF-β pathways induce Δ^4-DA biosynthesis through DAF-9–CYP450. (Right) DAF-12 with the ligand activates L3 programs and expression of *let-7s* and thereby inhibits HBL-1 and genes of L2 programs, which result in developmental progression (E). (Left) During unfavorable conditions, DAF-12 without the ligand, together with DIN-1, repress L3 programs and *let-7s*, which allows derepression of L2 programs or developmental arrest. Dauer signaling also has Δ^4-DA–independent outputs onto microRNAs.

References and Notes

1. D. J. Mangelsdorf *et al.*, *Cell* **83**, 835 (1995).
2. A. Antebi, J. G. Culotti, E. M. Hedgecock, *Development* **125**, 1191 (1998).
3. A. Antebi, W. H. Yeh, D. Tait, E. M. Hedgecock, D. L. Riddle, *Genes Dev.* **14**, 1512 (2000).
4. D. L. Motola *et al.*, *Cell* **124**, 1209 (2006).
5. N. Fielenbach, A. Antebi, *Genes Dev.* **22**, 2149 (2008).
6. D. P. Bartel, *Cell* **116**, 281 (2004).
7. R. C. Lee, R. L. Feinbaum, V. Ambros, *Cell* **75**, 843 (1993).
8. B. Wightman, I. Ha, G. Ruvkun, *Cell* **75**, 855 (1993).
9. A. E. Rougvie, *Development* **132**, 3787 (2005).
10. M. Chalfie, H. R. Horvitz, J. E. Sulston, *Cell* **24**, 59 (1981).
11. A. L. Abbott *et al.*, *Dev. Cell* **9**, 403 (2005).
12. B. J. Reinhart *et al.*, *Nature* **403**, 901 (2000).
13. Materials and methods are available as supporting material on *Science* Online.
14. Y. Shostak, M. R. Van Gilst, A. Antebi, K. R. Yamamoto, *Genes Dev.* **18**, 2529 (2004).
15. A. Esquela-Kerscher *et al.*, *Dev. Dyn.* **234**, 868 (2005).
16. B. Gerisch, C. Weitzel, C. Kober-Eisermann, V. Rottiers, A. Antebi, *Dev. Cell* **1**, 841 (2001).
17. K. Jia, P. S. Albert, D. L. Riddle, *Development* **129**, 221 (2002).
18. A. H. Ludewig *et al.*, *Genes Dev.* **18**, 2120 (2004).
19. G. D. Hayes, A. R. Frand, G. Ruvkun, *Development* **133**, 4631 (2006).
20. M. Li, M. W. Jones-Rhoades, N. C. Lau, D. P. Bartel, A. E. Rougvie, *Dev. Cell* **9**, 415 (2005).
21. H. Grosshans, T. Johnson, K. L. Reinert, M. Gerstein, F. J. Slack, *Dev. Cell* **8**, 321 (2005).
22. J. Varghese, S. M. Cohen, *Genes Dev.* **21**, 2277 (2007).
23. J. J. Repa *et al.*, *Science* **289**, 1524 (2000).
24. Our thanks go to G. Hayes, G. Ruvkun, V. Ambros, and A. Rougvie for strains; N. Timchenko for gel shift support; and D. Magner, S. Greene, and F. Schroeder for manuscript comments. This work was supported by NIH grant GM077201 and the Ellison Medical Foundation (A.A.), and the Howard Hughes Medical Institute and the Robert A. Welch Foundation (D.J.M.).

Supporting Online Material

www.sciencemag.org/cgi/content/full/324/5923/95/DC1
Materials and Methods
Figs. S1 to S5
Tables S1 and S2
References

20 August 2008; accepted 11 February 2009
10.1126/science.1164899

Evidence for Cardiomyocyte Renewal in Humans

Olaf Bergmann,[1]* Ratan D. Bhardwaj,[1]* Samuel Bernard,[2] Sofia Zdunek,[1] Fanie Barnabé-Heider,[1] Stuart Walsh,[3] Joel Zupicich,[1] Kanar Alkass,[4] Bruce A. Buchholz,[5] Henrik Druid,[4] Stefan Jovinge,[3,6] Jonas Frisén[1]†

It has been difficult to establish whether we are limited to the heart muscle cells we are born with or if cardiomyocytes are generated also later in life. We have taken advantage of the integration of carbon-14, generated by nuclear bomb tests during the Cold War, into DNA to establish the age of cardiomyocytes in humans. We report that cardiomyocytes renew, with a gradual decrease from 1% turning over annually at the age of 25 to 0.45% at the age of 75. Fewer than 50% of cardiomyocytes are exchanged during a normal life span. The capacity to generate cardiomyocytes in the adult human heart suggests that it may be rational to work toward the development of therapeutic strategies aimed at stimulating this process in cardiac pathologies.

Myocardial damage often results in chronic heart failure due to loss and insufficient regeneration of cardiomyocytes. This has prompted efforts to devise cardiomyocyte replacement therapies by cell transplantation or by the promotion of endogenous regenerative processes. The development of cell transplantation strategies is advancing rapidly, and some are currently being evaluated in clinical trials (*1*, *2*). Stimulating endogenous regenerative processes is attractive as it potentially could provide a noninvasive therapy and circumvent the immunosuppression required for allografts. However, it is unclear whether such regenerative strategies are realistic because it has been difficult to establish whether cardiomyocytes can be generated after the perinatal period in humans.

Stem/progenitor cells with the potential to generate cardiomyocytes in vitro remain in the adult rodent and human myocardium (*3*, *4*). Moreover, mature cardiomyocytes have been suggested to be able to reenter the cell cycle and duplicate (*5*). However, studies over several decades in rodents with labeled nucleotide analogs have led to conflicting results, ranging from no to substantial generation of cardiomyocytes postnatally (*6*). A recent genetic labeling study, which enabled detection of cardiomyocyte generation by stem/progenitor cells (but not by cardiomyocyte duplication), demonstrated cardiomyocyte renewal after myocardial injury, but not during 1 year in the healthy mouse (*7*).

It is possible that humans, who live much longer than rodents, may have a different requirement for cardiomyocyte replacement. Cell turnover has been difficult to study in humans because the use of labeled nucleotide analogs and other strategies commonly used in experimental animals cannot readily be adapted for studies in humans owing to safety concerns. The limited functional recovery after loss of myocardium and the fact that primary cardiac tumors are very rare indicate limited proliferation within the adult human heart (*8*). Several studies have described the presence of molecular markers associated with mitosis in the human myocardium (*5*), but this provides limited information because it is difficult to deduce the future fate of a potentially dividing cell in terms of differentiation and long-term survival.

We have measured carbon-14 (^{14}C) from nuclear bomb tests in genomic DNA of human myocardial cells, which allows retrospective birth dating (*9*–*11*). ^{14}C concentrations in the atmosphere remained relatively stable until the Cold War, when aboveground nuclear bomb tests caused a sharp increase (*12*, *13*). Even though the detonations were conducted at a limited number of locations, the elevated amounts of ^{14}C in the atmosphere rapidly equalized around the world as $^{14}CO_2$. After the Limited Nuclear Test Ban Treaty in 1963, the ^{14}C concentrations dropped exponentially, not primarily because of radioactive decay (half-life of 5730 years), but by diffusion from the atmosphere (*14*). Newly created atmospheric ^{14}C reacts with oxygen to form $^{14}CO_2$, which is incorporated by plants through photosynthesis. Humans eat plants, and animals that live off plants, so the ^{14}C concentration in the human body mirrors that in the atmosphere at any given time (*15*–*18*). Because DNA is stable after a cell has gone through its last cell division, the concentration of ^{14}C in DNA serves as a date mark for when a cell was born and can be used to retrospectively birth date cells in humans (*9*–*11*).

We first carbon-dated left ventricle myocardial cells, including cardiomyocytes and other cell types, to determine the extent of postnatal DNA synthesis in the human heart. DNA was extracted, and ^{14}C concentrations were measured by accelerator mass spectrometry (see tables S1 and S2 for ^{14}C values and associated data). The cellular birth dates can be inferred by determining the time at which the sample's ^{14}C concentration corresponded to the atmospheric concentration (Fig. 1A). ^{14}C concentrations from all individuals born around or after the nuclear bomb tests corresponded to atmospheric concentrations several years after the subjects' birth (Fig. 1B), indicating substantial postnatal DNA synthesis. Analysis of individuals born before the period of nuclear bomb tests allows for sensitive detection of any turnover after 1955, due to the marked increase in ^{14}C concentrations. By analyzing individuals born at different times before 1955 it is possible to establish the age up to which DNA synthesis occurs, or whether it continues beyond that age.

[1]Department of Cell and Molecular Biology, Karolinska Institutet, SE-171 77 Stockholm, Sweden. [2]CNRS UMR5208, Institut Camille Jordan, Université Claude Bernard Lyon 1, 69622 Villeurbanne cedex, France. [3]Lund Strategic Research Center for Stem Cell Biology and Cell Therapy, Lund University, SE-221 84 Lund, Sweden. [4]Department of Forensic Medicine, Karolinska Institutet, SE-171 77 Stockholm, Sweden. [5]Center for Accelerator Mass Spectrometry, Lawrence Livermore National Laboratory, 7000 East Avenue, L-397, Livermore, CA 94551, USA. [6]Department of Cardiology, Lund University Hospital, SE-221 85 Lund, Sweden.

*These authors contributed equally to this work.
†To whom correspondence should be addressed. E-mail: jonas.frisen@ki.se

In all studied cases, born up to 22 years before the onset of the nuclear bomb tests, ^{14}C concentrations were elevated compared to the levels before the nuclear bomb tests (Fig. 1C). Thus, DNA of myocardial cells is synthesized many years after birth, indicating that cells in the human heart do renew into adulthood.

Because cardiomyocytes constitute only about 20% of all cells within the human myocardium (*19*), it is not possible to infer from these data whether there is postnatal renewal of cardiomyocytes, or whether cell turnover in the myocardium is limited to other cell populations. We therefore set out to specifically birth date cardiomyocytes. Many cardiomyocytes are binucleated, and it is difficult to distinguish a binucleated cell from two aggregating mononucleated cells (of which one could be a noncardiomyocyte) in the flow cytometer. Hence, rather than separating myocardial cells on the basis of cell surface or cytoplasmic markers, we developed a strategy to isolate cardiomyocyte nuclei by flow cytometry.

We found that the well-characterized cardiomyocyte-specific proteins cardiac troponin I (cTroponin I, also known as TNNI3) and cardiac troponin T (cTroponin T, also known as TNNT2) [for review, see (*20*)] have evolutionar-

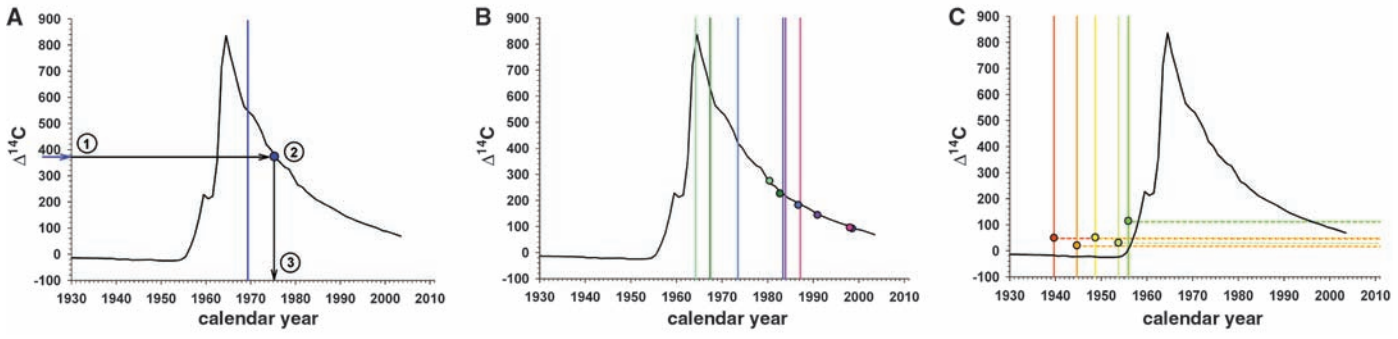

Fig. 1. Cell turnover in the heart. (**A**) Schematic figure demonstrating the strategy to establish cell age by ^{14}C dating. The black curve in all graphs shows the atmospheric concentrations of ^{14}C over the decades since 1930 [data from (*14*)]. The vertical bar indicates the date of birth of the individual. The measured ^{14}C concentration (1) is related to the atmospheric ^{14}C concentration by use of the established atmospheric ^{14}C bomb curve (2). The average birth date of the population can be inferred by determining where the data point intersects the *x* axis (3). ^{14}C concentrations in DNA of cells from the left ventricle myocardium in individuals born after (**B**) or before (**C**) the nuclear bomb tests correspond to time points substantially after the time of birth, indicating postnatal cell turnover. The vertical bar indicates the date of birth of each individual, and the similarly colored dots represent the ^{14}C data for the same individual. For individuals born before the increase in ^{14}C concentrations, it is not possible to directly infer an age because the measured concentration can be a result of ^{14}C incorporation during the rising and/or falling part of the atmospheric curve, and thus the concentration is indicated by a dotted horizontal line.

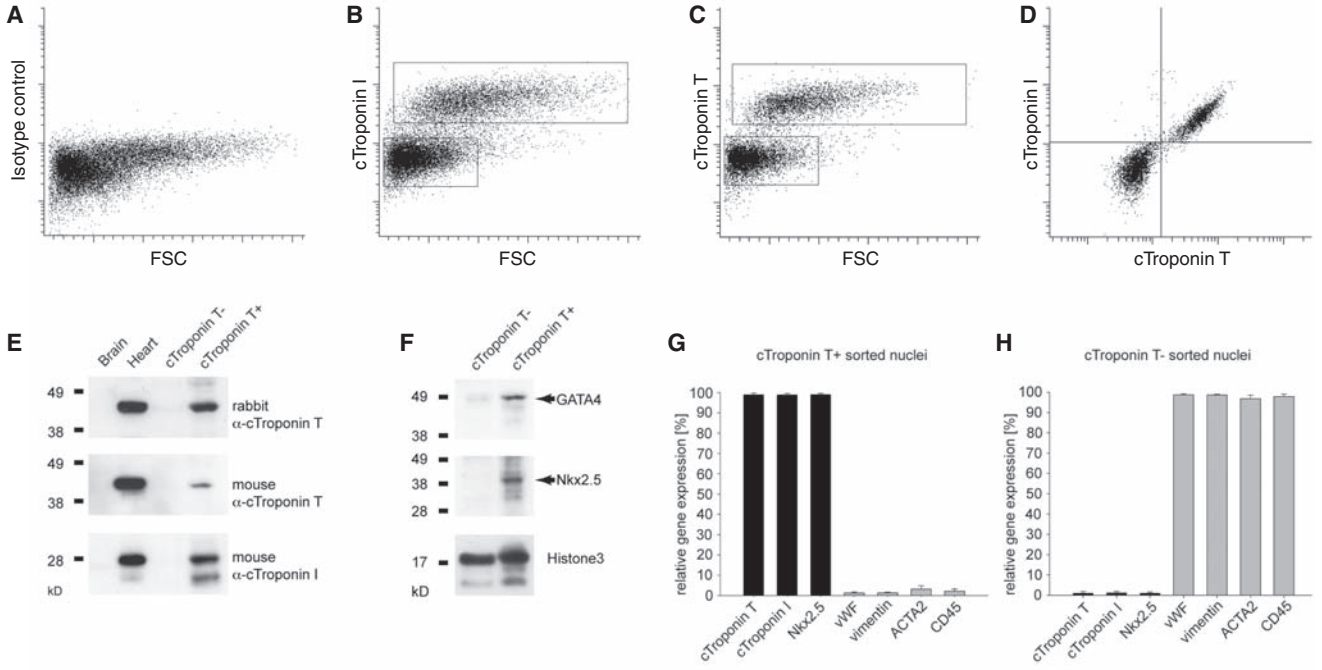

Fig. 2. Isolation of cardiomyocyte nuclei. (**A** to **C**) Flow cytometric analysis of cardiomyocyte nuclei from the left ventricle of the human heart with an isotype control antibody or antibodies to the cardiomyocyte-specific antigens cTroponin I or T. Boxes denote the boundaries for the positive and negative sorted populations. (**D**) cTroponin I and T are present in the same subpopulation of heart cell nuclei. (**E**) Western blot analysis of flow cytometry–isolated nuclei demonstrates nearly all detectable cTroponin T (analyzed with two different antibodies) and I protein in the cTroponin T–positive fraction. Brain and heart tissue were used as negative and positive controls, respectively. (**F**) The cardiac troponin T–positive population is enriched for the cardiomyocyte-specific transcription factors Nkx2.5 and GATA4. Both fractions contain similar amounts of the nuclear protein histone 3 (loading control). (**G**) Gene expression analysis of flow cytometry–isolated nuclei shows high expression of cardiomyocyte-specific genes in the cTroponin T–positive fraction (cTroponin I and T, Nkx2.5), whereas marker genes for endothelial cells (vWF), fibroblasts (vimentin), smooth muscle (ACTA2), and leukocytes (CD45) are highly expressed in the cTroponin T–negative fraction (**H**). Bars in (G) and (H) show the average from three independent experiments (±SD).

ily conserved nuclear localization signals and are partly localized in the nuclei of cardiomyocytes (figs. S1 and S2). Antibodies to cTroponin I and T identify the same subpopulation of nuclei in the myocardium (Fig. 2, A to D), and retrospective birth dating of nuclei isolated with antibodies against either epitope gave similar results (table S1). Western blot and quantitative reverse transcription polymerase chain reaction analysis of sorted nuclei demonstrated a high enrichment of cTroponin I and T in the positive fraction and a depletion in the negative, validating the efficiency of the strategy (Fig. 2, E to H). We assessed the potential transfer of cTroponin I and T during tissue processing by mixing cardiac tissue with another tissue devoid of these proteins, and found that there was negligible transfer of cTroponin I or T to noncardiomyocyte nuclei during tissue dissociation, nuclear preparation, or flow cytometric sorting (fig. S2).

We assessed the specificity of the isolation procedure with known cardiomyocyte-specific markers and markers of noncardiomyocytes present in the myocardium. There was a high enrichment of nuclei containing the known cardiomyocyte-specific nuclear markers Nkx2.5 and GATA4 in the cTroponin-positive fraction, with little contamination of nuclei expressing markers for fibroblasts, smooth muscle cells, endothelial cells, or hematopoietic cells (Fig. 2, F to H). Conversely, cardiomyocyte markers were depleted in the cTroponin-negative fraction (Fig. 2, F to H), indicating that nearly all cardiomyocytes were isolated in the positive fraction. Sorting whole cells with antibodies to a nonnuclear cardiomyocyte-specific epitope confirmed that nuclear cTroponin I and T are specific to cardiomyocytes, but resulted in lower purity compared to sorting nuclei (fig. S3). Flow cytometric reanalysis of all sorted samples demonstrated a DNA content-corrected cardiomyocyte purity of 96 ± 1.8% (mean ± SD; table S1 and fig. S4). Thus, flow cytometry with antibodies against cTroponin I or T allows specific isolation of cardiomyocyte and noncardiomyocyte nuclei.

We extracted DNA from cardiomyocyte nuclei [$(5 \pm 2) \times 10^7$, mean ± SD] and measured the ^{14}C concentration in genomic DNA. By analyzing the ^{14}C concentration also in unsorted myocardial nuclei ($>10^8$), we mathematically compensated for any contamination in the cardiomyocyte fraction in the individual cases, reducing the risk that contamination with a cell population with a different turnover rate would skew the result for cardiomyocytes. In all individuals born before the onset of the nuclear bomb tests, the ^{14}C concentrations in cardiomyocyte genomic DNA were higher than the pre-bomb atmospheric concentrations, demonstrating DNA synthesis after 1955 (Fig. 3A). Similarly, in all individuals born near or after the time of the nuclear bomb tests, the ^{14}C concentrations in cardiomyocyte DNA corresponded to the concentrations several years after their birth, establishing postnatal cardiomyocyte DNA synthesis (Fig. 3B).

There is no increase in the number of cardiomyocytes after the postnatal period but rather a slow, continuous decrease with age (*21*). About 25% of cardiomyocytes are binucleated in humans at birth, and this proportion stays constant throughout life (*22*). Thus, the postnatal cardiomyocyte DNA synthesis detected by ^{14}C analysis cannot be explained by an increase in cardiomyocyte number or binucleation. However, the heart grows during childhood, as the increasing demand of contractile capacity is met by hypertrophy of cardiomyocytes. Almost all cardiomyocyte nuclei are diploid at the time of birth, but the DNA of most nuclei is duplicated to become tetraploid in childhood when the cells undergo hypertrophy (Fig. 3C and fig. S5) (*23*–*25*). After the age of 10, there is no further increase in the DNA content of cardiomyocyte nuclei (R = 0.135, P = 0.384, Fig. 3C). The DNA synthesis associated with polyploidization of cardiomyocyte DNA results in incorporation of ^{14}C concentrations corresponding to the atmospheric levels during childhood.

Three of the individuals born before the nuclear bomb tests were more than 10 years old at the onset of the increase in atmospheric ^{14}C. That their ^{14}C concentration in cardiomyocyte DNA was above the prenuclear bomb test levels (Fig. 3A) cannot be explained by DNA synthesis associated with polyploidization, but indicates cardiomyocyte renewal after 1955. Moreover, in the individuals born after the nuclear bomb tests, the difference between the birth date of the person and the date corresponding to the ^{14}C concentration in cardiomyocyte DNA increased with the age of the individual (fig. S6 and table S1), demonstrating that cardiomyocyte DNA synthesis is not restricted to a limited period in childhood but continues in adulthood.

Polyploidization of cardiomyocyte DNA occurs in a stereotypical manner during a rather short period in childhood (Fig. 3C) (*23*–*25*), making it possible to calculate its impact on ^{14}C values in each individual [see supporting online text and (*26*)]. By subtracting the childhood polyploidization-associated ^{14}C incorporation from the measured value in each case, we could estimate polyploidization-independent ^{14}C values. In all cases, the polyploidization-independent ^{14}C values corresponded to time points after birth for each individual (Fig. 3D), indicating cardiomyocyte renewal. In the five oldest individuals, who all were born before or at the onset of the nuclear bomb tests, the ^{14}C values were lower than contemporary values (Fig. 3D), establishing that not all cardiomyocytes had been exchanged after 1955 but that a substantial fraction remains from early in life, even in the elderly.

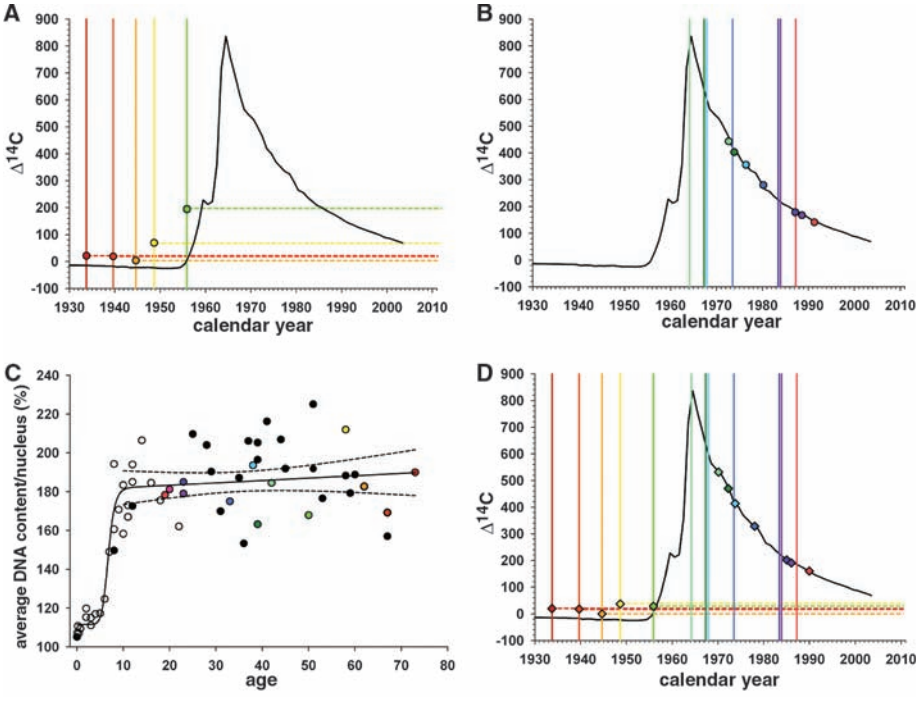

Fig. 3. Cardiomyocyte turnover in adulthood. (**A**) The ^{14}C concentrations in cardiomyocyte DNA from individuals born before the time of the atmospheric radiocarbon increase correspond to time points after the birth of all individuals. The vertical bar indicates year of birth, with the correspondingly colored data point indicating the $\Delta^{14}C$ value. (**B**) ^{14}C concentrations in cardiomyocyte DNA from individuals born after the time of the nuclear bomb test. (**C**) Average DNA content ($2n$ = 100%) per cardiomyocyte nucleus from individuals (without severe heart enlargement; see fig. S5) of different ages. Ploidy was measured by flow cytometry. Colored data points identify individuals analyzed for ^{14}C (n = 13). Black data points are from individuals analyzed only with regard to ploidy level (n = 23), and white data points are taken from Adler *et al*. (n = 26) (*24*, *26*). The dashed lines indicate the 95% confidence interval for the regression curve. (**D**) ^{14}C values corrected for the physiologically occurring polyploidization of cardiomyocytes during childhood for individuals born before and after the bomb-induced spike in ^{14}C concentrations, calculated on the basis of the individual average DNA content per cardiomyocyte nucleus. The ^{14}C content is not affected in individuals where the polyploidization occurred before the increase in atmospheric ^{14}C concentrations.

Increased cardiac workload in pathological situations often results in cardiomyocyte hypertrophy and heart enlargement, and at late stages can result in polyploidization in adulthood (fig. S5) (*24*). Although a few subjects had cardiac pathology (table S2), none had severe heart enlargement nor a pathological cardiomyocyte ploidy profile, and there was no significant difference in ^{14}C integration in cardiomyocyte DNA in the subjects with cardiac pathology (table S1, Fig. 3C, and fig. S5). Moreover, mathematical modeling of the kinetics of DNA synthesis and ^{14}C integration showed that the measured ^{14}C concentrations in cardiomyocyte DNA could not be a result of polyploidization during adulthood (see supporting online text). Furthermore, analysis of ^{14}C concentrations in DNA from only diploid or only polyploid cardiomyocyte nuclei demonstrated similar degrees of ^{14}C integration after childhood in both compartments, providing further evidence for cardiomyocyte renewal independently of polyploidization (see supporting online text, fig. S7, and table S3).

Several studies of sex-mismatched transplant recipients have indicated fusion of human cardiomyocytes with other cells (*27*). However, fusion appears to mainly occur transiently after transplantation, and even in the acute phase the fusion rate is too low to explain the ^{14}C data (fig. S8). DNA damage and repair are very limited in differentiated cells (*28*) and, at least in neurons, are well below the detection limit of the method used (*10*, *11*). Although cell fusion and DNA repair may affect ^{14}C concentrations in cardiomyocyte DNA, available data suggest that the magnitude of these processes makes them negligible in the current context and that the ^{14}C data we report here (after compensation for polyploidization) likely accurately reflects cell renewal.

Mathematical modeling of ^{14}C data from individuals born both before and after the nuclear bomb tests, which provides slightly different and complementary information, as well as of subjects of different age within these groups, can provide an integrated view on cell turnover (*9*). We used an analytical model that includes polyploidization in childhood to assess which one of many scenarios for cell birth and death best describes the data. Times at which cells are born, ploidize, and die are tracked. The atmospheric ^{14}C values corresponding to DNA synthesis events are integrated to yield a calculated ^{14}C level, on the basis of each subject's birth date, age at death, and DNA content. The calculated ^{14}C levels were fitted to the purity-corrected values to find the best renewal rates for each scenario (see supporting online text for a comprehensive description of the modeling). We first calculated what the annual turnover rate would be in each individual if the rate was constant throughout life. This indicated annual turnover rates of 0.2 to 2% (Fig. 4A). However, there was a clear negative correlation to age ($R = -0.84$; $P = 0.001$), establishing that the turnover rate declines with age. The strong negative correlation to age also indicates that there is limited interindividual variation in the cardiomyocyte turnover rate and its decrease with age.

We next tested a series of different models allowing turnover rates to change with age. The best fit was found with an inverse-linear declining turnover rate (Fig. 4B), in which younger cardiomyocytes were more likely than older ones to be replaced (see supporting online text). This model predicts that cardiomyocytes are renewed at a rate of ~1% per year at the age of 25 and 0.45% at the age of 75 (Fig. 4B). With this turnover rate, most cardiomyocytes will never be exchanged during a normal life span (Fig. 4C). At the age of 50, 55% of the cardiomyocytes remain from the time around birth and 45% have been generated later (Fig. 4C). The age of cardiomyocytes is on average 6 years younger than the individual (Fig. 4D). The ^{14}C data indicate a substantially higher renewal rate for noncardiomyocytes, with a median annual turnover of 18% and a mean age of 4.0 years (see supporting online text). Our data do not allow us to identify whether new cardiomyocytes derive from cardiomyocyte duplication or from a stem/progenitor pool, because both would result in similar ^{14}C integration in DNA.

Analysis of cell proliferation in the human myocardium has previously indicated a cardiomyocyte proliferation rate that could result in the exchange of all cardiomyocytes within 5 years (*29*), but the ^{14}C concentrations in DNA exclude such a high mitotic renewal rate. We asked whether cardiomyocytes may be heterogeneous, with an identifiable subpopulation turning over relatively fast and the rest not turning over at all. This scenario is incompatible with the data, and it is most likely that the vast majority of cardiomyocytes have a similar probability of being exchanged at a given age (see supporting online text).

The limited functional recovery in humans after myocardial injury clearly demonstrates insufficient regeneration of cardiomyocytes. The renewal of cardiomyocytes, indicated by the continuous integration of ^{14}C, suggests that the development of pharmacological strategies to stimulate this process may be a rational alternative or complement to cell transplantation strategies for cardiomyocyte replacement.

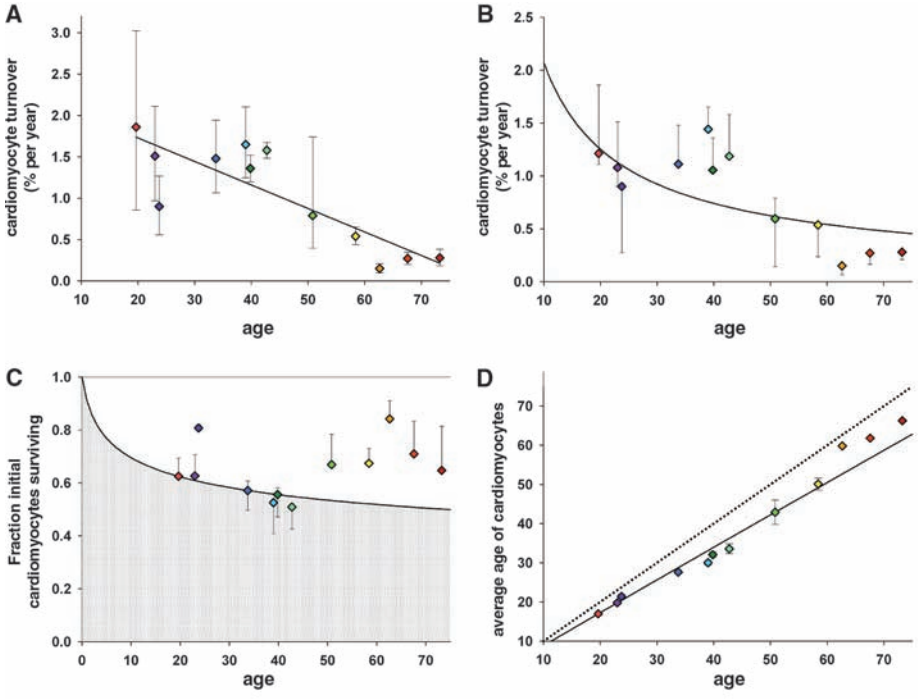

Fig. 4. Dynamics of cardiomyocyte turnover. (**A**) Individual data fitting assuming a constant turnover (see supporting online text) reveals an almost linear decline of cardiomyocyte turnover with age ($R = -0.84$; $P = 0.001$). A constant-turnover hypothesis might therefore not represent the turnover dynamics accurately. (**B**) Global fitting of all data points (see supporting online text, error sum of squares = 1.2×10^4) shows an age-dependent decline of cardiomyocyte turnover. (**C**) The gray area depicts the fraction of cardiomyocytes remaining from birth, and the white area is the contribution of new cells. Estimate is from the best global fitting. (**D**) Cardiomyocyte age estimates from the best global fitting. The dotted line represents the no-cell-turnover scenario, where the average age of cardiomyocytes equals the age of the individual. The black line shows the best global fitting. Colored diamonds indicate computed data points from ^{14}C-dated subjects. Error bars in (A) are calculated from the errors on ^{14}C measurements. Error bars in all other graphs are calculated for each subject individually and show the interval of possible values fitted with the respective mathematical scenario.

References and Notes

1. R. Passier, L. W. van Laake, C. L. Mummery, *Nature* **453**, 322 (2008).
2. M. A. Laflamme, C. E. Murry, *Nat. Biotechnol.* **23**, 845 (2005).
3. S. Martin-Puig, Z. Wang, K. R. Chien, *Cell Stem Cell* **2**, 320 (2008).
4. S. M. Wu, K. R. Chien, C. Mummery, *Cell* **132**, 537 (2008).
5. P. Anversa, B. Nadal-Ginard, *Nature* **415**, 240 (2002).

6. M. H. Soonpaa, L. J. Field, *Circ. Res.* **83**, 15 (1998).
7. P. C. Hsieh *et al.*, *Nat. Med.* **13**, 970 (2007).
8. J. Butany *et al.*, *Lancet Oncol.* **6**, 219 (2005).
9. K. L. Spalding *et al.*, *Nature* **453**, 783 (2008).
10. R. D. Bhardwaj *et al.*, *Proc. Natl. Acad. Sci. U.S.A.* **103**, 12564 (2006).
11. K. Spalding, R. D. Bhardwaj, B. Buchholz, H. Druid, J. Frisén, *Cell* **122**, 133 (2005).
12. H. De Vries, *Science* **128**, 250 (1958).
13. R. Nydal, K. Lovseth, *Nature* **206**, 1029 (1965).
14. I. Levin, B. Kromer, *Radiocarbon* **46**, 1261 (2004).
15. K. L. Spalding, B. A. Buchholz, L.-E. Bergman, H. Druid, J. Frisén, *Nature* **437**, 333 (2005).
16. W. F. Libby, R. Berger, J. F. Mead, G. V. Alexander, J. F. Ross, *Science* **146**, 1170 (1964).
17. D. D. Harkness, *Nature* **240**, 302 (1972).
18. E. M. Wild *et al.*, *Nucl. Instrum. Methods Phys. Res. B* **172**, 944 (2000).
19. M. Rubart, L. J. Field, *Annu. Rev. Physiol.* **68**, 29 (2006).
20. M. S. Parmacek, R. J. Solaro, *Prog. Cardiovasc. Dis.* **47**, 159 (2004).
21. G. Olivetti, M. Melissari, J. M. Capasso, P. Anversa, *Circ. Res.* **68**, 1560 (1991).
22. G. Olivetti *et al.*, *J. Mol. Cell. Cardiol.* **28**, 1463 (1996).
23. V. Brodsky, D. S. Sarkisov, A. M. Arefyeva, N. W. Panova, I. G. Gvasava, *Virchows Arch.* **424**, 429 (1994).
24. C. P. Adler, in *The Development and Regenerative Potential of Cardiac Muscle,* J. O. Oberpriller, J. C. Oberpriller, A. Mauro, Eds. (Harwood, New York, 1991), pp. 227–252.
25. P. Pfitzer, *Curr. Top. Pathol.* **54**, 125 (1971).
26. Materials and methods are available as supporting material on *Science* Online.
27. M. A. Laflamme, D. Myerson, J. E. Saffitz, C. E. Murry, *Circ. Res.* **90**, 634 (2002).
28. T. Nouspikel, P. C. Hanawalt, *DNA Repair (Amst.)* **1**, 59 (2002).
29. A. P. Beltrami *et al.*, *N. Engl. J. Med.* **344**, 1750 (2001).

30. We thank R. Lee, K. Spalding, and members of the Frisén lab for valuable discussions; M. Toro and K. Hamrin for help with flow cytometry; P. Reimer for assistance with radiocarbon interpretation; R. Cassidy, M. Müller, and E. Klaile for technical advice; M. Stahlberg and T. Bergman for help with high-performance liquid chromatography; and D. Kurdyla and P. Zermeno for producing graphite. This study was supported by grants from the Swedish Heart-Lung Foundation, the Swedish Research Council, Knut och Alice Wallenbergs Stiftelse, Human Frontiers Science Program, the Swedish Cancer Society, the Foundation for Strategic Research, the Karolinska Institutet, the Juvenile Diabetes Research Foundation, NIH/NCRR (RR13461), European Commission FP7 CardioCell, and the Tobias Foundation. This work was performed in part under the auspices of the U.S. Department of Energy by Lawrence Livermore National Laboratory under contract DE-AC52-07NA27344. R.D.B. and F.B.-H. were supported by fellowships from the Canadian Institutes of Health Research, and F.B.-H. was also supported by a fellowship from the Christopher and Dana Reeve Foundation.

Supporting Online Material

www.sciencemag.org/cgi/content/full/324/5923/98/DC1
Materials and Methods
SOM Text
Figs. S1 to S8
Tables S1 to S3
References

14 August 2008; accepted 29 January 2009
10.1126/science.1164680

S-Nitrosylation of Drp1 Mediates β-Amyloid–Related Mitochondrial Fission and Neuronal Injury

Dong-Hyung Cho,[1]*† Tomohiro Nakamura,[1]* Jianguo Fang,[1] Piotr Cieplak,[2] Adam Godzik,[2] Zezong Gu,[1]‡ Stuart A. Lipton[1]§

Mitochondria continuously undergo two opposing processes, fission and fusion. The disruption of this dynamic equilibrium may herald cell injury or death and may contribute to developmental and neurodegenerative disorders. Nitric oxide functions as a signaling molecule, but in excess it mediates neuronal injury, in part via mitochondrial fission or fragmentation. However, the underlying mechanism for nitric oxide–induced pathological fission remains unclear. We found that nitric oxide produced in response to β-amyloid protein, thought to be a key mediator of Alzheimer's disease, triggered mitochondrial fission, synaptic loss, and neuronal damage, in part via S-nitrosylation of dynamin-related protein 1 (forming SNO-Drp1). Preventing nitrosylation of Drp1 by cysteine mutation abrogated these neurotoxic events. SNO-Drp1 is increased in brains of human Alzheimer's disease patients and may thus contribute to the pathogenesis of neurodegeneration.

Disrupting the balance between mitochondrial fission and fusion can lead to excessive mitochondrial fragmentation. Fragmentation triggered by dysfunction of the fission-inducing protein Drp1 (dynamin-related protein 1), for example, contributes to synaptic damage and subsequent neuronal loss because of nitrosative/oxidative stress and impaired bioenergetics (*1*–*6*). Excessive fission results in abnormally small mitochondria with fragmented cristae (*2*), as observed in electron microscopy studies of neurons in human Alzheimer's disease (AD) (*7*). Drp1 homologs are S-nitrosylated, which regulates their activity (*8*, *9*). Furthermore, β-amyloid protein (Aβ) oligomers induce excessive mitochondrial fission and neuronal damage in a nitric oxide (NO)–mediated fashion (*2*, *10*). We sought to determine whether Drp1 is S-nitrosylated and thereby activated in AD.

Cerebrocortical neurons transfected with the mitochondrial marker mito-DsRed2 were exposed to the NO donor *S*-nitrosocysteine (SNOC) (*11*) and morphological changes in mitochondria were monitored by 3D-deconvolution fluorescence microscopy (*2*). Mitochondria normally displayed an elongated filamentous morphology, but addition of SNOC induced fragmented, smaller mitochondria in a dose-dependent manner, due to fission (Fig. 1, A and B) (*2*, *11*). Using a biotin-switch assay (*12*), we found that SNOC induced S-nitrosylation of Drp1 (forming SNO-Drp1) in neurons before inducing fission (Fig. 1C).

To investigate whether endogenously generated NO can induce SNO-Drp1, we used human embryonic kidney (HEK) 293 cells stably expressing neuronal NO synthase (nNOS). These cells were subjected to biotin-switch assay after incubation with the calcium ionophore A23187 to activate nNOS. Endogenous Drp1 was S-nitrosylated by endogenous NO; this reaction was blocked by the NOS inhibitor *N*-nitro-L-arginine (NNA; Fig. 2, A and B). SNO-Drp1 was not detected in controls performed without ascorbate to remove NO, thus preventing replacement of NO by biotin (which is detected in this assay), or without biotin-HPDP (*N*-[6-(biotinamido)hexyl]-3′-(2′-pyridyldithio)-propionamide).

Using the same conditions under which Aβ causes mitochondrial fragmentation and consequent neuronal damage (*2*), we found that Aβ could induce SNO-Drp1 formation. Cerebrocortical neurons were exposed to oligomers of the pathologically active fragment Aβ25-35 or, as a control, reverse-sequence Aβ35-25. Formation of SNO-Drp1 was observed only in Aβ25-35–treated neurons, not in the control (Fig. 2C). Additionally, we tested the effect of endogenously produced Aβ, generated from amyloid precursor protein (APP) in conditioned medium of N2a/APP695 stable neuronal cell lines or CHO cells stably expressing human APP with the $Val^{717} \rightarrow Phe$ mutation (designated 7PA2 cells). Exposing N2a cells to SNOC or conditioned medium resulted in SNO-Drp1 formation (Fig. 2C). We also found elevated levels of SNO-Drp1 in vivo in brains of the AD transgenic mouse model Tg2576, which expresses high levels of the Swedish APP mutation ($Lys^{670} \rightarrow Asn$, $Met^{671} \rightarrow Leu$) (fig. S1).

To extend these findings to humans, we examined brains obtained shortly after death from patients manifesting AD (table S1). We found increased SNO-Drp1 levels in 17 of 17 AD brains studied, but not in brains of deceased Parkinson's disease patients or controls who died of non-CNS causes (Fig. 2, D and E, and fig. S2). To determine whether the level of SNO-Drp1 in AD human

[1]Center for Neuroscience, Aging, and Stem Cell Research, Burnham Institute for Medical Research, 10901 North Torrey Pines Road, La Jolla, CA 92037, USA. [2]Bioinformatics and Systems Biology Program, Burnham Institute for Medical Research, 10901 North Torrey Pines Road, La Jolla, CA 92037, USA.

*These authors contributed equally to this work.
†Present address: Asan Medical Center, University of Ulsan College of Medicine, 388-1 Poongnap-2-dong Songpa-gu, Seoul 138-736, Korea.
‡Present address: University of Missouri–Columbia School of Medicine, Columbia, MO 65212, USA.
§To whom correspondence should be addressed. E-mail: slipton@burnham.org

brains is of pathophysiological importance, we used a technique to calculate the ratio of SNO-Drp1 (determined by biotin-switch assay) to total Drp1 (from immunoblots) (*13*). This ratio was comparable to that encountered in our cell-based models manifesting excessive mitochondrial fission and neuronal damage (Fig. 2E), consistent with the notion that pathophysiologically relevant amounts of SNO-Drp1 are present in human AD brains. Thus, SNO-Drp1 can potentially serve as a biomarker for AD.

We next sought to identify the target cysteine residue for S-nitrosylation on Drp1. Sequence alignment of Drp1 revealed four distinct structural domains: an N-terminal guanosine triphosphatase (GTPase) domain, a dynamin-like middle domain, an insert B domain, and a C-terminal GTPase effector domain (GED). The GED affects both GTPase activity and Drp1 dimer formation (*14*). In search of S-nitrosylated cysteine residue(s), we mutated each of the nine Drp1 cysteines. To assess S-nitrosylation, we performed a chemical assay using 2,3-diaminonaphthalene (DAN) on immunoprecipitates from HEK293 cells transfected with wild-type or mutant Drp1. This assay monitors release of NO from thiol by conversion of DAN to fluorescent 2,3-naphthyltriazole (NAT). Among the cysteine mutants, only C644A (Cys^{644} → Ala), located in the GED domain, decreased SNO-Drp1 formation (Fig. 3A). Cys^{644} was confirmed as the S-nitrosylated residue by biotin-switch assay.

A23187 exposure, to activate nNOS and produce endogenous NO, resulted in SNO-Drp1 formation, which was virtually eliminated in Drp1 (C644A) but not other cysteine mutant cells (Fig. 3B). Thus, Cys^{644} was essential for SNO-Drp1 generation. We then constructed an atomic model of Drp1 based on comparative homology using the structure of bacterial dynamin-like protein (PDB ID: 2J68-A) (*15*). With the software program MODELLER, we found that the Drp1-GED domain contains a consensus motif for S-nitrosylation flanking Cys^{644} (Fig. 3C) (*16*). Homology modeling also predicted that Cys^{644} is exposed to the protein surface, increasing its accessibility to NO and thus facilitating nitrosylation.

Dimer formation of the homologous protein dynamin, a process influenced by residues in the GED domain, increases dynamin GTPase activity (*14*, *17*). We tested whether NO could induce dimer formation of Drp1 and influence its GTPase activity. The Drp1-GED domain is critical for inter- and intramolecular interactions and GTPase activity (*14*, *18*). Indeed, S-nitrosylation of Cys^{644} in the GED domain led to dimerized SNO-Drp1 (Fig. 4A and fig. S3) and increased GTPase activity (Fig. 4B). In contrast, NO failed to induce dimerization/oligomerization or to increase GTPase activity of the Drp1(C644A) mutant. For this experiment, we measured GTPase activity of purified wild-type or mutant Drp1 proteins after exposure to SNOC or control solutions by monitoring absorbance at 635 nm, representing hydrolysis of GTP by GTPase. The GTPase activity of Drp1(C644A) protein was as reduced as that of dominant-negative Drp1 with a Lys^{38} → Ala mutation [DN-Drp1(K38A)] (*1*, *2*), consistent with the notion that S-nitrosylation of Drp1 at residue Cys^{644} increases its GTPase activity.

We then superimposed the atomic-resolution model for Drp1 onto a lower-resolution 3D reconstruction representing dimerization of the homologous dynamin molecule (Fig. 4C) (*19*). Superimposition allowed us to examine the potential effect of NO on Drp1 domain structure. This suggested that NO-induced dimerization triggered a conformation change in the stalk region, composed of the GED and middle domains, thereby regulating GTPase activity analogous to dynamin dimerization (*19*).

We next examined the effect of S-nitrosylation of Drp1 on mitochondrial fragmentation. An intact Drp1-GTPase domain is required for mitochondrial fission or fragmentation. Knockdown of Drp1 by RNA interference or mutation producing DN-Drp1(K38A), located in the GTPase domain, inhibits excessive mitochondrial fragmentation

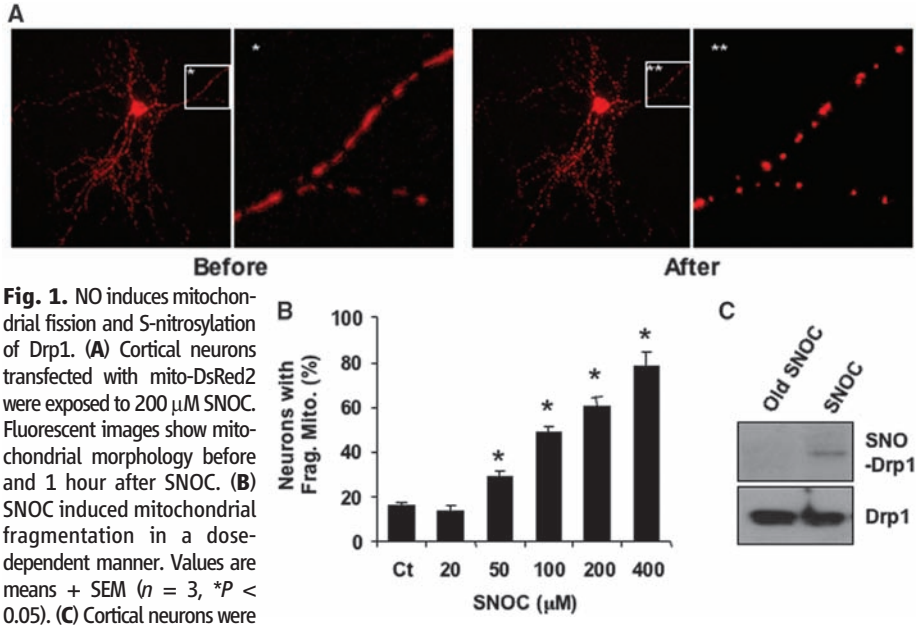

Fig. 1. NO induces mitochondrial fission and S-nitrosylation of Drp1. (**A**) Cortical neurons transfected with mito-DsRed2 were exposed to 200 μM SNOC. Fluorescent images show mitochondrial morphology before and 1 hour after SNOC. (**B**) SNOC induced mitochondrial fragmentation in a dose-dependent manner. Values are means + SEM (n = 3, *P < 0.05). (**C**) Cortical neurons were exposed to SNOC or decayed (old) SNOC for <15 min and subjected to biotin-switch assay.

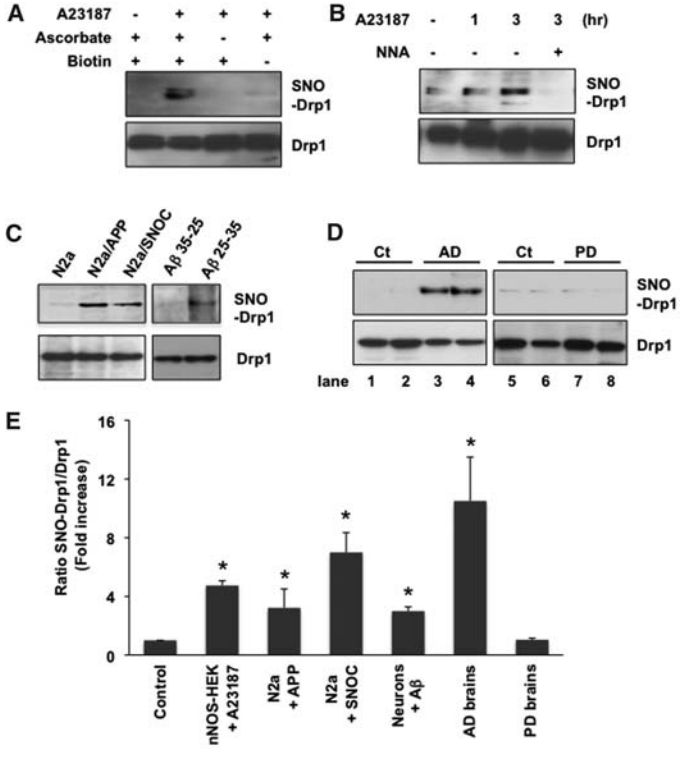

Fig. 2. SNO-Drp1 formation in vitro and in vivo. (**A** and **B**) Biotin-switch assay of nNOS-HEK293 cells activated with A23187 for 1 to 3 hours. (**C**) SNO-Drp1 formation by biotin-switch assay in neuronal cells. Left: N2a/APP695 cells were harvested after 30 hours in conditioned medium containing endogenously secreted Aβ soluble oligomers or 30 min after SNOC exposure. Right: Cortical neurons were exposed to 10 μM Aβ25-35 or control Aβ35-25 for 6 hours. (**D**) SNO-Drp1 detection in vivo by biotin-switch assay of representative human post-mortem control (Ct), AD, or Parkinson's disease (PD) brains. (**E**) Relative amounts of SNO-Drp1 formation. Biotin-switch assays and immunoblot analyses were quantified by densitometry, and the relative ratio of SNO-Drp1 to total Drp1 was calculated for all samples. Values are means + SEM ($n \geq 4$ for each group, *P < 0.02).

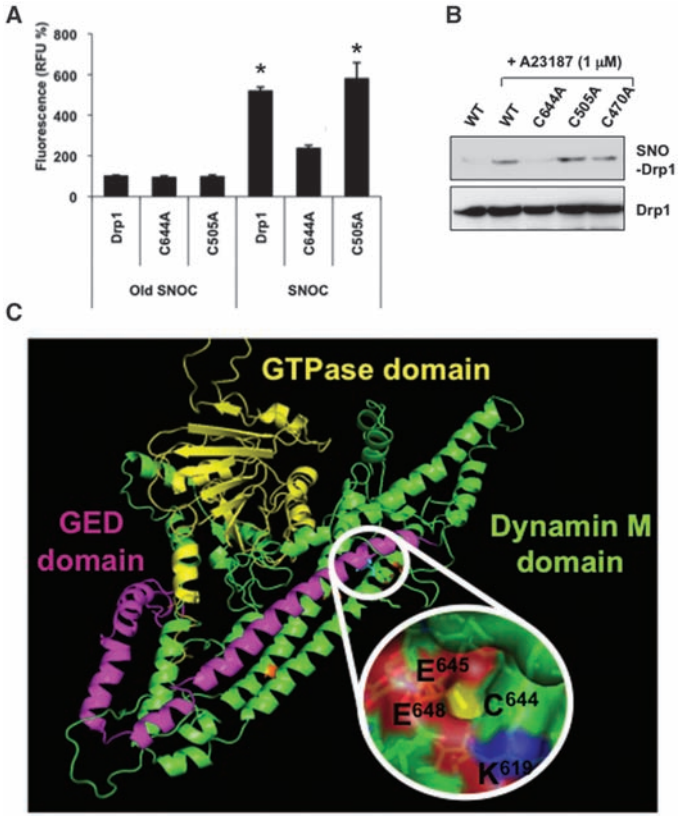

Fig. 3. S-Nitrosylation of Cys^{644} in Drp1. (**A**) HEK293 cells transiently transfected with green fluorescent protein (GFP)–fused constructs for wild-type or representative cysteine mutant Drp1 were exposed to SNOC, lysed, and subjected to immunoprecipitation with antibody to GFP. Precipitated Drp1 was analyzed for S-nitrosylation with the DAN assay by monitoring NO release spectrofluorometrically in relative fluorescence units (RFU). Values are means + SEM ($n = 3$, $^*P < 0.01$). (**B**) nNOS-HEK293 cells transfected with GFP-fused constructs for wild-type (WT) or representative cysteine mutant Drp1 were exposed to A23187 and subjected to biotin-switch assay. (**C**) Homology modeling of Drp1 atomic structure: Predicted ribbon structure of human Drp1 showing putative acid/base S-nitrosylation motif around Cys^{644}. Yellow, GTPase domain; green, middle (M) domain; magenta, GED domain; C, Cys; E, Glu; K, Lys.

(*1*, *2*, *20*). Because nitrosylation of Drp1 in the GED domain activates GTPase activity, we reasoned that SNO-Drp1 should activate mitochondrial fission. In cortical neurons, NO induced mitochondrial fragmentation (*2*, *21*), and overexpression of wild-type Drp1 slightly enhanced this effect (Fig. 4D). In contrast, expression of Drp1(C644A) or DN-Drp1(K38A) abrogated NO-mediated mitochondrial fission. Among the nine possible Drp1-cysteine mutants, only C644A suppressed NO-induced mitochondrial fragmentation (figs. S4 and S5), consistent with the observation that Cys^{644} was the predominant Drp1 nitrosylation site. As a control, Drp1(C644A) did not act as a dominant negative to decrease Drp1-mediated mitochondrial fission that was not triggered by NO (fig. S6).

Mitochondrial fragmentation induced by NO or Aβ contributes to neuronal cell injury or death and is abrogated by DN-Drp1(K38A) (*2*, *21*). Because SNO-Drp1 formation was induced here by Aβ, we next examined the effect of nitrosylation of Drp1 on neurotoxicity. Exposure to NO triggers neuronal damage or death in the presence of wild-type Drp1 (*2*, *21*). However, expression of Drp1(C644A) largely protected the neurons (Fig. 4E), consistent with the notion that S-nitrosylation of Drp1 at Cys^{644} is required for NO-mediated damage. During Aβ-induced neurotoxicity, synaptic damage is reported to represent one of its earliest manifestations (*22*). Exposure to oligomerized Aβ results in loss of

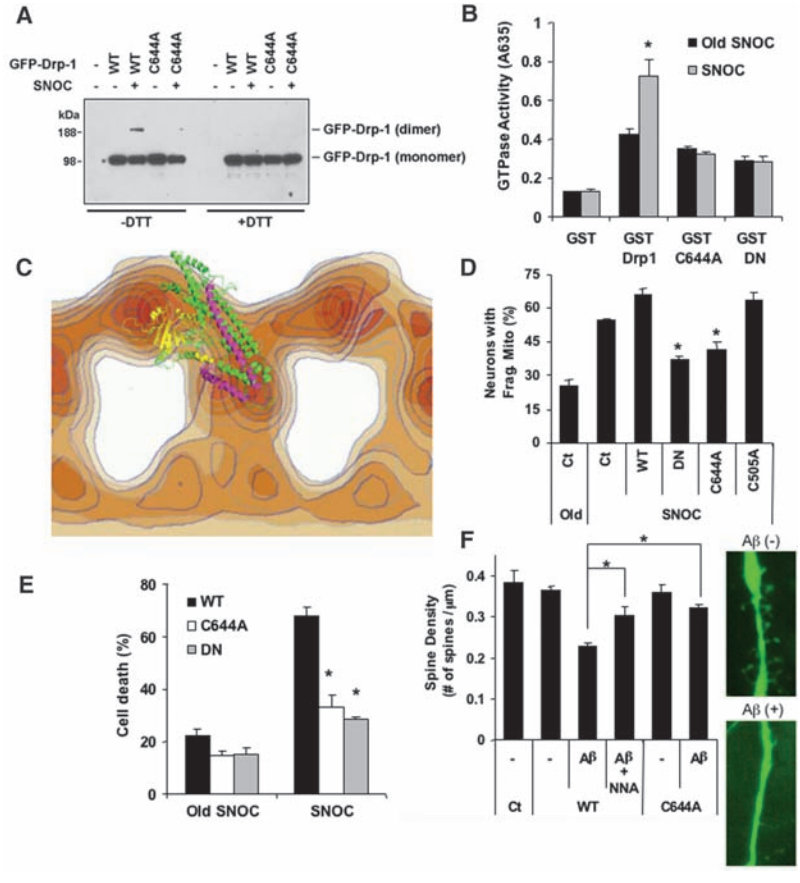

Fig. 4. S-Nitrosylation of Drp1 regulates dimerization, GTPase activity, mitochondrial fragmentation, and neuronal damage. (**A**) HEK cells expressing enhanced GFP (EGFP)–tagged WT-Drp1 or Drp1(C644A) were exposed to 200 μM SNOC or control decayed SNOC. Cell extracts were subjected to SDS–polyacrylamide gel electrophoresis, with or without dithiothreitol (DTT) to reduce disulfide bonds and thus inhibit dimer formation, and immunoblotted. (**B**) GST-fused WT-Drp1, Drp1(C644A), and DN-Drp1(K38A) were expressed and purified from bacteria, exposed to SNOC, and assayed for GTPase activity 30 min later ($^*P < 0.01$). (**C**) Atomic-resolution model of Drp1 superimposed onto electron-density map of homologous domains of dynamin dimer: GTPase (yellow), forming the head; middle (green) and GED (magenta) domains, forming the stalk. (**D**) S-Nitrosylation of Drp1 enhances mitochondrial fission. Cortical neurons transfected with mito-DsRed2 (Ct), mito-DsRed2 plus WT-Drp1, mito-DsRed2 plus DN-Drp1, mito-DsRed2 plus Drp1(C644A), or mito-DsRed2 plus Drp1(C505A) were exposed to SNOC and scored for fragmented mitochondria 1 hour later ($^*P < 0.05$). (**E**) SNO-Drp1 increases apoptotic cell death. Cortical neurons transfected with plasmid (p)EGFP, pEGFP plus WT-Drp1, pEGFP plus Drp1(C644A), or pEGFP plus DN-Drp1(K38A) were exposed to SNOC, and 18 hours later stained for NeuN (to identify neurons) and Hoechst 33342 (to assess nuclear morphology). Values are means + SEM ($n \geq 3$, $^*P < 0.02$). (**F**) Naturally secreted Aβ decreases dendritic spine density in cortical neurons via NO. Cultured cortical neurons were cotransfected with EGFP and pcDNA3 (Ct), WT-Drp1, or Drp1(C644A) and exposed for 5 days to 7PA2-conditioned medium containing oligomerized Aβ (+) or control (–). At the right are representative images of dendritic spines of neurons transfected with EGFP-Drp1 ($n \geq 7$, $^*P < 0.002$).

dendritic spines, representing neuronal postsynaptic sites; this form of Aβ-mediated injury is dependent on *N*-methyl-D-aspartate (NMDA)–type glutamate receptor activity (*22*). Additionally, dendritic mitochondria localize to developing synaptic sites in a Drp1-dependent manner (*4*, *5*).

Because NMDA receptor stimulation activates nNOS and thus generates NO, we asked whether Aβ-induced synaptic damage might be mediated at least in part by NO. Indeed, Aβ decreased the number of dendritic spines in an NO-dependent manner (Fig. 4F). Transfection with mutant Drp1(C644A), which lacks the nitrosylation site, abrogated the effect of Aβ on spine density, consistent with the notion that S-nitrosylation of Drp1 is involved in synaptic loss after exposure to Aβ.

Our results show that pathophysiologically relevant amounts of SNO-Drp1 form in human AD brains. Exposure of cerebrocortical neurons in culture to Aβ results in the formation of amounts of SNO-Drp1 relatively similar to those found in human AD brains. The S-nitrosylation of Drp1 causes dimer formation and increased GTPase activity, thus accelerating the process of mitochondrial fragmentation and contributing to neuronal synaptic damage or cell death. This relationship between nitrosative stress and mitochondrial fragmentation suggests that Drp1 can be a target of S-nitrosylation in AD. Drp1 is nitrosylated via a redox-mediated pathway in response to Aβ oligomers, causing mitochondrial fission and synaptic damage. This reaction may be facilitated by increased levels of copper, as observed in human AD brains (*23*). Copper(II)-mediated catalysis is responsible for generating bioactive S-nitrosothiols (*24*), such as SNO-Drp1. Thus, the redox consequences of nitrosative stress, resulting in Drp1 activation, may provide a mechanistic link among the actions of oligomeric Aβ, mitochondrial fission, and neuronal damage. Drp1 may represent a drug target to antagonize the progression of neurodegenerative disorders in which nitrosative stress and mitochondrial dysfunction play a key role.

References and Notes

1. R. J. Youle, M. Karbowski, *Nat. Rev. Mol. Cell Biol.* **6**, 657 (2005).
2. M. J. Barsoum *et al.*, *EMBO J.* **25**, 3900 (2006).
3. A. B. Knott, G. Perkins, R. Schwarzenbacher, E. Bossy-Wetzel, *Nat. Rev. Neurosci.* **9**, 505 (2008).
4. H. Li *et al.*, *Proc. Natl. Acad. Sci. U.S.A.* **105**, 2169 (2008).
5. Z. Li, K. Okamoto, Y. Hayashi, M. Sheng, *Cell* **119**, 873 (2004).
6. X. Wang *et al.*, *Proc. Natl. Acad. Sci. U.S.A.* **105**, 19318 (2008).
7. S. J. Baloyannis, *J. Alzheimers Dis.* **9**, 119 (2006).
8. N. Kang-Decker *et al.*, *J. Cell Sci.* **120**, 492 (2007).
9. G. Wang, N. H. Moniri, K. Ozawa, J. S. Stamler, Y. Daaka, *Proc. Natl. Acad. Sci. U.S.A.* **103**, 1295 (2006).
10. H. Yuan *et al.*, *Cell Death Differ.* **14**, 462 (2007).
11. See supporting material on *Science* Online.
12. S. R. Jaffrey, H. Erdjument-Bromage, C. D. Ferris, P. Tempst, S. H. Snyder, *Nat. Cell Biol.* **3**, 193 (2001).
13. T. Uehara *et al.*, *Nature* **441**, 513 (2006).
14. P. P. Zhu *et al.*, *J. Biol. Chem.* **279**, 35967 (2004).
15. H. H. Low, J. Lowe, *Nature* **444**, 766 (2006).
16. J. S. Stamler, E. J. Toone, S. A. Lipton, N. J. Sucher, *Neuron* **18**, 691 (1997).
17. R. Ramachandran *et al.*, *EMBO J.* **26**, 559 (2007).
18. K. R. Pitts, M. A. McNiven, Y. Yoon, *J. Biol. Chem.* **279**, 50286 (2004).
19. Y. J. Chen, P. Zhang, E. H. Egelman, J. E. Hinshaw, *Nat. Struct. Mol. Biol.* **11**, 574 (2004).
20. J. Estaquier, D. Arnoult, *Cell Death Differ.* **14**, 1086 (2007).
21. H. Yuan *et al.*, *Cell Death Differ.* **14**, 462 (2007).
22. G. M. Shankar *et al.*, *J. Neurosci.* **27**, 2866 (2007).
23. A. I. Bush, C. L. Masters, R. E. Tanzi, *Proc. Natl. Acad. Sci. U.S.A.* **100**, 11193 (2003).
24. D. T. Hess, A. Matsumoto, S. O. Kim, H. E. Marshall, J. S. Stamler, *Nat. Rev. Mol. Cell Biol.* **6**, 150 (2005).

25. We thank T. Newmeyer, J. Zaremba, J. Russo, E. Masliah, H. Xu, and Y. Zhang for help or reagents. Supported by the Japan Society for the Promotion of Science (T.N.) and NIH grants P01 HD29587, R01 EY05477, P01 ES016738, and P30 NS057096 (S.A.L.).

Supporting Online Material

www.sciencemag.org/cgi/content/full/324/5923/102/DC1
Materials and Methods
SOM Text
Figs. S1 to S6
Table S1
References

20 January 2009; accepted 13 February 2009
10.1126/science.1171091

Use-Dependent Plasticity in Clock Neurons Regulates Sleep Need in *Drosophila*

Jeffrey M. Donlea, Narendrakumar Ramanan, Paul J. Shaw*

Sleep is important for memory consolidation and is responsive to waking experience. Clock circuitry is uniquely positioned to coordinate interactions between processes underlying memory and sleep need. Flies increase sleep both after exposure to an enriched social environment and after protocols that induce long-term memory. We found that flies mutant for *rutabaga*, *period*, and *blistered* were deficient for experience-dependent increases in sleep. Rescue of each of these genes within the ventral lateral neurons (LN_Vs) restores increased sleep after social enrichment. Social experiences that induce increased sleep were associated with an increase in the number of synaptic terminals in the LN_V projections into the medulla. The number of synaptic terminals was reduced during sleep and this decline was prevented by sleep deprivation.

Although sleep is a process that is necessary for survival, the functions of sleep are unknown (*1*, *2*). Sleep is regulated by circadian influences and is important for consolidation of long-term memory (LTM) (*3*–*5*). Additionally, LTM is modulated by circadian mechanisms (*6*, *7*). Because the relationship between sleep, memory, and circadian rhythms seem to be phylogenetically conserved, *Drosophila* can be used to explain mechanisms that coordinate these processes. *Drosophila* show an increase in daytime sleep after exposure to socially enriched environments (*5*). Similarly, an increase in sleep after courtship conditioning is necessary for LTM (*5*).

Increased sleep after social enrichment is dependent upon genes that are required for learning and memory, including genes that alter cyclic adenosine monophosphate signaling (*5*). Although newly eclosed flies that are mutant for the adenylyl cyclase *rutabaga* (rut^{2080}) show increased sleep after social enrichment, 3- 4-day-old adult *rut* mutants do not respond to changes in the social environment (fig. S1). Elevating wild-type *rut* in adult flies with an RU486-inducible driver rescued experience-dependent increases in sleep in adult *rut* mutants (fig. S1); vehicle-treated siblings showed no increase in sleep (fig. S1). To identify circuits that mediate experience-dependent increases in sleep, we used a series of GAL4 lines to drive wild-type *rut* expression in brain circuits (Fig. 1A). Figure S2 illustrates the data analysis used to quantify each GAL4 rescue. Expression of UAS-*rut* using *pdf*-GAL4 restored the increase in daytime sleep and daytime sleep-bout duration, although to a lesser extent than *GSelav* (Fig. 1, B to E). The expression pattern of *pdf*-GAL4 is limited to the ventral lateral neurons (LN_Vs), a group of clock neurons that express *pigment-dispersing factor* (*pdf*) (*8*, *9*). Although *pdf* is the only known output from the LN_Vs, flies mutant for *pdf* show a wild-type increase in sleep (fig. S3).

Given this role of clock cells, we examined the clock gene *period* (*per*), which is expressed in the LN_Vs and is required for LTM (*6*). Rescue of wild-type *per* using a 7.2-kb fragment of the *per* genomic sequence (per^{01};*per*+7.2-2) restored expression of PER at CT0 within the LN_Vs as well as the dorsal lateral neurons, LN_Ds (Fig. 1F); mutant flies carrying a null mutation, per^{01}, expressed no PER (Fig. 1G). Although per^{01} mutants showed no increase in sleep after social enrichment, per^{01};*per*+7.2-2 flies displayed normal experience-dependent increases in sleep (Fig. 1H). per^{01} mutants have no LTM when tested 48 hours after training and only show a transient increase in sleep (Fig. 1, I and J). per^{01};*per*+7.2-2 flies displayed LTM (Fig. 1K) and increases in sleep (Fig. 1, L and M). Although *per* levels are low in mutants for *Clock* and *cycle*, both acquire LTM (*6*) and increase sleep after social enrichment (*5*). Thus, only a very small amount of *per* may be required to support increased sleep and LTM.

Department of Anatomy and Neurobiology, Washington University in St. Louis, 660 South Euclid Avenue, St. Louis, Missouri, USA.

*To whom correspondence should be addressed. E-mail: shawp@pcg.wustl.edu

To further investigate the role of synaptic plasticity in clock cells, we used the *Drosophila* homolog for *serum response factor* (*SRF*), *blistered* (*bs*). In mice, *SRF* is essential for activity-induced gene expression and plays an important role in synaptic long-term potentiation (*10*) and in contextual habituation (*11*). *bs* retains a 93% identity with *SRF* within the DNA-binding MCM1-ARG80-Agamous-Deficiens-SRF (MADS) domain (*12*). Social enrichment elevated the transcription of *bs* in wild-type *Canton-S* (*Cs*) flies (Fig. 2A). Mutants carrying a P element inserted into the *bs* gene (P{GAL4}bs^{1348}) do not increase sleep after social enrichment (Fig. 2B). This deficit was also found in flies carrying either of two other mutant alleles for *bs* (bs^{2} and bs^{3}) and was present in flies that are homozygous for mutant *bs* alleles and flies that have been outcrossed to either *Cs* or to flies carrying the In(2LR)Px^{4} deficiency (Fig. 2C). The P-element insertion in bs^{1348} preserves the MADS domain; similar N-terminal truncated mutant SRF acts as dominant negative (*13*). BS is expressed throughout the brain, including *pdf*-expressing LN_Vs (Fig. 2, D to F). When UAS-*egfp* was driven by P{GAL4}bs^{1348}, expression was restricted to a small number of neurons, including the LN_Vs (Fig. 2, G and I). Expression of *bs* using P{GAL4}bs^{1348} to drive either of two wild-type *bs* (UAS-*bs*) constructs rescued experience-dependent increases in sleep (Fig. 2J). Moreover, inducing *bs* expression within the LN_Vs using *pdf*-GAL4 increased sleep after social enrichment (Fig. 2K).

To establish whether expression of *bs* is required for LTM, we tested flies carrying the P{GAL4}bs^{1348} mutant allele using courtship conditioning. Although *P{GAL4}*bs^{1348}/+ flies acquire short-term memory (Fig. 2L), LTM was impaired (Fig. 2M, left). Rescue of wild-type *bs* using P{GAL4}bs^{1348} restored LTM (Fig. 2M, right). Next, we used the GAL4 repressor *cry*-GAL80 to block UAS-*bs* expression within the LNs. Although UAS-*bs*/+;*cry*-gal80/+ control flies showed significant courtship suppression (Fig. 2N, left), P{GAL4}bs^{1348}/UAS-*bs*;*cry*-GAL80/+ flies had no LTM (Fig. 2N, right), which suggests a role for the LNs, although we cannot exclude a role for the dorsal neurons (DNs). Although *SRF* deletion in mouse forebrain results in neurons with abnormal morphology (*14*), the morphology of LN_Vs in mutant P{GAL4}bs^{1348}/+ flies (fig. S4A) did not differ from that of LN_Vs in P{GAL4}bs^{1348}/UAS-*bs* rescue flies (fig. S4B). All three mutants for *bs* had intact circadian rhythms and showed anticipatory activity before light-dark transitions; only bs^{3} flies show an altered period under constant darkness (fig. S5, A to F). These findings suggest that there are no developmental abnormalities in the LN_Vs in *bs* mutants.

Hypomorphic alleles for *bs* prevent proper wing development through interactions with *Epidermal growth factor receptor* (*Egfr*) signaling (*15*–*17*). Because *Egfr* alters sleep in *Drosophila* (*18*), interactions between *bs* and *Egfr* may regulate responses to social experience. After social enrichment, transcription of *Egfr* was significantly elevated in *Cs* flies (Fig. 3A). The *Egfr* genomic sequence contains several CC(A/T)6GG CArG elements that can be bound by *bs* to promote transcription (Fig. 3B), and transcription of *Egfr* was significantly reduced in *bs* mutants (data not shown). Thus, we used P{GAL4}bs^{1348} to drive expression of a constitutively active *Egfr* construct (UAS-*Egfr**). Although P{GAL4}bs^{1348}/+ mutants showed no change in

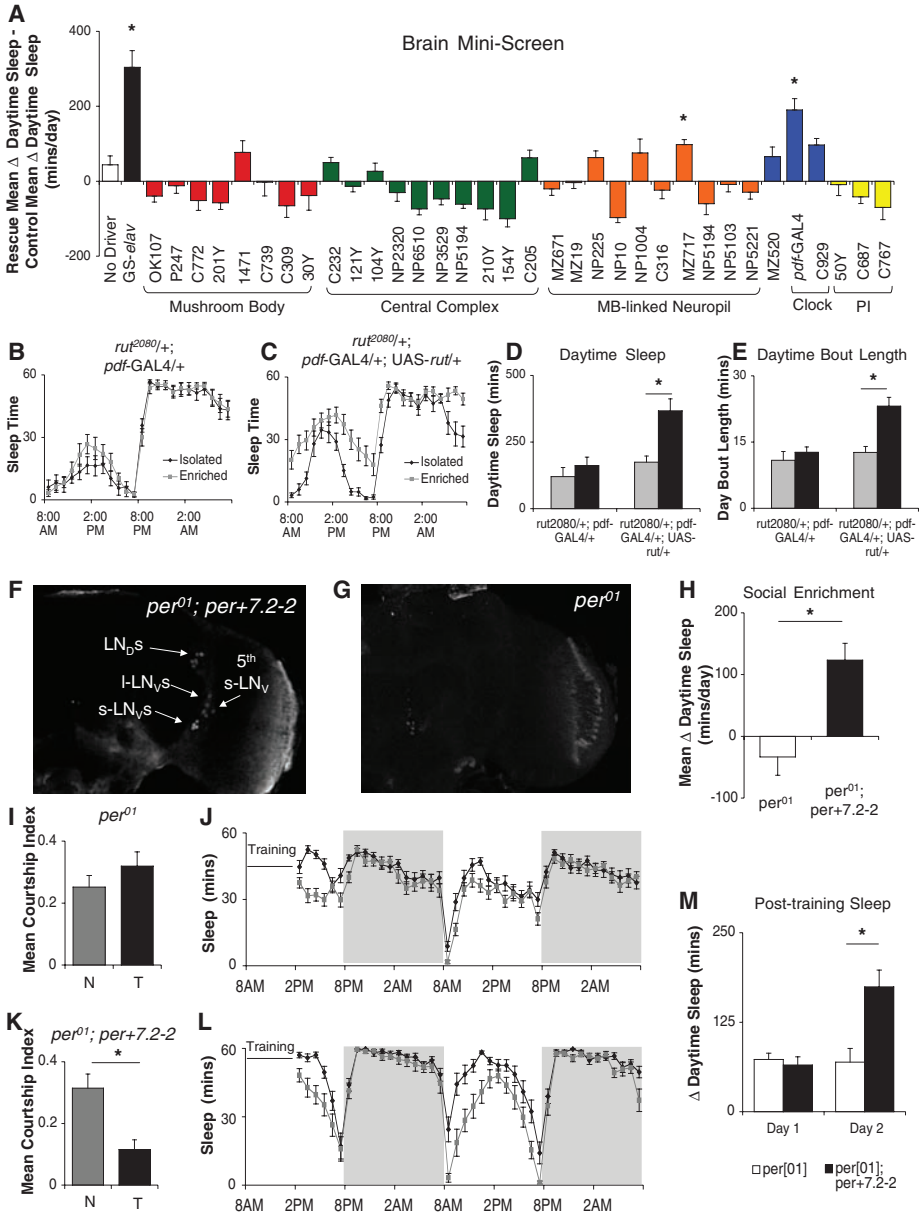

Fig. 1. Clock cells regulate experience-dependent increases in sleep. (**A**) Data for each GAL4 line (GAL4>/+:rut^{2080}/+;;UAS-*rut*/+) is compared to its parental line (GAL4/+:rut^{2080}/+). No increase in Δ daytime sleep is observed in the absence of GAL4 [(rut^{2080}/+;;UAS-*rut*/+)-(rut^{2080}/+); white bar]. The mean Δ daytime sleep for *Gs-elav*-GAL4 (RU+ versus RU–) is shown to facilitate comparisons (black). One-way analysis of variance (ANOVA) for genotype, $F_{(33,903)} = 9.09$. (*, $P < .05$ with correction for 34 comparisons; $n \geq 16$ for all groups). (**B** and **C**) Sleep after social enrichment in mutant rut^{2080}/+;*pdf*-GAL4/+ flies and rut^{2080}/+;*pdf*-GAL4/+;UAS-*rut*/+ flies ($n = 16$ in each group). (**D** and **E**) Average daytime sleep and sleep-bout duration in rut^{2080}/+;*pdf*-GAL4/+ mutant and rut^{2080}/+;*pdf*-GAL4/+;UAS-*rut*/+ rescue flies. Two-way ANOVA reveals a genotype by condition interaction for sleep [$F_{(1,57)} = 4.44$, $P = 0.03$] and bouts [$F_{(1,57)} = 6.59$, $P = 0.013$] (*, $P < .05$, planned pairwise comparisons with a Tukey correction; $n = 14$ to 16 for all groups). (**F** and **G**) PER immunohistochemistry of per^{01};*per*+7.2-2 and per^{01} mutants. (**H**) Δ daytime sleep in per^{01} mutants and per^{01};*per*+7.2-2 flies ($P = 0.0002$; $n = 30$ to 32 in each group). (**I**) Male per^{01} mutants do not exhibit a reduction in courtship 48 hours after a spaced courtship conditioning (N, Naïve; T, Trained; $n = 13$ to 14). (**J**) per^{01} flies only exhibit a transient increase in sleep immediately after training. (**K**) per^{01};*per*+7.2-2 flies exhibit suppression of courtship 48 hours after training ($P = 0.001$; $n = 13$ in each group). (**L**) per^{01};*per*+7.2-2 males also show sustained increases in sleep for 2 days. (**M**) Δ daytime sleep is quantified for per^{01} and per^{01};*per*+7.2-2 males Two-way ANOVA reveals a genotype by day interaction $F_{(1,39)} = 7.48$, $P = 0.009$ (*, $P < .05$ planned pairwise comparisons with a Tukey correction; $n = 13$ to 14 each group).

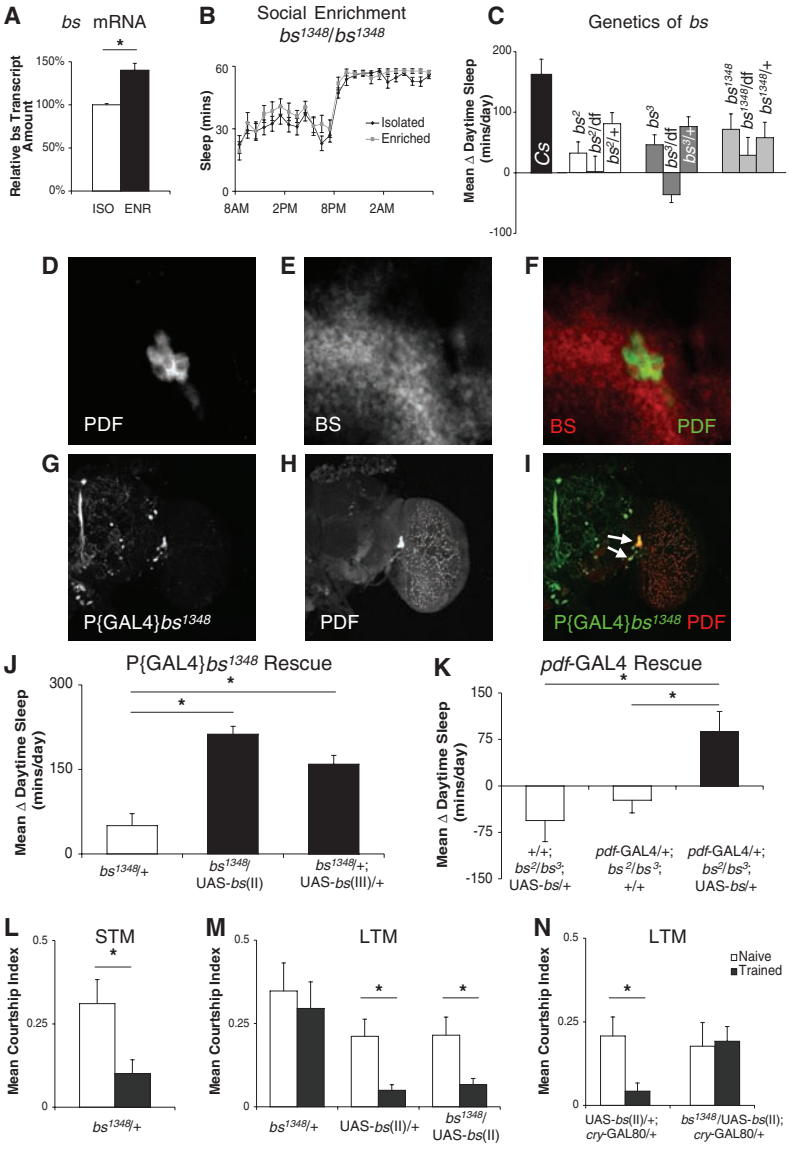

Fig. 2. *blistered* regulates experience-dependent increases in sleep. (**A**) *bs* transcripts are significantly elevated in socially enriched *Cs* flies compared with their isolated siblings ($P = 0.03$). (**B**) Flies homozygous for the P{GAL4}bs^{1348} insertion do not respond to social enrichment with an increase in sleep ($n = 16$ in each group). (**C**) Mean Δ daytime sleep is absent in bs^2 and bs^3 mutants and persists when each allele (bs^2, bs^3, or P{GAL4}bs^{1348}) is outcrossed to *Cs* or with the Deficiency In(2LR)Px^4. One-way ANOVA for genotype [$F_{(9,124)} = 2.73$; $P = 0.04$; $n = 32$ in each group]. (**D**) Expression of UAS-egfp using *pdf*-GAL4 labels the cell bodies of LN_Vs. (**E**) Immunohistochemistry using mouse antibody to BS (diluted 1:1000). (**F**) Colocalization of BS and *pdf*-GAL4 indicates that BS is expressed in *pdf*-expressing LN_Vs. (**G**) P{GAL4}bs^{1348} was used to drive UAS-egfp, and the expression pattern was evaluated using confocal microscopy. (**H**) Brains of P{GAL4}bs^{1348}/+;*UAS-egfp* flies were colabeled with guinea pig antibody to PDF (diluted 1:10,000) (**I**) Colocalization of GFP with PDF indicates that P{GAL4}bs^{1348} drives GAL4 expression in *PDF*-expressing LN_Vs (arrows). (**J**) The failure to respond to social enrichment with an increase in sleep can be rescued by combining P{GAL4}bs^{1348} with either of two separate UAS-*bs* alleles. One-way ANOVA for genotype [$F_{(2,45)} = 22.86$; $P = 1.4 \times 10^{-7}$; *, $P < .05$ Bonferroni post-hoc test; $n = 16$ in each group)]. (**K**) Expressing wild-type *bs* using *pdf*-GAL4 in an otherwise *bs* mutant background (*pdf*-GAL4/+;bs^2/bs^3;UAS-*bs*) rescues increases in Δ daytime sleep); parental lines are shown in white. The lower Δsleep versus 2] may indicate a partial rescue. One-way ANOVA for genotype [$F_{(2,45)} = 6.30$; $P = 0.003$; *, $P < .05$, Bonferroni post-hoc test; $n = 16$ in each group)]. (**L**) Courtship suppression in P{GAL4}bs^{1348} mutants tested 5 min after Courtship Conditioning White bars represent naïve males; dark bars represent trained males ($P = 0.02$; $n = 13$ in each group). (**M**) LTM is disrupted in P{GAL4}bs^{1348}/+ mutants tested 48 hours after training and rescued by expression of UAS-*bs*. Two-way ANOVA reveals a genotype by condition interaction [$F_{(2,72)} = 16.73$; $P = 0.0001$] (*, $P < .05$, planned pairwise comparisons with a Tukey correction; $n = 13$ in each group). (**N**) Blocking GAL4 expression in clock cells using *cry*-GAL80 prevents rescue of LTM. Genotype by condition interaction [$F_{(1,48)} = 2.32$; $P = 0.14$] (*, $P < .05$, planned pairwise comparisons with a Tukey correction; $n = 13$ in each group).

sleep after social enrichment (Fig. 3C), activation of *Egfr* in P{GAL4}bs^{1348}/+;UAS-*Egfr**/+ flies increased sleep (Fig. 3, D and E). Conversely, the expression of a dominant-negative construct for *Egfr* (UAS-$Egfr^{DN}$) using *pdf*-GAL4 prevented increases in sleep after social enrichment, but parental controls (*pdf*-GAL4/+ and UAS-$Egfr^{DN}$/+) were wild-type (Fig. 3F).

A recent theory proposes that a function of sleep is to downscale synaptic connections (*19*). Moreover, structural plasticity can be induced by environmental manipulation in *Drosophila* (*20*). To quantify the effect of social enrichment on the number of post-synaptic terminals in LN_V projections, we used *pdf*-GAL4 to drive expression of a green fluorescent protein (GFP)–tagged construct of the postsynaptic protein discs-large (UAS-*dlg*WT-gfp). After 5 days of social enrichment, LN_V projections into the medulla of *pdf*-GAL4/+;;UAS-*dlg*WT-gfp/+ flies contained significantly more GFP-positive terminals (Fig. 4, A to C). Although we have not demonstrated that the labeled synaptic terminals are functional, these tools have been used to quantify synapses (*21*). The expression of the UAS-*dlg*WT-GFP marker did not alter synaptic function in a wild-type background (*20*) and did not prevent the increase in sleep when expressed using pdf-GAL4 after social enrichment (fig. S6). To determine the effect of waking on synapse number, socially isolated *pdf*-GAL4/+;;UAS-*dlg*WT-gfp/+ flies and their enriched siblings either were allowed to sleep ad libitum or were sleep deprived for 48 hours after social enrichment. Although the number of *dlg*-GFP positive terminals remained elevated in sleep-deprived socially enriched flies, terminal number was significantly reduced in siblings that were allowed to sleep (Fig. 4D). Similarly, the number of presynaptic terminals in LN_V projections into the medulla using a GFP-tagged construct of the presynaptic protein synaptobrevin (UAS-*VAMP*-GFP) in *pdf*-GAL4/+;UAS-*VAMP*-GFP/+ flies was increased (Fig. 4, E to G). After 48 hours of recovery, socially enriched *pdf*-GAL4/+;UAS-*VAMP*-GFP/+ flies had a reduced number of *VAMP*-GFP–positive presynaptic terminals relative to their sleep-deprived siblings (Fig. 4H). A recent study has reported a clock-dependent remodeling in the axonal terminals of the PDF circuit that is highest during the day (*22*). Recent data indicates that hyperexcitation of a subset of the LN_Vs suppresses sleep in *Drosophila* (*23*–*25*). Together with our results, these data suggest that the PDF circuit is well suited to test the hypothesis that sleep acts to downscale synaptic connections that are potentiated during waking experience.

References and Notes

1. A. Rechtschaffen, M. A. Gilliland, B. M. Bergmann, J. B. Winter, *Science* **221**, 182 (1983).
2. P. J. Shaw, G. Tononi, R. J. Greenspan, D. F. Robinson, *Nature* **417**, 287 (2002).
3. M. P. Walker, T. Brakefield, A. Morgan, J. A. Hobson, R. Stickgold, *Neuron* **35**, 205 (2002).
4. L. A. Graves, E. A. Heller, A. I. Pack, T. Abel, *Learn. Mem.* **10**, 168 (2003).
5. I. Ganguly-Fitzgerald, J. Donlea, P. J. Shaw, *Science* **313**, 1775 (2006).
6. T. Sakai, T. Tamura, T. Kitamoto, Y. Kidokoro, *Proc. Natl. Acad. Sci. U.S.A.* **101**, 16058 (2004).

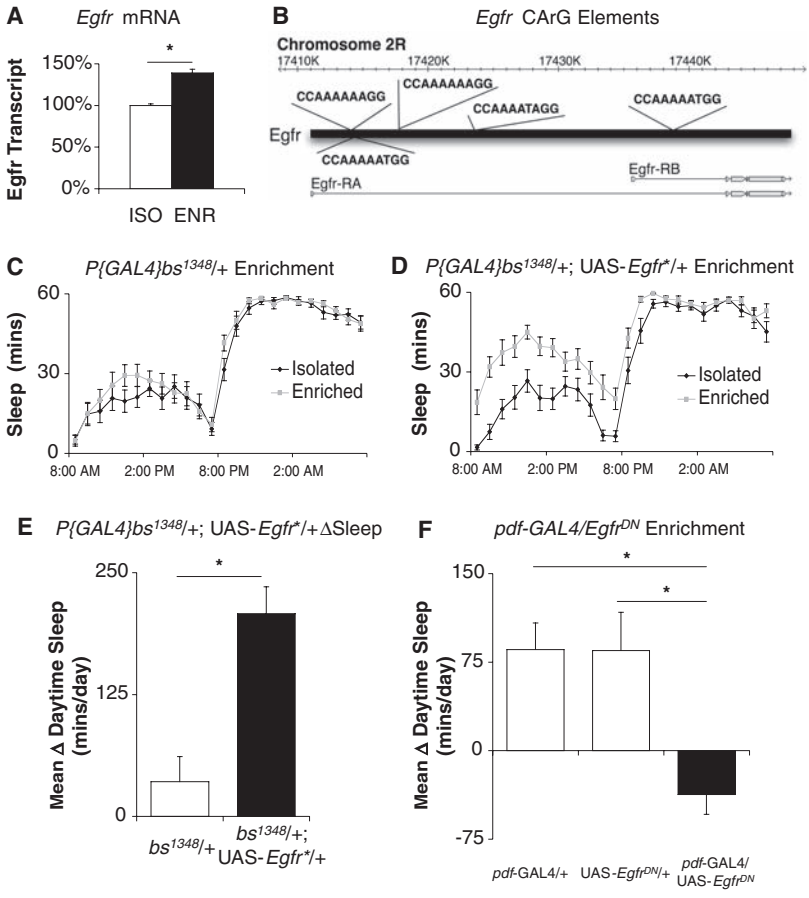

Fig. 3. *Egfr* mediates experience-dependent sleep. (**A**) Transcription of *Egfr* is significantly elevated in socially enriched *Cs* flies compared with their isolated siblings, as measured by quantitative polymerase chain reaction. (**B**) Genomic *Egfr* sequence contains several SRF-binding CArG elements. (**C** and **D**) Driving the expression of UAS-*Egfr** with P{GAL4}bs^{1348} restores ΔSleep after social enrichment. (**E**) Summary of the response for data shown in (C) and (D) (*, $P = 7 \times 10^{-5}$; $n = 16$ in each group). (**F**) No change in Δ sleep is observed in *pdf*-GAL4/UAS-$Egfr^{DN}$. One-way ANOVA for genotype $F_{(2,44)} = 7.75$, $P = 0.001$ (*, $P < .05$, Bonferroni correction; $n = 15$ to 16 in each group).

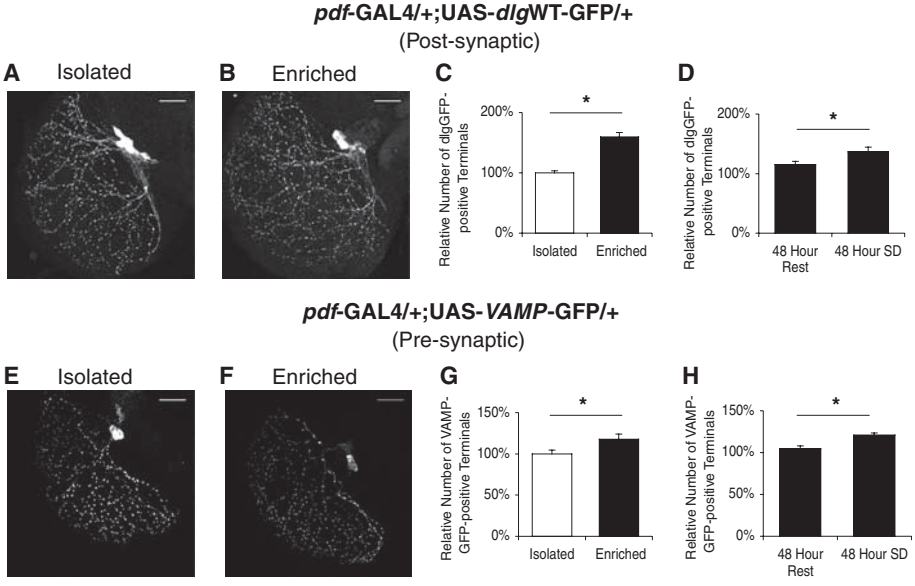

Fig. 4. LN_V synapse number in medulla. (**A** and **B**) LN_V projections in socially enriched *pdf*-GAL4/+;;UAS-*dlg*WT-gfp/+ flies contain more GFP-positive terminals than their socially isolated siblings when evaluated using confocal microscopy. (**C**) Relative quantification of *dlg*-GFP-immunopositive terminals in socially isolated *pdf*-GAL4/+;;UAS-*dlg*WT-gfp/+ flies versus socially enriched siblings ($P = 1.5 \times 10^{-9}$; $n = 33$ to 34 in each group). (**D**) *dlg*-GFP positive terminals 48 hours after social enrichment in sleep-deprived flies and their normally sleeping siblings. ($P = 0.003$; $n =$ 15 to 18 in each group). (**E** and **F**) Social enrichment of *pdf*-GAL4/+;UAS-*VAMP*-GFP/+ flies induces a modest increase of LN_V terminals relative to isolated siblings. (**G**) Relative quantification of *VAMP*-GFP-positive terminals in socially isolated *pdf*-GAL4/+;UAS-*VAMP*-gfp/+ flies and their socially enriched siblings ($P = 0.03$; $n = 16$ to 18 in each group). (**H**) UAS-*VAMP*-gfp-positive terminals 48 hours after social enrichment in sleep-deprived flies and their normally sleeping siblings ($P = 0.01$; $n = 18$ in each group).

7. S. Decker, S. McConnaughey, T. L. Page, *Proc. Natl. Acad. Sci. U.S.A.* **104**, 15905 (2007).
8. C. Helfrich-Forster, U. Homberg, *J. Comp. Neurol.* **337**, 177 (1993).
9. S. C. Renn, J. H. Park, M. Rosbash, J. C. Hall, P. H. Taghert, *Cell* **99**, 791 (1999).
10. N. Ramanan *et al.*, *Nat. Neurosci.* **8**, 759 (2005).
11. A. Etkin *et al.*, *Neuron* **50**, 127 (2006).
12. M. Affolter *et al.*, *Development* **120**, 743 (1994).
13. C. Gauthier-Rouviere *et al.*, *Exp. Cell Res.* **209**, 208 (1993).
14. B. Knoll *et al.*, *Nat. Neurosci.* **9**, 195 (2006).
15. D. Fristrom *et al.*, *Development* **120**, 2661 (1994).
16. J. Montagne *et al.*, *Development* **122**, 2589 (1996).
17. F. Roch, A. Baonza, E. Martin-Blanco, A. Garcia-Bellido, *Development* **125**, 1823 (1998).
18. K. Foltenyi, R. J. Greenspan, J. W. Newport, *Nat. Neurosci.* **10**, 1160 (2007).
19. G. Tononi, C. Cirelli, *Brain Res. Bull.* **62**, 143 (2003).
20. M. Barth, M. Heisenberg, *Learn. Mem.* **4**, 219 (1997).
21. Y. Zhang *et al.*, *Neuron* **53**, 201 (2007).
22. M. P. Fernández, J. Berni, M. F. Ceriani, *PLoS Biol.* **6**, e69 (2008).
23. V. Sheeba *et al.*, *Curr. Biol.* **18**, 1537 (2008).
24. K. M. Parisky *et al.*, *Neuron* **60**, 672 (2008).
25. Y. Shang, L. C. Griffith, M. Rosbash, *Proc. Natl. Acad. Sci. U.S.A.* **105**, 19587 (2008).

26. We thank M. Thimgan, W. Vanderheyden, P. Gray, and P. Taghert for comments. This study was funded by NIH grants R01-NS051305-01A1 and T32-GM008151.

Supporting Online Material

www.sciencemag.org/cgi/content/full/324/5923/105/DC1
Materials and Methods
Figs. S1 to S6
References

1 October 2008; accepted 12 February 2009
10.1126/science.1166657

Widespread Changes in Synaptic Markers as a Function of Sleep and Wakefulness in *Drosophila*

Giorgio F. Gilestro, Giulio Tononi,* Chiara Cirelli*

Sleep is universal, strictly regulated, and necessary for cognition. Why this is so remains a mystery, although recent work suggests that sleep, memory, and plasticity are linked. However, little is known about how wakefulness and sleep affect synapses. Using Western blots and confocal microscopy in *Drosophila*, we found that protein levels of key components of central synapses were high after waking and low after sleep. These changes were related to behavioral state rather than time of day and occurred in all major areas of the *Drosophila* brain. The decrease of synaptic markers during sleep was progressive, and sleep was necessary for their decline. Thus, sleep may be involved in maintaining synaptic homeostasis altered by waking activities.

There is increasing evidence for a link between sleep need and neuronal plasticity (*1*). Sleep need increases after learning, and learning tasks that involve local brain regions lead to local changes in sleep intensity. Neural activity during sleep can reactivate neural circuits involved in learning. Moreover, sleep consolidates memories, whereas sleep deprivation interferes with memory acquisition. Presumably, sleep exerts these effects by modifying synapses (*1*). In rats, the number of cortical and hippocampal glutamate AMPA receptors (AMPARs) containing the subunit GluR1 is high after waking and low after sleep, and the slope of cortical evoked responses is steeper after waking relative to sleep (*2*). These data suggest that periods of wakefulness are associated with a net increase in synaptic strength and that periods of sleep are associated with a net decrease. Sleep could therefore play an important role in renormalizing synaptic changes caused by learning during wakefulness (*3*). But how general is this finding, and does it apply to species with brains very different from those of mammals? Both plasticity and sleep are universal across animal species. If the opposing effects of wakefulness and sleep on synaptic markers reflect a fundamental function of sleep, they should also occur in nonmammalian species.

To address this issue, we turned to *Drosophila melanogaster*, whose sleep shares most of the features of mammalian sleep: It consists of long periods of behavioral immobility with increased arousal threshold (*4*, *5*) and is associated with changes in brain electrical activity and gene expression (*1*). In flies as in mammals, the duration and intensity of sleep both increase in proportion to the duration of prior waking, sleep deprivation reduces performance (*6*), and learning and enriched experience increase sleep need and sleep intensity (*7*, *8*). Fly brains are different from mammalian brains, but the central synapses of *Drosophila* and mammals share key pre- and postsynaptic components and use similar mechanisms of synaptic plasticity (*9*, *10*).

Here, we tested whether waking and sleep affect synaptic markers in the *Drosophila* central nervous system (CNS) by measuring changes in protein levels of several pre- and postsynaptic components (Fig. 1A). Bruchpilot (BRP) is an essential constituent of the active zone of all synapses (Fig. 1A), and excitatory synapses lacking BRP show reduced evoked release of glutamate (*11*). In vivo, a strong BRP signal is associated with fully formed synapses (*11*); BRP staining is used to quantify synapse number (*12*, *13*).

Wild-type Canton-S (CS) males were kept awake by an established mechanical method of sleep deprivation that causes a post-deprivation increase in sleep duration and intensity that is proportional to the amount of sleep lost (*6*). Sleep deprivation was performed for 6, 12, and 24 hours and was highly effective (flies lost at least 80% of their baseline sleep) (Fig. 1B). At the end of sleep deprivation, fly brains were dissected and BRP expression measured by Western blots. Sleep-deprived flies showed higher BRP levels relative to controls allowed to sleep ad libitum, and the increase in BRP expression was smaller after 6 hours of forced waking and larger when sleep was prevented for 12 to 24 hours (Fig. 1, C and E). Similar BRP increases were seen after sleep deprivation in males of another strain, $white^{1118}$ (fig. S1, A and C), and in CS females (Fig. 1, I and K). In the latter, BRP levels increased similarly after 12 and 24 hours of sleep deprivation (Fig. 1I), consistent with the fact that females concentrate most of their sleep at night (*5*, *6*), whereas males take a nap in the middle of the day (fig. S2).

To investigate whether sleep deprivation also increases the expression of postsynaptic proteins, we focused on Discs-large (DLG), the *Drosophila* homolog of the postsynaptic density protein PSD-95/SAP-90 (*14*). DLG is mainly expressed postsynaptically (Fig. 1A) (*15*) and is abundant at the neuromuscular junction and in the CNS neuropil, where its pattern of expression overlaps with that of BRP (*14*, *16*). DLG regulates glutamate release and postsynaptic structure (*17*) and controls the postsynaptic clustering of glutamate receptors (*12*). At the *Drosophila* neuromuscular junction, postsynaptic activation of DLG increases the number and size of the presynaptic active zones (*18*). In mammals, the synaptic delivery and incorporation of AMPARs depend in part on PSD-95 (*19*), and overexpression of PSD-95 enhances the activity of postsynaptic glutamate receptors and the number and size of dendritic spines (*20*). In CS male flies, sleep deprivation increased DLG levels in the CNS, and more so after 24 hours of sleep loss (Fig. 1, D and E). Similar results were observed in CS females (Fig. 1, J and K) and in two other strains (fig. S1, B and D).

We then tested whether sleep loss affects the expression not only of structural proteins such as BRP and DLG, but also of components of the secretory machinery (Fig. 1A): synapsin [Syn (*21*)], syntaxin [Syx (*22*)], and cystein string protein [CSP (*23*)]. After 24 hours of sleep deprivation, all three proteins increased their expression levels by ~30% (Fig. 1, F to H), with CSP showing a significant increase also after 12 hours of continuous waking.

Because both sleeping and sleep-deprived flies were collected at light onset (Fig. 1B), these results cannot be ascribed to circadian differences in the time of collection. However, because flies were stimulated mechanically to keep them awake, it was important to demonstrate that lack of sleep, and not stimulation per se, was responsible for the observed results. To do so, we carried out three sets of experiments. First, sleep loss was enforced for 24 hours via mechanical stimulation as before, but flies were grouped according to the efficiency of sleep deprivation. Even though all flies received the same amount of mechanical stimuli across the 24 hours, the more effective the sleep deprivation, the higher the level of BRP (Fig. 2, A and D), and the correlation was stronger for highly effective sleep deprivation (>70% sleep loss, corresponding to 75% of all flies; $r = 0.65$, $P < 0.001$). In a second set of experiments, we used a different method to keep flies awake. A wild-type (red-eyed) CS male was first kept in standard conditions for at least 2 days, and then a "guest" white-eyed male fly was introduced into the recording tube at dark onset. As confirmed by continuous video recording, both flies were awake most of the night (fig. S3, A to C). As soon as the guest fly was removed the next morning, the host fly showed a sleep rebound, and the increase in sleep duration over the first 3 hours of recovery sleep was similar to that observed after 12 hours of sleep loss by mechanical stimulation (fig. S3D). Relative to flies that slept as usual in single tubes, flies kept awake with this method showed increased levels of BRP, DLG, and CSP (Fig. 2, B and E). Thus, nonspecific factors due to the sleep deprivation methods cannot account for the effects of behavioral state on synaptic markers. Finally, we investigated whether the expression of synaptic proteins also increases after spontaneous waking. BRP levels were measured in flies collected in the middle of the day, after they had been spontaneously

Department of Psychiatry, University of Wisconsin, Madison, WI 53719, USA.

*To whom correspondence should be addressed. E-mail: ccirelli@wisc.edu (C.C.); gtononi@wisc.edu (G.T.)

awake almost continuously for 6 hours, and at the end of the night, after 6 hours spent mainly asleep (Fig. 2C). In both female and male CS flies, BRP levels were again higher after waking than after sleep (Fig. 2F). The increase after 6 hours of spontaneous wakefulness was not as pronounced as after 12 to 24 hours of sleep deprivation.

To determine the time course of the decline in BRP expression during sleep, we collected flies at the end of the light phase, after they had been mostly awake for several hours, and every 3 hours across the entire dark phase, when they slept. In both males and females, BRP levels declined progressively in the course of sleep, reaching the lowest level toward the end of the night (Fig. 3, A and C). Was sleep per se, or merely the passage of time, responsible for the decline in BRP expression? To answer this question, we conducted an experiment in which two groups of flies were sleep-deprived by mechanical stimulation for 12 hours during the night; one group was then allowed to recover sleep for the first 6 hours of the next day, while the other group was kept awake for the same period of time. BRP, DLG, and CSP levels were ~20 to 40% lower in flies that could sleep relative to those that could not (Fig. 3, B and D). Because BRP levels did not decrease, but rather increased, when flies remained awake spontaneously for 6 hours (Fig. 2F), these results are consistent with the idea that sleep is necessary for down-regulating the expression of synaptic proteins.

All changes described so far were detected using whole-brain homogenates, and thus it remained unclear whether they were restricted to select brain areas. We therefore used confocal microscopy to measure BRP levels in dissected brains of two groups of flies, both collected immediately after light onset. Controls slept undisturbed; the other group was sleep-deprived for the preceding 16 hours. An increase in the level of BRP protein relative to controls could be observed across the whole central brain of sleep-deprived flies (Fig. 4) and was due to sleep loss [two-way analysis of variance (ANOVA), sleep loss, $F = 16.27$, $P < 0.0001$; brain tissue, $F = 0.68$, $P = 0.56$; sleep × tissue interaction, $F = 0.24$, $P = 0.86$]. This increase was similar in four major structures of the fly brain: antennal lobes (mean percentage increase ± SEM, 69 ± 11%), β lobes of the mushroom bodies (40 ± 11%), ellipsoid body of the central complex (67 ± 18%), and entire central brain (76 ± 15%). In flies as in mammals, learning and memory—and activity-dependent structural plasticity in general—involve complex and widespread circuits that span most of the brain (*10*, *24*). Thus, it is perhaps not surprising that forcing flies to stay awake through a complex range of tactile, auditory, and visual stimuli affects synaptic activity in most brain regions.

Finally, we examined whether prolonged sleep loss is also associated with overall changes in the volume of antennal lobes, because activity-dependent plasticity leads to volumetric increases in this structure (*25*). In flies that were sleep-deprived for 16 hours, antennal lobes were slightly but significantly bigger than in flies that had slept (+15%, $P = 0.01$; N of flies, sleeping = 27; sleep-deprived = 19), a result that is compatible with a diffuse increase in either the number or the volume of synaptic connections.

Our main finding is that in *Drosophila*, the expression of several bona fide synaptic markers increases after wakefulness and decreases after sleep, independent of time of day. There are three documented examples of daily structural changes in *Drosophila* neuronal circuits: (i) Neuronal branches at the neuromuscular junction are thicker and carry larger synaptic boutons during the day, when flies are active, than during the night (*26*). (ii) Optic lobe interneurons have larger axons at

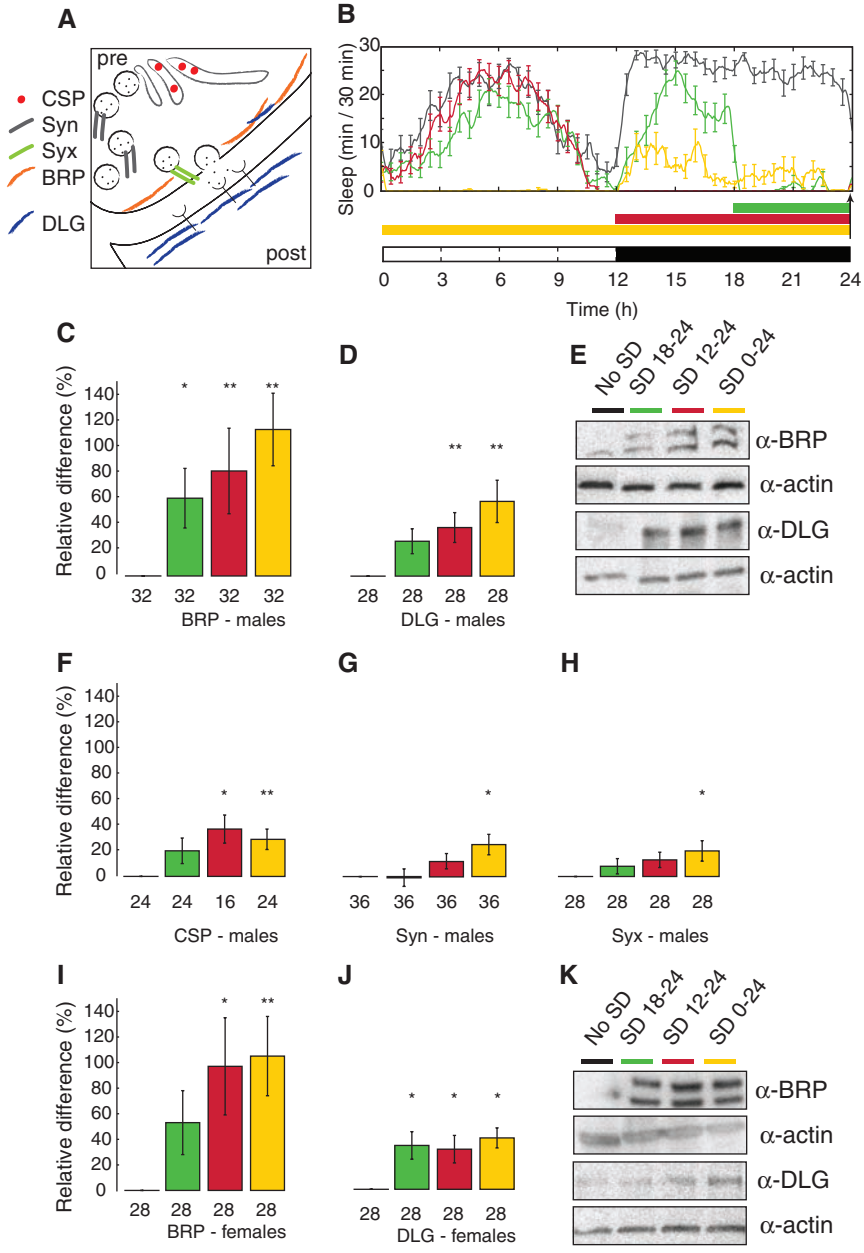

Fig. 1. Levels of synaptic proteins are high after sleep deprivation and low after sleep. (**A**) The *Drosophila* synapse. Abbreviations: pre, presynaptic; post, postsynaptic; BRP, Bruchpilot; CSP, cysteine string protein; DLG, Discs-large; Syn, synapsin; Syx, syntaxin. (**B**) Daily pattern of sleep in Canton-S males sleep-deprived for the last 6 hours of the night (green), 12 hours at night (red), or 24 hours (yellow) and control siblings left undisturbed (no sleep deprivation, black line). Arrow at right shows when flies were collected. White and black bars indicate light and dark periods. Each group includes 12 to 16 flies and represents one of the two or three experiments used for (C) to (H). (**C** to **H**) Representative immunoblots [(E); SD, sleep deprivation] and gel quantification (mean ± standard deviation; *n* of flies below each bar). SD values [color-coded as in (B)] represent percent change relative to sleep (= 0%). (**I** to **K**) Canton-S females. *$P < 0.05$, **$P < 0.01$ [one-way ANOVA followed by Tukey's HSD (honestly significant difference) post hoc test].

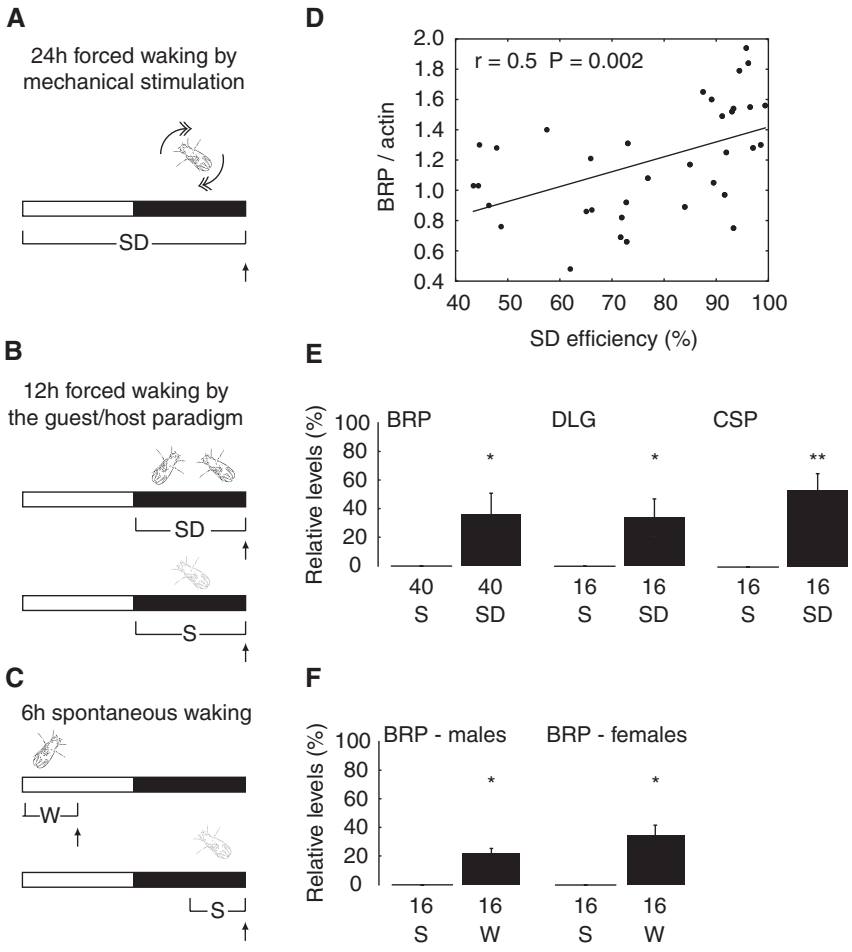

Fig. 2. The expression of synaptic proteins increases as a result of sleep loss. (**A** to **C**) SD, sleep deprivation; S, sleep; W, spontaneous waking. Vertical arrows show when flies were collected. (**D**) Correlation between BRP levels (BRP/actin ratio) and sleep deprivation efficiency during the preceding 24 hours in Canton-S males (Pearson correlation). Each dot represents four flies with similar SD efficiency. (**E** and **F**) Levels of synaptic proteins after SD or W, expressed as percent change relative to sleep (= 0%) (mean ± standard deviation; *n* of flies below each bar). **P* < 0.05, ***P* < 0.01 (Student's *t* test).

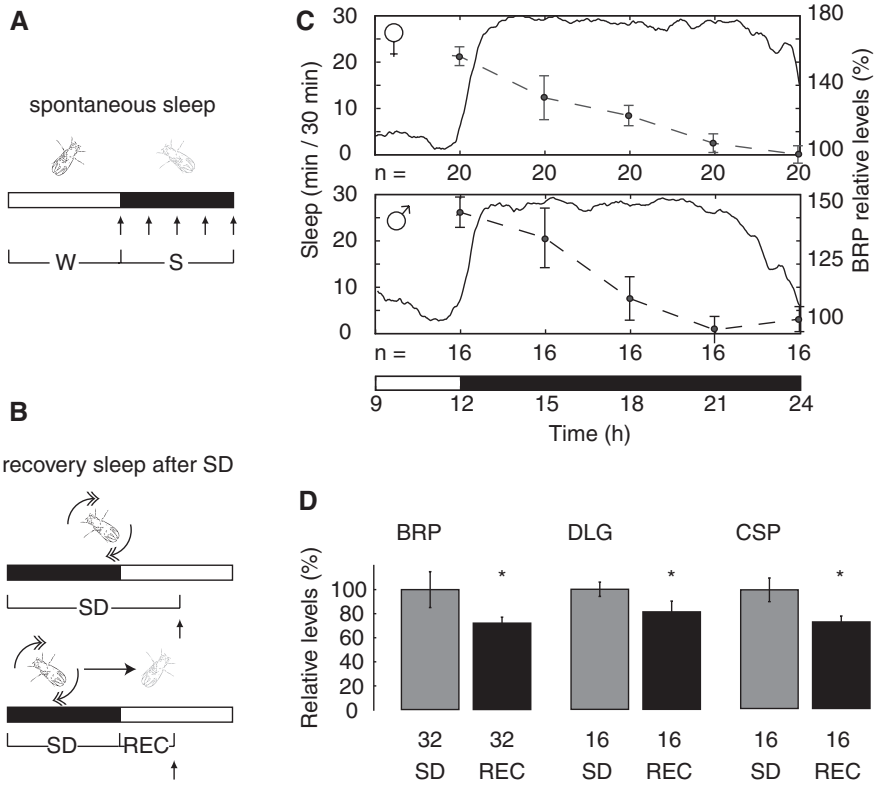

Fig. 3. Synaptic markers decrease during sleep. (**A** and **B**) Rec, recovery sleep after SD; other abbreviations as in Fig. 2. Vertical arrows show when flies were collected. (**C**) BRP levels (data points at 3-hour intervals) are expressed as percent change relative to sleep at the end of the night (= 100%); solid lines indicate mean sleep amount at 30-min intervals. (**D**) Levels of synaptic proteins after recovery sleep, expressed as % change relative to SD (=100%) (mean ± standard deviation; *n* of flies is below each bar). **P* < 0.05 (Student's *t* test).

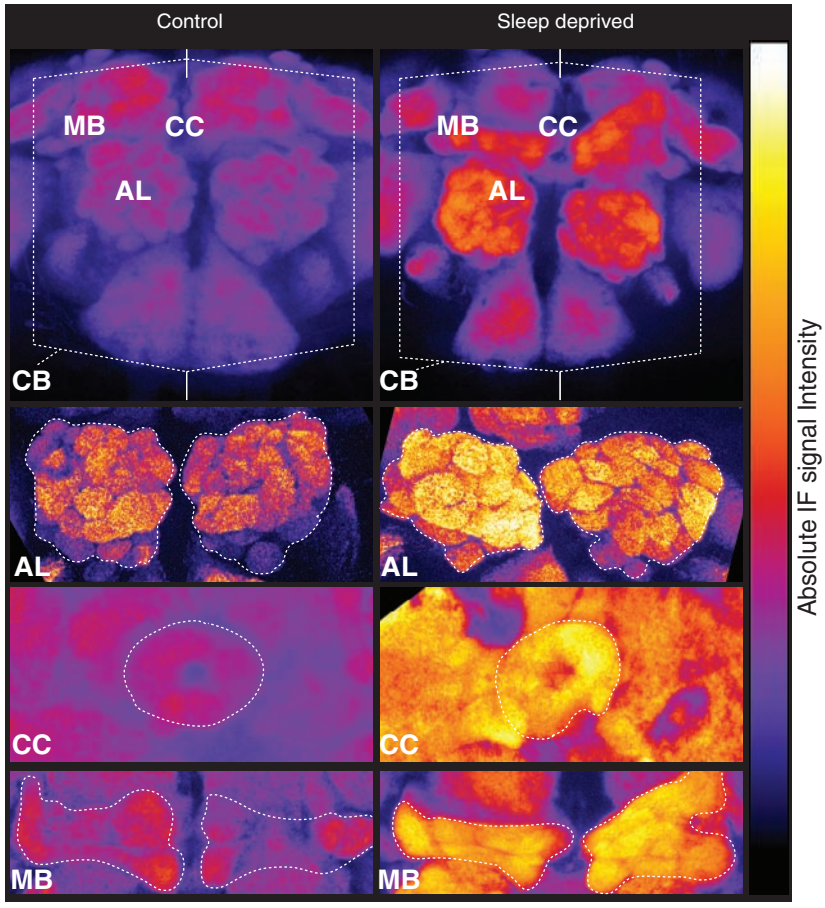

Fig. 4. Widespread BRP increase after sleep loss, as shown by representative examples of BRP immunofluorescence (IF) in controls and flies sleep-deprived for 16 hours (sleep loss >80%) ending at light onset (sum of selected optical stacks, false-colored on a quantitative scale). Immunoreactivity levels were measured in antennal lobes (AL), β lobes of the mushroom bodies (MB), ellipsoid body of the central complex (CC), and central cerebrum excluding the optic lobes (CB).

the beginning of the night than at the beginning of the day, and their dendritic trees also undergo daily morphological changes (*27*). (iii) The dorsal axonal projections of the small ventral lateral neurons, which are involved in rhythmic behavior, show a higher degree of arborization in the morning than at night (*28*). It is thought that these forms of structural plasticity are controlled by the circadian clock, because they are largely maintained in constant darkness and are abolished in flies carrying mutations of circadian genes (*26*, *28*, *29*). However, the sleep/waking cycle is an endogenous circadian rhythm; it persists in constant darkness and is disrupted by mutations of circadian genes. Thus, structural changes in neural circuits occurring between day and night may be due, at least in part, to changes in behavioral state. Consistent with this, the number of synaptic terminals in ventral lateral neurons is reduced during sleep, and this decline is prevented by sleep deprivation (*30*).

What could be the functional importance of the large, widespread decrease in synaptic markers that takes place during sleep? Processes of synaptic potentiation and depression, which are often associated with structural changes, are usually assumed to occur concurrently so as to maintain an overall synaptic balance (*3*). However, the increase in synaptic markers observed after periods of wakefulness in rats (*2*) and now in flies suggests that this balance may not be fully preserved. An increase of synaptic strength by the end of the waking day would result in higher energy consumption, larger synapses that take up precious space, and saturation of the capacity to learn (*3*). Also, a net strengthening of synapses likely represents a major source of cellular stress, resulting from the need to synthesize and deliver cellular constituents as varied as mitochondria and synaptic vesicles. Sleep may thus play an important role in renormalizing synapses to a baseline level that is sustainable and ensures cellular homeostasis. Because similar changes appear to occur in phylogenetically distant species with different brain organizations, synaptic homeostasis may represent a cellular correlate of wakefulness and sleep that is conserved across evolution.

References and Notes

1. C. Cirelli, G. Tononi, *PLoS Biol.* **6**, e216 (2008).
2. V. V. Vyazovskiy, C. Cirelli, M. Pfister-Genskow, U. Faraguna, G. Tononi, *Nat. Neurosci.* **11**, 200 (2008).
3. G. Tononi, C. Cirelli, *Sleep Med. Rev.* **10**, 49 (2006).
4. J. C. Hendricks *et al.*, *Neuron* **25**, 129 (2000).
5. P. J. Shaw, C. Cirelli, R. J. Greenspan, G. Tononi, *Science* **287**, 1834 (2000).
6. R. Huber *et al.*, *Sleep* **27**, 628 (2004).
7. R. Huber, M. F. Ghilardi, M. Massimini, G. Tononi, *Nature* **430**, 78 (2004).
8. I. Ganguly-Fitzgerald, J. Donlea, P. J. Shaw, *Science* **313**, 1775 (2006).
9. Z. Guan, S. Saraswati, B. Adolfsen, J. T. Littleton, *Neuron* **48**, 91 (2005).
10. C. Margulies, T. Tully, J. Dubnau, *Curr. Biol.* **15**, R700 (2005).
11. D. A. Wagh *et al.*, *Neuron* **49**, 833 (2006).
12. K. Chen, D. E. Featherstone, *BMC Biol.* **3**, 1 (2005).
13. See supporting material on *Science* Online.
14. D. F. Woods, P. J. Bryant, *Cell* **66**, 451 (1991).
15. T. Lahey, M. Gorczyca, X. X. Jia, V. Budnik, *Neuron* **13**, 823 (1994).
16. V. Albornoz *et al.*, *Gene Expr. Patterns* **8**, 443 (2008).
17. V. Budnik *et al.*, *Neuron* **17**, 627 (1996).
18. H. Kazama, A. Nose, T. Morimoto-Tanifuji, *Neuroscience* **145**, 1007 (2007).
19. I. Ehrlich, R. Malinow, *J. Neurosci.* **24**, 916 (2004).
20. A. E. El-Husseini, E. Schnell, D. M. Chetkovich, R. A. Nicoll, D. S. Bredt, *Science* **290**, 1364 (2000).
21. B. R. Klagges *et al.*, *J. Neurosci.* **16**, 3154 (1996).
22. K. L. Schulze, K. Broadie, M. S. Perin, H. J. Bellen, *Cell* **80**, 311 (1995).
23. K. E. Zinsmaier, K. K. Eberle, E. Buchner, N. Walter, S. Benzer, *Science* **263**, 977 (1994).
24. M. Heisenberg, M. Heusipp, C. Wanke, *J. Neurosci.* **15**, 1951 (1995).
25. S. Sachse *et al.*, *Neuron* **56**, 838 (2007).
26. K. I. Mehnert *et al.*, *Dev. Neurobiol.* **67**, 415 (2007).
27. J. Gorska-Andrzejak, A. Keller, T. Raabe, L. Kilianek, E. Pyza, *Photochem. Photobiol. Sci.* **4**, 721 (2005).
28. M. P. Fernandez, J. Berni, M. F. Ceriani, *PLoS Biol.* **6**, e69 (2008).
29. E. Pyza, I. A. Meinertzhagen, *J. Neurobiol.* **40**, 77 (1999).
30. J. M. Donlea, N. Ramanan, P. J. Shaw, *Science* **324**, 105 (2009).
31. Authors' contributions: G.F.G. performed the experiments; G.F.G., G.T., and C.C. designed the experiments; G.T. and C.C. conceived and coordinated the project. All authors wrote the manuscript and read and approved the final version. We thank D. Paasch, D. Denucci, and M. Uy for technical assistance with fly work; M. Pfister-Genskow for help with Western blot analysis; L. Rodenkirch and the UW Keck Laboratory for Biological Imaging for assistance in confocal microscopy; and D. Bushey for discussion and comments on the manuscript. Supported by National Institute of General Medical Sciences grant R01 GM075315 (C.C.) and an NIH Director's Pioneer award (G.T.).

Supporting Online Material

www.sciencemag.org/cgi/content/full/324/5923/109/DC1
Materials and Methods
Figs. S1 to S3
References

1 October 2008; accepted 11 February 2009
10.1126/science.1166673

Electrophoresis Systems

Two new gel systems are suited for high throughput electrophoresis of polymerase chain reaction (PCR) products from 96-well microtiter plates. The compact CSL multiSUB Midi 96 system is designed to be used in conjunction with samples from 96-well plates to allow direct loading and easy identification of samples. The run length between samples is 17 mm. The multiSUB MIDI96 stretch has a run length of 34 mm for extended separations. With an average run-time of just 15 to 30 minutes, the Midi 96 version allows rapid identification of samples. The eight-channel pipettes facilitate sample loading. Two comb types are available, one with eight wells plus an additional lane for DNA markers and one with eight wells plus two lanes for markers. Custom-made combs are also available. The buffer volume of the Midi 96 is just 300 ml, which can be reduced to 200 ml by using buffer saver blocks.

Cleaver Scientific
For information +44-(0)-1788-565-300
www.cleaverscientific.com

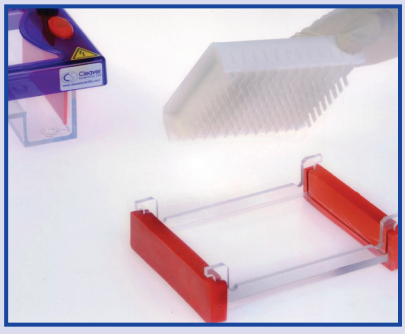

Tissue Culture Plates

A new product line features tissue culture plates coated with a selection of matrices that enhance cell growth and differentiation for stem cell, cancer, cell signaling, and other research applications. Millicoat Cultureware products are 6-well or 24-well tissue culture plates coated with either extracellular matrix (ECM) proteins or synthetic coatings, including collagen, fibronectin, and poly-D-lysine. ECM proteins provide a substrate necessary for many fastidious cells to attach to a surface. Studies show that anchorage-dependent cells growing on ECM undergo more efficient plating, have higher proliferation rates, reach a higher density, require lower serum and growth factor concentrations, and demonstrate enhanced differentiation potential. ECM helps with in vitro cell culture because it simulates aspects of the normal three-dimensional cellular environment.

Millipore
For information 978-762-5170
www.millipore.com

Automated Dispensing

Fill-It is a new product for rapidly dispensing cell suspensions and other liquids into screw-cap vials, including automatically removing and replacing vial caps. It can be coupled with Overlord 2 and the PAA Scara robot to fully automate filling of capped vials. Fill-It enables the rapid creation of high-quality, consistent stock vials for centralized cell-line laboratories, screening operations, or production cell banks, and can be used with both mammalian and microbial cell suspensions. The integrated Scara robot allows loading of vial racks for high throughput automation and the integration of additional instruments from the extensive range of Overlord drivers. Overlord 2 software provides a simple control interface that can interact with any database.

The Automation Partnership
For information +44-(0)-1252-37300
www.automationpartnership.com

Parallel Research System

The Synthesis 1 can be configured for parallel solid and liquid phase synthesis as well as multiple evaporation experiments. Interchangeable plug and play reaction blocks enable the user to quickly configure Synthesis 1 to perform a wide range of applications. Up to 24 reaction vessels can be accommodated in four separate heating zones, making the system suitable for reaction optimization experiments. Direct, in-vessel sample temperature feedback from each zone ensures temperature control within 1°C. Temperatures can be set anywhere from -80°C to 160°C. Unattended operation is aided by a process timer and ability to perform automatic ramping experiments with up to nine programmable steps. Sample mixing is performed by frequency-controlled shaking at speeds from 100 to 1,000 rpm. A connection for vacuum and inert gas supply allows reactions to be run under an inert atmosphere.

Heidolph UK
For information +44-1799-513320
www.heidolph-uk.co.uk

High Throughput HPLC System

The ExpressHT-Ultra HPLC (high performance liquid chromatography) system provides short cycle times and high throughput for liquid chromatography/mass spectrometry studies of pharmacokinetics and drug metabolism. With cycle times as short as 60 seconds, the ExpressHT-Ultra can run six 96-well sample plates overnight. Running at a maximum pressure of 10,000 psi, the system enables the use of small-particle stationary phases to deliver narrow peaks to the mass spectrometer. Featuring columns with diameters of 1 mm or smaller, the system uses up to 95 percent less solvent per analysis than traditional HPLC systems. Proprietary microfluidic flow control technology generates reproducible flow rates from nanoliters per minute to hundreds of microliters per minute.

Eksigent
For information 925-560-2628
www.eksigent.com

Molecular Modeling Software

FieldAlign and FieldTemplater are designed for molecular modelers and medicinal chemists who want to discover new ligands against a wide range of drug targets, including targets with no X-ray structural data, such as G-coupled protein receptors. Both products accept two-dimensional chemical sketches of compounds as inputs. The products feature proven Field Point technology to describe molecules of interest and suggest which molecules to make next. FieldAlign aligns molecules to a three-dimensional field template created from an active molecule. The molecules the user is considering synthesizing can be entered in two dimensions. FieldTemplater finds the three-dimensional bioactive conformation from known active compounds. Three active compounds are all that is needed to get started.

CambridgeSoft
For information 800-315-7300
www.cambridgesoft.com

Electronically submit your new product description or product literature information! Go to **www.sciencemag.org/products/newproducts.dtl** for more information.

Newly offered instrumentation, apparatus, and laboratory materials of interest to researchers in all disciplines in academic, industrial, and governmental organizations are featured in this space. Emphasis is given to purpose, chief characteristics, and availabilty of products and materials. Endorsement by *Science* or AAAS of any products or materials mentioned is not implied. Additional information may be obtained from the manufacturer or supplier.

Science Careers
Classified Advertising

For full advertising details, go to **ScienceCareers.org** and click **For Advertisers**, or call one of our representatives.

UNITED STATES & CANADA
E-mail: advertise@sciencecareers.org
Fax: 202-289-6742

Joribah Able
Industry – US & Canada
Phone: 202-326-6572

Alexis Fleming
Northeast Academic
Phone: 202-326-6578

Tina Burks
Southeast Academic
Phone: 202-326-6577

Daryl Anderson
Midwest/Canada Academic
Phone: 202-326-6543

Nicholas Hintibidze
West Academic
Phone: 202-326-6533

EUROPE & INTERNATIONAL
E-mail: ads@science-int.co.uk
Fax: +44 (0) 1223 326532

Tracy Holmes
Associate Director, *Science* Careers
Phone: +44 (0) 1223 326525

Alex Palmer
Phone: +44 (0) 1223 326527

Dan Pennington
Phone: +44 (0) 1223 326517

Susanne Kharraz Tavakol
Phone: +44 (0) 1223 326529

Louise Moore
Phone: +44 (0) 1223 326528

JAPAN
Mashy Yoshikawa
Phone: +81 (0) 3 3235 5961
E-mail: myoshikawa@aaas.org

To subscribe to *Science*:
In US/Canada call 202-326-6417 or 1-800-731-4939.
In the rest of the world call +44 (0) 1223 326515.

Science makes every effort to screen its ads for offensive and/or discriminatory language in accordance with US and non-US law. Since we are an international journal, you may see ads from non-US countries that request applications from specific demographic groups. Since US law does not apply to other countries we try to accommodate recruiting practices of other countries. However, we encourage our readers to alert us to any ads that they feel are discriminatory or offensive.

Science Careers
From the journal *Science* AAAS

POSITIONS OPEN

VIENNA DOCTORAL PROGRAMME on WATER RESOURCE SYSTEMS

The recently founded Water Research Centre at the Vienna University of Technology announces competition for the Doctoral Programme on Water Resource Systems. This is a dedicated program of the Austrian Science Fund (FWF) that promotes doctoral research and education at the highest standards and provides excellent opportunities for cross-disciplinary research in various water related fields including hydrology, hydrogeology, aquatic microbiology, water quality, resource management, remote sensing, mechanics of structures, and risk assessment. In the first round, eight Ph.D. student positions are available as well as one Postdoctoral position. The program is anticipated to host a total of 70 doctoral students over a period of 12 years.

Applicants for the Ph.D. student positions must have a Master's degree (or equivalent) in a discipline related to water resource systems. The Postdoctoral Fellow will particularly focus on the crosscutting themes of the program and assist in coordinating the research. The working language of the program is English.

The program provides a salary according to the FWF scheme, together with a significant allowance for travel and research support. The contracts will be for three years and extension to a fourth year is possible. The preferred starting date of the first round is October 1, 2009.

Candidates should send a letter of application, a statement of research interests, copies of education certificates, and curriculum vitae to: **e-mail: office@waterresources.at** (PDF format). Application deadline is May 15, 2009. Shortlisted candidates will be invited to a selection seminar. Financial support towards travel expenses is available on request. Information about the Doctoral Programme on Water Resource Systems may be viewed at **website: http://waterresources.at.**

TU Wien is an Equal Opportunity Employer.

POSTDOCTORAL FELLOWSHIPS in IMMUNOLOGY

Postdoctoral positions are available to pursue research supported by several NIH grants including the Center of Excellence for Complementary and Alternative Medicine on Autoimmune and Inflammatory Diseases **(website: http://www.med.sc.edu/1.html).** Studies will address the effects of plant products such as resveratrol and cannabidiol on inflammation, autoimmunity and cancer. Ph.D. in immunology or related areas is required. Other projects include role of CD44, cannabinoids, and TCDD on immune response. Send curriculum vitae and three references to: **Dr. Mitzi Nagarkatti, Professor and Chair, Department of Pathology, Microbiology and Immunology, University of South Carolina School of Medicine, Columbia, SC 29229 or e-mail: postdoccam@uscmed.sc.edu**.

University of South Carolina, Columbia is an Equal Opportunity Affirmative Action Employer and encourages applications from women and minorities.

POSTDOCTORAL POSITIONS in PROSTATE CANCER BIOLOGY

Positions available to participate in NIH-funded program studying mechanisms associated with progression of prostate cancer and metastasis, and drug discovery to prevent this process. Expertise in molecular biology (generation of constructs and mutagenesis) and the ability to work with transgenic rodents as well as cell cultures is essential. Some experience in cell biology/fluorescent microscopy is highly desirable. Please send curriculum vitae and contact information for three references to: **Girish V. Shah, Ph.D., Calhoun Endowed Professor of Pharmacology, University of Louisiana at Monroe, College of Pharmacy, 1800 Bienville Drive, Monroe, LA 71201 USA. E-mail: shah@ulm.edu.**

POSITIONS OPEN

POSTDOCTORAL POSITIONS IN MOLECULAR AND CELLULAR BIOLOGY
The Wine Research Centre, University of British Columbia, Vancouver, B.C., Canada

Two Postdoctoral positions are available immediately in the Wine Research Centre **(website: http://www.landfood.ubc.ca/wine/index.html)** for a 24-month appointment with potential for extending employment. These positions are funded by large-scale Genome British Columbia wine genomics grants to characterize fermentation stress response genes in *S. cerevisiae*. Successful candidates will be responsible for establishing function of each of these 62 genes induced during wine fermentation using a systems biology approach. Outstanding research facilities are available. Salary approximately $50,000 annually, including benefits.

A Ph.D. in molecular and cellular biology is required. Experience in transcriptomics/proteomics/metabolomics will be an asset. Interested candidates should apply with curriculum vitae and names of three references to: **Dr. Hennie J. J. van Vuuren, Director, e-mail: hjjvv@interchange.ubc.ca.**

Two **NEUROSCIENCE POSTDOCTORAL RESEARCH TRAINEE POSITIONS** are available immediately to work on NIH-funded projects at the University of Tennessee Health Science Center located in Memphis, Tennessee. One project investigates the neuronal mechanisms underlying the coordination of orofacial and respiratory movements in awake and behaving mice. The second project investigates the role of the cerebellum in the modulation of dopamine in the frontal cortex in a mouse model of autism spectrum disorder. Applicants must have a Ph.D. or M.D., and should have expertise in at least one of the following areas: extracellular or intracellular electrophysiology in vivo, neuroanatomical track tracing, cyclic voltammetry or mouse behavior. Position includes highly competitive salary and interaction with neuroscientists in the Department **(website: http://www.utmem.edu/anatomy-neurobiology/)** and Neuroscience Institute **(website: http://www.utmem.edu/neuroscience/)**. The Lab is set up with state of the art equipment and is embedded in a well-established, collaborative multidisciplinary neuroscience program. Memphis and its suburbs provide very affordable living with excellent schools, parks and year-round outdoor recreational activities. Applications will be accepted until position is filled. Please submit a curriculum vitae and names and contact information for three references to: **Dr. Detlef H. Heck, Dept. of Anatomy & Neurobiology, University of Tennessee Health Science Center, Memphis, TN 38163. E-mail: dheck@utmem.edu.** *The University of Tennessee is an Affirmative Action Employer, encourages applications from women and underrepresented minorities and is an Equal Opportunity Employer/Affirmative Action/Title VI/Title IX, Section 504/ADA/ADEA Employer.*

Multiple **POSTDOCTORAL/RESEARCH ASSOCIATE POSITIONS** are available to study cell calcium, ion channels, and signal transduction in cardiovascular, respiratory and other systems. Candidates who apply for **Electrophysiologist** positions should have patch clamp and/or calcium imaging experience. For **Molecular Biologist** positions, applicants should have training in molecular biology, protein biochemistry, embryonic stem cells, cancer, or development. If interested, please send application letter and curriculum vitae to: **e-mail: wangy@mail.amc.edu** to **Dr. Yong-Xiao Wang, Center for Cardiovascular Sciences, Albany Medical College, Albany, NY 12208.**

Albany Medical College supports a diversified, smokefree environment and is proud to be an Equal Opportunity/Affirmative Action Employer, encouraging women and minorities to apply. In support of a safe, drugfree environment, criminal background checks and drug testing are part of our hiring process.

IT'S GETTING EASIER TO BE GREEN: JOBS IN GREEN SCIENCE

***"People well versed in environmental topics, or productive in developing methods that lighten the environmental footprint, will be highly sought, key players in the development of the new economy—and well rewarded."*—Mario Mettich, communications manager for environmental health and safety at Con Edison.**

Green jobs are red hot. For scientists, an expanding employment spectrum deals with the survival of people, plants, and planet. **By Carol Milano**

Whatever you've studied—physical science, medicine, engineering, any life science from agriculture to zoology—qualifies you for some kind of environmental job. Many don't require Ph.D.s; most will utilize, and often expand, your skills and training.

Which green problems catch your attention—pesticides in foods, new recycling possibilities, fossil fuel alternatives, causes of polar ice melt? The list is as endless as the approaches. Here are some examples:

Greg Koch of Coca-Cola leads an international team of over 300 groups involved in the integrated global water strategy he helped establish. They strive to reduce the amount of, and safely recycle, water used to manufacture Coke's beverages, and replenish community water supplies through locally relevant projects.

As vice president for research at the Environmental Working Group, **Jane Houlihan** oversees scientists at the Washington, D.C., nonprofit's busy labs. Their thorough reports about consumer product safety—from sunblock to toys to bottled water—garner wide attention.

Kathy Loftus, national energy manager for Whole Foods Market, coordinates energy procurement and management. She supervises green design, construction, and maintenance for Whole Foods' 270 sites, and helped develop the US Green Building Council's coveted certification for supermarkets.

New York City Department of Environmental Protection ecologist **John McLaughlin** leads a project exploring urban oyster beds as natural water filters. Challenges include introducing shellfish restoration in locations as unlikely, and possibly uninviting, as wastewater treatment plants.

Skills and Specialties

Green jobs typically involve a range of proficiencies. *The ability to conduct research* in widely varied roles and settings, in labs or on location, is clearly a critical skill. Scientists study particular environmental factors, seeking ways to identify, predict, and lessen negative impacts. Through *monitoring and evaluating* activities, scientists track algal blooms, rainfall shifts, frog survival, air quality, possible toxins in decomposing trash—anything affecting or resulting from an environmental factor. Findings are sometimes controversial, requiring some skill in communicating with the public and media, too. Scientists in a specific green area might need to *design, develop, and implement* problem-solving approaches. These may be local and short-term, like testing water quality, or as widespread and complex as reducing greenhouse gas emissions. *Training, educating, and communicating* is of increasing importance these days; employees and the public need updates on new findings and approaches. Environmental health and safety (EHS) managers often handle internal training, while outreach specialists—typically at government or nonprofit organizations—inform citizens and spur support for environmental improvements.

Where the Jobs Are

Every employment sector now has environmental concerns and green jobs:

Academia: Besides faculty and research positions, some universities have prominent environmental affiliates, like Scripps Institute for Oceanography (University of California, San Diego), or Strategic Energy Institute (Georgia Institute of Technology).

Industry: Amidst efforts to reduce energy use and pollution, EHS is a rapidly growing profession. Fortune 500 corporations have become leaders in seeking national environmental reforms. One example, the outdoor clothing maker, Patagonia, was an early adapter of green technologies for its buildings and products.

Government: Municipal, state, and federal departments regulate everything from emissions to agriculture to water safety. California Department of Toxic Substances scientists explore innovative dioxin cleanup—even bioremediative mushrooms. The Recycling Bureau at New York City's Department of Sanitation conducts an ambitious composting program. continued »

The list of green science jobs is as endless as the approaches.

Kathleen Sayce

"It took the guaranteed support I get from federal agencies. I'm very happy with my great freedom as a federal employee"
—Ron Neilson

Nonprofits: Thousands of associations, organizations, and foundations handle green issues through advocacy, education, research, recreation, or a combination of these. Nonprofits can be small and local like Sustainable South Bronx, or high profile and nationally active like the Environmental Defense Fund, or global innovators, like the Bill & Melinda Gates Foundation.

Quasi-public: Privately-owned, government-regulated companies like Detroit Edison or the Port Authority of New York/New Jersey provide essential services including water, electricity, and transportation. Their scientists explore newer, cleaner, more affordable energy sources.

Profiles in Green: It's All About the Science

Botanist **Kathleen Sayce** is the bank scientist at Shorebank in Ilwaco, Washington, a 12-year-old financial institution committed to a sustainable economy. Known for her work as science director at a local waterfront alliance, she was invited to apply, joined the bank in 1998, and helped develop evaluation criteria for loans.

"We consider where an applicant is now, the environmental impacts of how they do things, and steps they can take toward their goals," Sayce explains. "When our evaluation shows problems we consider important, we can help solve them, starting with simple actions like more recycling or better windows for daylighting."

Reporting directly to Shorebank CEO (and Ph.D. physicist), **David Williams,** Sayce sets her own work schedule and annual goals. One-third of her time is at client meetings, often about developing more efficient, cost-effective energy use. Scientific training is "important background for a lot of our processes. If you don't keep anchored in the science, you'll get lost," Sayce and Williams believe.

Sayce says she's been surprised at how easily traditional scientists "cross over to insurance, finance, brokerage, or analytic work. Scientific training gives you comfort with numbers and logic," Sayce finds. "I love the job and the pace—never knowing day to day what I'll be asked to work on."

Profiles in Green: Forecasting Climate Change

No one was hiring biogeologists when **Ron Neilson** completed his Ph.D. during the 1980s recession. Before climate change became a global issue, a series of academic jobs led him to merge population biology and pipeline ecology. Using math and computer skills, he developed systems models showing 150 years of climate variability.

When 1986 legislation funded a national climate change research facility at the US Environmental Protection Agency's Portland, Oregon, environmental lab, Neilson called to offer a seminar on Northwest acid rain. It was a success; he instantly volunteered another, on climate change and vegetation. "When I wandered in, my [current] job was ending," he recalls. "They were looking for someone to hire. With my huge perspective on jet streams, weather, and global currents, my visit became a job interview, with an immediate offer."

As chief scientist, he established nationwide cooperative agreements for massive case studies among 50 institutions. Displeased with EPA politics, he moved to the US Forest Service's Corvallis, Oregon, research lab. As their bioclimatologist, Neilson and several postdocs he'd hired developed one of the first—and statistically most accurate—biogeographic climate models. Adapted by other nations, NOAA, and the Weather Channel, Neilson's model is now used to forecast seasonal forest fire risks.

"I don't think I could have built [this] research infrastructure and capability on soft money," he reflects. "It took the guaranteed support I get from federal agencies. I'm very happy with my great freedom as a federal employee."

GREEN JOBS CHECKLIST

Pros

Transferable skills. Apply training learned at other jobs.
Earning potential. Shortage of qualified scientists in many specialties boosts salaries.
Gratification. Make a difference!
Employer awareness. There is increasing respect for environmental responsibility.

Cons

Slow growth. Environmental positions will evolve gradually in newer areas.
Unfamiliar workplaces. Managerial or analytic responsibility can mean more time indoors or away from research sites.
Increasing demands. With skyrocketing need for environmental information, some fields are swamped with requests.
New collaborators. You may have to persuade nonscientists that certain environmental factors affect them.
Enormous scale. It can be challenging to work on such big issues, especially when policy lags innovation.

Profiles in Green: Listening to the Oceans

Scuba diving heightened **Nancy Rabalais's** marine biology interests during high school, in coastal Corpus Christi, Texas. She surveyed natural reef sea squirts for her Master's, gave beach walks and slide shows as a national park seashore naturalist, and assessed Texas's continental shelf while a research associate. Seasick on large boats and disliking small ones, Rabalais found a land-based marine specialty for her zoology Ph.D.: fiddler crabs.

Increasing involvement in invertebrate taxonomy and community ecology led her in 1983 to a job at a statewide nonprofit, exploring oil and gas development's effects on marine ecology. She became Louisiana Universities Marine Consortium's executive director in 2005. "It's challenging, a real chance to help LUMCON grow," Rabalais reflects. "We try to increase ocean literacy, for example. Our Bayouside Classroom for middle school kids won a National Science Foundation award."

Rabalais team-teaches biological oceanography at Louisiana State University, and continues her own research on Mississippi River-Gulf of Mexico interactions, forming the world's second largest dead zone. Serving on many boards and panels, she travels frequently for LUMCON. "This is an exciting time for ocean and marine biology. They're a growth opportunity—or should be: oceans drive climate. People moving to coasts put more pressure on coastal habitats. Ecology isn't one estuary or gulf—it's global," she declares.

Profiles in Green: Heeerrre's... Mario

As EHS communications manager at Con Edison in New York, **Mario Mettich** updates the company's 1,400 employees on environmental initiatives and important procedures, like handling hazardous substances safely.

For the quasi-public corporation's annual report—featuring environmental consequences of company operations—his data-gathering, coordination, and writing take six months. He produces and writes a monthly Intranet video news magazine, ghostwrites safety and environmental speeches, and organizes an annual environmental forum conference for Fortune 500 executives. "I'm the Johnny Carson of EHS," jokes Mettich.

His physics degree "acquaints me with the scientific method when evaluating data, providing a very broad foundation. Many continued »

CREDITS: PHOTO BY AVERY S. NEILSON, NATIONAL ARBORETUM, 6/2003

UNIVERSITY OF OTTAWA
HEART INSTITUTE

INSTITUT DE CARDIOLOGIE
DE L'UNIVERSITÉ D'OTTAWA

SEEKING RESEARCH SCIENTIST IN GENETICS AND GENOMICS

GENETIC RESEARCH HIGHLIGHTS

- Identified 9p21, the strongest genetic risk factor for coronary artery disease and heart attack to date.
- Discovered the genetic basis for atrial fibrillation, the most common form of cardiac arrhythmia.
- Unlocked the mechanism controlling the ACSL5 weight loss gene.

UOHI RESEARCH FOCUS AREAS

- Genetics of cardiovascular disorders
- Molecular medicine and cellular therapy
- Cardiac imaging
- Obesity
- Vascular biology
- Hypertension
- Cardiovascular endocrinology
- Clinical trials (drugs and devices)
- Behaviour and risk modification

UOHI KEY RESEARCH STATS

- Principal Investigators: 60
- Research Staff: 175
- Funding (2008): $65 million
- Research funding has increased 300% since 2004
- Endowment funds have doubled in 5 years

The University of Ottawa Heart Institute (UOHI) is Canada's largest academic cardiovascular centre and has established a major focus in genomic approaches to the study of cardiovascular disease and its associated traits.

The Institute is seeking a dynamic investigator with an international research profile in genetics and genomics. The candidate should have either a PhD or MD and must have an outstanding publication and grant procurement record. Additional expertise in biostatistics or bioinformatics would be considered an asset but is not essential. The candidate should also have the strong leadership, interpersonal and networking skills required to direct his/her own laboratory and work with the Ruddy Canadian Cardiovascular Genetics Centre.

An extensive biobank and database contains more than 8,000 phenotypically defined patients and controls that have been genotyped in a genome-wide association study (GWAS), and further recruitment is ongoing. The core genetics laboratory is fully equipped for GWAS with four Affymetrix GeneChip scanners and sixteen fluidics stations dedicated to high-throughput SNP genotyping and expression analysis, a Roche FLX Genome Sequencer, and sophisticated, highly advanced facilities for cellular imaging and animal models of disease.

Qualified candidates would be eligible for Tier 1 or Tier 2 Canada Research Chairs, substantial peer-reviewed funding from Canadian granting agencies, and additional infrastructure support from the Canada Foundation for Innovation (CFI).

Send applications to:

Robert Roberts, MD, FRCPC, MACC
President and Chief Executive Officer
University of Ottawa Heart Institute
Tel: 613-761-4779
Fax: 613-761-4650
email: rroberts@ottawaheart.ca

40, RUE RUSKIN STREET, OTTAWA, ON K1Y 4W7
T 613.761.5000 WWW.OTTAWAHEART.CA

"We're busier than ever, and don't see any lack of money."
—Frank DeSafey

physics principles are in applied technologies like engineering or process controls," observes Mettich, whose first job was editing an American Institute of Physics journal. He later became marketing communications vice president at an electronics manufacturer.

Mettich sees the EHS role growing continually, across industries. "My peers at ABC, Colgate-Palmolive, or Disney all work on the same issues. The mission of environmental specialists remains [consistent]: conducting sustainable practices."

Profiles in Green: The Human Factor

"Climate change is an intellectually stimulating sector, very complex, with many possibilities for how this will come together," says **Heather Kaplan Coleman,** senior policy adviser on climate change for Oxfam America. "I see it crossing many fields—a global humanitarian issue and an energy issue."

Working at a Washington, D.C., advocacy center in 1997 inspired her to seek some green experience. By 2001, "I knew why I was interested in the environment—it was about changing the way we think about and use energy in the United States. I became more interested in human communities, not just animals and air." Instead of pursuing federal climate-related jobs after earning her Master's, Coleman chose regional and state climate policy, "where the action has been."

She built her reputation at a regional air use consortium and a think tank, Environment Northeast. When Boston-based Oxfam America began addressing climate issues, "they had no one with climate change or policy experience, and found me," recalls Coleman, who was eager to move into international negotiations. "It's a hugely expansive, eye-opening learning experience, bringing a different perspective to people around the world, seeing that we can support those who need to adapt. How do we get the developing world on track with us? This is much more advocacy-based than what I'd been doing, more analytic."

Job Hunting

It's an exciting time for green employment, reports **Frank DeSafey,** vice president of Sequence Staffing, an environmental and engineering placement firm in Roseville, California. "We're busier than ever, and don't see any lack of money. The world's limited amount of resources means shortages, pollution problems, and more competition for land, water, and other natural resources. They're all becoming critical."

Already, Sequence Staffing is recognizing specific environmental areas with new opportunities for scientists. Geologists, environmental chemists, and engineers are needed for remediation programs, which face challenges like water purification and decontamination of brownfields. They're developing innovative biochemical processes that go beyond carbon, filtering, and dilution.

Demand for emissions scientists exceeds their availability. In particular, dealing with greenhouse gas emissions is about to "become as professionalized an industry as IT did in the '80s," predicts DeSafey. In February, Sequence Staffing released a major study, "2009 Green-house Gas and Climate Change Workforce Needs Assessment Survey," available at www.sequencestaffing.com/industry-survey-results/employer-content/services/industry-survey-results.html.

Any environmental science background can open several doors. One is at the intersection of agribusiness and recycling, where waste management and water reuse are two rapidly growing examples. Another evolving sector is sustainable building practices. Both residential and commercial buyers are increasingly asking for green(er) buildings, with recycled materials and a smaller environmental footprint. Aside from environmental science, employers in these areas welcome land use or chemistry experience.

Renewable energy is on a fast track, too, with everything from biofuels to nuclear to hydropower being explored. Each energy source requires its own gamut of specialists, and demand is surging. In 2008, the solar energy field employed 35,000 people in the United States. If the US Department of Energy pursues its goal of 20 percent wind power by 2030, Desafey forecasts increases in this field of 10 times the current 50,000 jobs. Specialists needed for windpower positions include ecologists, climatologists, and electrical engineers.

As early environmental specialists' retirements create significant mid-level demand, especially for project managers, Sequence seeks people with technical degrees and management experience. With periodic hiring freezes, federal agencies have relatively few younger employees, notes Neilson, anticipating some upcoming opportunities for scientists.

Even in a thorny job market, prospects in the green sector remain (at least relatively) encouraging. And many professionals working in green fields discover that their rewards go well beyond the paycheck. Rabalais of LSU is often called to Capitol Hill to review bills or testify before Senate and House committees on natural resources. "My testimony has helped lead to appropriations," she says with pride. "My job is very fulfilling. I never expected this when I was chasing around fiddler crabs!"

Featured Participants

Bill & Melinda Gates Foundation
www.gatesfoundation.org

California Department of Toxic Substances
www.dtsc.ca.gov

Coca-Cola
www.coca-cola.com

Con Edison
www.coned.com

Detroit Edison
www.dteenergy.com

Environmental Defense Fund
www.edf.org

Environment Northeast
www.env-ne.org

Environmental Working Group
www.ewg.org

Louisiana State University
www.lsu.edu

Louisiana University Marine Consortium
www.lumcon.edu

New York City Department of Environmental Protection
www.nyc.gov/html/dep/html/home/home.shtml

New York City Department of Sanitation
www.nyc.gov/sanitation

Oxfam America
www.oxfamamerica.org

Port Authority of New York/New Jersey
www.panynj.gov

Scripps Institute for Oceanography
www.sio.ucsd.edu

Sequence Staffing
www.sequencestaffing.com

Shorebank
www.shorebankcorp.com

Strategic Energy Institute
www.energy.gatech.edu

Sustainable South Bronx
www.ssbx.org

US Environmental Protection Agency
www.epa.gov

US Forest Service
www.fs.fed.us

Whole Foods Market
www.wholefoods.com

The views expressed by interviewees do not necessarilty represent those of their employers or affiliated institutions.

Carol Milano is an independent journalist in New York City, covering health care and science.

DOI: 10.1126/science.opms.r0900069

Full-Time Professor Positions
at the Department of Earth Sciences
Tsinghua University P.R.C

清华大学地球科学系(筹)诚聘海内外优秀学者加盟

Tsinghua University is planning to establish a new department in Earth Sciences in 2009. We invite applications for **professors and senior research scientists** whose interests include but not limited to: Geochemistry and Biogeochemistry, Structural Geology, Planetary Science, Atmospheric Science, Ocean Sciences, Earth System Science, Climate Change, Earth System Modeling and Earth Observations.

Candidates must hold a Ph.D. and have publications in high profile journals. Senior Scientists with full professorship and extensive research experiences are preferred. The university will offer a generous startup package, competitive salaries, and benefits etc. Applicants should submit full curriculum vitae, statements of research interests, 3-5 representative research papers and proof of exceptional achievements, three to five letters of recommendation to **rckfb@mail.tsinghua.edu.cn** or **mail to Mr. Wang Wei, Personnel Office, Tsinghua University, Haidian District, Beijing,100084 P.R.China.**

SCHOOL OF MEDICINE
INDIANA UNIVERSITY

ENDOWED CHAIR, GASTROINTESTINAL CANCER

The Division of Gastroenterology and Hepatology at Indiana University School of Medicine, in conjunction with the IU Simon Cancer Center, is seeking applications from qualified individuals for a senior level, tenured/tenure-track position to expand basic and translational research to complement existing excellent clinical research and clinical practice in the area of GI cancer. The institution is particularly strong in colon, pancreatic, biliary, and liver cancers. Qualified applicants will also be considered for an Endowed Professorship in the School of Medicine. The position requires a strong record of productive independent research and a record of peer-reviewed extramural funding.

Interested individuals should send their curriculum vitae, a brief overview of research plans, and three (3) letters of reference (NOTE: full professors must submit six (6) letters of reference) to: **Naga Chalasani, MD, Chief, Division of Gastroenterology and Hepatology, Indiana University School of Medicine, RG 4100, 1050 Wishard Blvd., Indianapolis, IN 46202**. Or email application materials to **bjcraig@iupui.edu**; reference "Faculty Position" in the subject line. To ensure full consideration, applications should be received by **June 1, 2009**.

Indiana University is an Affirmative Action, Equal Opportunity Employer. Applications from women and minorities are encouraged.

RIKEN

RIKEN
Researcher and technical staff positions for FY 2009

RIKEN has openings for researchers and technical staff at the following laboratories.

1. **Research Department**: Organometallic Chemistry Laboratory (Chief Scientist: Zhaomin Hou)
Area of Research: http://www.riken.jp/engn/r-world/research/lab/wako/organometallic/index.html
Available Position: One ASI Research Scientist
Job Description: http://www.riken.jp/engn/r-world/info/recruit/090610k.html
Qualifications:
- The successful candidate must have a PhD or must be confirmed to acquire it by the starting date.
- At least one year of overseas research experience desirable.

2. **Research Department**: Research Infrastructure Group, SR Life Science Instrumentation Unit (Group Director: Masaki Yamamoto)
Area of Research: http://www.harima.riken.go.jp/eng/labo/37.html
Available Position: One Research Scientist or Technical Scientist
Job Description: http://www.riken.jp/engn/r-world/info/recruit/090610k_2.html
Qualifications:
- PhD (or equivalent research ability and background) in the relevant field of research.
- At least one year of overseas research experience is desirable.
- Preferable to be experienced with R&D for experimental instruments in synchrotron radiation science.

3. **Research Department**: Lipid Biology Laboratory (Chief Scientist: Toshihide Kobayashi)
Area of Research: http://www.riken.jp/engn/r-world/research/lab/wako/lipid/index.html
Available Position: One ASI Research Scientist
Job Description: http://www.riken.jp/engn/r-world/info/recruit/090610k_4.html
Qualifications:
- The successful candidate must have a PhD or must be confirmed to acquire it by the starting date.
- At least one year of overseas research experience desirable.

4. **Research Department**: Advanced Device Laboratory (Chief Scientist: Koji Ishibashi)
Area of Research: http://www.riken.jp/engn/r-world/research/lab/wako/device/index.html
Available Position: One ASI Research Scientist
Job Description: http://www.riken.jp/engn/r-world/info/recruit/090610k_3.html
Qualifications:
- The successful candidate must have a PhD or must be confirmed to acquire it by the starting date.
- At least one year of overseas research experience desirable.

5. **Research Department**: Radioactive Isotope Physics Laboratory (Chief Scientist: Hiroyoshi Sakurai)
Area of Research: http://www.riken.jp/engn/r-world/research/lab/nishina/isotope/index.html
Available Position: One RNC Research Scientist
Job Description: http://www.riken.jp/engn/r-world/info/recruit/090610k_5.html
Qualifications:
- The successful candidate must have a PhD or must be confirmed to acquire it by the starting date.
- At least one year of overseas research experience desirable.

Common conditions

Location: Research Infrastructure Group: RIKEN Harima Institute, 1-1-1, Kouto, Sayo-cho, Sayo-gun, Hyogo 679-5148, Japan

All other positions: RIKEN Wako Institute, 2-1 Hirosawa, Wako-shi, Saitama, Japan

Conditions: A tenured fulltime position until RIKEN's retirement age of 60. However, the successful applicant may be offered instead a five-year fixed-term employment contract depending on the selection results. In this case, the employee can move to a tenured position after undergoing a successful review to be held at the end of the first 3 years of employment. Annual salary and other conditions of the fixed-term contract position are the same as for the tenured position. Salary shall be determined on an annual basis subject to the applicant's experience and performance. Social health insurance, commuting and housing allowances are provided. Days off are weekends, public holidays, New Year's holidays (Dec 29 - Jan 3) and RIKEN Foundation Day. These and other provisions are in accordance with RIKEN regulations. Recipients of JASSO category 1 scholarship loans may be eligible to have loan repayments waived (those awarded through FY2003). The researcher in this position will be eligible to apply for research grants offered by MEXT or JSPS.

Application Documents: The required documents differ according to the laboratory. Please refer to the following URL to find out what documents are required.
http://www.riken.jp/engn/r-world/info/recruit/index.html
Note 1: Submitted documents are strictly protected under the RIKEN Privacy Policy and will be used only for the purpose of applicant screening. Personal information will not be disclosed, transferred or loaned to a third party under any circumstances without legitimate reason.
Note 2: Submitted documents will not be returned.

Deadline: 5pm on Wednesday, June 10, 2009 (Japan Standard Time)

Selection Process: Selection will be made based on application screening and interviews.

Start of Employment: October 1, 2009 or later, but negotiable.

Contact Information for Submitting Documents and Making Inquiries:
Research Personnel Section, Advanced Research Promotion Division, RIKEN, 2-1 Hirosawa, Wako, Saitama 351-0198 (3rd floor of the RIKEN Gallery building)
E-mail: rps-saiyo (please add "@riken.jp" to complete the address)
Telephone calls cannot be accepted. When you mail your application, please send as certified mail so that there will be a record of delivery. Please write in red on the front of the envelope, the name of the laboratory you are applying for. Email attachments cannot be accepted.

DEPARTMENT OF HEALTH AND HUMAN SERVICES (DHHS)
NATIONAL INSTITUTES OF HEALTH (NIH)
National Institute of Arthritis and Musculoskeletal and Skin Diseases (NIAMS)
Director, Division of Extramural Research Activities (DERA)

The Department of Health and Human Services (DHHS) and the National Institutes of Health (NIH) are seeking exceptional candidates for the position of Director, Division of Extramural Research Activities (DERA), National Institute of Arthritis and Musculoskeletal and Skin Diseases (NIAMS) to support research into the causes, treatment, and prevention of arthritis and musculoskeletal and skin diseases, the training of basic and clinical scientists to carry out this research, and the dissemination of information on research progress in these diseases, while promoting public health and addressing issues of health disparities. This position offers a unique opportunity to direct, manage, and provide oversight to the Grants Management Branch (GMB) and the Scientific Review Branch (SRB), as well as, to oversee human subject protection and clinical trial activities under the extramural programs of NIAMS.

The DERA Director manages and directs all DERA program activities, which includes developing and justifying the yearly budget request. The DERA Director provides guidance and leadership to the GMB and SRB Chiefs on the development of new programs and projects, directs collaboration with Federal organizations, grantees, contractors, and private industry to develop models for DERA programs, and best practice models for providing DERA services, and provide leadership and advice to the Director, NIAMS, on developing, implementing, and coordinating extramural research contract, grant, and training program policies. The DERA Director maintains ongoing analysis and evaluation of the review of applications and the management of grants and contracts to support overall policy research, development and reporting for the extramural activities of the Institute. In addition, the DERA Director will collaborate with leading figures in the scientific community at NIH and other government organizations, representatives of academic institutions, and members of foreign governments and scientific organizations to exchange information on scientific research and coordinate projects of mutual interest. The DERA Director is a full partner in the executive leadership of the NIAMS.

Applicants may browse the NIAMS Home Page at http://www.niams.nih.gov/ for additional information on the Institute. Applicants must possess an M.D., Ph.D., or equivalent degree in a biomedical field related to the mission of NIAMS and have professional experience with a broad national programmatic or scientific background; be able to interact with the Scientific Program Division with equal authority; have the demonstrated capability to plan and direct programs of national and international importance; and have the ability to communicate with and obtain the cooperation of public, private and national and international organizations and individuals. Salary is commensurate with his/her qualifications and experience. Full Federal benefits including leave, health and life insurance, long-term care insurance, retirement, and a savings plan (401k equivalent). A detailed vacancy announcement that includes application procedures is available at: **http://www.jobs.nih.gov (under vacancy announcement NIAMS-09-327761)**. Questions may be addressed to **Ms. Ruth Fritz, 301-496-6051 e-mail: fritzr@mail.nih.gov. A CV and bibliography, including a statement addressing the qualifications and interest in the position, should be received by April 30, 2009**. *Applications received after this date will be considered until the position is filled.*

Department of Health and Human Services
National Institutes of Health
National Institute of Arthritis and Musculoskeletal and Skin Diseases
Intramural Research Program

Staff Scientist (Biostatistician)
Clinical Sciences Section
Orthopaedic Surgery

The Clinical Sciences Section (CSS) in the Office of the Clinical Director, National Institute of Arthritis and Musculoskeletal and Skin Diseases (NIAMS) is recruiting for a Biostatistician. Research in the CSS is in the broad areas of clinical epidemiology and health services research. The CSS focuses on studies of health outcomes of patients with musculoskeletal diseases. This is accomplished using observational studies, clinical trials, and analyses of large administrative datasets.

The successful candidate will be expected to be skilled in statistical computing, the application of statistics in epidemiology, longitudinal data analysis, and the analysis of clinical trials. He/she will assist in hypothesis development, data acquisition, data analysis, and manuscript preparation for projects designed to improve clinical care in orthopaedic surgery and musculoskeletal medicine. He/she will have the opportunity to conduct independent methodological research.

The ideal candidate will have a doctoral degree in statistics, health services research, economics or a related field. A record of peer-reviewed publications in one of these fields is required. Experience with programming using common statistical software is expected. Prior experience analyzing large administrative datasets would be advantageous. The successful candidate should have strong communication skills and the ability to work independently. Applications will be evaluated on demonstrated ability to analyze epidemiologic and clinical trial data and to collaborate effectively.

Salary will be commensurate with experience. A full package of benefits, including retirement, health, life, and long-term care insurance, and a Thrift Savings Plan is available.

Interested individuals should send a cover letter, curriculum vitae, a brief summary of research experience, accomplishments and research interests and goals, copies of three publications or reprints, and three letters of reference electronically to **Ms. Penny J. Mowery at mowerypj@mail.nih.gov** or mailed to the address below by **June 30, 2009: Timothy Bhattacharyya, MD, c/o Penny J. Mowery, NIAMS (National Institute of Arthritis and Musculoskeletal and Skin Diseases), National Institutes of Health, DHHS, Building 10 - Magnuson CC, 6N204, 10 Center Drive , Bethesda, MD 20892 Desk phone: 301-402-2679; Office phone: 301-435-3050**.

WWW.NIH.GOV

Tenure Track/Tenure Investigator Positions in Systems Immunology and Infectious Disease Modeling

The National Institute of Allergy and Infectious Diseases (NIAID), Division of Intramural Research (DIR), is seeking several outstanding individuals for its new Program in Systems Immunology and Infectious Disease Modeling (PSIIM — http://www3.niaid.nih.gov/labs/aboutlabs/psiim/).

Modern technology allows the deep analysis of biological systems at multiple levels—from intracellular signaling networks to individual cell behavior to the functioning of a tissue, organ, and even the whole organism. The challenge is not only to collect the large amounts of data these technologies can generate, but also to organize it in a manner that enhances our understanding of how such systems operate. To do this, it is necessary to develop quantitative models that can be used to predict behavior of these complex systems.

Achieving this goal requires an interdisciplinary effort, and for this reason PSIIM is organized as an integrated team of scientists and support staff. Within PSIIM, there will be groups with expertise in the areas of computational biology, bioinformatics, proteomics, genomics, cell biology, immunology, and infectious diseases. These groups will have access to the latest technology for gene expression profiling, high content screening of RNAi libraries for the discovery of pathway components, imaging tools, genomic and proteomic analysis, cores for the genetic manipulation of animals, and a substantial computer infrastructure. They will also have access to BSL-3 facilities for working with infectious agents of high priority for human health and biodefense.

Although PSIIM has been established within NIAID and has an immune/infectious disease focus, it is also expected to play a major role in fostering the growth of systems biology efforts throughout NIH and involving diverse biomedical areas. PSIIM staff will interact extensively with investigators in other components of the NIH intramural research program, including but not limited to the National Center for Biotechnology Information, NIH Chemical Genomics Center, Center for Information Technology, and Center for Human Immunology, all of which have activities emphasizing systems and informatic approaches to biomedicine.

Current groups in the PSIIM include Computational Biology—Modeling and Simulation, Molecular/ Cell Biology—High-throughput Screening, Proteomics, and Immunology. PSIIM is now recruiting for tenure-track or tenure level team leader appointments in the following areas:

Bioinformatics/Biostatistics: The incumbent will lead a group focused on developing and implementing computational tools and statistical methods for the analysis of large-scale genomic, proteomic, and cell biological datasets. The ideal candidate will have a strong background in statistics, mathematics, programming, and modeling biological systems, as well as a strong interest in collaborating with experimentalists to elucidate biological mechanisms through application of informatic methods, including construction of networks suitable for predictive analysis. The group will include expertise in statistics, software development (C++, Java, Perl, SQL, etc.), knowledge of existing and emerging bioinformatic tools, databases and algorithms, and experience with heterogeneous computer environments.

Genomics: The incumbent will be responsible for applying and, when necessary, developing novel methods for the systems-wide analysis of such issues as transcription factor and epigenetic control of gene expression, quantitative measurement of gene expression, and the role of non-coding regions and small RNAs in regulating gene/gene product expression patterns. PSIIM is especially interested in recruiting an individual with a strong interest in the application of these methods to the study of gene regulatory circuits and to the integration of information on cell signaling events, developmental state, and such gene regulatory circuits into comprehensive models of the control of cellular differentiation, for example, of effector CD4+ T cells or iPS.

These positions and the research activities they conduct are fully funded by the intramural research program of NIAID. Each team leader is expected to build a working group consisting of postdoctoral fellows, students, technicians, and staff scientists. The team leaders will work with the program director to help set the goals for PSIIM and to determine how best to reach these goals as an integrated group. To ensure appropriate career trajectories for those joining the PSIIM team effort, NIH has modified its tenure policies to take specific account of contributions made in such a team science setting. Members of PSIIM will be expected to play a major role in development of an integrated computational systems approach to biology, the application of these methods to questions of substantial biomedical importance, and the dissemination of the tools and techniques developed in PSIIM across the NIH intramural program and in the extramural academic and industrial spheres. Applicants should be seeking a challenge in which creativity, technical expertise, and a strong desire to achieve in a team setting will be critical for success

Interested candidates may contact:

Ronald Germain, M.D., Ph.D., Program Director, PSIIM, DIR, NIAID, at 301-496-1904 or **rgermain@niaid.nih.gov** for additional information about these positions.

Applicants must have a Ph.D., M.D., or equivalent degree in a relevant field with extensive post-doctoral experience, as well as a strong publication record demonstrating potential for creative research.

To apply, submit your curriculum vitae, bibliography, and a detailed statement of how your expertise can contribute to the success of the PSIIM program to Wanda Jackson at **NIAID.DIR.Search@niaid.nih.gov**. In addition, three letters of reference must be sent directly from the referee to Robert Hohman, Ph.D., Chair, NIAID Search Committee, c/o Wanda Jackson at **NIAID.DIR.Search@niaid.nih.gov** or 10 Center Drive, MSC 1356, Building 10, Room 4A22, Bethesda, MD 20892-1356. Email is preferred. **Completed applications MUST be received by May 1, 2009.**

Further information regarding the DIR laboratories is available at **http://www3.niaid.nih.gov/about/organization/dir/default.htm**, and information on working at NIAID is available on our Web site at **http://www.niaid.nih.gov/careers/dps**.

For more information about the NIAID systems biology program, please visit **http://www.nih.gov/catalyst/2006/06.09.01/page1.html**

NIAID

National Institute of Allergy and Infectious Diseases

U.S. DEPARTMENT OF HEALTH AND HUMAN SERVICES
National Institutes of Health

National Institute of Allergy and Infectious Diseases

Proud to be Equal Opportunity Employers

USDA ARS Agricultural Research Service
www.ars.usda.gov

"The premier food and agricultural research agency of USDA"

Center Director

Western Regional Research Center (WRRC)
Albany, California

Senior Executive Service (SES) – Career Reserved
ES-1301, 0401-00/00
Salary Range of $117,787 - $177,000 per year

Announcement Open: March 3, 2009 through May 1, 2009

The ARS is seeking highly qualified candidates for the Center Director of the Western Regional Research Center (WRRC), in Albany, California. This is a permanent full-time SES position, leading a regional Center of excellence with state-of-the-art research facilities and unique scientific expertise in molecular biology, genomics, biochemistry, food technology, materials engineering and ecology. The WRRC is recognized for its impact on the Nation's priority issues in biofuels, bioproducts, food quality and safety, new healthy food products, and the control of invasive weeds. The Center Director leads a dynamic group of more than 80 scientists in developing and implementing internationally renowned research programs, and in leveraging strategic collaborations with national and international research institutions, and private industry.

Join us in enhancing the
health and wealth of the Nation and its people
solving problems, expanding knowledge, delivering answers

To apply, print a copy of vacancy announcement ARS:SES-09-03 from the ARS Careers Website at **www.ars.usda.gov/careers**, and follow the application directions provided. To have a printed copy mailed or for questions about these positions, call **Deborah Crump** at **(301) 504-1448** or E-Mail: **deborah.crump@ars.usda.gov**. U.S. citizenship is required. Applications must be received by **May 1, 2009**.

USDA/ARS is an Equal Opportunity Employer and Provider.

---

aimen

The Technology Center AIMEN, located in Galicia (Spain), is a highly professionalized organisation specialised in the field of Materials Engineering and Manufacturing Processes. Around 100 industrial member organisations and 500 industrial customers covering a wide range of industrial sectors ensure the applicability of the R&D&I projects, which can be grouped into the following research fields:

- Joining technologies.
- Materials processing through advanced technologies (Laser and Friction Stir Based Techniques).
- Non Destructive testing technologies.
- Development of new materials and coatings.
- Environment.

To lead some of these areas, AIMEN is looking for candidates to fill in the following positions:

DIRECTOR OF THE CHARACTERIZATION AND MATERIALS RESEARCH LINE. (Ref. IMAN 007)

Candidates with a PhD in Physics, Chemistry or Materials Engineering are expected to have 10 years post-doctoral experience in research project management of materials, technical know-how on a welding basis and a high impact publication record in the field.

DIRECTOR OF LASER TECHNOLOGY. (Ref. IMAN 008)

Candidates with a PhD plus major in Laser Assisted Materials Processing should have at least 15 years experience in research project management on Laser Material Processing. European projects, high impact publication record and patents in the field together with management skills are also expected.

The Center will make all its facilities and technical resources available to the successful candidates.

Salary range: negotiable, commensurate with qualifications and experience of the appointee.

For further details and how to apply please visit: **www.programaiman.eu**

Application deadline: **May 31st, 2009**.

XUNTA DE GALICIA

iman

School of Pharmacy
Philadelphia College of Osteopathic Medicine-Georgia Campus

Academic Administrative and Faculty Opportunities

Philadelphia College of Osteopathic Medicine (PCOM) will seek Pre-Candidate accreditation status from ACPE in summer, 2009 and enroll its inaugural class in fall, 2010. PCOM is a nationally-recognized institution with an enrollment of 1426 medical students and 736 graduate students on two campuses.

The PCOM Georgia campus is a 19-acre site approximately 25 miles northeast of Atlanta in Gwinnett County, and currently serves 338 medical students and 75 graduate students. The proposed Doctor of Pharmacy program will have a strong regional emphasis, with a focus on increasing the pharmacist cohort in Georgia and the Southeast. Dr. Mark Okamoto, Founding Dean and Chief Academic Officer of the School of Pharmacy and the PCOM administration and are now engaged in formation of the pharmacy school leadership team and faculty. Qualified candidates are sought for the following positions:

Assistant/Associate Dean for Academics & Assessment

Assistant/Associate Dean for Experiential Education

Chair, Department of Pharmacy Practice

Chair, Department of Pharmaceutical Sciences

Director of Experiential Education

Faculty: Pharmacy Administration, Pharmaceutical Sciences, Pharmacy Practice

Salary and appointment level will be commensurate with qualifications and experience. Review of applications is in progress and will continue until the positions are filled. Application for the positions will require submission of a detailed curriculum vitae, a statement of practice, teaching, and research interests and names and addresses of three references, preferably from current or former supervisors. Additional information about the school and position descriptions are available at **www.pcom.edu.**

All inquiries must include salary history and requirements and should be directed to:

Department of Human Resources
Medical Office Building, 4190 City Avenue,
Suite 144, Philadelphia, PA 19131
Call (215) 871-6500, Fax (215) 871-6506,
Email: hr@pcom.edu

PCOM
PHILADELPHIA COLLEGE OF OSTEOPATHIC MEDICINE
PCOM is an Equal Opportunity Employer

USDA ars Agricultural Research Service

www.ars.usda.gov

The USDA, Agricultural Research Service (ARS), Animal and Natural Resources Institute in Beltsville, Maryland, is seeking an **Associate Institute Director** for a permanent full-time position. Salary is commensurate with experience and can range between $120,830 to $153,200 per annum, plus benefits. The mission of the institute is to conduct research and technology transfer programs that ensure high quality and safe food and other animal products while protecting the natural resource base and the environment. The mission is accomplished through fundamental and applied research in 8 laboratories, and a Veterinary Services Unit and Animal Care Compliance Office. The Associate Director participates with the Director in planning, coordinating, and evaluating the institute's programs, and provides leadership and operational accountability for the institute's research and technology transfer programs. The position requires thorough knowledge of animal, natural resources, and/or environmental sciences; knowledge of budgetary processes and procedures; and managerial skills in establishing goals and priorities and in the assessment and assignment of human resources to accomplish goals.

Refer to announcement **ARS-X9E-0098** at: **http://www.afm.ars.usda.gov/divisions/hrd/vacancy/VAC2.HTM** for detailed information regarding qualification requirements and for complete application information and instructions. Applications must be postmarked by **April 10, 2009**.

U.S. Citizenship is required.
USDA/ARS is an Equal Opportunity Employer and Provider.

FACULTY POSITIONS AT THE ROCKEFELLER UNIVERSITY

The Rockefeller University seeks exceptional, interactive, and creative scientists to join its faculty. We invite applications from outstanding candidates for tenure-track positions and also encourage tenured Professors to apply, provided that they are early on in their careers.

The Rockefeller University provides strong financial support for the research work of its faculty. The positions offer highly competitive salary, benefits and start-up funds, new or recently renovated laboratory space, access to numerous state-of-the-art core facilities and extensive opportunities for collaboration both within the University and with neighboring institutions. The University also provides very strong continuing support for research work beyond start-up, including full support for graduate students.

The University has a laboratory-based organization structure that fosters interdisciplinary research in the following areas:

- **Biology of Single Cells**
- **Chemical Biology**
- **Evolution, Ecology, & Developmental Biology**
- **Medical Sciences & Human Genetics**
- **Microbiology & Immunology**
- **Neurobiology & Behavior**
- **Physics & Biology**
- **Physiology of Multicellular Organisms**

Details about specific subjects of research can be found at: **http://www.rockefeller.edu/facultysearch.**

Applications are being accepted electronically through our **Online Application System** at **http://oas.rockefeller.edu.** Applicants should follow the online application procedure.

The deadline for receipt of applications is May 15, 2009.

If you have questions regarding submitting an application, please contact our Administrator at **facultysearch@rockefeller.edu.**

The Rockefeller University is an Affirmative Action/Equal Opportunity/VEVRAA Employer and solicits applications from women and underrepresented minorities.

BIOZENTRUM Universität Basel

UNI BASEL

OPPORTUNITIES FOR EXCELLENCE

International PhD program at the BIOZENTRUM University of Basel, Switzerland

The **Biozentrum** together with the **Werner Siemens - Foundation (WSF)** launches the **International PhD program** in **Molecular Life Sciences** and encourages excellent students to apply for one of the prestigious WSF fellowships.

The Biozentrum provides an internationally renowned research environment centered around three focal areas (Infection Biology, Growth and Development, Neurobiology) and two core programs (Structural Biology & Biophysics and Computational & Systems Biology) and is dedicated to basic molecular and biomedical research (http://www.biozentrum.unibas.ch/). We offer advanced Interdisciplinary training in the field of modern biology, a lively and interactive educational atmosphere, and competitive salaries with respect to European standards. University graduates admitted to the program receive theoretical and practical training and conduct a three-year research project under the supervision of a Biozentrum faculty member, monitored by a Thesis Advisory Committee.

Basel is an international center for biology research with major academic life science institutes and a high density of globally operating biotech companies.

Applications to the PhD fellowship program have to be submitted online. Application forms, requirements, and additional information can be found at: **http://www.biozentrum.unibas.ch/phd/.**

Application deadline: June 30, 2009.

Call for applications for FY2010 Foreign Postdoctoral Researcher (FPR) RIKEN, Japan

RIKEN is one of Japan's largest research organizations with institutes and centers in various locations in Japan and overseas. RIKEN carries out advanced basic and applied research in a wide range of fields, including physics, chemistry, medical science, biology, and engineering.

RIKEN is now accepting applications for the position of Foreign Postdoctoral Researcher (FPR) for FY2010. This position is for young foreign scientists who have demonstrated creative and innovative ideas and who can be expected to achieve broad international recognition in the future.

The FPR program will provide an opportunity for young foreign scientists to apply their creative and innovative ideas, under the direction of RIKEN's laboratory heads, to research currently being conducted at RIKEN.

Job Description Summary

1. Number of openings: Around 15
2. Qualifications:
   (1) Applicants should be none Japanese citizens.
   (2) Applicants must have a PhD in the natural sciences awarded in or after 2003, or expect to be awarded a PhD by the date of hire.
   (3) Applicants must be able to start working at RIKEN within fiscal year 2010 (April 1, 2010 to March 31, 2011).
3. Contract duration;
   (1) From date of hire to March 31, 2011
   (2) This contract may be extended for up to a maximum of 3 years.
4. Remuneration:

Salary is 487,000 yen per month. Commuting and housing allowances are also available. An annual research budget of 1 million yen will be allocated to the host laboratory.

Send an e-mail indicating your desire to apply for the position of FPR to RIKEN by **Friday, May 22, 2009**. Reference material will be sent to those with an interest in applying.

Application Deadline : 5pm on Friday, May 29, 2009 (Japan Standard Time)

Additional information on the program and application procedures is available at http://www.riken.go.jp/engn/r-world/info/recruit/index.html

FPR Desk, Research Personnel Section, Advanced Research Promotion Division, RIKEN, 2-1 Hirosawa, Wako, Saitama 351-0198 Japan. Fax +81-48-463-3687 Email: fpr@riken.jp

EINSTEIN

Albert Einstein College of Medicine
OF YESHIVA UNIVERSITY

Post-doctoral positions available: HIV-1 Biology, Pathogenesis and HIV host factors

Two post-doctoral positions are available immediately to work on exciting HIV research projects.

1. HIV-1 Biology and Pathogenesis

One project is aimed at perturbing specific steps of HIV-1 replication using RNA aptamers directed to HIV targets including Gag, Nef, Protease, Reverse Transcriptase and Tat. These preclinical/basic projects entail mechanistic studies to dissect the early and late events of HIV replication and developing effective inhibitors. A second project attempts to delineate determinants of HIV neuropathogenesis. The latter project also offers opportunities for global health projects in developing countries. Individuals interested in learning more, can visit the laboratory website at: **http://www.aecom.yu.edu/home/faculty/profile.asp?id=6706&k=&O=1&P=1**.

Candidates must have experience in molecular biology, virology and cell culture methods. If interested, email curriculum vitae listing 3 references to **prasad@aecom.yu.edu**.

2. Structure function analysis of HIV-1 host proteins

We have two ongoing research projects aimed at: (i) the analysis of host factors for HIV-1 and (ii) studying the essential interactions between viral proteins. These structural and genetic approaches to study HIV-1 replication can shed light on complex host-pathogen interactions ultimately leading to anti-HIV-1 inhibitors. For additional information: **http://molgen.aecom.yu.edu/index.php?option=com_content&task=view&id=58&Itemid=78**.

Candidates must have experience in protein biochemistry, crystallography, and molecular biology. If interested, email curriculum vitae listing 3 references to: **kalpana@aecom.yu.edu**.

Albert Einstein College of Medicine, Jack and Pearl Resnick Campus, 1300 Morris Park Avenue, Bronx NY 10461 USA

Equal Opportunity Employer.

Ψ

HERMAN B WELLS CENTER
FOR PEDIATRIC RESEARCH

INDIANA UNIVERSITY
School of Medicine

Asthma and Allergic Disease Program
Assistant/Associate Professor

The Department of Pediatrics, Section of Pulmonology, Critical Care and Allergy and the HB Wells Center for Pediatric Research (**www.wellscenter.iupui.edu**) is recruiting for a faculty position at the Assistant/Associate Professor level. We are particularly interested in candidates working in asthma and allergic disease related research to complement existing strengths in cytokine and T cell biology, and airway physiology in the areas of epithelial cell biology and viral infection. Candidates will have a PhD, MD or MD/PhD with a strong research background and either current, or potential for, independent funding. New faculty will be provided with generous start-up packages and join an active multi-disciplinary Immunology and Airway Disease research community.

Interested candidates are encouraged to submit a curriculum vitae and a short description of research interests to:

Mark H. Kaplan, PhD
Director of Pediatric Pulmonary Basic Research
Wells Center for Pediatric Research
Department of Pediatrics
Indiana University School of Medicine
702 Barnhill Drive, Room 2612
Indianapolis, IN 46202
airway@iupui.edu

Indiana University is an EEO/AA Educator, Employer and Contractor (M/F/D).

VIDRC

Vaccine and Infectious Disease Research Center

TRANSLATIONAL HEALTH SCIENCE AND TECHNOLOGY INSTITUTE

Faridabad, National Capital Region, India

Advertisement for scientific positions

The Department of Biotechnology, Ministry of Science & Technology (Government of India) is establishing the Translational Health Science and Technology Institute (THSTI), an autonomous institution, as a part of the interdisciplinary Health Biotech Science cluster, located at Faridabad in the National Capital Region. The institute is being mentored by globally recognized National Institute of Immunology (NII) and the Harvard-MIT Division of Health Science and Technology (HM-HST). The THSTI is designed to be a dynamic and interactive organization with a mission to conduct innovative translational research and develop research collaborations across disciplines and professions to accelerate the development of concepts into tangible products to improve human health. The other members of the cluster include the Regional Center for Biotechnology (RCB) under the aegis of UNESCO and the NII with which THSTI will have seamless scientific collaboration to achieve the interdisciplinary expertise. The cluster institutions will have access to state of the art experimental animal facility and the platform technology center for the sophisticated instrumentation.

Vaccine and Infectious Disease Research Center (VIDRC) is an independent research center of the THSTI with mission to study infectious disease and pathogens with the aim to generate translational knowledge for developing prophylactic and therapeutic measures against diseases prevalent in India. The center is looking for highly motivated individuals with expertise in relevant areas of immunology, virology, microbiology, structural, chemical, and systems biology with interest in furthering the center's mission. Research areas involving host-pathogen interactions, covering the entire range of expertise and interest from the statistical and epidemiological to the cellular and molecular levels will be considered.

Appointments are offered Assistant Professor upwards at various levels depending on the quantum of experience and the quality of the scientific productivity. The candidates must have an MD or PhD degree from a recognized university in any area of life sciences. A demonstrated record of scientific output in the form of recent peer-reviewed publications in scientific journals of high international repute and/or internationally valid and productive patents is essential. At the Assistant Professor level, three years of post-doctoral experience is desirable with some indication of independent scientific thinking. Appropriately higher experience and scientific accomplishment must be demonstrated for appointment at senior level. The investigators will be provided shared laboratory space and adequate start-up resources. They are expected to generate extramural project based funding for their research program.

The permanent laboratories of the center will come up at Faridabad in the next three years. The interim laboratories of the center will function from Gurgaon in the South Delhi area with adequate housing, transportation and schooling facilities. Campus housing may be made available when center moves to Faridabad.

Interested scientists holding Indian citizenship may send their bio-data containing details of qualification, positions held, professional experience/distinctions and copies of notable publications, with names and email addresses of three potential referees to the Director, Vaccine and Infectious Disease Research Center, Translational Health Science and Technology Institute, NII Campus, New Delhi 110067 and a soft copy by email to **vidrcindia@gmail.com**. The application should accompany a two-page write up on the proposed scientific program stating how it would complement the mission of the center. People working in public sector institutions within India are required to have their applications forwarded through proper channels. Applications will be accepted round the year; the first round of appointments is expected to be offered before **September 2009** for which the closing date is **May 15, 2009**. Only short listed candidates will be contacted for further discussion.

Faculty Position
Plastic Surgery/Developmental Biology

The Divisions of Plastic Surgery and Developmental Biology are jointly recruiting for a faculty position in Craniofacial Developmental Biology/ Developmental Genetics research. Candidates must hold M.D., Ph.D., or M.D./Ph.D. Degree and will be expected to maintain a federally funded independent research program. Faculty at CCHMC have access to high-quality graduate and M.D./Ph.D. programs and training programs for post-doctoral fellows, clinical fellows, residents and clinical faculty. Candidates will be considered at any level from Assistant to Full Professor.

Our Children's Hospital is currently ranked number three in the country in terms of NIH funding, just behind those at Harvard and the University of Pennsylvania. **Dr. Chris Wylie** heads the Division of Developmental Biology, which includes about twenty primary faculty appointments, with a wide range of developmental biology research interests. The many research credits of Children's include the development of the oral polio vaccine by Sabin. **http://www.cincinnatichildrens.org/ed/research/degree/mdb/default.htm**

The Children's Hospital Medical Center is resource rich and recently completed construction of a new 415,000 square foot research building, where we expect the Craniofacial Development Center to be housed.

Interested candidates should submit a curriculum vitae, a summary of past research accomplishments and future goals, and contact information for three references. Send to: **Julie Burns, Cincinnati Children's Hospital Research Foundation, 3333 Burnet Avenue ML 7007, Cincinnati, OH 45229-3039; Phone: 513-636-5620; julie.burns@cchmc.org .**

Cincinnati Children's Hospital Medical Center Visit our website at www.cincinnatichildrens.org

BROWN UNIVERSITY
Division of Biology and Medicine

Structural Biology Faculty Position
Assistant Professor/Associate Professor

The Center for Genomics and Proteomics at Brown University announces the opening of a faculty position at the rank of Assistant Professor or Associate Professor, effective **July 1, 2009**. Qualifications include a Ph.D. and/or M.D. degree with relevant postdoctoral research training and a record of excellence in research. The successful applicant will be an experimentalist in the general area of structural biology who will be expected to pursue an independent, externally funded research program. Special attention will be given to NMR spectroscopists, however structural biologists using other techniques, such as X-ray crystallography among others, are also encouraged to apply. The applicant should demonstrate a commitment to graduate and undergraduate education, and will have the opportunity to participate in predoctoral training programs within the Division of Biology and Medicine and campus at large. Research space will be provided in a new, state-of-the-art facility with access to modern core facilities, NMR spectrometers, in-house X-ray equipment, crystallization robotics, mass spectrometry, and biophysical analysis instrumentation, such as ITC, DSC, CD, and SPR among others. An attractive start-up package will be provided.

Candidates should submit a curriculum vitae with complete bibliography, a 3-5 page description of research plans, and a one-page teaching statement. Applicants should arrange for at least three reference letters to be sent under separate cover. Review of materials will commence on **April 15, 2009**, and will continue until the position is filled. Materials should be submitted electronically in PDF format to **MPPB@brown.edu** or by mail to: **Dr. Wayne Bowen, c/o Ms. Monique Victor, Department of Molecular Pharmacology, Physiology & Biotechnology, Brown University, Box G-B3, Providence, RI 02912**.

Brown University is an Equal Opportunity/Affirmative Action Employer and welcomes applications from women and minorities.

UMBI life. science. works.

The Medical Biotechnology Center (MBC) of the University of MD Biotechnology Institute (UMBI) is actively seeking a Research Associate in the Institute of Fluorescence. The applicants will be expected to undertake day-to-day laboratory experiments in Fluorescence Spectroscopy and metal-enhanced fluorescence within the Institute of Fluorescence. This will include the operation of fluorescence and absorption spectrometers, optical detectors such as CCD cameras, fiber optics and the measurement of fluorescence lifetimes using TCSPC as well as molecular diffusion times using FCS. The candidate will have a good working knowledge of fluorescence theory and its applications and be familiar with FCS and single molecule detection. The development, use and application of fluorescence-based immunoassays will also be undertaken by the successful applicants.

The candidate must have a Ph.D. in Fluorescence Spectroscopy or in a related spectroscopy discipline. The candidate will also have experience in textile processes, staining and the implementation of nanotechnology to clothing fibers. Expertise in optical spectroscopy is desirable. Salary is commensurate with experience.

Postdoctoral and Senior Researchers are encouraged to apply.

ALL APPLICANTS ARE REQUIRED TO APPLY ONLINE AT **WWW.UMBI.UMD.EDU/JOBS** TO POSITION NUMBER **300991**. Application review will begin immediately and will continue until a suitable candidate is selected.

UMBI is an EEO/ADA/AA Employer.

The University of New Mexico
DataONE (Observation Network for Earth)
Director, Information Technology

The Office of the Vice President for Research seeks highly qualified candidates for the position of Director of Information Technology for DataONE—a distributed global data center for earth observations, supporting the biological, environmental and earth sciences. The Director provides overall leadership for the design of system architecture, cyberinfrastructure implementation, and operations for the global data network.

Applicants must possess an M.S. or Ph.D. in Computer Science, Library and Information Science, or the Biological, Environmental, or Earth Sciences, plus demonstrated senior-level management experience and outstanding knowledge of information system architecture and operation. Expertise in software and systems engineering, Linux, modern programming languages, and open source development approaches is essential.

Salary is commensurate with experience, and a complete benefits package (including retirement, health/dental/life/long-term care insurance, etc.) is available. A detailed announcement including mandatory qualifications and application procedures can be obtained at the UNM Jobs website: **https://unmjobs.unm.edu**. Questions on application procedures may be addressed to **The University of New Mexico Human Resource Department** at **(505) 277-6947**.

A letter of interest (including a statement addressing the qualifications requirements), CV, and three references must be received by close of business **May 1st, 2009**.

The University of New Mexico is an Equal Opportunity, Affirmative Action Employer.

Fundación **BBVA**

2009 **BBVA** Foundation **Frontiers of Knowledge Awards**

The BBVA Foundation expresses the corporate responsibility of BBVA, a global financial services group committed to working for the improvement of the societies where it does business.

The Foundation supports knowledge generation, scientific research and the promotion of culture, ensuring that the results of its work are relayed to society at large. Among its preferred areas of activity are basic sciences, biomedicine, ecology and conservation biology, the social sciences, literary creation and contemporary music.

The **BBVA Foundation Frontiers of Knowledge Awards**, whose second edition is now open, seek to recognize and encourage world-class research and artistic creation, prizing contributions of broad impact for their originality and theoretical significance. The **BBVA Foundation Frontiers of Knowledge Awards** honor fundamental advances in a series of basic, natural, social and technological sciences, as well as creative activity of excellence in the classical music of our time. Categories are also reserved for two core concerns of early 21st century society, climate change and socioeconomic development.

The BBVA Foundation Frontiers of Knowledge Awards take in the following categories:

- Basic Sciences (Physics, Chemistry, Mathematics)
- Biomedicine
- Ecology and Conservation Biology
- Information and Communication Technologies
- Economics, Finance and Management
- Contemporary Music
- Climate Change
- Development Cooperation

With the collaboration of:

CSIC

CONSEJO SUPERIOR
DE INVESTIGACIONES
CIENTÍFICAS

The **BBVA Foundation Frontiers of Knowledge Awards** consist of 400,000 euros prize money in each category and are granted on an annual basis.

Candidates may be one or more natural persons, without limit of number, of any nationality. This means recognition may go to achievements resulting from cooperation within or across teams. In the categories of Climate Change and Development Cooperation, entries are also open to public or private non-profit organizations.

Nominations will be indirect and may come from any of the following institutions: scientific or artistic societies and organizations; national or regional academies of the sciences or the arts; public or private R&D centers; university departments and schools and university or research institutes; hospital departments and biomedical research centers; conservatories and schools of music; scholarly music and musicology journals; orchestras and orchestra associations; radio and television broadcasters running symphony or chamber orchestras; museums of the arts and sciences; and public agencies and international, national or regional organizations substantially engaged in analysis and/or activities relating to climate change and development cooperation. Winners of the Nobel Prize in any of its categories and past winners of the BBVA Foundation Frontiers of Knowledge Awards shall likewise be entitled to nominate. The BBVA Foundation may also invite nominations from researchers and creative practitioners who have made outstanding contributions in their respective fields.

Entries can be submitted from January 1 to June 30, 2009, using the form provided on the dedicated website: www.fbbva.es/awards.

Candidate selection will be guided by the principles of objectivity and independence and will rely on the best standards and metrics of excellence in each prize area. The Foundation will be partnered in the selection process by the **Spanish National Research Council (CSIC)**, Spain's premier multidisciplinary research organization. The prize juries in each category will be made up of eminent international specialists.

Fundación BBVA

Plaza de San Nicolás, 4
48005 Bilbao · Spain

Paseo de Recoletos, 10
28001 Madrid · Spain

awards-info@fbbva.es
www.fbbva.es

POSITIONS OPEN

ASSISTANT/ASSOCIATE/FULL PROFESSOR Pharmaceutical Sciences
Auburn University

The Department of Pharmacal Sciences at Auburn University's Harrison School of Pharmacy invites applications for multiple **12-Month Tenure-Track Faculty Positions** in pharmaceutical sciences and related disciplines. Individuals with expertise in drug metabolism, pharmacokinetics and drug delivery are of particular interest. These positions offer the opportunity to join an expanding enterprise in research in pharmaceutical and biomedical sciences. Successful candidates are expected to actively participate in the teaching mission of the Harrison School of Pharmacy at the graduate (Ph.D.) and professional (Pharm.D.) levels; develop and/or maintain an independent extramurally funded research program; be involved in collaborative research programs; demonstrate a high level of scholarly activity as evidenced by quality publications in peer-reviewed scientific journals and active participation in professional societies and contribute to Department, School and University service activities.

Applicants must have a demonstrated interest in education of health professionals and graduate students. They must have a Ph.D. or equivalent degree, postdoctoral training and demonstrated research abilities. A professional degree in pharmacy is desirable but not essential. The successful candidate must meet eligibility requirements to work in the United States at the time the appointment is scheduled to begin and continue to work legally for the proposed term of employment; excellent communication skills required. Review of applications will begin April 1, 2009 and will continue until the positions are filled. Candidates should submit a letter of application, curriculum vitae, statements of research and teaching interests as well as the names and addresses (include e-mail address and phone number) of three-five references.

Preferably applications should be submitted electronically to **Ms. Kandi Dawson, e-mail: dawsokp@auburn. edu, fax: 334-844-8331.**

Auburn University is an Equal Opportunity/Affirmative Action Employer. Women and minorities are encouraged to apply.

POSTDOCTORAL FELLOW
Department of Molecular Medicine
College of Medicine

The Department of Molecular Medicine within the University South Florida Health College of Medicine is seeking candidates for a Postdoctoral Fellow candidate in the laboratory of **Dr. Robert Deschenes, Ph.D.** in the Department of Molecular Medicine at the University of South Florida in Tampa, Florida. The research focuses on the molecular mechanisms of cancer cell signaling with an emphasis on posttranslational control and spatial distribution of Ras oncogene proteins. The Department of Molecular Medicine is comprised of biochemists, molecular biologists, microbiologists, and immunologists with expertise in genetic mechanisms of disease, structure-function relationships, microbial genetics and pathogenesis, and cellular and molecular immunology.

Applicants must have a Ph.D. at the time of employment in biochemistry, molecular biology, chemistry, or related areas. First-author publications in peer reviewed journals and experience with isolation and purification of membrane proteins, enzymology, and protein lipidation is desirable. Salary will be commensurate with experience and benefits are provided.

Please submit a cover letter, curriculum vitae, and three references to: **Robert J. Deschenes, Ph.D., Chair, Department of Molecular Medicine, College of Medicine, University of South Florida, 12901 Bruce B. Downs Boulevard, MDC 7, Tampa, FL 33612-4799, telephone: 813-974-8320, e-mail: rdeschen@health. usf.edu, website:http://molecularmedicine.health. usf.edu.** Applications will be accepted until the position is filled.

University of South Florida is an Equal Opportunity/Equal Access/Affirmative Action Employer. For disability accommodations, contact Rochelle Morris at telephone: 813-974-8349 a minimum of five working days in advance. According to Florida law, applications and meetings regarding them are open to the public.

POSITIONS OPEN

POSTDOCTORAL FELLOWSHIP POSITIONS
Center for Environmental Health Sciences
College of Health Professions and Biomedical Sciences
University of Montana – Missoula

Two or more postdoctoral positions funded by an NIH Centers of Biomedical Research Excellence grant and individual NIH grants are available as part of our training program at the Center for Environmental Health Sciences (CEHS) in various fields of investigation including immunotoxicology, respiratory diseases, neurotoxicology, cardiovascular diseases, and related fields. More information can be found at **website: http://www.umt.edu/cehs/.** Previous training in a relevant field in biomedical research is required; applicants must have a Ph.D., M.D., or comparable degree at the time of appointment. Postdoctoral fellows will be expected to apply for independent funding in their first year. Please send curriculum vitae, a career statement, and three letters of reference to: **Dr. Andrij Holian, CEHS, 280 Skaggs Building, 32 Campus Drive, Missoula, MT 59812. E-mail: andrij.holian@umontana.edu.**

An Equal Opportunity/Affirmative Action Employer.

The University of Georgia (UGA) Complex Carbohydrate Research Center (CCRC) is accepting applications for several **ASSISTANT RESEARCH SCIENTISTS.** A Ph.D. in a biological or chemical science field is required along with three years of research experience in the study of complex carbohydrates in plant, animal, or microbial cells and/or tissues. If interested please send a letter of application, curriculum vitae, and three letters of recommendation to: **Lynn Berryman, CCRC, 315 Riverbend Road, Athens, GA 30602-4712. E-mail: lberry@ccrc.uga.edu.** To ensure full consideration applications must be received by April 25, 2009. *UGA is an Equal Employment Opportunity/Affirmative Action Employer.*

ALASKA SEALIFE CENTER

CHIEF SCIENTIST will be responsible for overall center scientific leadership, reporting to the president and chief executive officer. We are seeking a visionary and proven science leader to broaden our marine research horizons. Ph.D. required, Alaskan experience preferred. For full position description, see our **website: http://www.alaskasealife.org.** Send curriculum vitae to: **Dr. Ian Dutton** at **e-mail: ian_dutton@alaskasealife.org.**

GRANTS

National Brain Tumor Society
Leading through research and support

BRAIN TUMOR RESEARCH GRANTS

National Brain Tumor Society requests proposals focused on improving treatments and finding a cure. Standard Awards: $100,000-$200,000 (one to two years); Advanced Awards: $600,000 (three years); Innovation Awards: $300,000 (two years); letter of intent deadline: April 30, 2009. For details and application packets, visit **website: http://www.braintumor.org.**

POSITIONS OPEN

MARKETPLACE

Les prix CANADA GAIRDNER Awards

50 years ago, James Gairdner created The Gairdner Awards to recognize the breakthroughs of the world's leading medical scientists and to bring the workings of 'high science' to the public. The Gairdners are now Canada's top international prize and one of the most esteemed awards in the world of science.

The importance of the Gairdners to Canada's future as a world leader in scientific research was underscored when the Government of Canada last year announced an endowment to increase its awards to $100,000 each and to create the world's first individual award for Global Health. Starting this year, they will be named the Canada Gairdner International Awards and the Canada Gairdner Global Health Award.

Supported nationally by:

CIHR IRSC
Canadian Institutes of Health Research / Instituts de recherche en santé du Canada

www.gairdner.org

SEVEN OF THE WORLD'S LEADING SCIENTISTS ARE RECIPIENTS OF THE 2009 CANADA GAIRDNER AWARDS

The 2009 Canada Gairdner International Awardees are:

Dr. Shinya Yamanaka

Professor, Department of Stem Cell Biology
Institute for Frontier Medical Sciences
Director, Centre for iPS Cell Research and Applications
Institute for Integrated Cell-Material Sciences
Kyoto University
Japan

"for his demonstration that the key transcription factors which specify pluripotency may become reprogrammed somatic cells to pluripotent stem cells"

Dr. Lucy Shapiro

D.K. Ludwig Professor
Department of Developmental Biology
Director, Beckman Center for Molecular and Genetic Medicine
Stanford University School of Medicine
Stanford, CA

"for their discovery of mechanisms that define cell polarity and asymmetric cell division, processes key in cell differentiation and in the generation of cell diversity"

Dr. Richard Losick

Maria Moors Cabot Professor of Biology
Howard Hughes Medical Institute Professor
Faculty of Arts and Sciences
Harvard University
Cambridge, MA

Dr. Kazutoshi Mori

Professor, Department of Biophysics
Graduate School of Science
Kyoto University
Japan

"for their dissection and elucidation of a key pathway in the unfolded protein response which regulates protein folding in the cell"

Dr. Peter Walter

Howard Hughes Medical Institute
Department of Biochemistry and Biophysics
University of California, San Fransicso
San Francisco, CA

Gairdner Wightman Award

Dr. David Sackett. MD, ScD

Professor Emeritus
McMaster University
Hamilton, Ontario
Canada

"for his leadership in the fields of clinical epidemiology and evidence-based medicine, which have had major impacts internationally in applied clinical research and in the practice of medicine"

The Inaugural Canada Gairdner Global Health Awardee is:

Dr. Nubia Muñoz

Visiting Scientist
Catalan Institute of Oncology
Barcelona, Spain

"for her epidemiological studies that defined the essential role of the human papilloma virus in the etiology of cervical cancer on a global level which led to the development of successful prophylactic vaccines"

R&D Systems
High Performance Antibodies.

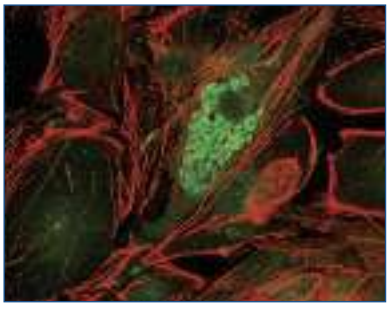
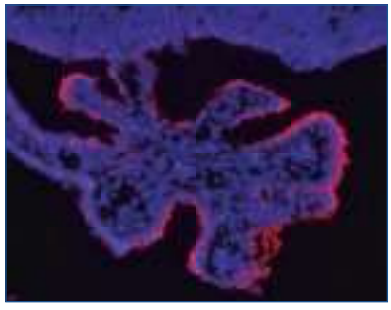
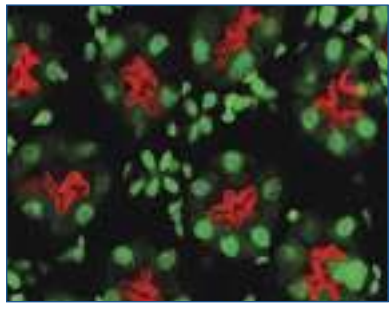
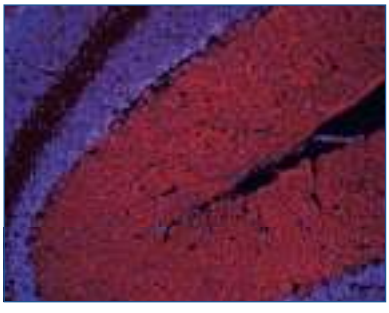

We deliver.

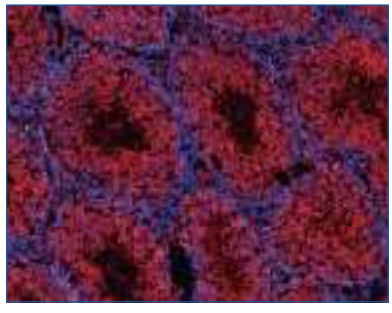
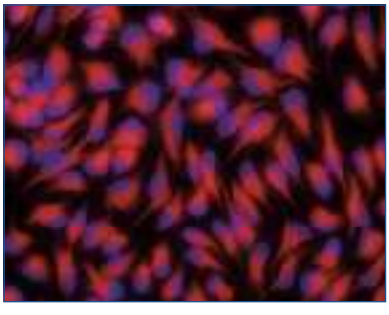
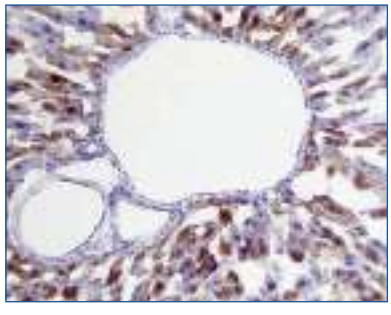
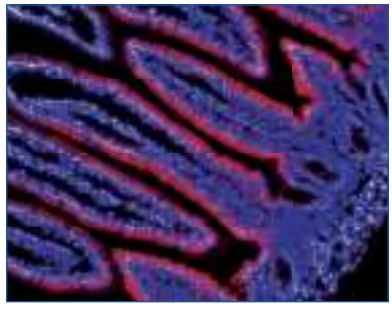
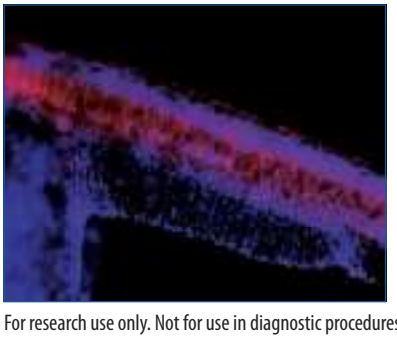
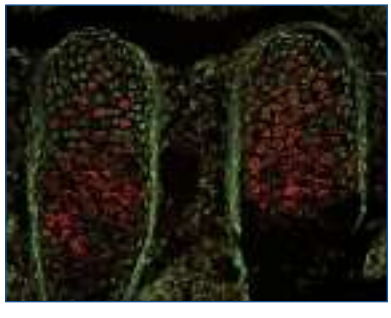
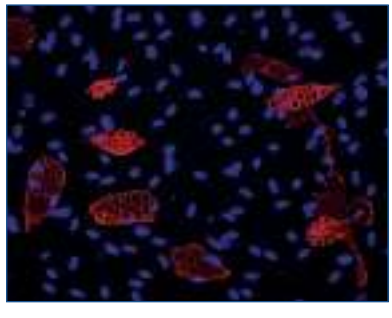

For research use only. Not for use in diagnostic procedures.

For details about the images above, please visit our website at www.RnDSystems.com/go/AntibodyAd

R&D Systems Tools for Cell Biology Research™

USA & Canada **R&D Systems, Inc.** Tel: (800) 343-7475 info@RnDSystems.com

Europe **R&D Systems Europe, Ltd.** Tel: +44 (0)1235 529449 info@RnDSystems.co.uk

Selection expanding weekly—visit **www.RnDSystems.com/go/request** to sign up for weekly new product updates.

R&D SYSTEMS®